CRANFIELD UNIVERSITY

Byoung-Ju Jeon

Nonlinear Flight Control with Reduced Model Dependency

School of Aerospace, Transport and Manufacturing

PhD Thesis

Cranfield University

School of Aerospace, Transport and Manufacturing

PhD Thesis

Academic Year 2017-2020

Byoung-Ju Jeon

Nonlinear flight control with reduced model dependency

Supervisors: Prof. Hyo-Sang Shin
Prof. Antonios Tsourdos

May 2020

This thesis is submitted in partial fulfillment of the requirements for the degree of Doctor of Philosophy.

Abstract

This thesis aims to innovate knowledge on nonlinear flight control algorithms with reduced model dependency by resolving the research gaps for practical applications. Two control schemes with different principles on reducing model dependency are considered in this thesis; incremental control scheme and adaptive control scheme. In incremental control scheme, state derivative and control surface deflection angle measurements are additionally utilized to substitute required model information except control effectiveness. In adaptive control scheme, uncertain model parameters are estimated online via adaptation law and these estimates are utilized in control input command calculation. Discussions in this thesis are based on incremental backstepping control (IBKS) and composite adaptive backstepping control (C-ABKS) which are obtained by applying those control schemes to backstepping control (BKS). Contributions of this thesis with each algorithm are detailed as follows.

This thesis provides critical understandings on IBKS in a systematic way via theoretical analysis under various defects. As a starting point, closed-loop analyses under the model uncertainties are conducted with IBKS and BKS for theoretical interpretations on reduced model dependency in IBKS. Stability and performance of the closed-loop system with IBKS are shown to be not affected by the model uncertainties, while they significantly influence the closed-loop characteristics with BKS. One interesting observation is that the uncertainty on control effectiveness information, which is still required to implement IBKS, does not have any impact on the closed-loop system with IBKS if a control input is calculated, transmitted and reflected fast enough to an actual control surface. The next two analyses are conducted to identify how the defects on the additional measurements together with the model uncertainties affect stability and performance of the closed-loop system with IBKS. First, the closed-loop characteristics with IBKS is analyzed under biases on the additional measurements and the model uncertainties. The measurement biases result in a steady state error while not affecting the closed-loop system stability with IBKS. Unlike the analysis results only with the model uncertainties, the uncertainty in control effectiveness information has an impact on the steady-state error of the closed-loop system. Second, the closed-loop system with IBKS under delays on the additional measurements and the model uncertainties is examined with the analysis framework proposed in this thesis. New analysis framework with optimization concept is proposed to systematically and efficiently test the closed-loop

system stability under measurement delays. The key finding is that the delays on the additional measurements should satisfy a specific relationship for the closed-loop stability with IBKS. Besides, it is identified that this stability condition is affected by the uncertainty on control effectiveness information.

A new C-ABKS is designed by resolving research gaps of the composite adaptive control for a practical application as follows. First, parameter convergence under finite excitation (FE) is guaranteed with a new paradigm for the information matrix design which is suggested by developing a modulation-based approach. It is proven that the new information matrix is positive definite for all the time from the beginning under FE, while the accumulation-based approach in previous studies requires uncertain amount of time to populate the information matrix to be full rank. The closed-loop system with the C-ABKS utilizing the new information matrix is guaranteed to be globally exponentially stable for all the time under FE. Comparing to the accumulation-based approach, the new modulation-based approach provides advantages in adaptation speed and system robustness since the information matrix is designed to have all eigenvalues with moderate level of magnitudes. Second, the adaptation speed is improved without excessive increase of the adaptation gains in the new logarithmic regression-based composite adaptive control system. The parameter convergence speed is enhanced by slowing down the adaptation speed degeneration at the later stage where the estimation error is small; a concave and monotonically increasing characteristics of a logarithmic function is utilized for the regression term design in this research. The closed-loop system with the proposed logarithmic regression-based C-ABKS is shown to be asymptotically stable under FE by applying Lyapunov theory. Within the system boundary, the new logarithmic regression-based algorithm is proven to be always faster than the well-known linear regression-based algorithm under the same adaptation gain if its design parameters satisfy the suggested condition. In order to make the linear regression-based approach to become faster than the logarithmic regression-based approach with the design parameters satisfying this condition, the adaptation gain of the linear regression term should be increased and this can result in reduced robustness.

Important findings for IBKS and C-ABKS are suggested and verified with simulations throughout the thesis. A comparative study is additionally conducted to show different properties of IBKS and C-ABKS under model uncertainties and measurement delays via numerical simulations.

Acknowledgements

I would like to give sincere gratitude for every support I had in studying period for my PhD.

First, I would like to express my great appreciation to my supervisors, Prof. Hyo-Sang Shin and Prof. Antonios Tsourdos, from the wonderful opportunity for PhD research in Cranfield to their helpful supervision. I also would like to thank my friends, Shaoming, Hae-In, Teng, In-Mo, Sang-Jun, Ju-Hyeon, Dmitry, On and Yun-Ha for sharing their valuable experiences with practical helps in PhD life.

I am particularly grateful to my parents Jae-Hwang and Il-Sun for their endless encouragement. Above all, I would like to express my deepest gratitude to my love, Min-Guk.

Contents

List of Figures

List of Tables

Chapter 1

Introduction

1.1 Background and Motivation

There have been extensive and valuable researches on nonlinear flight control algorithms [1–15] which have advantages comparing to linear controllers as follows. First, time-consuming tasks for gain scheduling are not required. Second, nonlinear controllers can show improved performance especially for flight envelope with significant nonlinearities. One of the biggest limitations in nonlinear flight controllers is that they are highly dependent on aircraft model information identified off-line. By utilizing the model information to cancel out undesired nonlinearities in dynamics, most nonlinear controllers make error dynamics of a closed-loop system to achieve desired behaviors.

Since it is difficult to obtain accurate model information from aero-prediction or wind tunnel test in reality, model uncertainties are inevitable. Besides, there exist possibilities of accidents in flight which significantly change original characteristics of an airplane in unpredictable manner. Hence, it is important to reduce model dependency of nonlinear flight control algorithms.

Backstepping(BKS) control [16] is one of the most widely and successfully applied nonlinear flight control algorithms [1–10]. BKS is sensitive to model uncertainties like other nonlinear controllers, but it has additional merits as follows. Since BKS has a cascade control structure, a control law design for a system with large dimension can be split into recursive design for several subsystems with smaller dimensions. Besides, the closed-loop system with BKS fulfills desired response with known stability and convergence properties, as it is designed under Lyapunov framework. This

thesis focuses on BKS among nonlinear flight control algorithms and mainly considers two sensor dependent approaches to reduce its model dependency as follows.

Incremental backstepping(IBKS) controller is proposed in previous studies [17–20] to reduce model dependency of BKS with supplementary measurements. Comparing to BKS, IBKS additionally utilizes state derivative and control surface deflection angle measurements which replace required knowledge about a model except control effectiveness information for its implementation. It is evident that stability and performance with IBKS are strongly influenced by quality of these additional measurements, but measurement defects are inevitable in practical applications. Hence, it is essential to have critical understandings on the impacts of defects in these additional measurements and uncertainty in control effectiveness information to the system with IBKS.

Adaptive control [21–45] can be considered as another sensor dependent approach for reduced model dependency of BKS. Note that adaptive control algorithm can be designed to estimate uncertain model information on-line via an adaptation law with existing measurements and utilize these estimates in control command calculation. This thesis focuses on composite adaptive backstepping(C-ABKS) control for improved estimation and tracking performance with enhanced system robustness. There are practical issues with this parameter estimation-based control scheme; persistent excitation(PE) is required for parameter convergence and high adaptation gain is utilized to enhance convergence speed. PE results in persistent oscillations of state and control input signals, which is unrealistic. Fast convergence is essential for online adaptation, but excessively large adaptation gain amplifies noise.

To this end, it is important to reduce model dependency of BKS while responding research gaps for practical applications in considered methodologies mentioned above.

1.2 Research Aim and Objective

The overall scientific aim of this thesis is to innovate knowledge on nonlinear flight control algorithms with reduced model dependency by resolving research gaps for practical applications in considered methodologies.

This thesis considers BKS among nonlinear flight control algorithms and focuses on incremental and adaptive control schemes to reduce its model dependency. The

individual objectives against the overall aim are addressed as follows, considering technical issues to be tackled in each considered approach i.e. IBKS and C-ABKS.

- **O1. Analysis with IBKS under Model Uncertainty**: Suggest critical understandings obtained from theoretical closed-loop analysis under model uncertainty with IBKS comparing to one with BKS.

  O2. Analysis with IBKS under Measurement Bias and Model Uncertainty: Suggest critical understandings on closed loop system characteristics with IBKS under measurement bias and model uncertainty obtained from theoretical analysis.

  O3. Analysis with IBKS under Measurement Delay and Model Uncertainty: Propose new stability analysis framework and suggest critical understandings about closed-loop characteristics with IBKS under measurement delay and model uncertainty.

- **O4. Design of C-ABKS**: Propose C-ABKS which reduces model dependency of BKS and design an adaptation law with less computational complexity which takes advantage of cascade control structure of BKS.

  O5. Design of C-ABKS with new information matrix: Propose C-ABKS with new information matrix, which achieves parameter convergence without PE.

  O6. New C-ABKS Design for adaptation speed enhancement: Propose new C-ABKS which enhances adaptation speed without high gains.

- **O7. Comparative study between IBKS and New C-ABKS**: Compare pros and cons of IBKS and New C-ABKS under various defect circumstances e.g. model uncertainty and measurement delay, demonstrating their advantages from reduced model dependency comparing to BKS.

1.3 Thesis Overview and Contribution

This thesis is written in a paper-format; each chapter from 2 to 7 is based on the corresponding paper published or submitted. Accordingly, each chapter becomes a self-contained description of all aspects of the research, which provides introduction with research context and relevant literature review, methodologies, results, discussions, conclusions and references.

Connections between research objectives, chapters and papers are illustrated in Fig 1.1.

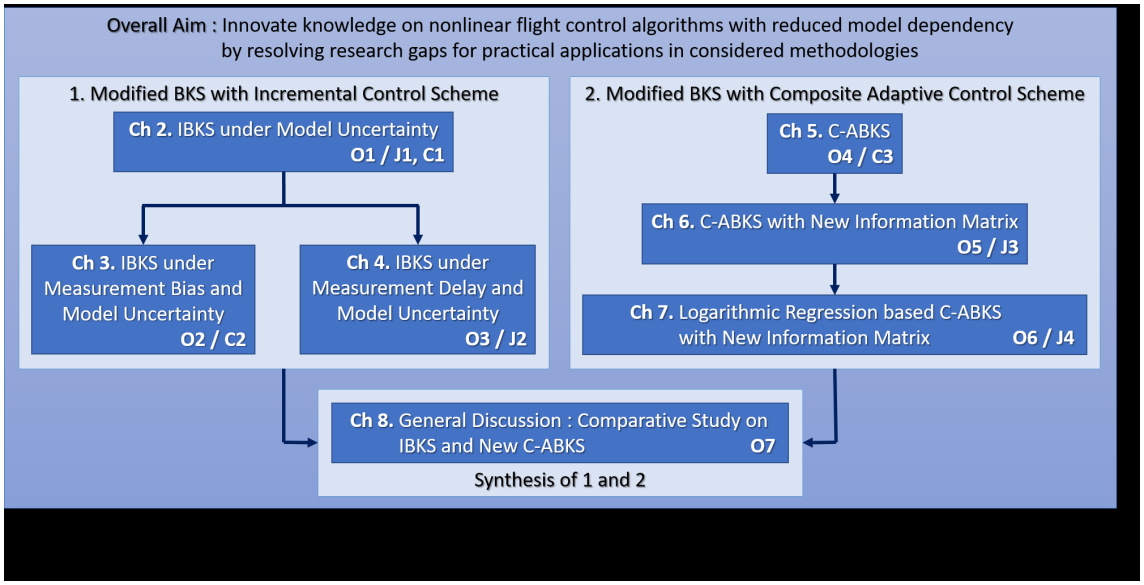

Figure 1.1: Thesis Outline

Chapter 2, 3 and 4 deal with incremental control scheme to reduce model dependency of BKS, providing knowledge on IBKS under various critical defects in a systematic way. Note that IBKS additionally utilizes state derivative and control surface deflection angle measurements to replace required knowledge about a model except control effectiveness information, comparing to BKS. Chapter 2 suggests theoretical closed-loop analysis results under the model uncertainties with IBKS comparing to the ones with BKS. Chapter 3 provides closed loop characteristics with IBKS considering biases in the additional measurements and the model uncertainty in control effectiveness information via theoretical analysis. In Chapter 4, delays in the additional measurements together with the model uncertainty in control effectiveness information are considered for the analysis of the closed-loop system with IBKS. For this delayed system with the model uncertainty, new stability analysis framework is proposed and critical understandings about the closed-loop characteristics are investigated.

Chapter 5, 6 and 7 deal with composite adaptive control scheme to reduce model dependency of BKS, providing new C-ABKS where research gaps for practical applications in the considered scheme are resolved step by step. Chapter 5 corresponds to a basis for Chapter 6 and 7 where new C-ABKS is proposed. In Chapter 5, model dependency of BKS is reduced via parameter estimation in the composite adaptation law which has less computational complexity by taking advantage of cascade

control structure of BKS. Note that linear regression based approach and accumulation based information matrix design method in previous studies are utilized in Chapter 5. In Chapter 6, a new paradigm in the information matrix design for parameter convergence without PE is proposed, which resolves issues arising from the existing accumulation based design method. In Chapter 7, a novel idea to enhance adaptation speed without an excessive increase in gains is proposed, resulting in logarithmic regression based approach. Finally, new C-ABKS is proposed in Chapter 7 with new information matrix in Chapter 6 and logarithmic regression based composite adaptation law in Chapter 7.

Comparative study between IBKS in Chapter 2-4 and new C-ABKS in Chapter 7 is conducted for general discussions in Chapter 8. Their pros and cons under various defect circumstances are investigated from the simulation results with a short period mode dynamics of an aircraft under the model uncertainty and the measurement delay. Note that Chapter 2-4 with IBKS are based on short period mode dynamics due to its importance in flight control and simplicity in theoretical analysis, but more general and complicated dynamics are considered especially in Chapter 6-7 for verification of newly proposed algorithms.

Each chapter from 2 to 7 which corresponds to each block in Fig 1 is overviewed in detailed way as below, underpinning its contributions.

- **Chapter 2. Incremental Backstepping Control under Model Uncertainty**

  C1. B.-J. Jeon, M.-G. Seo, H.-S. Shin, and A. Tsourdos, "Understandings of the Incremental Backstepping Control through Theoretical analysis under the Model Uncertainties," in 2018 IEEE Conference on Control Technology and Applications (CCTA). IEEE, 2018, pp. 318-323. (Published)

  J1. B.-J. Jeon, M.-G. Seo, H.-S. Shin, and A. Tsourdos, "Understandings of Classical and Incremental Backstepping Controllers with Model Uncertainties," IEEE Transactions on Aerospace and Electronic Systems, 2019. (Online published)

  Chapter 2 suggests theoretical closed-loop analysis results with BKS and IBKS under model uncertainties. Note that both BKS and IBKS are designed to achieve asymptotic stability of the system for the nominal case. For the case with and without model uncertainties, closed-loop analyses with BKS and IBKS are conducted under a piecewise approach, whose results are systematically assessed as follows. First, transfer functions with BKS and IBKS

under the model uncertainties are compared with the ones for the nominal case. This shows important changes on the transfer functions due to consider model uncertainties, resulting in conditions to maintain stability and performance metrics under the model uncertainties. Second, distinctions between the transfer functions with two algorithms are investigated to clarified how the effect of the model uncertainties to the closed-loop system becomes different depending on the applied control algorithm. The key finding can be summarized as follows; unlike the system with BKS, the closed-loop system with IBKS is not affected by the uncertainties on any model information including control effectiveness which is still required for IBKS implementation, if the control input is calculated, transmitted, and reflected fast enough to the actual control surface. To have more insight from simplified situations, case studies are conducted for BKS and IBKS under the assumption that the uncertainty exists only in one aerodynamic derivative estimate while the other estimates have true values. This facilitates systematic interpretations on the impacts of the uncertainty on the specific aerodynamic derivative estimate to the closed-loop system, which is represented as weight factors derived for each case. Simulation is performed to verify properties obtained from the analysis.

- **Chapter 3. Incremental Backstepping Control under Measurement Bias and Model Uncertainty**

  C2. B.-J. Jeon, M.-G. Seo, H.-S. Shin, and A. Tsourdos, "Closed-loop Analysis with Incremental Backstepping Controller considering Measurement Bias," in the 21st IFAC Symposium on Automatic Control in Aerospace, vol. 52, no. 12, pp. 405-410, 2019. (Published, One of six finalist papers for the young author award)

  In Chapter 3, closed loop characteristics with IBKS obtained from theoretical analysis when both measurement bias and model uncertainty exist, are examined. Comparing to BKS, measurements about state derivatives and control surface deflection angles are additionally required to implement IBKS, so biases on them are mainly considered in this analysis. Considering measurement biases and model uncertainty, a transfer function with IBKS is derived under a piecewise approach and following properties are suggested from the analysis. First, the measurement biases cause a steady state error, but they do not have any impact to the characteristic equation. Second, a model uncertainty in control effectiveness information has an impact to this steady state error, which is the key difference between properties provided in Chapter 2 and 3. Note

that in Chapter 2 where the closed-loop characteristics with IBKS considering only model uncertainties are investigated, it is shown that system stability and performance are not affected by any model uncertainty even in control effectiveness information if a control command is calculated, transmitted and reflected fast enough to a real control surface deflection. Properties obtained from the theoretical analysis are verified through simulations.

- **Chapter 4. Incremental Backstepping Control under Measurement Delay and Model Uncertainty**

  J2. B.-J. Jeon, M.-G. Seo, H.-S. Shin, and A. Tsourdos, "Understandings of Incremental Backstepping Controller considering Measurement Delay with Model Uncertainty," Aerospace Science and Technology, 2020. (In revision to submit)

  Chapter 4 suggests closed loop characteristics with IBKS under measurement delay along with model uncertainty, obtained from a proposed analysis framework. Delays on state derivative and control surface deflection angle measurements which are additionally utilized in IBKS comparing to BKS are mainly considered in this closed loop analysis. To judge absolute stability for the system with IBKS under measurement delays and model uncertainty, new numerical framework with an optimization concept is proposed. Note that a transfer function can be derived under a piecewise approach but it is difficult to find analytic solutions of the characteristic equation because of the exponential terms generated from considered delays. The proposed numerical framework utilizes an optimization concept to search unstable poles in efficient and systematic manner even for a metric function with high nonlinearity due to the considered measurement delays. By applying the suggested numerical framework, critical system characteristics with IBKS under measurement delays and model uncertainty are obtained in absolute stability point of view as follows. First, a stability condition is found as a relationship between delays on state derivative and control surface deflection angle measurements. Second, this stability condition is shown to be affected by the model uncertainty in control effectiveness information, which is the main difference with the analysis results in Chapter 2 and 3. Verification and validation of the obtained properties about the absolute stability are performed through simulations. From simulation results, robustness and performance under the measurement delays together with the model uncertainty are additionally investigated for better understandings. Comparative study provides valuable insights about

individual and integrated effects of the measurement delays and the model uncertainty to the closed loop system with IBKS.

- **Chapter 5. Composite Adaptive Backstepping Control**

  C3. B.-J. Jeon, H.-S. Shin, and A. Tsourdos, "Composite Adaptive Backstepping Control considering Computational Complexity and Relaxation of Persistent Excitation," in the 21st IFAC World Congress, 2020. (Accepted)

  In Chapter 5, adaptive control is examined as another sensor dependent approach for reduced model dependency of BKS. Note that composite adaptive control is considered for improved estimation and tracking performance with enhanced system robustness. The adaptation law for C-ABKS is designed to estimate model parameters in each loop separately by taking an advantage from a cascade control structure of BKS. Comparing to the adaptation laws in previous studies which estimate whole model parameters of the dynamic system at once, the designed adaptation law deals with smaller estimation problems, resulting in reduced computational complexity. Relaxation of PE requirement for parameter convergence has not been discussed for C-ABKS, which is one of main technical issues to be tackled in adaptive control. In Chapter 5, PE requirement is relaxed to FE condition by utilizing the information matrix design method in previous studies. Note that new paradigm in the information matrix design for parameter convergence without PE will be proposed in Chapter 6.

- **Chapter 6. Composite Adaptive Backstepping Control with New Information Matrix**

  J3. B.-J. Jeon, H.-S. Shin, and A. Tsourdos, "Composite Adaptive Control with New Information matrix for Parameter Convergence without Persistent Excitation," Automatica, 2020. (Submitted)

  Chapter 6 proposes a composite adaptive control algorithm with new information matrix, which aims to achieve parameter convergence without PE. If parameter estimates do not converge to their true values, parameter drift can occur especially under the existence of non-parametric uncertainties such as noise and unmodeled dynamics, resulting in instability phenomena with sudden bursting. Hence, the convergence of the parameter estimation should be guaranteed, but PE requirement is unrealistic for practical applications since this leads to continuous oscillations of state and control input signals. In Chapter 6, a new paradigm for the information matrix design is proposed

to accomplish full rank under FE for parameter convergence by developing a modulation-based approach. This novel approach has substantially different design principle from the accumulation based approaches in previous studies; the proposed design framework is based on linear independency between the signals via multiple filters with different modulation effects. Multiple filtered regressor vectors are modified to be orthogonal with each other while maintaining their magnitudes, and the information matrix is constructed with these modified filtered regressor vectors. The new information matrix is shown to be positive definite for all the time from the beginning and it is proven to be bounded. The new information matrix has moderate level of eigenvalues, which is beneficial for adaptation speed and system robustness. The closed-loop system with the proposed composite adaptive control utilizing the new information matrix is shown to be globally exponentially stable based on Lyapunov stability theory. Numerical simulations are conducted for verification of the theoretical findings and demonstration of advantages over the existing information matrix design approaches.

- **Chapter 7. Logarithmic Regression based Composite Adaptive Backstepping Control**

  J4. B.-J. Jeon, H.-S. Shin, and A. Tsourdos, "Composite Adaptive Control with Logarithmic Regression for Fast Adaptation," IEEE Transactions on Automatic Control, 2020. (In revision to submit)

  In Chapter 7, new logarithmic regression-based composite adaptive control is proposed to accomplish fast parameter convergence without excessive increase of the adaptation gain. In order to achieve this aim, Chapter 7 suggests a new paradigm for composite adaptation law design with regression pattern shaping. Comparing to linear regression-based approach in previous studies, logarithmic function with concave and monotonically increasing characteristics is introduced for the regression term of the proposed approach to enhance parameter convergence speed by relaxing the adaptation speed degeneration at the later stage. With the proposed logarithmic regression-based composite adaptation law, the asymptotic stability of the closed-loop system is guaranteed and this is proven under the Lyapunov theory. The condition on the design parameters of the logarithmic regression-based composite adaptation law to make it always faster than the linear regression-based composite adaptation law for the same adaptation gain is provided within the system boundary. When this condition is satisfied, the adaptation gain of the linear regression-

based approach is required to be increased to make this approach always faster than the new logarithmic regression-based approach, which can result in lack of system robustness. Numerical simulations are performed for demonstration of advantages over the existing linear regression-based composite adaptation law and verification of the theoretical findings. Note that new information matrix in Chapter 6 is utilized to the logarithmic regression based composite adaptation law in Chapter 7, resulting in the final new C-ABKS which achieves both parameter convergence under FE and fast adaptation without excessive increase of the adaptation gain.

1.4 List of Publications

List of journal and conference papers submitted or published is addressed below, which are related to this PhD research.

Journal Papers

J1. B.-J. Jeon, M.-G. Seo, H.-S. Shin, and A. Tsourdos, "Understandings of Classical and Incremental Backstepping Controllers with Model Uncertainties," IEEE Transactions on Aerospace and Electronic Systems, 2019. (Online published)

J2. B.-J. Jeon, M.-G. Seo, H.-S. Shin, and A. Tsourdos, "Understandings of Incremental Backstepping Controller considering Measurement Delay with Model Uncertainty," Aerospace Science and Technology, 2020. (In revision to submit)

J3. B.-J. Jeon, H.-S. Shin, and A. Tsourdos, "Composite Adaptive Control with New Information matrix for Parameter Convergence without Persistent Excitation," Automatica, 2020. (Submitted)

J4. B.-J. Jeon, H.-S. Shin, and A. Tsourdos, "Composite Adaptive Control with Logarithmic Regression for Fast Adaptation," IEEE Transactions on Automatic Control, 2020. (In revision to submit)

Conference Papers

C1. B.-J. Jeon, M.-G. Seo, H.-S. Shin, and A. Tsourdos, "Understandings of the Incremental Backstepping Control through Theoretical analysis under the Model Uncertainties," in 2018 IEEE Conference on Control Technology and Applications (CCTA). IEEE, 2018, pp. 318-323. (Published)

C2. B.-J. Jeon, M.-G. Seo, H.-S. Shin, and A. Tsourdos, "Closed-loop Analysis with Incremental Backstepping Controller considering Measurement Bias," in the 21st IFAC Symposium on Automatic Control in Aerospace, vol. 52, no. 12, pp. 405-410, 2019. (Published, One of six finalist papers for the young author award)

C3. B.-J. Jeon, H.-S. Shin, and A. Tsourdos, "Composite Adaptive Backstepping Control considering Computational Complexity and Relaxation of Persistent Excitation," in the 21st IFAC World Congress, 2020. (Accepted)

References

[1] Taeyoung Lee and Youdan Kim. Nonlinear adaptive flight control using backstepping and neural networks controller. *Journal of Guidance, Control, and Dynamics*, 24(4):675–682, 2001.

[2] Jay Farrell, Manu Sharma, and Marios Polycarpou. Backstepping-based flight control with adaptive function approximation. *Journal of Guidance, Control, and Dynamics*, 28(6):1089–1102, 2005.

[3] Hann-Shing Ju and Ching-Chih Tsai. Longitudinal axis flight control law design by adaptive backstepping. *IEEE Transactions on Aerospace and Electronic Systems*, 43(1):311–329, 2007.

[4] Liang Sun and Wei Huo. 6-dof integrated adaptive backstepping control for spacecraft proximity operations. *IEEE Transactions on Aerospace and Electronic Systems*, 51(3):2433–2443, 2015.

[5] LR García Carrillo, Alejandro Dzul, and Rogelio Lozano. Hovering quad-rotor control: A comparison of nonlinear controllers using visual feedback. *IEEE Transactions on Aerospace and Electronic Systems*, 48(4):3159–3170, 2012.

[6] Xu Huang and Ye Yan. Saturated backstepping control of underactuated spacecraft hovering for formation flights. *IEEE Transactions on Aerospace and Electronic Systems*, 53(4):1988–2000, 2017.

[7] Lars Sonneveldt, QP Chu, and JA Mulder. Nonlinear flight control design using constrained adaptive backstepping. *Journal of Guidance, Control, and Dynamics*, 30(2):322–336, 2007.

[8] Baohua Lian and Hyochoong Bang. Momentum transfer-based attitude control of spacecraft with backstepping. *IEEE transactions on aerospace and electronic systems*, 42(2):453–463, 2006.

[9] Yoonsoo Kim and Byoung Soo Kim. Pitch autopilot design for agile missiles with uncertain aerodynamic coefficients. *IEEE Transactions on Aerospace and Electronic Systems*, 49(2):907–914, 2013.

[10] Jawhar Ghommam and Maarouf Saad. Autonomous landing of a quadrotor on a moving platform. *IEEE Transactions on Aerospace and Electronic Systems*, 53(3):1504–1519, 2017.

[11] Stephen H Lane and Robert F Stengel. Flight control design using non-linear inverse dynamics. *Automatica*, 24(4):471–483, 1988.

[12] Chang-Hun Lee, Byung-Eul Jun, and Jin-Ik Lee. Connections between linear and nonlinear missile autopilots via three-loop topology. *Journal of Guidance, Control, and Dynamics*, pages 1426–1432, 2016.

[13] Yunjun Xu. Multi-timescale nonlinear robust control for a miniature helicopter. *IEEE Transactions on Aerospace and Electronic systems*, 46(2):656–671, 2010.

[14] Romulus Lungu, Mihai Lungu, and Lucian Teodor Grigorie. Automatic control of aircraft in longitudinal plane during landing. *IEEE Transactions on Aerospace and Electronic Systems*, 49(2):1338–1350, 2013.

[15] Yuankai Li, Zhongliang Jing, and Guangjun Liu. Maneuver-aided active satellite tracking using six-dof optimal dynamic inversion control. *IEEE Transactions on Aerospace and Electronic Systems*, 50(1):704–719, 2014.

[16] Petar V Kokotovic. The joy of feedback: nonlinear and adaptive. *IEEE Control Systems Magazine*, 12(3):7–17, 1992.

[17] Pieter van Gils, Erik-Jan Van Kampen, Coen C de Visser, and Q Ping Chu. Adaptive incremental backstepping flight control for a high-performance aircraft with uncertainties. In *AIAA Guidance, Navigation, and Control Conference*, 2016.

[18] Abdelouahed Ait Haddou Ali, Q Ping Chu, Erik-Jan Van Kampen, and Coen C de Visser. Exploring adaptive incremental backstepping using immersion and invariance for an f-16 aircraft. In *AIAA Guidance, Navigation, and Control Conference*, 2014.

[19] Paul Acquatella, E van Kampen, and Qi Ping Chu. Incremental backstepping for robust nonlinear flight control. In *Proceedings of the EuroGNC 2013, 2nd CEAS Specialist Conference on Guidance, Navigation and Control*, pages 1444–1463, 2013.

[20] Guillermo P Falconí, Valentin A Marvakov, and Florian Holzapfel. Fault tolerant control for a hexarotor system using incremental backstepping. In *2016 IEEE Conference on Control Applications (CCA)*, pages 237–242. IEEE, 2016.

[21] Jean-Jacques E Slotine and Weiping Li. On the adaptive control of robot manipulators. *The international journal of robotics research*, 6(3):49–59, 1987.

[22] Jean-Jacques E Slotine and Weiping Li. Composite adaptive control of robot manipulators. *Automatica*, 25(4):509–519, 1989.

[23] Hanlei Wang. Adaptive control of robot manipulators with uncertain kinematics and dynamics. *IEEE Transactions on Automatic Control*, 62(2):948–954, 2016.

[24] Nazli E Kahveci and Petros A Ioannou. Adaptive steering control for uncertain ship dynamics and stability analysis. *Automatica*, 49(3):685–697, 2013.

[25] J Van Amerongen. Model reference adaptive control applied to steering of ships. In *Methods and applications in adaptive control*, pages 199–208. Springer, 1980.

[26] HJ Tol, CC De Visser, LG Sun, E van Kampen, and QP Chu. Multivariate spline-based adaptive control of high-performance aircraft with aerodynamic uncertainties. *Journal of Guidance, Control, and Dynamics*, 39(4):781–800, 2016.

[27] Ye Zhou, Erik-Jan van Kampen, and QiPing Chu. Nonlinear adaptive flight control using incremental approximate dynamic programming and output feedback. *Journal of Guidance, Control, and Dynamics*, 40(2):493–496, 2016.

[28] Nhan Nguyen, Kalmanje Krishnakumar, John Kaneshige, and Pascal Nespeca. Flight dynamics and hybrid adaptive control of damaged aircraft. *Journal of guidance, control, and dynamics*, 31(3):751–764, 2008.

[29] DE Seborg, Thomas F Edgar, and SL Shah. Adaptive control strategies for process control: a survey. *AIChE Journal*, 32(6):881–913, 1986.

[30] A Galip Ulsoy and Yoram Koren. Applications of adaptive control to machine tool process control. *IEEE Control Systems Magazine*, 9(4):33–37, 1989.

[31] Chengshuai Wu, Jian Chen, Chenfeng Xu, and Zhiyang Liu. Real-time adaptive control of a fuel cell/battery hybrid power system with guaranteed stability. *IEEE Transactions on Control Systems Technology*, 25(4):1394–1405, 2016.

[32] Dezhi Xu, Jianxing Liu, Xing-Gang Yan, and Wenxu Yan. A novel adaptive neural network constrained control for a multi-area interconnected power system with hybrid energy storage. *IEEE Transactions on Industrial Electronics*, 65(8):6625–6634, 2017.

[33] Manuel A Duarte and Kumpati S Narendra. Combined direct and indirect approach to adaptive control. *IEEE Transactions on Automatic Control*, 34(10):1071–1075, 1989.

[34] Manuel A Duarte and Kumpati S Narendra. A new approach to model reference adaptive control. *International Journal of Adaptive Control and Signal Processing*, 3(1):53–73, 1989.

[35] Kumpati S Narendra and Manuel A Duarte. Application of robust adaptive control using combined direct and indirect methods. *International Journal of Adaptive Control and Signal Processing*, 3(2):131–142, 1989.

[36] Eugene Lavretsky. Combined/composite model reference adaptive control. *IEEE Transactions on Automatic Control*, 54(11):2692–2697, 2009.

[37] M Kemal Ciliz. Combined direct and indirect adaptive control for a class of nonlinear systems. *IET Control Theory & Applications*, 3(1):151–159, 2009.

[38] Parag M Patre, William MacKunis, Marcus Johnson, and Warren E Dixon. Composite adaptive control for euler–lagrange systems with additive disturbances. *Automatica*, 46(1):140–147, 2010.

[39] MK Ciliz. Adaptive backstepping control using combined direct and indirect adaptation. *Circuits, Systems & Signal Processing*, 26(6):911–939, 2007.

[40] Parag M Patre, Shubhendu Bhasin, Zachary D Wilcox, and Warren E Dixon. Composite adaptation for neural network-based controllers. *IEEE Transactions on Automatic Control*, 55(4):944–950, 2010.

[41] Yongping Pan, Yiqi Liu, and Haoyong Yu. Online data-driven composite adaptive backstepping control with exact differentiators. *International Journal of Adaptive Control and Signal Processing*, 30(5):779–789, 2016.

[42] Yongping Pan and Haoyong Yu. Composite learning from adaptive dynamic surface control. *IEEE Transactions on Automatic Control*, 61(9):2603–2609, 2015.

[43] Girish Chowdhary, Tansel Yucelen, Maximillian Mühlegg, and Eric N Johnson. Concurrent learning adaptive control of linear systems with exponentially convergent bounds. *International Journal of Adaptive Control and Signal Processing*, 27(4):280–301, 2013.

[44] Girish Chowdhary, Maximilian Mühlegg, and Eric Johnson. Exponential parameter and tracking error convergence guarantees for adaptive controllers without persistency of excitation. *International Journal of Control*, 87(8):1583–1603, 2014.

[45] Namhoon Cho, Hyo-Sang Shin, Youdan Kim, and Antonios Tsourdos. Composite model reference adaptive control with parameter convergence under finite excitation. *IEEE Transactions on Automatic Control*, 63(3):811–818, 2017.

[46] Hassan K Khalil. *Nonlinear systems*. Upper Saddle River, 1996.

[47] Jean-Jacques E Slotine, Weiping Li, et al. *Applied nonlinear control*. Prentice hall Englewood Cliffs, NJ, 1991.

[48] I. Kanellakopoulos M. Krstic and P. Kokotovic. *Nonlinear and Adaptive Control*. John Wiley and Sons, Inc., New York, 1995.

[49] B. Kim et al. *Flight Dynamics and Control*. Kyung Moon Sa, 2004.

[50] Farid Golnaraghi and Benjamin C Kuo. *Automatic Control Systems*. John Wiley and Sons Ltd, 2009.

[51] Donald McLean. *Automatic flight control systems*. Prentice Hall, New York, 1990.

[52] Gang Tao. *Adaptive control design and analysis*, volume 37. John Wiley & Sons, 2003.

Chapter 2

Incremental Backstepping Control under Model Uncertainty

2.1 Introduction

Backstepping algorithm [1] is one of the most widely and successfully applied nonlinear flight control methods [2–11]. The backstepping(BKS) controller design starts from dynamics farthest from a control input and then steps back through integrators by considering augmented Lyapunov functions, to obtain the controller which fulfils desired motions with known stability and convergence properties. Since BKS requires explicit model information to implement the algorithm, it can be regarded as a model based approach. The issue is that a model based control strategy is normally sensitive to model uncertainties, but it could be hard to obtain accurate model information.

Incremental backstepping(IBKS) method [12–15] is suggested to reduce model dependency of BKS. This incremental controller utilizes additional measurements such as state derivatives and control surface deflection angles, replacing a part of required model information. This algorithm becomes implicit, not totally residing in explicit model to be cancelled. Because IBKS still requires knowledge about control effectiveness for its implementation, it lies in between model based and sensor based approach.

Not only for BKS but also for IBKS, it is essential to identify and understand the effects of the model uncertainties on each closed-loop system. There have been some

studies [12–15] that investigated their closed-loop characteristics under the model uncertainties, but only by numerical simulations or experiments. Since results obtained from simulations or experiments are valid for particular plants under specific conditions, theoretical analysis is necessary for general interpretations on the effects of the model uncertainties to the closed-loop systems with BKS and IBKS. To the best of our knowledge, it is difficult to find existing studies that successfully provide theoretical analysis on BKS and IBKS considering the model uncertainties. Hence, Chapter 2 aims to suggest the closed-loop analysis results on BKS and IBKS, especially in consideration of the model uncertainties.

Unlike BKS and IBKS, there have been several researches [16–20] in which closed-loop analysis under the model uncertainties was carried out for nonlinear dynamic inversion(NDI) and incremental nonlinear dynamic inversion(INDI). Note that NDI[21] is another representative nonlinear control approach, most widely developed and applied[22–25]. NDI explicitly cancels out undesired nonlinearities in system using inverse dynamics, and INDI is its incremental version, similar to IBKS. BKS and NDI have some similarities, since both nonlinear controllers ultimately try to make error dynamics of a closed-loop system to achieve desired behaviors by cancelling undesired nonlinearities in dynamics. Therefore, it would be worth to examine previous analyses on NDI / INDI and investigate possibility to extend them to the analysis of BKS / IBKS.

In [16], each of NDI and INDI was applied to an inner-loop of 6-DoF nonlinear dynamics for an unmanned aerial vehicle. Under model uncertainties, a transfer function with INDI was suggested, but closed-loop analysis with NDI was difficult to proceed further due to remaining nonlinearities. For the closed-loop analysis with INDI, incremental dynamics utilized in control law derivation process was applied instead of true system dynamics. This makes difficult to comprehend the effects of the control surface deflection measurement to the system. Besides, it is hard to find comparative study between INDI and NDI in closed-loop characteristics under the model uncertainties. [18] performed analysis with NDI and INDI under a general type of nonlinear dynamics based on Lyapunov stability theory. Consequently, proof of bounded stability for the closed-loop systems and conditions to achieve it were provided. This Lyapunov-based analysis was mathematically rigorous, but it had limitations to get physical understandings for applications on real systems. Additionally, analysis considering the model uncertainties was conducted, addressing rough understandings about their effects. It is difficult to investigate detailed effects of the model uncertainties on stability and performance.

The review on analysis of NDI and INDI suggests that they could shed some lights on potential direction of our analysis. However, they cannot be direct references for our research with BKS and IBKS, due to the following difference between BKS and NDI. NDI disregards interconnections between the loops under the time-scale separation assumption. On the contrary, BKS intermediately adopts the time-scale separation assumption, but it considers the transient responses in the end. This difference can make the analysis with BKS and IBKS more challenging than the one with NDI and INDI.

To this end, Chapter 2 suggests theoretical closed-loop analysis with BKS and IBKS under the model uncertainties. This analysis enables critical understandings on system characteristics related to the model uncertainties. Note that short period mode dynamics for an aircraft is utilized for simplicity of the analysis. BKS and IBKS are designed to achieve asymptotic stability of the system for the nominal case. Considering the model uncertainties, closed-loop analysis is conducted with a piece-wise approach. Transfer functions with BKS and IBKS under the model uncertainties, are compared with the ones for the nominal case. This shows important changes on the transfer functions due to the model uncertainties, resulting in conditions to maintain stability and performance metrics under the model uncertainties. By investigating distinctions between the transfer functions with two algorithms, it is clarified how the effect of the model uncertainties to the closed-loop system becomes different depending on the applied control algorithm. This comparative study also enriches understandings about the effect of additional measurements in IBKS. To have more insights from simplified situations, case studies are conducted under the assumption that the uncertainty exists only in one aerodynamic derivative estimate while the other estimates have true values. This facilitates systematic interpretations on the impacts of the uncertainty on the specific aerodynamic derivative estimate to the closed-loop system. Simulation is performed to verify properties obtained from the analysis.

2.2 Preliminaries : Dynamics

From Newton's law of motion about conservation of linear and angular momentum, 6-DoF nonlinear coupled dynamics for an aircraft can be derived. Taylor series expansion provides the first order approximation in the neighborhood of trim points. Then, longitudinal and lateral motions can be decoupled under several flight conditions like a level flight. Short period mode is one of the longitudinal oscillation

modes with high natural frequency. This mode is of paramount importance in flight control, because one of the main purposes of a stability augmentation system for an aircraft is to improve short period mode characteristics. Since the oscillation lasts for relatively short time, velocity change is assumed to be negligible. This results in the dynamics (2.1) below [26], and in Chapter 2, it is applied for control law derivation and closed-loop analysis.

$$
\begin{aligned}
&\dot{\alpha} = Z_{\alpha}^{*}(M,\alpha)\,\alpha + q + Z_{\delta}^{*}(M,\alpha)\,\delta \\
&\dot{q} = M_{\alpha}^{*}(M,\alpha)\,\alpha + M_{q}^{*}(M,\alpha)\,q + M_{\delta}^{*}(M,\alpha)\,\delta \\
&\text{where} \\
&Z_{\alpha}^{*}(M,\alpha) = \frac{\bar{q}S}{m} C_{Z_{\alpha}}(M,\alpha)\,\frac{1}{U_0} \\
&Z_{\delta}^{*}(M,\alpha) = \frac{\bar{q}S}{m} C_{Z_{\delta}}(M,\alpha)\,\frac{1}{U_0} \\
&M_{\alpha}^{*}(M,\alpha) = \frac{\bar{q}S\bar{c}}{I_y} C_{M_{\alpha}}(M,\alpha) \\
&\qquad\qquad + \frac{\bar{q}S\bar{c}^{2}}{2I_yU_0} C_{M_{\dot{\alpha}}}(M,\alpha)\,\frac{\bar{q}S}{m} C_{Z_{\alpha}}(M,\alpha)\,\frac{1}{U_0} \\
&M_{q}^{*}(M,\alpha) = \frac{\bar{q}S\bar{c}^{2}}{2I_yU_0} C_{M_{q}}(M,\alpha) + \frac{\bar{q}S\bar{c}^{2}}{2I_yU_0} C_{M_{\dot{\alpha}}}(M,\alpha) \\
&M_{\delta}^{*}(M,\alpha) = \frac{\bar{q}S\bar{c}}{I_y} C_{M_{\delta}}(M,\alpha) \\
&\qquad\qquad + \frac{\bar{q}S\bar{c}^{2}}{2I_yU_0{}^{2}} C_{M_{\dot{\alpha}}}(M,\alpha)\,\frac{\bar{q}S}{m} C_{Z_{\delta}}(M,\alpha)
\end{aligned}
\tag{2.1}
$$

State variables α and q represent an angle of attack and a pitch rate. Control input δ corresponds to a deflection of an elevator. $\bar{q}$ indicates a dynamic pressure, U_0 means a constant velocity of an aircraft, and M stands for Mach number. For notational convenience, aerodynamic derivatives will be expressed in shorthand form as Z_{α}^{*}, Z_{δ}^{*}, M_{α}^{*}, M_{q}^{*} and M_{δ}^{*}, but they are still functions of M and α. $C_{(\cdot)}$ denotes dimensionless aerodynamic coefficients. S, $\bar{c}$, m and I_y are reference area, reference length, mass and moment of inertia in y-axis of an aircraft.

Dynamics (2.1) represents a linear parameter-varying(LPV) system, i.e., a nonlinear system which can be described as a parameterized linear system whose parameters change with the states. This simplified version of dynamics, not full 6-DoF dynamics, is utilized for simplicity of the analysis, because complex dynamics can make analysis with model uncertainties more complicated. Since the main objective in this study is to have critical understandings about the closed-loop characteristics with BKS and IBKS under the model uncertainties, dynamics (2.1) is reasonable for this purpose.

As a future work, this research can be extended to the analysis with full 6-DoF dynamics.

2.3 Derivation of Control Laws

Before derivation of BKS and IBKS, following modification and assumption widely accepted in controller design phase, are applied to dynamics (2.1).

First, aerodynamic derivatives estimates $\hat{(\cdot)}$ are utilized instead of real Z^*_α, Z^*_δ, M^*_α, M^*_q and M^*_δ, as only estimated values are available in controller design phase. Those derivatives are calculated from the dimensionless aerodynamic coefficients $C_{(\cdot)}$ identified from wind tunnel test or aeroprediction, and the aircraft parameters S, $\bar{c}$, m and I_y measured before flight. Hence, the aerodynamic derivatives estimates $\hat{(\cdot)}$ are most likely to contain uncertainties which make them different with their true values. Nevertheless, in Section 2.3, both controllers are designed to accomplish asymptotic stability assuming that the estimates are the same as their true values. The effects of the model uncertainties, which can make aimed performance and stability characteristics in this design phase difficult to be achieved, will be investigated in the closed-loop analysis part IV.

Second, $\hat{Z}^*_\delta\delta$ related to non-minimum phase is neglected, to make the system in lower-triangular form. Both control laws are based on the backstepping method, which requires that the dynamics should be in strict feedback form. Therefore, it is assumed that a fin surface is a pure moment generator. This is a valid assumption for most of aircrafts, often made in flight control systems design, because C_{Z_δ} is usually small enough [26].

Under these modification and assumption, the dynamics (2.2) below is utilized for the control law derivations.

$$\begin{aligned} \dot{\alpha} &= \hat{Z}^*_\alpha\alpha + q \\ \dot{q} &= \hat{M}^*_\alpha\alpha + \hat{M}^*_q q + \hat{M}^*_\delta\delta \end{aligned} \tag{2.2}$$

State errors are defined as follows.

$$\begin{aligned} z_1 &= \alpha - \alpha_c \\ z_2 &= q - q_c \end{aligned} \tag{2.3}$$

where subscript c represents a command.

2.3.1 Backstepping Control

If Lyapunov function candidate becomes positive definite and its derivative becomes negative definite, asymptotic stability can be guaranteed for the system. To derive BKS control command which satisfies asymptotic stability, 2 cascaded steps are performed as follows.

First, Lyapunov function candidate V_1 considering only z_1 is selected as

$$V_1 = \frac{1}{2} z_1^2 \tag{2.4}$$

which is positive definite. It's for the outer-loop related to the force equation, and the time-scale separation assumption is intermediately adopted here. In this step, it is assumed that the fast state has already achieved its desired value, without any considerations about its transient response (i.e. z_2 is zero).

Derivative of Lyapunov function candidate V_1 becomes

$$\begin{aligned} \dot{V}_1 &= z_1 \dot{z}_1 \\ &= z_1 \left(\hat{Z}_\alpha^* \alpha + q - \dot{\alpha}_c \right) \end{aligned} \tag{2.5}$$

In order to satisfy Lyapunov stability condition, a pseudo-command q_c is derived as

$$q_c = -C_1 z_1 - \hat{Z}_\alpha^* \alpha + \dot{\alpha}_c \tag{2.6}$$

which makes negative definite $\dot{V}_1 = -C_1 z_1^2$ where C_1 is a positive design parameter. The state of the fast dynamics is regarded as a control input for the state of the slow dynamics.

Second, Lyapunov function candidate V_2 considering both z_1 and z_2 is selected as

$$V_2 = \frac{1}{2} z_1^2 + \frac{1}{2} z_2^2 \tag{2.7}$$

which is positive definite. V_2 can be interpreted as an augmented V_1 with the additional term to penalize z_2, considering the transient response of the fast state. Another explanation about V_2 is also possible. For the inner-loop related to the moment equation, it's hard to assume that the slow state has already achieved its desired value (i.e. z_1 can't be assumed to be zero here). Hence, not only z_2, but also z_1 is considered in the inner-loop controller design. Regardless how this step is explained, the time-scale separation assumption is significantly relaxed, as a result.

Derivative of V_2 can be calculated as below.

$$\begin{aligned}\dot{V}_2 &= z_1\dot{z}_1 + z_2\dot{z}_2 \\ &= z_1\left(\hat{Z}_\alpha^*\alpha + q - \dot{\alpha}_c\right) + z_2\left(\hat{M}_\alpha^*\alpha + \hat{M}_q^* q + \hat{M}_\delta^*\delta - \dot{q}_c\right)\end{aligned} \tag{2.8}$$

By using the pseudo-command (2.6), $\dot{V}_2$ becomes

$$\dot{V}_2 = z_1\left(-C_1 z_1 + z_2\right) + z_2\left(\hat{M}_\alpha^*\alpha + \hat{M}_q^* q + \hat{M}_\delta^*\delta - \dot{q}_c\right) \tag{2.9}$$

To satisfy Lyapunov stability condition, the control command δ is derived as

$$\delta = \frac{1}{\hat{M}_\delta^*}\left(-C_2 z_2 - z_1 - \hat{M}_\alpha^*\alpha - \hat{M}_q^* q + \dot{q}_c\right) \tag{2.10}$$

which makes negative definite $\dot{V}_2 = -C_1 z_1^2 - C_2 z_2^2$ where C_1 and C_2 are positive design parameters.

The final form of BKS controller derived in Section 2.3.1 can be suggested as follows.

$$\begin{aligned}q_c &= -C_1 z_1 - \hat{Z}_\alpha^*\alpha + \dot{\alpha}_c \\ \delta &= \frac{1}{\hat{M}_\delta^*}\left(-C_2 z_2 - z_1 - \hat{M}_\alpha^*\alpha - \hat{M}_q^* q + \dot{q}_c\right)\end{aligned} \tag{2.11}$$

The pseudo-command q_c to make the angle of attack α achieve its desired value α_c, is derived. q goes to q_c by the derived control input δ. The model information about $\hat{Z}_\alpha^*, \hat{M}_\delta^*, \hat{M}_\alpha^*$ and $\hat{M}_q^*$ is required to implement the control algorithm.

2.3.2 Incremental Backstepping Control

For the outer-loop controller design, BKS, not IBKS, is utilized in Section 2.3.2. If IBKS is applied here, it additionally requires measurements about current state derivative and control in the outer-loop (i.e. $\dot{\alpha}_0$ and q_0). Instead of using those

measurements hard to be obtained, more practical ways exist to compensate the model information $\hat{Z}_\alpha^*$. For example, more general measurements like a normal force and a velocity can directly substitute for $\hat{Z}_\alpha^*\alpha$. For this reason, the incremental law is not normally used for the outer-loop, and it can be seen in other papers [12] [14] [17] which just applied BKS or PID for it. In Chapter 2, BKS is utilized for the outer-loop, to make the comparison easier with a pure BKS proposed in Section 2.3.1. Therefore, the first step is identically applied, so the pseudo-command becomes the same with (2.6).

For the inner-loop controller design, q dynamics in (2.2) is modified assuming that the states α, q and the control input δ can be expressed as combinations of reference points $(\cdot)_0$ and disturbances $\Delta(\cdot)$ around them. This assumption is reasonable especially with a sufficiently high sampling rate.

$$\begin{aligned}\dot{q} &= \hat{M}_\alpha^* (\alpha_0 + \Delta\alpha) + \hat{M}_q^* (q_0 + \Delta q) + \hat{M}_\delta^* (\delta_0 + \Delta\delta) \\ &= \dot{q}_0 + \hat{M}_\alpha^* \Delta\alpha + \hat{M}_q^* \Delta q + \hat{M}_\delta^* \Delta\delta\end{aligned} \tag{2.12}$$

As in [12], [16], [19] and [20], the increments in states, $\Delta\alpha$ and Δq, can be ignored, since they have much smaller effects than the increment in input, $\Delta\delta$. This becomes acceptable as the control surface deflection directly and instantly affects the pitch moment, whereas the effect of $\Delta\alpha$ and Δq on the pitch moment is not direct. Note that α and q first create lift force and this force then induces the pitch moment. This implies that the effect of α and q on the pitch moment is slower than that of δ. Hence, comparing to the increment on control input, the effect of increments on state variables becomes negligible, especially when a sampling time is small enough. Then, q dynamics for the inner-loop controller design with IBKS becomes

$$\dot{q} \simeq \dot{q}_0 + \hat{M}_\delta^* \Delta\delta \tag{2.13}$$

In the second step, Lyapunov function candidate V_2 considering both z_1 and z_2 is selected as

$$V_2 = \frac{1}{2} z_1^2 + \frac{1}{2} z_2^2 \tag{2.14}$$

which is positive definite. It can be interpreted in the same way with Section 2.3.1.

Derivative of V_2 can be calculated as below.

$$\begin{aligned}\dot{V}_2 &= z_1\dot{z}_1 + z_2\dot{z}_2 \\ &= z_1\left(\hat{Z}_\alpha^*\alpha + q - \dot{\alpha}_c\right) + z_2\left(\dot{q}_0 + \hat{M}_\delta^*\Delta\delta - \dot{q}_c\right)\end{aligned} \tag{2.15}$$

The only difference with (2.8) is that the dynamics (2.13) which is expressed into an incremental form is applied. By using the pseudo-command which is the same as (2.6), $\dot{V}_2$ becomes

$$\dot{V}_2 = z_1\left(-C_1 z_1 + z_2\right) + z_2\left(\dot{q}_0 + \hat{M}_\delta^*\Delta\delta - \dot{q}_c\right) \tag{2.16}$$

To satisfy Lyapunov stability condition, the control command $\Delta\delta$ is derived as

$$\Delta\delta = \frac{1}{\hat{M}_\delta}\left(-C_2 z_2 - z_1 - \dot{q}_0 + \dot{q}_c\right) \tag{2.17}$$

which makes negative definite $\dot{V}_2 = -C_1 z_1^2 - C_2 z_2^2$ where C_1 and C_2 are positive design parameters.

The final form of IBKS controller derived in Section 2.3.2 can be suggested as follows.

$$\begin{aligned}q_c &= -C_1 z_1 - \hat{Z}_\alpha^*\alpha + \dot{\alpha}_c \\ \delta &= \delta_0 + \Delta\delta \\ &= \frac{1}{\hat{M}_\delta^*}\left(-C_2 z_2 - z_1 - \dot{q}_0 + \dot{q}_c\right) + \delta_0\end{aligned} \tag{2.18}$$

Like BKS, q goes to q_c by δ, and α goes to α_c by q_c. Comparing to pure BKS control command in Section 2.3.1, $\hat{M}_\alpha^*$ and $\hat{M}_q^*$ related terms are disappeared, because $\Delta\alpha$ and Δq are neglected in q dynamics (2.13) during the control law derivation. Only $\hat{Z}_\alpha^*$ and $\hat{M}_\delta^*$ are necessary for the implementation of the algorithm, so less model information is required. Instead of reduced model dependency, additional measurements δ_0 and $\dot{q}_0$, current control surface deflection and state derivative, are required to implement the control algorithm.

2.4 Closed-loop Analysis

Closed-loop analysis is performed by substituting each control input (2.11) and (2.18) to the dynamics (2.1) with $Z_\delta^* = 0$. In general, C_{Z_δ} is small enough to be neglected, especially for large aircrafts [26]. Comparing to the dynamics (2.2)

utilized for the control law derivation, the main difference in the dynamics for the analysis is that the real aerodynamic derivatives, not the estimates, are considered. As in [22], analysis is performed in piece-wise way in order to easily utilize the existing analysis framework for linear time-invariant(LTI) system.

In Section 2.4, analysis starts with the nominal case, where transfer functions with both algorithms are derived assuming that the uncertainties do not exist in the aerodynamic derivative estimates. The next step is to consider the model uncertainties in the closed-loop analysis, so their effects to the systems with each controller can be investigated in stability and performance point of view. Under the model uncertainties, a condition to maintain stability and a steady state error are suggested for each closed-loop system. Although the control laws are designed to always ensure asymptotic stability with the positive design parameters in the nominal case, it cannot be guaranteed if real model information is different with the estimates utilized in the controller design phase due to the model uncertainties. Closed-loop characteristics with BKS and IBKS under the model uncertainties can be directly compared using derived common metrics, which reinforces critical understandings about the algorithms. To have more insights from simplified situations, case studies are carried out, assuming that the uncertainty exists only in one aerodynamic derivative estimate and the other estimates have true values.

2.4.1 Nominal Case

Under the assumption of perfect model information without any uncertainties, ideal measurements without any delays, and constant α_c (i.e. $\dot{\alpha}_c = \ddot{\alpha}_c = 0$), transfer functions with BKS and IBKS are derived for the nominal case. Their detailed derivation processes are addressed in Appendix A and B, and the results are suggested as (2.19).

$$\begin{aligned}
&\frac{\alpha(s)}{\alpha_c(s)} = \frac{T_N}{s^2 + 2\zeta_{_N}\omega_{n_{_N}} s + \omega_{n_{_N}}^2} \\
&\text{where} \\
&T_N = C_1 C_2 + 1 \\
&2\zeta_{_N}\omega_{n_{_N}} = C_1 + C_2 \\
&\omega_{n_{_N}}^2 = C_1 C_2 + 1
\end{aligned} \tag{2.19}$$

$\zeta_{_N}$ and $\omega_{n_{_N}}$ represent a damping ratio and a natural frequency for the closed-loop systems with BKS and IBKS in the nominal case.

Poles with BKS and IBKS for the nominal case, $p_{N,1}$ and $p_{N,2}$, are given from (2.19) as follows.

$$p_{N,1} = p_{N,2} = \frac{-\left(C_1 + C_2\right) \pm \sqrt{\left(C_1 - C_2\right)^2 - 4}}{2} \tag{2.20}$$

From the equation (2.20) above, following properties can be identified. First, with the positive design parameters, poles are always located in left half plane, which means that the systems always become stable with BKS and IBKS. Second, poles can be expressed as a function of the design parameters only. This implies that the system characteristics become uniform in the entire flight envelope.

Steady state error, e_{ss}, can be calculated using following relationships.

$$e_{ss} = \alpha_c - \lim_{t\to\infty} \alpha(t) = \alpha_c - \lim_{s\to 0} s\alpha(s) \tag{2.21}$$

A step input $\alpha_c = K$ in time-domain is expressed in the frequency-domain as below.

$$\alpha_c(s) = \frac{K}{s} \tag{2.22}$$

By applying (2.19) and (2.22) to (2.21), steady state errors with BKS and IBKS for the nominal case, $e_{ss_{_N},1}$ and $e_{ss_{_N},2}$, can be calculated, resulting in zero values.

$$e_{ss_{_N},1} = e_{ss_{_N},2} = 0 \tag{2.23}$$

Because the transfer functions with both algorithms are suggested, various performance metrics can be discussed further. For instance, a settling time, when the magnitude of the state error is reduced within 5%, can be calculated by the approx-

imated equation (2.24) suggested below [27].

$$t_{s_N} = \begin{cases} \dfrac{3.2}{\zeta_N \omega_{n_N}} & \text{if } 0 < \zeta_N < 0.69 \\ \\ \dfrac{4.5}{\omega_{n_N}} \zeta_N & \text{if } \zeta_N > 0.69 \end{cases} \tag{2.24}$$

where

$$\begin{aligned} \omega_{n_N} &= \sqrt{C_1 C_2 + 1} \\ \zeta_N &= \frac{C_1 + C_2}{2\sqrt{C_1 C_2 + 1}} \end{aligned} \tag{2.25}$$

This performance metric t_{s_N}, related to fast response, is also determined only by the design parameters C_1 and C_2.

For the nominal case, asymptotic stability is achieved in both closed-loop systems, which is expected in the design stage of the controllers. Although the incremental dynamics (2.13) is applied in the IBKS controller derivation process, the closed-loop analysis shows that the desired characteristics are accomplished, because the sampling rate is assumed to be fast enough for this sensor based approach.

2.4.2 Closed-loop Analysis under the Model Uncertainties

If the model uncertainties are considered, asymptotic stability cannot be achieved only with the positive design parameters, and performance cannot be uniform in whole flight envelope, unlike the nominal case. In Section 2.4.2, for each closed-loop system, a condition to maintain stability under the model uncertainties is investigated, along with performance metrics like a steady state error. To have more insights from simplified situations, case studies are carried out for each closed-loop system, assuming that the uncertainty exists only in one aerodynamic derivative estimate and the others have true values. Detailed description for each case is suggested in Table 2.1, where $\Delta_{(\cdot)}$ denotes the uncertainty in the estimate for real aerodynamic derivative $(\cdot)$.

Table 2.1: Case Description

	$\hat{M}_{\alpha}^{*}$	$\hat{M}_{q}^{*}$	$\hat{Z}_{\alpha}^{*}$	$\hat{M}_{\delta}^{*}$
Case 1	$M_{\alpha}^{*}(1+\Delta_{M_{\alpha}^{*}})$	M_{q}^{*}	Z_{α}^{*}	M_{δ}^{*}
Case 2	M_{α}^{*}	$M_{q}^{*}(1+\Delta_{M_{q}^{*}})$	Z_{α}^{*}	M_{δ}^{*}
Case 3	M_{α}^{*}	M_{q}^{*}	$Z_{\alpha}^{*}(1+\Delta_{Z_{\alpha}^{*}})$	M_{δ}^{*}
Case 4	M_{α}^{*}	M_{q}^{*}	Z_{α}^{*}	$M_{\delta}^{*}(1+\Delta_{M_{\delta}^{*}})$

2.4.2.1 Backstepping Control

If there exist the uncertainties in the aerodynamic derivative estimates, a transfer function with BKS can be derived as (2.26), under the assumption of perfect measurements without any delays and constant α_c. Detailed derivation process is listed in Appendix A.

$$\frac{\alpha(s)}{\alpha_c(s)} = \frac{T_{\Delta,1}}{s^2 + 2\zeta_{\Delta,1}\omega_{n_{\Delta,1}} s + \omega_{n_{\Delta,1}}^2}$$

where

$$\begin{aligned}
T_{\Delta,1} &= \frac{M_{\delta}^{*}}{\hat{M}_{\delta}^{*}}\left(C_1 C_2 + 1\right) \\
2\zeta_{\Delta,1}\omega_{n_{\Delta,1}} &= -\left\{ Z_{\alpha}^{*} + M_{q}^{*} - \frac{M_{\delta}^{*}}{\hat{M}_{\delta}^{*}}\left(C_1 + C_2 + \hat{M}_{q}^{*} + \hat{Z}_{\alpha}^{*}\right)\right\} \\
\omega_{n_{\Delta,1}}^2 &= \left\{\left(Z_{\alpha}^{*} M_{q}^{*} - M_{\alpha}^{*}\right) - \frac{M_{\delta}^{*}}{\hat{M}_{\delta}^{*}}\left(Z_{\alpha}^{*}\hat{M}_{q}^{*} - \hat{M}_{\alpha}^{*}\right)\right\} \\
&\quad + \frac{M_{\delta}^{*}}{\hat{M}_{\delta}^{*}}\left\{C_2\left(\hat{Z}_{\alpha}^{*} - Z_{\alpha}^{*}\right) + \left(C_1 C_2 + 1\right)\right\}
\end{aligned} \tag{2.26}$$

$\zeta_{\Delta,1}$ and $\omega_{n_{\Delta,1}}$ represent a damping ratio and a natural frequency for the system with BKS under the model uncertainties. Because the model uncertainties are considered, not only C_1 and C_2, but also the aerodynamic derivatives and their estimates with the uncertainties, have impacts on the closed-loop system and explicitly appear in the transfer function as (2.26), unlike (2.19) for the nominal case.

For a damped system, stability is normally guaranteed. Hence, a condition $\mathscr{G}_{\Delta,1}$ to maintain stability for the system with BKS under the model uncertainties can be obtained from $2\zeta_{\Delta,1}\omega_{n_{\Delta,1}} > 0$ (Cond.1) under $\omega_{n_{\Delta,1}}^2 > 0$ (Cond.2) as below.

$$
\begin{aligned}
&\mathscr{G}_{\Delta,1} = \left\{ C_1, C_2 \in \mathbb{R}_{>0} | \text{ Cond. 1 \& Cond. 2} \right\} \\
&\text{Cond. 1 : } C_1 + C_2 > \left(\frac{\hat{M}_\delta^*}{M_\delta^*} Z_\alpha^* - \hat{Z}_\alpha^* \right) + \left(\frac{\hat{M}_\delta^*}{M_\delta^*} M_q^* - \hat{M}_q^* \right) \\
&\text{Cond. 2 : } \left(C_1 + \hat{Z}_\alpha^* - Z_\alpha^* \right) C_2 > -\frac{\hat{M}_\delta^*}{M_\delta^*} \left(Z_\alpha^* M_q^* - M_\alpha^* \right) \\
&\qquad\qquad + \left(Z_\alpha^* \hat{M}_q^* - \hat{M}_\alpha^* \right) - 1
\end{aligned}
\tag{2.27}
$$

if M_δ^* and $\hat{M}_\delta^*$ have the same sign. This stability condition can be interpreted into constraints on the design parameters for BKS under the model uncertainties.

A steady state error $e_{ss_\Delta,1}$ with BKS controller can be obtained from (2.21), (2.22) and (2.26).

$$
e_{ss_\Delta,1} = K \frac{\eta_2 + \frac{\hat{M}_\delta^*}{M_\delta^*} \eta_3}{\eta_1 + \eta_2 + \frac{\hat{M}_\delta^*}{M_\delta^*} \eta_3} \tag{2.28}
$$

η_1, η_2 and η_3 in (2.28) can be written as follows.

$$
\begin{aligned}
\eta_1 &= C_1 C_2 + 1 \\
\eta_2 &= C_2 \left(\hat{Z}_\alpha^* - Z_\alpha^* \right) \\
\eta_3 &= \left\{ \left(Z_\alpha^* M_q^* - M_\alpha^* \right) - \frac{M_\delta^*}{\hat{M}_\delta^*} \left(Z_\alpha^* \hat{M}_q^* - \hat{M}_\alpha^* \right) \right\}
\end{aligned}
\tag{2.29}
$$

η_1, the only difference between the numerator and the denominator in the derived steady state error equation (2.28), is dependent only upon the design parameters. η_2 is a function of the model information for the outer-loop and the design parameter for the inner-loop. η_3 is highly related to the model information for the inner-loop. Unlike the nominal case, $e_{ss_\Delta,1}$ cannot be zero due to the model uncertainties. It can be reduced with high C_1, since η_1 increases as C_1 go up. It is difficult to generalize this property with the design parameter for the inner-loop C_2, because η_2 which is also affected by C_2, becomes effective to $e_{ss_\Delta,1}$ when the uncertainty exists in $\hat{Z}_\alpha^*$. The steady state error becomes $\frac{\left(\hat{Z}_\alpha^* - Z_\alpha^*\right)}{C_1 + \left(\hat{Z}_\alpha^* - Z_\alpha^*\right)}$ if C_2 goes to infinity, while $e_{ss_\Delta,1}$ goes to zero as C_1 goes to infinity.

To have better understandings about the effects of the uncertainty in each aerodynamic derivative estimate to the system with BKS, case studies are performed as

below. Depending on where the uncertainty exists, even with the same level of the uncertainty, its impact to the closed-loop system can be different.

For each case, a transfer function with BKS (2.26) can be simplified into (2.30) with perturbed parameters ${T'}_{\Delta,1}$, $2{\zeta'}_{\Delta,1}{\omega'}_{n_{\Delta,1}}$ and ${\omega'}^2_{n_{\Delta,1}}$ from the nominal T_N, $2\zeta_N\omega_{n_N}$, and $\omega^2_{n_N}$. These parameters are addressed in Table 2.2.

$$\frac{\alpha(s)}{\alpha_c(s)} = \frac{{T'}_{\Delta,1}}{s^2 + 2{\zeta'}_{\Delta,1}{\omega'}_{n_{\Delta,1}} s + {\omega'}^2_{n_{\Delta,1}}} \tag{2.30}$$

Table 2.2: Case Study : Parameters for Transfer Function with BKS

Case	${T'}_{\Delta,1}$	$2{\zeta'}_{\Delta,1}{\omega'}_{n_{\Delta,1}}$	${\omega'}^2_{n_{\Delta,1}}$
1	T_N	$2\zeta_N\omega_{n_N}$	$\omega^2_{n_N} + M^*_\alpha\Delta_{M^*_\alpha}$
2	T_N	$2\zeta_N\omega_{n_N} + M^*_q\Delta_{M^*_q}$	$\omega^2_{n_N} - Z^*_\alpha M^*_q\Delta_{M^*_q}$
3	T_N	$2\zeta_N\omega_{n_N} + Z^*_\alpha\Delta_{Z^*_\alpha}$	$\omega^2_{n_N} + C_2 Z^*_\alpha\Delta_{Z^*_\alpha}$
4	$\frac{T_N}{1+\Delta_{M^*_\delta}}$	$\frac{2\zeta_N\omega_{n_N}}{1+\Delta_{M^*_\delta}} - \frac{\left(Z^*_\alpha + M^*_q\right)\Delta_{M^*_\delta}}{1+\Delta_{M^*_\delta}}$	$\frac{\omega^2_{n_N}}{1+\Delta_{M^*_\delta}} + \frac{\left(Z^*_\alpha M^*_q - M^*_\alpha\right)\Delta_{M^*_\delta}}{1+\Delta_{M^*_\delta}}$

Note that, except the case 4, ${T'}_{\Delta,1}$ becomes the same as the nominal one, and the additive perturbation term appears in the parameters $2{\zeta'}_{\Delta,1}{\omega'}_{n_{\Delta,1}}$ and ${\omega'}^2_{n_{\Delta,1}}$ respectively. This perturbation term can be described as a product of the weight factor and the uncertainty $\Delta_{(\cdot)}$. The parameters for the case 4 show similar forms with the others, but they are additionally divided by $\left(1+\Delta_{M^*_\delta}\right)$.

For each case, using the parameters $2{\zeta'}_{\Delta,1}{\omega'}_{n_{\Delta,1}}$ and ${\omega'}^2_{n_{\Delta,1}}$ in Table 2.1, a stability condition can be simplified into (2.31) with Table 2.3.

$$\begin{aligned} &\mathscr{G}'_{\Delta,1} = \left\{C_1, C_2 \in \mathbb{R}_{>0} |\ \text{Cond. 1 \& Cond. 2}\right\} \\ &\text{Cond. 1}: C_1 + C_2 > \kappa_{1,1} \\ &\text{Cond. 2}: C_1C_2 + 1 > \kappa_{2,1} \end{aligned} \tag{2.31}$$

$\kappa_{1,1}$ and $\kappa_{2,1}$, which are related to the feasible boundary of the design parameters, appear to be the perturbation term of $2{\zeta'}_{\Delta,1}{\omega'}_{n_{\Delta,1}}$ and ${\omega'}^2_{n_{\Delta,1}}$ with the opposite sign. Depending on where the uncertainty exists, the boundary value of each $\Delta_{(\cdot)}$ for the stable closed-loop system can be different. It becomes small if the corresponding

Table 2.3: Case Study : Parameters for Stability Conditions with BKS

Case	$\kappa_{1,1}$	$\kappa_{2,1}$
1	0	$-M_{\alpha}^{*}\Delta_{M_{\alpha}^{*}}$
2	$-M_{q}^{*}\Delta_{M_{q}^{*}}$	$Z_{\alpha}^{*}M_{q}^{*}\Delta_{M_{q}^{*}}$
3	$-Z_{\alpha}^{*}\Delta_{Z_{\alpha}^{*}}$	$-C_2 Z_{\alpha}^{*}\Delta_{Z_{\alpha}^{*}}$
4	$\left(Z_{\alpha}^{*}+M_{q}^{*}\right)\Delta_{M_{\delta}^{*}}$	$-\left(Z_{\alpha}^{*}M_{q}^{*}-M_{\alpha}^{*}\right)\Delta_{M_{\delta}^{*}}$

weight factor is large. It is observed from Table 2.3 that, for the case 1, Cond.1 is always satisfied with the positive design parameters, so only Cond.2 is effective.

By comparing the cases, more simplified structure for the steady state error equation can be found as (2.32). η_1 in (2.32) is identical with the one in (2.28), defined only by the design parameters. For each case, the weight factor to the model uncertainty ${\eta'}_{2,1}$ only changes, and it is listed in Table 2.4.

$$e'_{ss_{\Delta},1} = K\frac{{\eta'}_{2,1}\Delta_{(\cdot)}}{\eta_1 + {\eta'}_{2,1}\Delta_{(\cdot)}} \tag{2.32}$$

Table 2.4: Case Study : Parameters for Steady State Error with BKS

Case	${\eta'}_{2,1}$
1	M_{α}^{*}
2	$-Z_{\alpha}^{*}M_{q}^{*}$
3	$C_2 Z_{\alpha}^{*}$
4	$Z_{\alpha}^{*}M_{q}^{*}-M_{\alpha}^{*}$

As can be seen in Table 2.3 and 2.4, $\kappa_{2,1} = -{\eta'}_{2,1}\Delta_{(\cdot)}$. Depending on where the uncertainty exists, even with the same level of the uncertainty, $|e_{ss_{\Delta},1}|$ gets larger for the case with greater weight factor. Additionally, $|e_{ss_{\Delta},1}|$ goes up as $|\Delta_{(\cdot)}|$ increases.

2.4.2.2 Incremental Backstepping Control

For successful analysis with IBKS, it is necessary to decide how to deal with the additional measurements $\dot{q}_0$ and δ_0. In Chapter 2, they are suggested as follows.

$$\begin{aligned} \dot{q}_0 &= M_{\alpha}^{*}\alpha + M_{q}^{*}q + M_{\delta}^{*}\delta_0 \\ \delta_0 &= \delta(t-\tau) \end{aligned} \tag{2.33}$$

The model for the current state derivative measurement $\dot{q}_0$ comes from the piecewise version of (2.1). For an ideal actuator, a control surface deflection directly follows a generated control command. Then, the current control surface deflection measurement δ_0 can be regarded as a control command generated in the previous step, where τ indicates a step size.

If the uncertainties exist in the aerodynamic derivative estimates, a transfer function with IBKS can be obtained as (2.34), under the assumption of perfect measurements without any delays and constant α_c. Detailed derivation process is addressed in Appendix B.

$$\frac{\alpha(s)}{\alpha_c(s)} = \frac{D_{\Delta,2}(s)}{s^2 + N_{\Delta,2}(s)s + N'_{\Delta,2}(s)}$$

where

$$\begin{aligned}
D_{\Delta,2}(s) &= \frac{M^*_\delta}{\phi(s)}\left(C_1C_2 + 1\right) \\
N_{\Delta,2}(s) &= -\left\{Z^*_\alpha + M^*_q - \frac{M^*_\delta}{\phi(s)}\left(C_1 + C_2 + M^*_q + \hat{Z}^*_\alpha\right)\right\} \\
N'_{\Delta,2}(s) &= \left(1 - \frac{M^*_\delta}{\phi(s)}\right)\left(Z^*_\alpha M^*_q - M^*_\alpha\right) \\
&\quad + \frac{M^*_\delta}{\phi(s)}\left\{C_2\left(\hat{Z}^*_\alpha - Z^*_\alpha\right) + \left(C_1C_2 + 1\right)\right\}
\end{aligned} \tag{2.34}$$

$\phi(s)$ is defined as below.

$$\phi(s) = \hat{M}^*_\delta\left(1 - e^{-\tau s}\right) + M^*_\delta e^{-\tau s} \tag{2.35}$$

Since the model uncertainties are considered, not only C_1 and C_2, but also the aerodynamic derivatives and their estimates with the uncertainties, have impacts on the closed-loop system and explicitly appear in the transfer function as (2.34), unlike (2.19) for the nominal case. Comparing to (2.26) with BKS, there are the two main differences in the transfer function (2.34). First, the true values for the stability derivatives in the inner-loop, not the estimated ones, appear in (2.34). Second, the effect of the control derivative estimate $\hat{M}^*_\delta$ resides in $\phi(s)$.

The transfer function with IBKS can be simplified as (2.36) with $\tau \simeq 0$ assumption for the analysis purpose.

$$\frac{\alpha(s)}{\alpha_c(s)} = \frac{T_{\Delta,2}}{s^2 + 2\zeta_{\Delta,2}\omega_{n_{\Delta,2}} s + \omega_{n_{\Delta,2}}^2}$$

where

$$\begin{aligned} T_{\Delta,2} &= C_1 C_2 + 1 \\ 2\zeta_{\Delta,2}\omega_{n_{\Delta,2}} &= (C_1 + C_2) + \left(\hat{Z}_\alpha^* - Z_\alpha^*\right) \\ \omega_{n_{\Delta,2}}^2 &= (C_1 C_2 + 1) + C_2\left(\hat{Z}_\alpha^* - Z_\alpha^*\right) \end{aligned} \tag{2.36}$$

$\zeta_{\Delta,2}$ and $\omega_{n_{\Delta,2}}$ denote a damping ratio and a natural frequency for the system with IBKS under the model uncertainties. An interesting observation from (2.36) is that, under the $\tau \simeq 0$ assumption, the effects of M_δ^* and its estimate with the uncertainty are vanished in the closed-loop system with IBKS, while they still remain in the system with BKS. This implies that, if the control command is calculated, transmitted and reflected fast enough to the real control surface deflection, the closed-loop system with IBKS becomes insensitive to the uncertainty in $\hat{M}_\delta^*$, although this information is still required to implement the control algorithm.

The differences in the analysis results with IBKS to the ones with BKS, can be explained as follows. The incremental controller for the inner-loop utilizes the additional measurements $\dot{q}_0$ and δ_0. In $\dot{q}_0$ measurement obtained in flight, the effects of true M_α^* and M_q^* are included in implicit way. Hence, model information about M_α^* and M_q^* is not required for IBKS, unlike BKS. Not only these stability derivatives, but also the control derivative M_δ^* are involved in this $\dot{q}_0$ measurement. If there is no uncertainty in $\hat{M}_\delta^*$ utilized to implement the algorithm, the effect of M_δ^* in the $\dot{q}_0$ measurement can be totally compensated with the δ_0 measurement, in the suggested control law (2.18). Generally, they cannot be fully cancelled out due to the uncertainty, resulting in $\phi(s)$ for the closed-loop system with IBKS. However, if $\tau \simeq 0$, $\phi(s)$ becomes just M_δ^*, even if $\hat{M}_\delta^*$ has uncertainty. Hence, the closed-loop system with IBKS becomes robust with respect to the uncertainty in $\hat{M}_\delta^*$ utilized to implement the algorithm, if the control command is calculated, transmitted and reflected fast enough to the real control surface deflection. To sum up, all model uncertainties do not affect the system with IBKS when computation and transmission of the control command are fast enough. This is the key difference in the system behaviors with IBKS, comparing to the ones with BKS.

For the same reason in Section 2.4.2.1 above with BKS, a condition $\mathscr{G}_{\Delta,2}$ to maintain stability for the system with IBKS under the model uncertainties can be obtained

from $2\zeta_{\Delta,2}\omega_{n_{\Delta,2}} > 0$ (Cond.1) under $\omega^2_{n_{\Delta,2}} > 0$ (Cond.2) as below.

$$\begin{aligned} &\mathscr{G}_{\Delta,2} = \left\{C_1, C_2 \in \mathbb{R}_{>0} | \text{ Cond. 1 \& Cond. 2}\right\} \\ &\text{Cond. 1 : } C_1 + C_2 > -\left(\hat{Z}^*_\alpha - Z^*_\alpha\right) \\ &\text{Cond. 2 : } \left(C_1 + \hat{Z}^*_\alpha - Z^*_\alpha\right) C_2 > -1 \end{aligned} \tag{2.37}$$

This stability condition can be interpreted into constraints on the design parameters for IBKS under the model uncertainties. Note that the stability condition is affected only by the uncertainty on $\hat{Z}^*_\alpha$ utilized for the outer-loop controller design with BKS.

Through the same process above using (2.21), (2.22) and (2.36), a steady state error $e_{ss_\Delta,2}$ with IBKS controller can be suggested as follows.

$$e_{ss_\Delta,2} = K\frac{\eta_2}{\eta_1 + \eta_2} \tag{2.38}$$

where

$$\begin{aligned} \eta_1 &= C_1C_2 + 1 \\ \eta_2 &= C_2\left(\hat{Z}^*_\alpha - Z^*_\alpha\right) \end{aligned} \tag{2.39}$$

Unlike the nominal case, the steady state error exist as (2.38) with (2.39) due to the model uncertainties. Comparing to (2.28) with (2.29) for pure BKS, there exist the same η_1 and η_2 in (2.38) with (2.39) for IBKS. However, there is no η_3 which is mainly related to the model information for the inner-loop, unlike pure BKS. The steady state error occurs only when there exists uncertainty on $\hat{Z}^*_\alpha$ utilized for the outer-loop controller design with BKS. In both (2.28) and (2.38), the denominator is bigger than the numerator by η_1 which increases as the design parameters go up. It indicates that high C_1 can also reduce $e_{ss_\Delta,2}$. For the same reason in Section 2.4.2.1 above with pure BKS, it is difficult to generalize this property with the design parameter for the inner-loop C_2.

Case studies are conducted to clearly show the effects of the uncertainty in each aerodynamic derivative estimate to the system with IBKS. Since $\hat{M}^*_\alpha$ and $\hat{M}^*_q$ are not required to implement IBKS thanks to the additional $\dot{q}_0$ measurement, the closed-loop system with IBKS is not affected by $\Delta_{M^*_\alpha}$ and $\Delta_{M^*_q}$. Hence, the analysis results with IBKS for the case 1 and 2 are the same with the ones for the nominal case. In addition, under the $\tau \simeq 0$ assumption, the analysis results with IBKS for the case 4 also become identical to the ones for the nominal case. It is shown that the

closed-loop system with IBKS becomes robust with respect to $\Delta_{M_\delta^*}$, if the control command is calculated, transmitted and reflected fast enough to the real control surface deflection. For the case 3 where the model uncertainty only exists in dynamics for the outer-loop, the analysis results with IBKS appear to be the same with the corresponding case study results with pure BKS in Section 2.4.2.1. This can be explained from the fact that each outer-loop controller is designed with BKS in common, and inner-loop controllers with BKS and IBKS become the same when there are no model uncertainties in dynamics for the inner-loop, which is the case 3.

2.5 Simulation

In Section 2.5, simulations are performed to verify the proposed theoretical analysis results. Since a piece-wise approach is considered to handle the LPV system as in [22], several points assigned to each grid were simulated. The aerodynamic derivatives shown in Fig. 2.7 of Appendix C and zero Z_δ^* are utilized for the simulations. As an example, simulation results when altitude is 7.6200km and $U_0 = 185.9280$m/s are suggested in Chapter 2.

Simulation parameters about the angle of attack command, the design parameters, and the level of the model uncertainties are suggested in Table 2.5. The simulation parameter $\Delta_{(\cdot)}$ which represents the level of the model uncertainty, indicates how much percentage of error exists in the aerodynamic derivative estimate utilized in the control system design, comparing to the actual aerodynamic derivative $(\cdot)$. For example, $\Delta_{(\cdot)} = -0.75$ means that an aerodynamic derivative estimate used in the flight controller is 75% smaller than its real value for $(\cdot)$. $\Delta_{(\cdot)} = 1$ implies that the flight controller utilizes an aerodynamic derivative estimate twice larger than its real value for $(\cdot)$. Initial values for the state variables α and q are set to be 0° and 0°/s. Small enough τ is applied as $0.001sec$ for the simulation. With BKS, simulations are carried out for case 1, 2, 3 and 4 respectively. With IBKS, simulations are performed for each case 3 and 4.

Table 2.5: Simulation Parameters

Parameter	Value
α_c	1.5°
C_1, C_2	1.5
$\Delta_{(\cdot)}$	$[-0.75,\ -0.5,\ -0.25,\ 0,\ 0.25,\ 0.5,\ 0.75,\ 1]$

The stability condition and the performance metric like e_{ss} predicted by the analysis, can be examined in pole trajectories and time response graphs. Besides, simulation results show which model uncertainty has much influence in stability and performance for this aircraft.

2.5.1 Simulation results with BKS

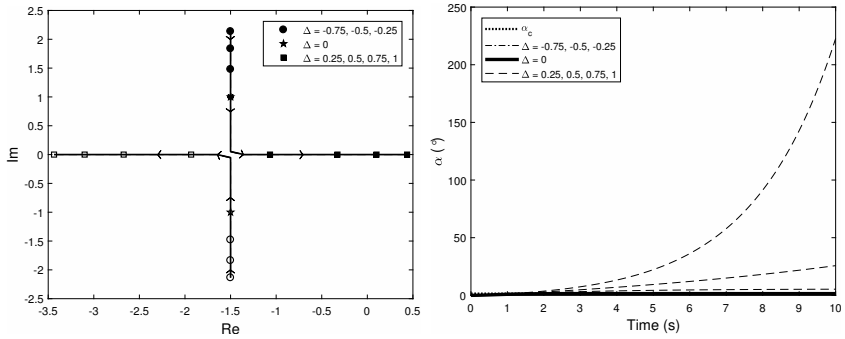

(a) Pole Trajectory (b) Time Response

Figure 2.1: Closed-loop System Response with BKS under the uncertainty in $\hat{M}_{\alpha}^{*}$

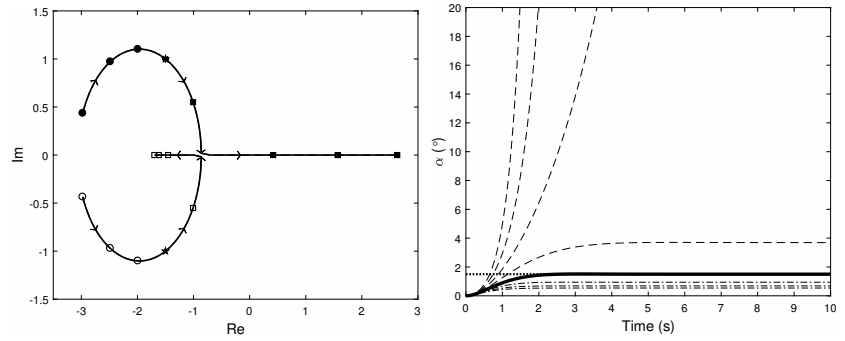

(a) Pole Trajectory (b) Time Response

Figure 2.2: Closed-loop System Response with BKS under the uncertainty in $\hat{M}_{q}^{*}$

Fig. 2.1 shows that the system becomes unstable when $\Delta_{M_{\alpha}^{*}} = 0.75$ and 1. From Fig. 2.2, it is observed that $\Delta_{M_{q}^{*}} = 0.5, 0.75$ and 1 can result in unstable behaviors of the system. Fig. 2.3 indicates that the closed-loop system is stable with every $\Delta_{Z_{\alpha}^{*}}$. It can be seen from Fig. 2.4 that $\Delta_{M_{\delta}^{*}} = -0.5$ and -0.75 can make the system unstable.

These observations can be clearly explained by the stability condition (2.31) with Table 2.3. Under this simulation environment, the Cond. 2 in (2.31) is appeared to be a dominant condition for stability. The Cond. 2 implies that, for larger $|\eta'_{2,1}|$

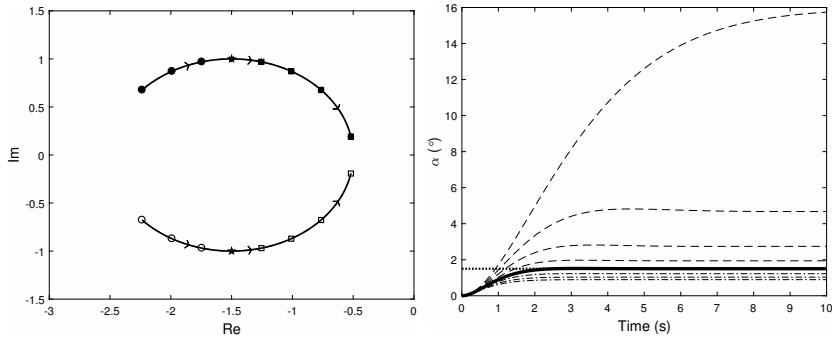

(a) Pole Trajectory (b) Time Response

Figure 2.3: Closed-loop System Response with BKS under the uncertainty in $\hat{Z}^*_\alpha$

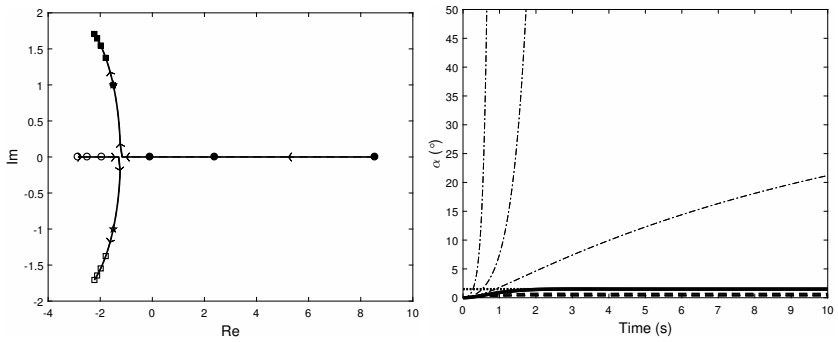

(a) Pole Trajectory (b) Time Response

Figure 2.4: Closed-loop System Response with BKS under the uncertainty in $\hat{M}^*_\delta$

case, the closed-loop system becomes unstable with smaller $|\Delta_{(\cdot)}|$. $\eta'_{2,1} = -4.7488$, -7.7182, -2.9439 and 12.4670 for Case 1, 2, 3 and 4, respectively. Thus, $|\Delta_{(\cdot)}|$ resulting in unstable behavior to the system is predicted to be smaller for the Case 4 than for the Case 2, 1 and 3 where it becomes the largest. This coincides with the observations above obtained from Fig. 2.1 to 2.4.

By rewriting the stability condition (2.31), a minimum C_1 to guarantee stability for each case under fixed C_2 and every $|\Delta_{(\cdot)}|$ in this simulation, can be predicted. It is expected that, in the stability point of view, $C_1 > 2.4992$ for the Case 1, $C_1 > 4.4788$ for the Case 2, $C_1 > 1.2960$ for the Case 3, and $C_1 > 5.5668$ for the Case 4, under this simulation environment. Thus, all simulations with the BKS in Chapter 2 for every case will show stable results, by increasing C_1 larger than 5.5668, which is the minimum C_1 for the Case 4 where $|\eta'_{2,1}|$ is the largest.

Steady state errors $e_{ss,1}$ are given in Table 2.6 for stable instances. It is interpreted from (2.32) that, $|e_{ss,1}|$ is larger for the case with greater $|\eta'_{2,1}|$, under the same $|\Delta_{(\cdot)}|$. The comparison should be carefully carried out between the cases with the

Table 2.6: Steady State Error for system with BKS, $e_{ss,1}$

Case \ $\Delta_{(\cdot)}$	-0.75	-0.5	-0.25	0	0.25	0.5	0.75	1
1	0.7843	0.6332	0.4013	0	-0.8632	-3.8281	-	-
2	0.9606	0.8143	0.5588	0	-2.1919	-	-	-
3	0.6068	0.4676	0.2770	0	-0.4391	-1.2418	-3.1749	-14.4279
4	-	-	-35.0820	0	0.7343	0.9859	1.1131	1.1898

same sign of $\eta'_{2,1}\Delta_{(\cdot)}$. $\eta'_{2,1} = -4.7488$, -7.7182, -2.9439 and 12.4670 for the Case 1, 2, 3 and 4, respectively. Thus, $|\eta'_{2,1}|$ is predicted to be smaller for the Case 3 than for the Case 1, 2 and 4 where it becomes the largest. The sign of $\eta'_{2,1}$ is positive only for the Case 4 and it is negative for the other three cases. Thus, the Case 1, 2 and 3 with $\Delta_{(\cdot)}$ and the Case 4 with $-\Delta_{(\cdot)}$ should be compared with each other. By applying this comparison scheme to Table 2.6, the interpretation from (2.32) is shown to agree with the simulation results.

Additionally, it is observed from Table 2.6 that $|e_{ss,1}|$ becomes larger as $|\Delta_{(\cdot)}|$ grows, which coincides with the analysis result.

2.5.2 Simulation results with IBKS

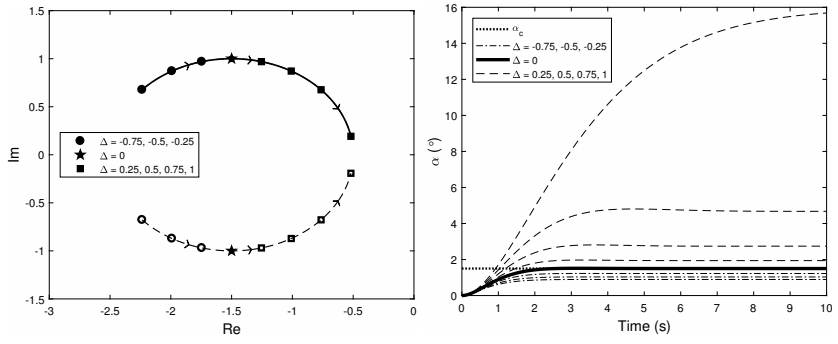

(a) Pole Trajectory (b) Time Response

Figure 2.5: Closed-loop System Response with IBKS under the uncertainty in $\hat{Z}^*_\alpha$

Fig. 2.5 shows the identical results with Fig. 2.3. For case 3, the system behaviors with IBKS and BKS become the same, which has been already predicted and explained in the analysis part. Under this simulation environment, the closed-loop system is stable with every $\Delta_{Z^*_\alpha}$. $|e_{ss,1}|$ increases as $|\Delta_{Z^*_\alpha}|$ gets larger, and the system

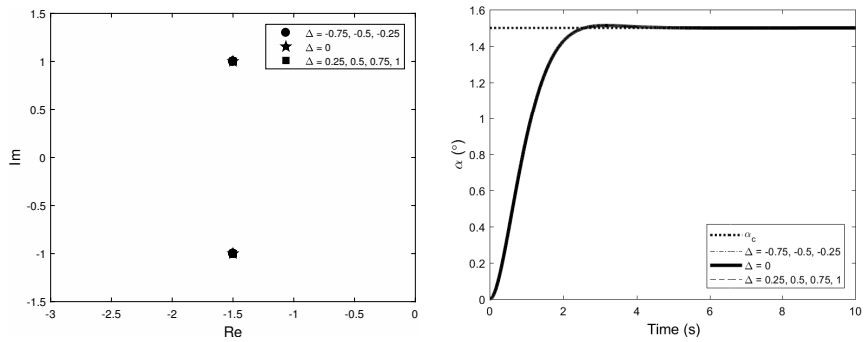

(a) Pole Trajectory (b) Time Response

Figure 2.6: Closed-loop System Response with IBKS under the uncertainty in $\hat{M}_\delta^*$

response becomes slower as $\Delta_{Z_\alpha^*}$ rises.

Fig. 2.6 shows that the closed-loop system is insensitive to the model uncertainty $\Delta_{M_\delta^*}$ in $\hat{M}_\delta^*$, with $\tau = 0.001$ which is set to be small enough for the simulation. Poles are always in the left half plane, so the system is stable all the time. There is no change in the location of poles depending on the variation of $\Delta_{M_\delta^*}$. Consequently, ω_n, ζ and t_s remain the same, and $e_{ss,2}$ doesn't exist. These simulation results coincide with the prediction from the analysis under the assumption that the control command is calculated, transmitted and reflected fast enough to the real control surface deflection.

2.6 Conclusion

Chapter 2 suggests closed-loop analysis results with BKS and IBKS methods under model uncertainties. The proposed analysis enables critical understandings and insights about system characteristics under the model uncertainties. Transfer functions with BKS and IBKS under the model uncertainties are compared with the ones for the nominal case. The effects of the model uncertainties on the closed-loop systems are figured out, resulting in the condition to maintain stability and the steady state error. The closed-loop characteristics with BKS and IBKS under the model uncertainties are directly compared using derived common metrics, which clarifies how the effects of the model uncertainties to the closed-loop system become different depending on the applied control algorithm. Unlike BKS, IBKS is not affected by the uncertainties on any model parameters, including control effectiveness which is still required for IBKS implementation, when the control input is calculated, trans-

mitted and reflected fast enough to the actual control surface. Under the assumption that the uncertainty exists only in one aerodynamic derivative estimate while the other estimates have true values, case studies are conducted to find the impact of the uncertainty on the specific aerodynamic derivative estimate to the closed-loop system. Depending on where the uncertainty exists, even with the same level of the uncertainty, its impact to the closed-loop system becomes different, and this is explained with the weight factors for each case. As a future work, the short period mode dynamics can be extended to full 6-DoF dynamics.

Appendix

A Derivation of Transfer Function with BKS

Dynamics (2.1) with $Z_\delta^* = 0$ can be expressed as a state space equation below.

$$\begin{aligned} &\dot{\mathbf{x}} = \mathbf{A}\mathbf{x} + \mathbf{B}\mathbf{u} \qquad \mathbf{y} = \mathbf{C}\mathbf{x} \\ &\mathbf{x} = \begin{bmatrix} \alpha & q \end{bmatrix}^T \qquad \mathbf{u} = \delta \\ &\mathbf{A} = \begin{bmatrix} Z_\alpha^* & 1 \\ M_\alpha^* & M_q^* \end{bmatrix} \quad \mathbf{B} = \begin{bmatrix} 0 \\ M_\delta^* \end{bmatrix} \quad \mathbf{C} = \begin{bmatrix} 1 & 0 \end{bmatrix} \end{aligned} \tag{2.40}$$

Using (2.11) with (2.1) and (2.3) under the assumption of constant α_c and zero Z_δ^*, δ can be rearranged as follows.

$$\begin{aligned} &\delta = \begin{bmatrix} -\frac{1}{\hat{M}_\delta^*}\nu_{1,\alpha} & -\frac{1}{\hat{M}_\delta^*}\nu_{1,q} \end{bmatrix} \mathbf{x} + \frac{1}{\hat{M}_\delta^*}\left(C_1 C_2 + 1\right)\alpha_c \\ &\text{where} \\ &\nu_{1,\alpha} = \left\{ \left(C_1 + \hat{Z}_\alpha^*\right)\left(C_2 + Z_\alpha^*\right) + \hat{M}_\alpha^* + 1 \right\} \\ &\nu_{1,q} = \left(C_1 + C_2 + \hat{M}_q^* + \hat{Z}_\alpha^*\right) \end{aligned} \tag{2.41}$$

Closed-loop system with BKS can be derived by substituting (2.41) into (2.40).

$$
\begin{aligned}
&\dot{\mathbf{x}} = \mathbf{A}_1\mathbf{x} + \mathbf{B}_1\alpha_c \qquad \mathbf{y} = \mathbf{C}\mathbf{x} \\
&\mathbf{A}_1 = \begin{bmatrix} a_{1,11} & a_{1,12} \\ a_{1,21} & a_{1,22} \end{bmatrix} \\
&\quad = \begin{bmatrix} Z_\alpha^* & 1 \\ M_\alpha^* - \frac{M_\delta^*}{\hat{M}_\delta^*}\nu_{1,\alpha} & M_q^* - \frac{M_\delta^*}{\hat{M}_\delta^*}\nu_{1,q} \end{bmatrix} \\
&\mathbf{B}_1 = \begin{bmatrix} 0 \\ \frac{M_\delta^*}{\hat{M}_\delta^*}\left(C_1C_2+1\right) \end{bmatrix} \\
&\mathbf{C} = \begin{bmatrix} 1 & 0 \end{bmatrix}
\end{aligned}
\tag{2.42}
$$

Transfer function for the closed-loop system with BKS can be derived as below.

$$
\begin{aligned}
&\frac{\alpha(s)}{\alpha_c(s)} = \mathbf{C}(s)\left(s\mathbf{I} - \mathbf{A}_1(s)\right)^{-1}\mathbf{B}_1(s) \\
&\quad = \frac{a_{1,12}\frac{M_\delta^*}{\hat{M}_\delta^*}\left(C_1C_2+1\right)}{s^2 - \left(a_{1,11}+a_{1,22}\right)s + \left(a_{1,11}a_{1,22} - a_{1,12}a_{1,21}\right)} = \frac{T(s)}{s^2 + 2\zeta\omega_n s + \omega_n^2}
\end{aligned}
$$

where

$$
\begin{aligned}
&T(s) = a_{1,12}\frac{M_\delta^*}{\hat{M}_\delta^*}\left(C_1C_2+1\right) = \frac{M_\delta^*}{\hat{M}_\delta^*}\left(C_1C_2+1\right) \\
&2\zeta\omega_n = -\left(a_{1,11}+a_{1,22}\right) \\
&\qquad = -\left\{Z_\alpha^* + M_q^* - \frac{M_\delta^*}{\hat{M}_\delta^*}\left(C_1 + C_2 + \hat{M}_q^* + \hat{Z}_\alpha^*\right)\right\} \\
&\omega_n^2 = a_{1,11}a_{1,22} - a_{1,12}a_{1,21} = \left\{\left(Z_\alpha^*M_q^* - M_\alpha^*\right) - \frac{M_\delta^*}{\hat{M}_\delta^*}\left(Z_\alpha^*\hat{M}_q^* - \hat{M}_\alpha^*\right)\right\} \\
&\qquad\qquad + \frac{M_\delta^*}{\hat{M}_\delta^*}\left\{C_2\left(\hat{Z}_\alpha^* - Z_\alpha^*\right) + \left(C_1C_2+1\right)\right\}
\end{aligned}
\tag{2.43}
$$

When the uncertainties in every aerodynamic derivative estimate are neglected in (2.43), the closed-loop transfer function with BKS for the nominal case can be obtained as (2.19).

B Derivation of Transfer Function with IBKS

Using (2.18) with (2.1), (2.3) and (2.33) under the assumption of constant α_c and zero Z^*_δ, δ can be rearranged as follows.

$$\begin{aligned}\delta = &-\frac{1}{\hat{M}^*_\delta}\nu_{2,\alpha}\alpha - \frac{1}{\hat{M}^*_\delta}\nu_{2,q}q + \frac{1}{\hat{M}^*_\delta}\left(C_1C_2+1\right)\alpha_c \\ &+ \left(1 - \frac{M^*_\delta}{\hat{M}^*_\delta}\right)\delta\left(t-\tau\right) \\ &\text{where} \\ \nu_{2,\alpha} = &\left\{\left(C_1 + \hat{Z}^*_\alpha\right)\left(C_2 + Z^*_\alpha\right) + M^*_\alpha + 1\right\} \\ \nu_{2,q} = &\left(C_1 + C_2 + M^*_q + \hat{Z}^*_\alpha\right)\end{aligned} \tag{2.44}$$

Applying Laplace transform to (2.44) and arranging the equation with respect to δ,

$$\begin{aligned}\delta(s) = &\left[\begin{array}{cc} -\frac{1}{\phi(s)}\nu_{2,\alpha}(s) & -\frac{1}{\phi(s)}\nu_{2,q}(s)\end{array}\right]\mathbf{X}(s) \\ &+ \frac{1}{\phi(s)}\left(C_1C_2+1\right)\alpha_c(s) \\ &\text{where} \\ \phi(s) = &\hat{M}^*_\delta\left(1-e^{-\tau s}\right) + M^*_\delta e^{-\tau s}\end{aligned} \tag{2.45}$$

Dynamics for closed-loop analysis with IBKS is the same with (2.40) mentioned in the closed-loop analysis with BKS. If Laplace transform is applied to (2.40) and $\delta(s)$ in (2.45) is substituted into that equation, the closed-loop system with the IBKS can be derived, as follows.

$$\begin{aligned}&s\mathbf{X}(s) = \mathbf{A}_2(s)\mathbf{X}(s) + \mathbf{B}_2(s)\alpha_c(s) \qquad \mathbf{Y} = \mathbf{C}(s)\mathbf{X}(s) \\ &\mathbf{A}_2(s) = \left[\begin{array}{cc} a_{2,11}(s) & a_{2,12}(s) \\ a_{2,21}(s) & a_{2,22}(s)\end{array}\right] \\ &\quad = \left[\begin{array}{cc} Z^*_\alpha & 1 \\ M^*_\alpha - \frac{M^*_\delta}{\phi(s)}\nu_{2,\alpha}(s) & M^*_q - \frac{M^*_\delta}{\phi(s)}\nu_{2,q}(s)\end{array}\right] \\ &\mathbf{B}_2(s) = \left[\begin{array}{c} 0 \\ \frac{M^*_\delta}{\phi(s)}\left(C_1C_2+1\right)\end{array}\right] \\ &\mathbf{C}(s) = \left[\begin{array}{cc} 1 & 0\end{array}\right]\end{aligned} \tag{2.46}$$

Transfer function for the closed-loop system with IBKS can be derived as below.

$$\begin{aligned}
\frac{\alpha(s)}{\alpha_c(s)} &= \mathbf{C}(s)\left(s\mathbf{I} - \mathbf{A}_2(s)\right)^{-1}\mathbf{B}_2(s) \\
&= \frac{a_{2,12}\frac{M_\delta^*}{\phi(s)}\left(C_1C_2+1\right)}{s^2 - \left(a_{2,11}+a_{2,22}\right)s + \left(a_{2,11}a_{2,22} - a_{2,12}a_{2,21}\right)} = \frac{T(s)}{s^2+2\zeta\omega_n s+\omega_n^2}
\end{aligned}$$

where

$$\begin{aligned}
T(s) &= a_{2,12}(s)\frac{M_\delta^*}{\phi(s)}\left(C_1C_2+1\right) = \frac{M_\delta^*}{\phi(s)}\left(C_1C_2+1\right) \\
2\zeta\omega_n &= -\left(a_{2,11}(s)+a_{2,22}(s)\right) \\
&= -\left\{Z_\alpha^* + M_q^* - \frac{M_\delta^*}{\phi(s)}\left(C_1+C_2+M_q^*+\hat{Z}_\alpha^*\right)\right\} \\
\omega_n^2 &= a_{2,11}(s)a_{2,22}(s) - a_{2,12}(s)a_{2,21}(s) \\
&= \left(1-\frac{M_\delta^*}{\phi(s)}\right)\left(Z_\alpha^*M_q^* - M_\alpha^*\right) + \frac{M_\delta}{\phi(s)}\left\{C_2\left(\hat{Z}_\alpha^* - Z_\alpha^*\right) + \left(C_1C_2+1\right)\right\}
\end{aligned} \tag{2.47}$$

When the uncertainties do not exist in any aerodynamic derivative estimates, (2.47) becomes identical to (2.19), which is the closed-loop transfer function with IBKS for the nominal case.

C Aerodynamic Derivatives for Simulation

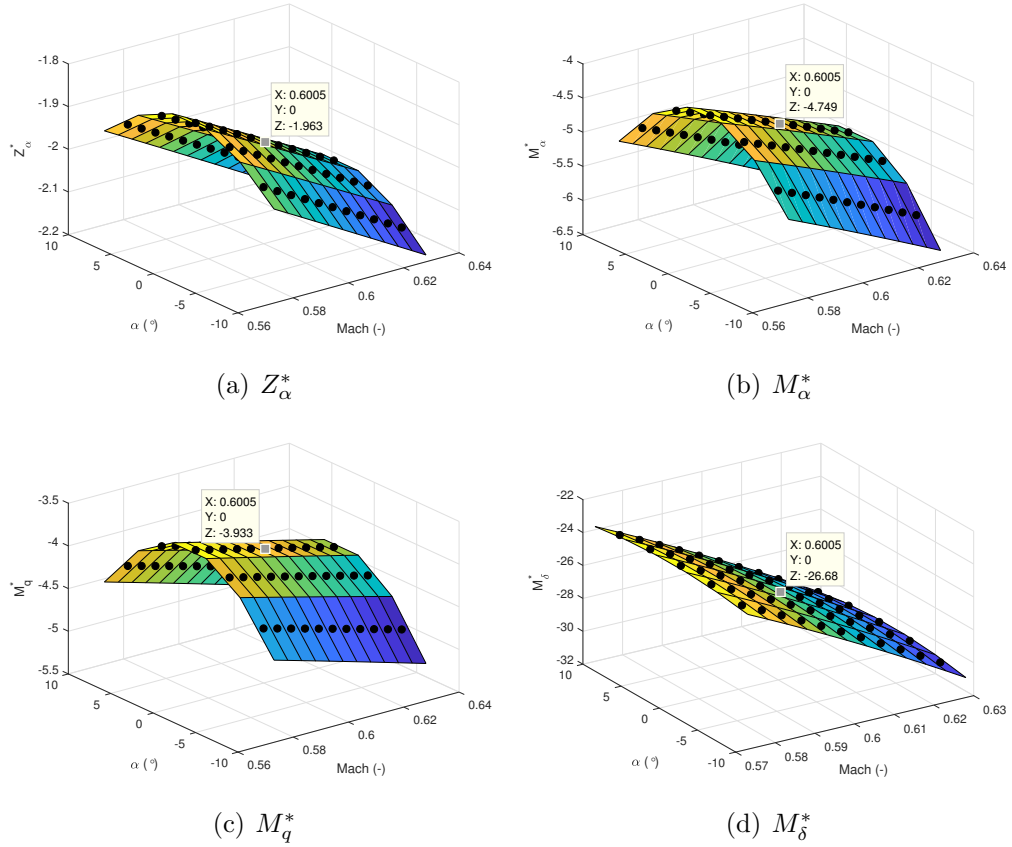

(a) Z^*_α (b) M^*_α

(c) M^*_q (d) M^*_δ

Figure 2.7: Aerodynamic Derivatives for Simulation

References

[1] Petar V Kokotovic. The joy of feedback: nonlinear and adaptive. *IEEE Control Systems Magazine*, 12(3):7–17, 1992.

[2] Taeyoung Lee and Youdan Kim. Nonlinear adaptive flight control using backstepping and neural networks controller. *Journal of Guidance, Control, and Dynamics*, 24(4):675–682, 2001.

[3] Jay Farrell, Manu Sharma, and Marios Polycarpou. Backstepping-based flight control with adaptive function approximation. *Journal of Guidance, Control, and Dynamics*, 28(6):1089–1102, 2005.

[4] Hann-Shing Ju and Ching-Chih Tsai. Longitudinal axis flight control law design by adaptive backstepping. *IEEE Transactions on Aerospace and Electronic Systems*, 43(1):311–329, 2007.

[5] Liang Sun and Wei Huo. 6-dof integrated adaptive backstepping control for spacecraft proximity operations. *IEEE Transactions on Aerospace and Electronic Systems*, 51(3):2433–2443, 2015.

[6] LR García Carrillo, Alejandro Dzul, and Rogelio Lozano. Hovering quad-rotor control: A comparison of nonlinear controllers using visual feedback. *IEEE Transactions on Aerospace and Electronic Systems*, 48(4):3159–3170, 2012.

[7] Xu Huang and Ye Yan. Saturated backstepping control of underactuated spacecraft hovering for formation flights. *IEEE Transactions on Aerospace and Electronic Systems*, 53(4):1988–2000, 2017.

[8] Lars Sonneveldt, QP Chu, and JA Mulder. Nonlinear flight control design using constrained adaptive backstepping. *Journal of Guidance, Control, and Dynamics*, 30(2):322–336, 2007.

[9] Baohua Lian and Hyochoong Bang. Momentum transfer-based attitude control of spacecraft with backstepping. *IEEE transactions on aerospace and electronic systems*, 42(2):453–463, 2006.

[10] Yoonsoo Kim and Byoung Soo Kim. Pitch autopilot design for agile missiles with uncertain aerodynamic coefficients. *IEEE Transactions on Aerospace and Electronic Systems*, 49(2):907–914, 2013.

[11] Jawhar Ghommam and Maarouf Saad. Autonomous landing of a quadrotor on a moving platform. *IEEE Transactions on Aerospace and Electronic Systems*, 53(3):1504–1519, 2017.

[12] Pieter van Gils, Erik-Jan Van Kampen, Coen C de Visser, and Q Ping Chu. Adaptive incremental backstepping flight control for a high-performance aircraft with uncertainties. In *AIAA Guidance, Navigation, and Control Conference*, 2016.

[13] Abdelouahed Ait Haddou Ali, Q Ping Chu, Erik-Jan Van Kampen, and Coen C de Visser. Exploring adaptive incremental backstepping using immersion and invariance for an f-16 aircraft. In *AIAA Guidance, Navigation, and Control Conference*, 2014.

[14] Paul Acquatella, E van Kampen, and Qi Ping Chu. Incremental backstepping for robust nonlinear flight control. In *Proceedings of the EuroGNC 2013, 2nd CEAS Specialist Conference on Guidance, Navigation and Control*, pages 1444–1463, 2013.

[15] Guillermo P Falconí, Valentin A Marvakov, and Florian Holzapfel. Fault tolerant control for a hexarotor system using incremental backstepping. In *2016 IEEE Conference on Control Applications (CCA)*, pages 237–242. IEEE, 2016.

[16] S Sieberling, QP Chu, and JA Mulder. Robust flight control using incremental nonlinear dynamic inversion and angular acceleration prediction. *Journal of guidance, control, and dynamics*, 33(6):1732–1742, 2010.

[17] Ewoud JJ Smeur, Qiping Chu, and Guido CHE de Croon. Adaptive incremental nonlinear dynamic inversion for attitude control of micro air vehicles. *Journal of Guidance, Control, and Dynamics*, 38(12):450–461, 2015.

[18] Xuerui Wang, Erik-Jan Van Kampen, Qiping Chu, and Peng Lu. Stability analysis for incremental nonlinear dynamic inversion control. *Journal of Guidance, Control, and Dynamics*, 42(5):1116–1129, 2019.

[19] Paul Acquatella, Wouter Falkena, Erik-Jan van Kampen, and Q Ping Chu. Robust nonlinear spacecraft attitude control using incremental nonlinear dynamic inversion. In *AIAA Guidance, Navigation, and Control Conference*, 2012.

[20] P Simplício, MD Pavel, E Van Kampen, and QP Chu. An acceleration measurements-based approach for helicopter nonlinear flight control using incremental nonlinear dynamic inversion. *Control Engineering Practice*, 21(8):1065–1077, 2013.

[21] Stephen H Lane and Robert F Stengel. Flight control design using non-linear inverse dynamics. *Automatica*, 24(4):471–483, 1988.

[22] Chang-Hun Lee, Byung-Eul Jun, and Jin-Ik Lee. Connections between linear and nonlinear missile autopilots via three-loop topology. *Journal of Guidance, Control, and Dynamics*, pages 1426–1432, 2016.

[23] Yunjun Xu. Multi-timescale nonlinear robust control for a miniature helicopter. *IEEE Transactions on Aerospace and Electronic systems*, 46(2):656–671, 2010.

[24] Romulus Lungu, Mihai Lungu, and Lucian Teodor Grigorie. Automatic control of aircraft in longitudinal plane during landing. *IEEE Transactions on Aerospace and Electronic Systems*, 49(2):1338–1350, 2013.

[25] Yuankai Li, Zhongliang Jing, and Guangjun Liu. Maneuver-aided active satellite tracking using six-dof optimal dynamic inversion control. *IEEE Transactions on Aerospace and Electronic Systems*, 50(1):704–719, 2014.

[26] Donald McLean. *Automatic flight control systems*. Prentice Hall, New York, 1990.

[27] Farid Golnaraghi and Benjamin C Kuo. *Automatic Control Systems*. John Wiley and Sons Ltd, 2009.

[28] Hassan K Khalil. *Nonlinear systems*. Upper Saddle River, 1996.

[29] Jean-Jacques E Slotine, Weiping Li, et al. *Applied nonlinear control*. Prentice hall Englewood Cliffs, NJ, 1991.

[30] I. Kanellakopoulos M. Krstic and P. Kokotovic. *Nonlinear and Adaptive Control*. John Wiley and Sons, Inc., New York, 1995.

[31] B. Kim et al. *Flight Dynamics and Control*. Kyung Moon Sa, 2004.

[32] Byoung-Ju Jeon, Min-Guk Seo, Hyo-Sang Shin, and Antonios Tsourdos. Understandings of the incremental backstepping control through theoretical analysis under the model uncertainties. In *2018 IEEE Conference on Control Technology and Applications (CCTA)*, pages 318–323. IEEE, 2018.

Chapter 3

Incremental Backstepping Control under Measurement Bias and Model Uncertainty

3.1 Introduction

Backstepping(BKS) method has been widely applied as one of nonlinear flight controllers. Nevertheless, it has a crucial drawback to be sensitive to model uncertainties because it requires explicit model information for its implementation. In reality, it is difficult to get an accurate model, so incremental backstepping(IBKS) algorithm is proposed to reduce model dependency of BKS. Thanks to additional measurements about state derivatives and control surface deflection angles, only control effectiveness information is required to implement IBKS.

There have been several researches [1–4] where closed loop characteristics with IBKS under model uncertainties can be found from numerical simulations or experiments. [5] suggested theoretical closed loop analysis results to have critical understandings about them. Previous studies indicate that IBKS has a strong advantage when model uncertainties exist; one of important characteristics obtained from the analysis in [5] is that a system is robust with respect to an uncertainty even in control effectiveness information if a control command is calculated, transmitted and reflected fast enough to a real control surface deflection. However, there is a limitation in previous works that measurements are assumed to be ideal, which is hard to be achieved in practical applications. If measurement related issues like a bias, a noise and a delay are

additionally considered, IBKS which lies in between model based and sensor based approach, might show worse performance than BKS.

In Chapter 3, closed loop analysis with IBKS considering both measurement biases and model uncertainties, is performed. The main purpose of this research is to have critical understandings about the effects of biases to system characteristics with IBKS, which can make aimed performance and stability characteristics difficult to be achieved. As previously mentioned, measurements about state derivatives and control surface deflection angles are additionally required to implement IBKS comparing to BKS, so biases on them are mainly considered in this analysis. Besides, in Chapter 3, it will be investigated whether closed loop system with IBKS is still robust with respect to model uncertainties although those biases are additionally considered.

In Section 3.2, dynamics for control law derivation will be suggested as a preliminary. In Section 3.3, a control algorithm using IBKS will be derived and proposed. In Section 3.4, closed loop analysis with IBKS considering both measurement biases and model uncertainties, is performed to have critical understandings especially about the effects of biases to a system. To verify properties obtained from Section 3.4, simulations will be carried out and following results will be suggested in Section 3.5.

3.2 Preliminary : Dynamics

For control law derivation and closed loop analysis, short period mode dynamics (3.1), one of the longitudinal oscillation modes with a high natural frequency, is applied. This simplified version of dynamics, not full 6-DoF dynamics, is utilized for simplicity of analysis. This short period mode is of paramount importance in flight control, because one of the main purposes of a stability augmentation system for an airplane is to improve characteristics about this mode. Since the main objective of Chapter 3 is to have critical understandings about closed loop characteristics with IBKS especially considering measurement biases, dynamics (3.1) is reasonable for this purpose.

$$\begin{aligned} \dot{\alpha} =& Z_{\alpha}^{*}(M,\alpha)\,\alpha + q + Z_{\delta}^{*}(M,\alpha)\,\delta \\ \dot{q} =& M_{\alpha}^{*}(M,\alpha)\,\alpha + M_{q}^{*}(M,\alpha)\,q + M_{\delta}^{*}(M,\alpha)\,\delta \end{aligned} \tag{3.1}$$

The state variables α and q indicate angle of attack and pitch rate. The control input δ represents elevator deflection angle. Z^*_α, Z^*_δ, M^*_α, M^*_q and M^*_δ denote aerodynamic derivatives where M corresponds to Mach number. Dynamics (3.1) can be regarded as a linear parameter-varying(LPV) system i.e., a nonlinear system which can be expressed into a parameterized linear system whose parameters change with the states.

3.3 Control Law Derivation

Before derivation of a control algorithm, dynamics (3.1) is modified as follows. First, aerodynamic derivatives estimates $\hat{(\cdot)}$ are utilized instead of real aerodynamic derivatives $(\cdot)$, because only estimated values are available in a controller design phase. Second, $\hat{Z}^*_\delta\delta$ related to non-minimum phase is neglected. IBKS control law is also based on backstepping method, so a system is required to be in strictly feedback form. This is valid for most of aircraft, often made in flight control systems' design process, because $\hat{Z}^*_\delta\delta$ is usually small enough comparing to the other terms in $\dot{\alpha}$ equation.

$$\begin{aligned} \dot{\alpha} &= \hat{Z}^*_\alpha\alpha + q \\ \dot{q} &= \hat{M}^*_\alpha\alpha + \hat{M}^*_q q + \hat{M}^*_\delta\delta \end{aligned} \tag{3.2}$$

The state errors are defined as follows.

$$\begin{aligned} z_1 &= \alpha - \alpha_c \\ z_2 &= q - q_c \end{aligned} \tag{3.3}$$

where subscript c represents a command.

If Lyapunov candidate function becomes positive definite and its derivative becomes negative definite, asymptotic stability for a nonlinear system can be guaranteed. To derive a control command which satisfies asymptotic stability assuming that $\hat{(\cdot)}$ have their true values, following 2 cascaded steps are performed.

First, Lyapunov function candidate V_1 considering only z_1 for an outer-loop controller design is selected as

$$V_1 = \frac{1}{2}z_1^2 \tag{3.4}$$

which is positive definite. The derivative of V_1 becomes

$$\begin{aligned}\dot{V}_1 &= z_1 \dot{z}_1 \\ &= z_1 \left(\hat{Z}_\alpha^* \alpha + q - \dot{\alpha}_c \right)\end{aligned} \tag{3.5}$$

In order to satisfy Lyapunov stability condition, a pseudo-command q_c is derived as

$$q_c \triangleq -C_1 z_1 - \hat{Z}_\alpha^* \alpha + \dot{\alpha}_c \tag{3.6}$$

which makes negative definite $\dot{V}_1 = -C_1 z_1^2$ where C_1 is a positive design parameter.

For the outer-loop controller design, classical BKS, not IBKS, is applied in Chapter 3. If IBKS is applied here for the outer loop control, $\dot{\alpha}_0$ measurement is additionally required instead of model information $\hat{Z}_\alpha^*$. There exist more practical ways to replace $\hat{Z}_\alpha^*$ information, so an incremental algorithm is not normally used for an outer loop control. This can be seen also in other papers [1] [3] [6] [7] which just applied BKS or PID for it.

For the second step to design an inner-loop controller, q dynamics in (3.2) is modified assuming that the states α, q and the control input δ can be expressed as combination of reference points $(\cdot)_0$ and perturbations $\Delta(\cdot)$ around them. This is a valid assumption especially with a sufficiently high sampling rate.

$$\begin{aligned}\dot{q} &= \hat{M}_\alpha^* (\alpha_0 + \Delta\alpha) + \hat{M}_q^* (q_0 + \Delta q) + \hat{M}_\delta^* (\delta_0 + \Delta\delta) \\ &= \dot{q}_0 + \hat{M}_\alpha^* \Delta\alpha + \hat{M}_q^* \Delta q + \hat{M}_\delta^* \Delta\delta\end{aligned} \tag{3.7}$$

The increments in states, $\Delta\alpha$ and Δq, are negligible comparing to the increment in input, Δu, since a control surface deflection directly affects pitch moment, while integrations are required first for states. Then, final incremental q dynamics for the inner loop controller design with IBKS is given as below.

$$\dot{q} \simeq \dot{q}_0 + \hat{M}_\delta^* \Delta\delta \tag{3.8}$$

In the second step, Lyapunov function candidate V_2 considering both z_1 and z_2 is selected as

$$V_2 = \frac{1}{2} z_1^2 + \frac{1}{2} z_2^2 \tag{3.9}$$

which is positive definite. The derivative of V_2 becomes

$$\begin{aligned}\dot{V}_2 &= z_1\dot{z}_1 + z_2\dot{z}_2 \\ &= z_1\left(\hat{Z}_\alpha^*\alpha + q - \dot{\alpha}_c\right) + z_2\left(\dot{q}_0 + \hat{M}_\delta^*\Delta\delta - \dot{q}_c\right)\end{aligned} \tag{3.10}$$

Using the pseudo-command (3.6), $\dot{V}_2$ becomes

$$\dot{V}_2 = z_1\left(-C_1 z_1 + z_2\right) + z_2\left(\dot{q}_0 + \hat{M}_\delta^*\Delta\delta - \dot{q}_c\right) \tag{3.11}$$

To satisfy Lyapunov stability condition, $\Delta\delta$ is derived as

$$\Delta\delta \triangleq \frac{1}{\hat{M}_\delta^*}\left(-C_2 z_2 - z_1 - \dot{q}_0 + \dot{q}_c\right) \tag{3.12}$$

which makes negative definite $\dot{V}_2 = -C_1 z_1^2 - C_2 z_2^2$ where C_1 and C_2 are positive design parameters.

Final form of the control law can be suggested as follows.

$$\begin{aligned}q_c &= -C_1 z_1 - \hat{Z}_\alpha^*\alpha + \dot{\alpha}_c \\ \delta &= \delta_0 + \Delta\delta \\ &= \frac{1}{\hat{M}_\delta^*}\left(-C_2 z_2 - z_1 - \dot{q}_0 + \dot{q}_c\right) + \delta_0\end{aligned} \tag{3.13}$$

δ makes q to achieve q_c, and α goes to its desired value α_c by q_c. For implementation of a control algorithm, only $\hat{Z}_\alpha^*$ and $\hat{M}_\delta^*$ are required, and $\hat{M}_\alpha^*$ and $\hat{M}_q^*$ are not necessary because the incremental dynamics about q is utilized for a derivation process of IBKS as an inner loop controller. Hence, comparing to BKS only controller, model information is less required and a system becomes robust with respect to the uncertainties in $\hat{M}_\alpha^*$ and $\hat{M}_q^*$. Instead, the additional measurements δ_0 and $\dot{q}_0$ are required to compensate them.

3.4 Closed-loop Analysis

Closed-loop analysis considering both biases on additional measurements and model uncertainties, is performed. As in [8], analysis is carried out in piece-wise way to easily apply existing analysis framework for a linear time-invariant(LTI) system. The effects of measurement biases, which can make aimed performance and stability

characteristics in a controller design phase difficult to be achieved, are investigated.

Dynamics (3.1) with $Z_\delta^* = 0$ can be expressed as a state space equation (3.14) below. In general, $\hat{Z}_\delta^*$ is small enough to be neglected, especially for large airplanes.

$$\begin{aligned}
&\dot{\mathbf{x}} = \mathbf{A}\mathbf{x} + \mathbf{B}\mathbf{u} \qquad \mathbf{y} = \mathbf{C}\mathbf{x} \\
&\text{where} \\
&\mathbf{x} = \begin{bmatrix} \alpha & q \end{bmatrix}^T \qquad \mathbf{u} = \delta \\
&\mathbf{A} = \begin{bmatrix} Z_\alpha^* & 1 \\ M_\alpha^* & M_q^* \end{bmatrix} \quad \mathbf{B} = \begin{bmatrix} 0 \\ M_\delta^* \end{bmatrix} \quad \mathbf{C} = \begin{bmatrix} 1 & 0 \end{bmatrix}
\end{aligned} \tag{3.14}$$

Comparing to the dynamics (3.2) for the control law derivation, real aerodynamic derivatives, not estimates, are considered in this dynamics (3.14) for the analysis.

In (3.13), δ can be rewritten as follows by substituting q_c, under the assumption of constant α_c (i.e. $\dot{\alpha}_c = \ddot{\alpha}_c = 0$).

$$\begin{aligned}
\delta = &\frac{1}{\hat{M}_\delta^*} \Big\{ - \left(C_1 + \hat{Z}_\alpha^* \right) \left(C_2 + Z_\alpha^* \right) \alpha - \left(C_1 + C_2 + \hat{Z}_\alpha^* \right) q \\
&+ C_1 C_2 \alpha_c - z_1 \Big\} - \frac{1}{\hat{M}_\delta^*} \dot{q}_0 + \delta_0
\end{aligned} \tag{3.15}$$

As mentioned in Section 3.3, measurements δ_0 and $\dot{q}_0$ are additionally required to implement IBKS. Hence, if there exist biases on these additional measurement, as an innerloop controller, IBKS might show worse performance than BKS. In Chapter 3, biases on δ_0 and $\dot{q}_0$ measurements, $b_{\dot{q}_0}$ and b_{δ_0}, are considered in closed loop analysis as follows, to have critical understandings about the effects of them to system characteristics with IBKS.

$$\begin{aligned}
\dot{q}_0 &= \dot{q}_{0,true} + b_{\dot{q}_0} \\
\delta_0 &= \delta_{0,true} + b_{\delta_0} \\
&\text{where} \\
\dot{q}_{0,true} &= M_\alpha^* \alpha + M_q^* q + M_\delta^* \delta_{0,true} \\
\delta_{0,true} &= \delta(t - \tau)
\end{aligned} \tag{3.16}$$

From a piece-wise version of (3.1), the model for $\dot{q}_{0,true}$ in (3.16) is suggested. Under the assumption of an ideal actuator, a control surface deflection becomes the same as a generated control command. Then, $\delta_{0,true}$ can be regarded as a control command generated in previous step, where τ indicates a step size.

By substituting (3.16) to (3.15), δ can be rearranged as below.

$$\begin{aligned}\delta = &-\frac{1}{\hat{M}_\delta^*}\nu_{2,\alpha}\alpha - \frac{1}{\hat{M}_\delta^*}\nu_{2,q}q + \frac{1}{\hat{M}_\delta^*}\left(C_1C_2+1\right)\alpha_c \\ &+ \left(1-\frac{M_\delta^*}{\hat{M}_\delta^*}\right)\delta\left(t-\tau\right) - \frac{1}{\hat{M}_\delta^*}b_{\dot{q}_0} + b_{\delta_0} \\ &\text{where} \\ &\nu_\alpha = \left\{\left(C_1+\hat{Z}_\alpha^*\right)\left(C_2+Z_\alpha^*\right) + M_\alpha^* + 1\right\} \\ &\nu_q = \left(C_1+C_2+M_q^*+\hat{Z}_\alpha^*\right)\end{aligned} \tag{3.17}$$

Applying Laplace transform to (3.17) and arranging this equation with respect to δ,

$$\begin{aligned}\delta(s) = &\left[\begin{array}{cc} -\frac{1}{\phi(s)}\nu_\alpha(s) & -\frac{1}{\phi(s)}\nu_q(s)\end{array}\right]\mathbf{X}(s) \\ &+ \frac{1}{\phi(s)}\left(C_1C_2+1\right)\alpha_c(s) - \frac{1}{\phi(s)}b_{\dot{q}_0} + \frac{\hat{M}_\delta^*}{\phi(s)}b_{\delta_0} \\ &\text{where} \\ &\phi(s) = \hat{M}_\delta^*\left(1-e^{-\tau s}\right) + M_\delta^* e^{-\tau s}\end{aligned} \tag{3.18}$$

If Laplace transform is applied to (3.14) and $\delta(s)$ in (3.18) is substituted into that equation, a closed loop system can be suggested, as follows.

$$
\begin{aligned}
&s\mathbf{X}(s) = \mathbf{A}(s)\mathbf{X}(s) + \mathbf{B}(s)\alpha_c(s) + \mathbf{D}(s)\mathbf{b}(s) \\
&\mathbf{Y} = \mathbf{C}(s)\mathbf{X}(s) \\
&\text{where} \\
&\mathbf{A}(s) = \begin{bmatrix} a_{2,11}(s) & a_{2,12}(s) \\ a_{2,21}(s) & a_{2,22}(s) \end{bmatrix} \\
&\qquad = \begin{bmatrix} Z_\alpha^* & 1 \\ M_\alpha^* - \frac{M_\delta^*}{\phi(s)}\nu_{2,\alpha}(s) & M_q^* - \frac{M_\delta^*}{\phi(s)}\nu_{2,q}(s) \end{bmatrix} \\
&\mathbf{B}(s) = \begin{bmatrix} 0 \\ \frac{M_\delta^*}{\phi(s)}\left(C_1C_2+1\right) \end{bmatrix} \\
&\mathbf{C}(s) = \begin{bmatrix} 1 & 0 \end{bmatrix} \\
&\mathbf{D}(s) = \begin{bmatrix} 0 & 0 \\ -\frac{M_\delta^*}{\phi(s)} & \frac{M_\delta^*\hat{M}_\delta^*}{\phi(s)} \end{bmatrix} \\
&\mathbf{b}(s) = \begin{bmatrix} b_{\dot{q}_0}(s) \\ b_{\delta_0}(s) \end{bmatrix}
\end{aligned}
\tag{3.19}
$$

Then $\alpha(s)$ can be derived as below.

$$
\begin{aligned}
\alpha(s) &= \mathbf{C}(s)\left\{s\mathbf{I} - \mathbf{A}(s)\right\}^{-1}\left\{\mathbf{B}(s)\alpha_c(s) + \mathbf{D}(s)\mathbf{b}(s)\right\} \\
&= \frac{1}{s^2 - \left(a_{2,11} + a_{2,22}\right)s + \left(a_{2,11}a_{2,22} - a_{2,12}a_{2,21}\right)} \\
&\left\{\frac{M_\delta^*}{\phi(s)}\left(C_1C_2+1\right)\alpha_c(s) - \frac{M_\delta^*}{\phi(s)}b_{\dot{q}_0}(s) + \frac{M_\delta^*\hat{M}_\delta^*}{\phi(s)}b_{\delta_0}(s)\right\}
\end{aligned}
\tag{3.20}
$$

(3.20) can be simplified as (3.21) assuming $\tau \simeq 0$ for analysis purpose.

$$
\begin{aligned}
&\alpha(s) = \frac{T(s)}{s^2 + 2\zeta\omega_n s + \omega_n^2} \\
&\text{where} \\
&T(s) = \left(C_1C_2+1\right)\alpha_c(s) - b_{\dot{q}_0}(s) + \hat{M}_\delta^* b_{\delta_0}(s) \\
&2\zeta\omega_n = \left(C_1 + C_2\right) + \left(\hat{Z}_\alpha^* - Z_\alpha^*\right) \\
&\omega_n^2 = \left(C_1C_2+1\right) + C_2\left(\hat{Z}_\alpha^* - Z_\alpha^*\right)
\end{aligned}
\tag{3.21}
$$

ζ and ω_n represent a damping ratio and a natural frequency for the closed loop system.

Absolute stability is normally guaranteed for a damped system, so a condition $\mathscr{G}$ to maintain stability under measurement biases and model uncertainties can be proposed from $2\zeta\omega_n > 0$ (Cond.1) under $\omega_n^2 > 0$ (Cond.2) as follows.

$$\begin{aligned} \mathscr{G} &= \left\{C_1, C_2 \in \mathbb{R}_{>0} | \text{Cond. 1 \& Cond. 2}\right\} \\ \text{Cond. 1} &: C_1 + C_2 > -Z_\alpha^* \Delta_{Z_\alpha^*} \\ \text{Cond. 2} &: C_1 C_2 + C_2 Z_\alpha^* \Delta_{Z_\alpha^*} > -1 \end{aligned} \tag{3.22}$$

$\Delta_{(\cdot)}$ indicates an uncertainty in aerodynamic derivative estimates $\hat{(\cdot)} = (\cdot)\left\{1 + \Delta_{(\cdot)}\right\}$.

$\alpha_c(s) = \frac{\alpha_c}{s}$, $b_{\dot{q}_0}(s) = \frac{b_{\dot{q}_0}}{s}$, and $b_{\delta_0}(s) = \frac{b_{\delta_0}}{s}$ for a step input and constant biases. Then, $\alpha(s)$ becomes

$$\alpha(s) = \frac{\left(C_1 C_2 + 1\right)\alpha_c - b_{\dot{q}_0} + \hat{M}_\delta^* b_{\delta_0}}{s^2 + 2\zeta\omega_n s + \omega_n^2} \frac{1}{s} \tag{3.23}$$

Steady state error e_{ss} can be derived from

$$e_{ss} = \alpha_c - \lim_{t\to\infty} \alpha(t) = \alpha_c - \lim_{s\to 0} s\alpha(s) \tag{3.24}$$

Then, e_{ss} can be suggested as below.

$$\begin{aligned} e_{ss} &= \frac{\eta_2}{\eta_1 + \eta_2}\alpha_c + \frac{1}{\eta_1 + \eta_2} b_{\dot{q}_0} + \frac{\eta_3}{\eta_1 + \eta_2} b_{\delta_0} \\ &\text{where} \\ \eta_1 &= C_1 C_2 + 1 \\ \eta_2 &= C_2\left(\hat{Z}_\alpha - Z_\alpha\right) \qquad \eta_3 = -\hat{M}_\delta^* \end{aligned} \tag{3.25}$$

From the closed loop analysis above, following two main observations can be found, and they can be further understood by comparing to [5] where closed-loop analysis with the same control structure was carried out only considering model uncertainties under the assumption of perfect measurements.

First, $b_{\dot{q}_0}$ and b_{δ_0} do not affect the characteristic equation which is the same as the one in [5] without considering biases. Hence, the condition for absolute stability (3.22) becomes the same with the one in [5] to maintain stability just under the model uncertainties. Unlike $\Delta_{Z_\alpha^*}$ from BKS for the outerloop, $\Delta_{M_\delta^*}$ from IBKS for

the innerloop doesn't have any impact.

Second, $b_{\dot{q}_0}$ and b_{δ_0} additionally cause the second and the third terms in steady state error (3.24) where the first term is identical to the one in [5]. One of important characteristics obtained from the analysis in [5] is that the system is robust with respect to $\Delta_{M_\delta^*}$ if a control command is calculated, transmitted and reflected fast enough to a real control surface deflection, even though M_δ^* information is required for implementation of IBKS. However, if $b_{\dot{q}_0}$ and b_{δ_0} are considered, $\Delta_{M_\delta^*}$ starts to have an impact to the steady state error, as it can be seen especially in b_{δ_0} related term of (3.25).

3.5 Simulation

Simulations are carried out to verify theoretical analysis results suggested in Section 3.4. With a piece-wise approach as in [8], several points for each grid were simulated, and as an example, results when altitude is 7.6200km and $U_0 = 185.9280$m/s are suggested in Chapter 3. The corresponding aerodynamic derivatives are $Z_\alpha^* = -1.963$, $Z_\delta^* = 0$, $M_\alpha^* = -4.749$, $M_q^* = -3.933$ and $M_\delta^* = -26.68$.

Simulation parameters such as an angle of attack command, design parameters, level of a model uncertainty in control effectiveness information, and biases on additional measurements are suggested in table 1. The initial values for α and q are 0° and 0°/s. Small enough $\tau = 0.001sec$ is applied for the simulation. The effects of $\Delta_{Z_\alpha^*}$ to this closed loop system comes from BKS for the outerloop. Since the main objective of this research is to have critical understandings with IBKS, it is assumed in this simulation that there is no model uncertainty in $\hat{Z}_\alpha^*$. As suggested in Section 3.4, the condition to guarantee absolute stability for the system is only affected by $\Delta_{Z_\alpha^*}$. Without $\Delta_{Z_\alpha^*}$, absolute stability can be accomplished just with positive design parameters, as intended in previous controller design process. Theoretical analysis results indicate that a primary effect of biases on additional measurements is in a steady state error, so stable cases with $\Delta_{Z_\alpha^*} = 0$ are examined in this simulation.

Closed loop system responses obtained from simulations considering only $b_{\dot{q}_0}$ are suggested in Fig.3.1, and e_{ss} values predicted by (3.25) for corresponding cases are summarized in Table 3.2. When b_{δ_0} is only considered, simulation results are proposed in Fig.3.2 and predicted steady state errors by (3.25) are suggested in Table 3.3. Since $\hat{Z}_\alpha^*$ information is assumed not to have any uncertainty in this

Table 3.1: Simulation Parameters

Parameter	Value
α_c	$1.5°$
C_1, C_2	1.5
$\Delta_{\hat{M}_\delta^*}$	$[-0.25,\ 0,\ 0.25]$
$b_{\dot{q}_0}, b_{\delta_0}$	$[-0.1,\ 0.1]$

Table 3.2: Predicted Steady State Error e_{ss} by (3.25) with $b_{\dot{q}_0}$

$\Delta_{M_\delta^*}$ \ $b_{\dot{q}_0}$	$-0.1°/s$	$0.1°/s$
-0.25	$-0.0308°$	$0.0308°$
0	$-0.0308°$	$0.0308°$
0.25	$-0.0308°$	$0.0308°$

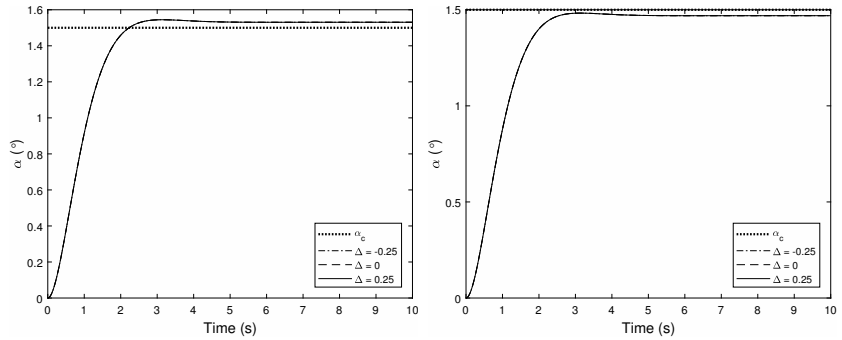

(a) Time response when $b_{\dot{q}_0} = -0.1$ (b) Time response when $b_{\dot{q}_0} = 0.1$

Figure 3.1: Closed-loop System Response with $b_{\dot{q}_0}$

simulation, ζ and ω_n of the system doesn't change depending on cases as expected, resulting in the same rising and settling time for Fig.3.1 and Fig.3.2. Steady state errors identified from simulations and predicted from the analysis result (3.25) are shown to be the same for every cases. Additionally, following phenomena observed in Fig.3.1 and Fig.3.2 can be also understood from (3.25). While $\Delta_{M_\delta^*}$ has an impact on steady state errors induced by b_{δ_0}, steady state errors induced by $b_{\dot{q}_0}$ are not affected by $\Delta_{M_\delta^*}$. Besides, the effect of b_{δ_0} is appeared to be bigger than of $b_{\dot{q}_0}$ in steady state error point of view, because $|\hat{M}_\delta^*| > 1$ in this simulation.

Table 3.3: Predicted Steady State Error e_{ss} by (3.25) with b_{δ_0}

$\Delta_{M_\delta^*}$ \ b_{δ_0}	$-0.1°$	$0.1°$
-0.25	$-0.6158°$	$0.6158°$
0	$-0.8211°$	$0.8211°$
0.25	$-1.0263°$	$1.0263°$

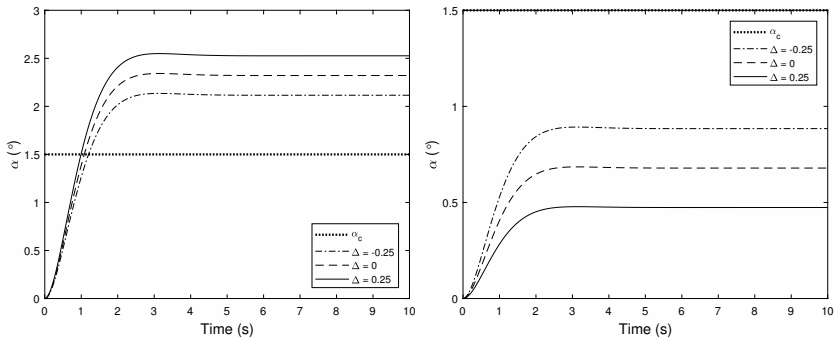

(a) Time response when $b_{\delta_0} = -0.1$ (b) Time response when $b_{\delta_0} = 0.1$

Figure 3.2: Closed-loop System Response with b_{δ_0}

3.6 Conclusion

In Chapter 3, closed loop analysis with IBKS considering both measurement biases and model uncertainties, is performed to have critical understandings especially about measurement bias effects. In previous study where closed loop characteristics with IBKS considering only model uncertainties are investigated, it is shown that a system is robust with respect to an uncertainty even in control effectiveness information if a control command is calculated, transmitted and reflected fast enough to a real control surface deflection. However, if measurement biases are additionally considered, the analysis results in Chapter 3 indicate that a model uncertainty in control effectiveness information starts to have an impact to a steady state error. These biases on additional measurements cause a steady state error, but they do not have any impact to the characteristic equation. These properties obtained from the analysis are verified through simulations.

References

[1] Pieter van Gils, Erik-Jan Van Kampen, Coen C de Visser, and Q Ping Chu. Adaptive incremental backstepping flight control for a high-performance aircraft with uncertainties. In *AIAA Guidance, Navigation, and Control Conference*, 2016.

[2] Abdelouahed Ait Haddou Ali, Q Ping Chu, Erik-Jan Van Kampen, and Coen C de Visser. Exploring adaptive incremental backstepping using immersion and invariance for an f-16 aircraft. In *AIAA Guidance, Navigation, and Control Conference*, 2014.

[3] Paul Acquatella, E van Kampen, and Qi Ping Chu. Incremental backstepping for robust nonlinear flight control. In *Proceedings of the EuroGNC 2013, 2nd CEAS Specialist Conference on Guidance, Navigation and Control*, pages 1444–1463, 2013.

[4] Guillermo P Falconí, Valentin A Marvakov, and Florian Holzapfel. Fault tolerant control for a hexarotor system using incremental backstepping. In *2016 IEEE Conference on Control Applications (CCA)*, pages 237–242. IEEE, 2016.

[5] Byoung-Ju Jeon, Min-Guk Seo, Hyo-Sang Shin, and Antonios Tsourdos. Understandings of the incremental backstepping control through theoretical analysis under the model uncertainties. In *2018 IEEE Conference on Control Technology and Applications (CCTA)*, pages 318–323. IEEE, 2018.

[6] S Sieberling, QP Chu, and JA Mulder. Robust flight control using incremental nonlinear dynamic inversion and angular acceleration prediction. *Journal of guidance, control, and dynamics*, 33(6):1732–1742, 2010.

[7] Ewoud JJ Smeur, Qiping Chu, and Guido CHE de Croon. Adaptive incremental nonlinear dynamic inversion for attitude control of micro air vehicles. *Journal of Guidance, Control, and Dynamics*, 38(12):450–461, 2016.

[8] Chang-Hun Lee, Byung-Eul Jun, and Jin-Ik Lee. Connections between linear and nonlinear missile autopilots via three-loop topology. *Journal of Guidance, Control, and Dynamics*, pages 1426–1432, 2016.

[9] Jean-Jacques E Slotine, Weiping Li, et al. *Applied nonlinear control*. Prentice hall Englewood Cliffs, NJ, 1991.

[10] Hassan K Khalil. *Nonlinear systems*. Upper Saddle River, 1996.

[11] I. Kanellakopoulos M. Krstic and P. Kokotovic. *Nonlinear and Adaptive Control*. John Wiley and Sons, Inc., New York, 1995.

[12] B. Kim et al. *Flight Dynamics and Control*. Kyung Moon Sa, 2004.

[13] Farid Golnaraghi and Benjamin C Kuo. *Automatic Control Systems*. John Wiley and Sons Ltd, 2009.

Chapter 4

Incremental Backstepping Control under Measurement Delay and Model Uncertainty

4.1 Introduction

Backstepping control [1] is one of the most widely and successfully applied nonlinear methodologies for a flight control system design [2–10]. One of the issues about a classical backstepping(BKS) controller is that it is sensitive to model uncertainties, because full model information is explicitly required for its implementation. Note that it is difficult to get an accurate model from a wind tunnel test or an aero-prediction in general. To reduce model dependency of BKS, incremental backstepping(IBKS) controller [11–19] is proposed. Comparing to BKS, IBKS additionally utilizes state derivative and control surface deflection angle measurements which replace required knowledge about a model except control effectiveness information. This algorithm becomes implicit, not totally relying on explicit model information for its implementation.

Since IBKS lies in between sensor based and model based approaches, it is essential to understand the effects of measurement defects such as bias, noise, and delay along with model uncertainties to the closed loop system. There have been some researches investigating closed loop characteristics with IBKS only considering model uncertainties [11–16]. One of the key findings from theoretical analyses in [15] and [16] is that the system is robust with respect to any model uncertainties even in con-

trol effectiveness information if a control command is calculated, transmitted and reflected fast enough to a real control surface deflection. The limitation of analyses in previous studies is that measurements are assumed to be ideal, which is impossible in practical applications. If measurement defects are additionally considered, IBKS might show worse performance than BKS. [17] suggested closed loop analysis results with consideration of measurement biases together with model uncertainties. This study indicates that measurement biases only cause additional steady state error. One of the interesting observations is that a model uncertainty in control effectiveness information starts to have an impact to the closed loop system when these measurement biases are additionally considered. To the best of our knowledge, there are no existing researches about IBKS analysis considering measurement delays along with model uncertainties.

Unlike IBKS, there have been some studies [20–22] about incremental nonlinear dynamic inversion(INDI) with consideration of measurement delays. INDI[20–25] is an incremental version of NDI[26], as IBKS to BKS. Relevant studies with INDI can shed some lights on our analysis with IBKS, but they also have limitations as follows. [20] and [21] only consider delay in the state derivative measurement induced by a filter to attenuate noise which is amplified during state differentiation process. In [22], induced delay from a filter on the state derivative measurement path for noise attenuation together with sensor delays are considered during a flight test. [20–22] briefly mention that measurement delays have critical impacts on the closed loop system with the incremental algorithm. [22] indicates that synchronization between state derivative and control surface deflection angle measurements is essential for a successful flight test with INDI. However, [20–22] just focused on algorithm designs to avoid delay issues without systematic analysis or sufficient interpretations on the effects of measurement delays to the system.

Despite their limitation in detailed analysis, there is a valuable lesson to be learned from the previous studies with INDI [20–22] that it is important to have critical understandings and insights about the effects of measurement delays to the closed loop system with the incremental algorithm. Besides, the literature review about IBKS [17] shows possibility that the model uncertainty in control effectiveness information starts to have an impact on the closed loop system when measurement defects like delays are additionally considered. Hence, analysis framework and results considering both measurement delays and model uncertainties which are inevitable in reality, should be beneficial in designing and applying IBKS algorithm to actual aircraft systems.

To this end, Chapter 4 aims to suggest a closed loop analysis framework and system characteristics for IBKS, especially with consideration of measurement delays along with model uncertainties. One of the biggest challenges to achieve this research goal is that it is difficult to judge even absolute stability of the system in an analytic way due to exponential terms in a characteristic equation generated from measurement delays. There have been several studies [27–33] about analysis for delayed systems. For the analysis, [27, 28, 30] approximate the exponential term using Taylor series expansion, assuming that delay is small enough. One of the limitations in this approach is that it is difficult to judge whether the existing delay is within an acceptable range so that this assumption holds. Besides, with a simple example, [29] shows that stability conditions obtained with Taylor series expansion are too sensitive to the order of the approximation and they do not even match well with those of the actual system. Rekasius substitution and Routh-Hurwitz criterion are applied in [31] for stability analysis of time-delayed LTI systems, which is applicable only when magnitudes of delays are identical for all the delayed signals. [33] utilizes Euler's formula to handle the exponential terms, and finds poles by defining a positive semi-definite metric function to become zero only at the poles. The pole search is conducted in a heuristic way as discretizing a complex plane and figuring out grid points in the right half plane where each metric function value becomes smaller than a threshold value. This implies that performance of the algorithm is highly dependent on grid settings, so it might be difficult to guarantee system stability even when no grid point was found in the right half plane with the metric function value under the threshold. If a grid size is reduced, probability of having grid points right on the poles could be increased. Still, it does not guarantee an accurate search while elevating the computation load.

To tackle the main technical issue mentioned above which makes difficult to suggest the aimed research results, Chapter 4 proposes analysis framework with an optimization concept to efficiently and systematically examine the existence of the poles in the right half plane. Proposed framework successfully works, even for a highly nonlinear metric function with a complex shape due to the considered measurement delays. By applying the suggested numerical framework, closed loop characteristics under measurement delays and model uncertainties especially in stability point of view are investigated. A stability condition for the closed-loop system with IBKS about the relationship between delays on state derivative and control surface deflection angle measurements is provided, and it is shown that this condition is affected by the model uncertainty. A comparative study which enables critical understandings about individual and integrated effects of the measurement delays and the model

uncertainties to the closed loop system with IBKS is suggested.

The rest of Chapter 4 is organized as follows. In Section 4.2, dynamics and derived control algorithm with IBKS are provided as preliminaries. Section 4.3 performs closed loop analysis with IBKS when both measurement delays and model uncertainties are considered. Numerical analysis framework is proposed and system characteristics obtained from the framework are suggested. A comparative study is performed to have critical understandings about individual and integrated effects of these defects to the system. Simulations are carried out for verification and validation of the analysis results obtained from the proposed framework. From simulation results, properties about robustness and performance are additionally investigated.

4.2 Preliminaries

For the closed loop analysis in Section 4.3, dynamics and control algorithm are suggested in Section 4.2. Short period mode dynamics and derived control law with IBKS are given in Section 4.2.1 and 4.2.2 respectively. Note that Chapter 4 utilizes IBKS for the inner controller design and BKS for the outer loop controller design. As can be seen in [11, 13, 16, 20] and [21], the incremental control algorithm is not generally applied for the outer loop, because more practical ways are available to compensate the required model information without utilizing additional measurements in the outerloop.

4.2.1 Dynamics

Chapter 4 considers short period mode dynamics in [34]. Note that the short period mode is of paramount importance in the flight control design because one of the main purposes of a stability augmentation system(SAS) for an aircraft is to enhance this short period mode characteristics.

$$
\begin{aligned}
\dot{\alpha} =& Z_{\alpha}^{*}(M,\alpha)\,\alpha + q + Z_{\delta}^{*}(M,\alpha)\,\delta \\
\dot{q} =& M_{\alpha}^{*}(M,\alpha)\,\alpha + M_{q}^{*}(M,\alpha)\,q + M_{\delta}^{*}(M,\alpha)\,\delta
\end{aligned}
$$

where

$$
\begin{aligned}
Z_{\alpha}^{*}(M,\alpha) &= \frac{\bar{q}S}{m} C_{Z_{\alpha}}(M,\alpha)\,\frac{1}{U_0} \\
Z_{\delta}^{*}(M,\alpha) &= \frac{\bar{q}S}{m} C_{Z_{\delta}}(M,\alpha)\,\frac{1}{U_0} \\
M_{\alpha}^{*}(M,\alpha) &= \frac{\bar{q}S\bar{c}}{I_y} C_{M_{\alpha}}(M,\alpha) \\
&\quad + \frac{\bar{q}S\bar{c}^2}{2I_y U_0} C_{M_{\dot{\alpha}}}(M,\alpha)\,\frac{\bar{q}S}{m} C_{Z_{\alpha}}(M,\alpha)\,\frac{1}{U_0} \\
M_{q}^{*}(M,\alpha) &= \frac{\bar{q}S\bar{c}^2}{2I_y U_0} C_{M_q}(M,\alpha) + \frac{\bar{q}S\bar{c}^2}{2I_y U_0} C_{M_{\dot{\alpha}}}(M,\alpha) \\
M_{\delta}^{*}(M,\alpha) &= \frac{\bar{q}S\bar{c}}{I_y} C_{M_{\delta}}(M,\alpha) \\
&\quad + \frac{\bar{q}S\bar{c}^2}{2I_y {U_0}^2} C_{M_{\dot{\alpha}}}(M,\alpha)\,\frac{\bar{q}S}{m} C_{Z_{\delta}}(M,\alpha)
\end{aligned}
\tag{4.1}
$$

State variables α and q denote for an angle of attack and a pitch rate, respectively. Control input δ indicates a deflection angle of an elevator. $\bar{q}$, U_0 and M are dynamic pressure, constant velocity and Mach number of an aircraft. For notational convenience, aerodynamic derivatives given as functions of M and α will be represented in shorthand form as Z_{α}^{*}, Z_{δ}^{*}, M_{α}^{*}, M_{q}^{*} and M_{δ}^{*}. $C_{(.)}$ indicates dimensionless aerodynamic coefficients. S, $\bar{c}$, m and I_y denote reference area, reference length, mass and moment of inertia in y-axis of an aircraft, respectively.

Dynamics (4.1) describes a linear parameter-varying(LPV) system, i.e., a nonlinear system which can be expressed as a parameterized linear system with parameters changing with state variables. In Chapter 4, short period mode dynamics (4.1), not full 6-DoF dynamics, is utilized for simplicity of the analysis. This research could be extended for the analysis with full 6-DoF dynamics in a future work.

Since IBKS is based on the backstepping algorithm which requires that dynamics should be in strict feedback form, $\hat{Z}_{\delta}^{*}\delta$ term related to non-minimum phase is ignored in (4.1), resulting in (4.2).

$$\begin{aligned} \dot{\alpha} &= Z_{\alpha}^{*}\alpha + q \\ \dot{q} &= M_{\alpha}^{*}\alpha + M_{q}^{*}q + M_{\delta}^{*}\delta \end{aligned} \tag{4.2}$$

In order to make the system in lower-triangular form, a fin surface is assumed to be a pure moment generator. This is a reasonable assumption for most of aircraft, often made in flight controller design, since C_{Z_δ} is generally small enough to be neglected [34].

For the inner-loop control algorithm design with IBKS, q dynamics in (4.2) is modified as (4.3), under the assumption that the states α, q and the control input δ can be represented as combinations of reference points $(\cdot)_0$ and perturbations $\Delta(\cdot)$ around them, which is valid especially with a sufficiently high sampling rate.

$$\begin{aligned} \dot{q} &= M_{\alpha}^{*}\left(\alpha_0 + \Delta\alpha\right) + M_{q}^{*}\left(q_0 + \Delta q\right) + M_{\delta}^{*}\left(\delta_0 + \Delta\delta\right) \\ &= \dot{q}_0 + M_{\alpha}^{*}\Delta\alpha + M_{q}^{*}\Delta q + M_{\delta}^{*}\Delta\delta \end{aligned} \tag{4.3}$$

As described in [11, 16, 20, 23] and [24], the increments of states, $\Delta\alpha$ and Δq, have much less effects on q dynamics than the increments of control input, $\Delta\delta$. This results in the incremental dynamics (4.4) for the inner loop control system design with IBKS, which is obtained by neglecting $\Delta\alpha$ and Δq in (4.3).

$$\dot{q} \simeq \dot{q}_0 + M_{\delta}^{*}\Delta\delta \tag{4.4}$$

Here is the final form of dynamics for the controller design.

$$\begin{aligned} \dot{\alpha} &= Z_{\alpha}^{*}\alpha + q \\ \dot{q} &= \dot{q}_0 + M_{\delta}^{*}\Delta\delta \end{aligned} \tag{4.5}$$

State errors are defined as (4.6).

$$\begin{aligned} z_1 &= \alpha - \alpha_c \\ z_2 &= q - q_c \end{aligned} \tag{4.6}$$

where subscript c indicates a command.

4.2.2 Derivation of Control Law

When Lyapunov function candidate is positive definite and its derivative is negative definite, asymptotic stability can be guaranteed for the closed loop system. A control command satisfying asymptotic stability of the system is derived from 2 cascaded designing steps as follows.

First, for the outer loop controller design, Lyapunov function candidate V_1 considering only z_1 is selected as

$$V_1 = \frac{1}{2} z_1^2 \tag{4.7}$$

which is positive definite.

The derivative of Lyapunov function candidate V_1 is obtained as

$$\begin{aligned} \dot{V}_1 &= z_1 \dot{z}_1 \\ &= z_1 \left(Z_\alpha^* \alpha + q - \dot{\alpha}_c \right) \end{aligned} \tag{4.8}$$

In order to satisfy the Lyapunov stability condition, a pseudo-command q_c is designed as

$$q_c = -C_1 z_1 - Z_\alpha^* \alpha + \dot{\alpha}_c \tag{4.9}$$

which makes negative definite $\dot{V}_1 = -C_1 z_1^2$ with a positive design parameter C_1. The state of the fast dynamics, q, is regarded as a control input for the slow dynamics.

Second, for the inner loop controller design, Lyapunov function candidate V_2 considering both z_1 and z_2 is defined as

$$V_2 = \frac{1}{2} z_1^2 + \frac{1}{2} z_2^2 \tag{4.10}$$

which is positive definite.

The derivative of V_2 can be calculated as (4.11), by utilizing the incremental dynamics of q in (4.4) for the inner loop controller design with IBKS.

$$\begin{aligned} \dot{V}_2 &= z_1 \dot{z}_1 + z_2 \dot{z}_2 \\ &= z_1 \left(Z_\alpha^* \alpha + q - \dot{\alpha}_c \right) + z_2 \left(\dot{q}_0 + M_\delta^* \Delta\delta - \dot{q}_c \right) \end{aligned} \tag{4.11}$$

From the pseudo-command (4.9), $\dot{V}_2$ becomes

$$\dot{V}_2 = z_1 \left(-C_1 z_1 + z_2\right) + z_2 \left(\dot{q}_0 + M_\delta^* \Delta\delta - \dot{q}_c\right) \tag{4.12}$$

To satisfy Lyapunov stability condition, $\Delta\delta$ is designed as

$$\Delta\delta = \frac{1}{M_\delta} \left(-C_2 z_2 - z_1 - \dot{q}_0 + \dot{q}_c\right) \tag{4.13}$$

which makes negative definite $\dot{V}_2 = -C_1 z_1^2 - C_2 z_2^2$ with positive design parameters C_1 and C_2.

The final form of derived control algorithm can be suggested as follows.

$$\begin{aligned} q_c &= -C_1 z_1 - \hat{Z}_\alpha^* \alpha + \dot{\alpha}_c \\ \delta &= \delta_0 + \Delta\delta \\ &= \frac{1}{\hat{M}_\delta^*} \left(-C_2 z_2 - z_1 - \dot{q}_0 + \dot{q}_c\right) + \delta_0 \end{aligned} \tag{4.14}$$

Note that aerodynamic derivatives estimates $\hat{(\cdot)}$ are utilized in (4.14) instead of real Z_α^* and M_δ^*, because only estimated values for the model information are available in controller design phase. The pseudo-command q_c makes the angle of attack α converge to its desired value α_c, and q achieves q_c by the designed control input δ. Comparing to a control command with pure BKS, explicit utilization of $\hat{M}_\alpha^*$ and $\hat{M}_q^*$ related terms is not required, since $\Delta\alpha$ and Δq are neglected in q dynamics (4.4) for the inner loop control algorithm design with IBKS. This implies that model dependency is reduced because $\hat{Z}_\alpha^*$ and $\hat{M}_\delta^*$ are only required for implementation of the algorithm. Instead, measurements δ_0 and $\dot{q}_0$, current control surface deflection and state derivative in the inner loop, are additionally required to implement the control algorithm with IBKS.

A flight controller is designed to accomplish asymptotic stability under Lyapunov framework, assuming that there are no measurement defects like delays and model uncertainties. The effects of measurement delays and model uncertainties, which can make aimed performance and stability characteristics in this design phase difficult to be achieved, will be investigated in following closed loop analysis part 4.3.

4.3 Closed-loop Analysis

In Section 4.3, the closed loop analysis is performed considering measurement delays and model uncertainties, under the piece-wise approach to handle this LPV system as in [35]. For better understandings about the obtained closed loop characteristics through a comparative study, relevant analysis results in [16] under the assumption of perfect measurements are briefly summarized and suggested in Section 4.3.1. If measurement delays are additionally considered in the closed loop analysis, it is difficult to even judge absolute stability of the system in analytic way. Therefore, a numerical framework is proposed in Section 4.3.2 to examine the system stability under measurement delays and model uncertainties. An optimization concept is utilized to search unstable poles efficiently and systematically, even for a highly nonlinear metric function due to the measurement delays considered. By applying the numerical framework suggested in Section 4.3.2, closed loop characteristics under measurement delays and model uncertainties especially in stability point of view are identified, which are presented in Section 4.3.3. A stability condition about a relationship between delays on state derivative and control surface deflection angle measurements is suggested, and it is shown that this condition is affected by the model uncertainty. Simulations are carried out for verification and validation of the framework results about the absolute stability, and they additionally provides understandings about the relative stability. From the simulation results, system performance is also investigated, which is addressed in Section 4.3.4.

4.3.1 Analysis without Measurement Delays

With the same control structure of Chapter 4, [16] performed theoretical closed loop analysis for the nominal case and the case only considering model uncertainties. For the comparative study in Section 4.3.3, relevant studies in [16] without considering measurement delays are reviewed as follows.

In [16], the transfer function is shown to be insensitive to the uncertainty in $\hat{M}_\delta^*$, if a control command is calculated, transmitted and reflected fast enough to a real control surface deflection. As a result, the closed loop system is only affected by the uncertainty in $\hat{Z}_\alpha^*$. Note that $\hat{Z}_\alpha^*$ is utilized for the outer loop controller design with BKS, and $\hat{M}_\delta^*$ is required for the inner loop controller design with IBKS. Since Chapter 4 aims to have critical understandings about IBKS, the model uncertainty

$\Delta_{M_\delta^*}$ on $\hat{M}_\delta^* = M_\delta^*(1 + \Delta_{M_\delta^*})$ is mainly considered in Chapter 4, resulting in the transfer function (4.15) which becomes the same with the one for the nominal case.

$$\begin{aligned} &\frac{\alpha(s)}{\alpha_c(s)} = \frac{T}{s^2 + 2\zeta\omega_n s + \omega_n^2} \\ &\text{where} \\ &T = C_1C_2 + 1 \\ &2\zeta\omega_n = C_1 + C_2 \\ &\omega_n^2 = C_1C_2 + 1 \end{aligned} \tag{4.15}$$

ζ and ω_n represent a damping ratio and a natural frequency of the system. A detailed derivation process of the transfer function (4.15) can be found in [16].

Poles p are obtained from (4.15) as (4.16).

$$p = \frac{-(C_1 + C_2) \pm \sqrt{(C_1 - C_2)^2 - 4}}{2} \tag{4.16}$$

With the positive design parameters, poles are always located in the left half plane, which means that the closed loop system always becomes stable. Besides, poles are given as a function of the design parameters only. This implies that the system characteristics become uniform in the entire flight envelope.

A steady state error, e_{ss}, can be calculated using following relationship.

$$e_{ss} = \alpha_c - \lim_{t\to\infty} \alpha(t) = \alpha_c - \lim_{s\to 0} s\alpha(s) \tag{4.17}$$

A step input $\alpha_c = K$ in the time-domain is expressed in the frequency-domain as below.

$$\alpha_c(s) = \frac{K}{s} \tag{4.18}$$

By applying (4.15) and (4.18) to (4.17), the steady state error can be calculated, resulting in zero value.

$$e_{ss} = 0 \tag{4.19}$$

4.3.2 Stability Analysis Framework under Measurement Delays

Comparing to classical BKS, state derivative and control surface deflection angle measurements are additionally utilized and consequently, model information about control effectiveness is only required for IBKS implementation. Hence, delays $\tau_{\dot{q}}$ and τ_δ on $\dot{q}_0$ and δ_0 measurements together with the model uncertainty $\Delta_{M_\delta^*}$ on $\hat{M}_\delta^*$ are mainly considered in Section 4.3.2 for the closed loop analysis. Note that the measurement delays in Chapter 4 are defined as final delays on the measurements for control command calculation, including delays from sensors, communication links, and processors with estimation algorithms. $\hat{M}_\delta^*$ is assumed to have the same sign with M_δ^*.

The first step for the stability analysis framework is to derive the transfer function of the closed loop system with IBKS considering $\tau_{\dot{q}}$ and τ_δ along with $\Delta_{M_\delta^*}$, resulting in (4.20).

$$\begin{aligned}
&\frac{\alpha(s)}{\alpha_c(s)} = \frac{\frac{M_\delta^*}{\hat{M}_\delta^*}(C_1C_2+1)}{\phi_1(s)s^2+\phi_2(s)s+\phi_3(s)} \\
&\text{where} \\
&\phi_1(s) = 1 - e^{-\tau_\delta s} + \frac{M_\delta^*}{\hat{M}_\delta^*}e^{-\tau_{\dot{q}}s} \\
&\phi_2(s) = -(Z_\alpha^* + M_q^*)(1-e^{-\tau_\delta s}) + \frac{M_\delta^*}{\hat{M}_\delta^*}(C_1 + C_2 + Z_\alpha^* - Z_\alpha^* e^{-\tau_{\dot{q}}s}) \\
&\phi_3(s) = (Z_\alpha^* M_q^* - M_\alpha^*)(1-e^{-\tau_\delta s}) + \frac{M_\delta^*}{\hat{M}_\delta^*}(C_1C_2+1)
\end{aligned} \tag{4.20}$$

A detailed derivation of the transfer function (4.20) under the piece-wise approach [35] is addressed in Appendix A.

The stability of the closed loop system can be examined by searching unstable poles from its characteristic equation in (4.20). The biggest challenge to obtain poles is that there exist exponential functions from the considered measurement delays. If the exponential functions are approximated as in [27–30], it is difficult to figure out the feasible range of delay for the valid approximation. In addition, [29] addresses that the stability characteristics obtained with Taylor series expansion can be highly sensitive to the order of the approximation. The proposed analysis framework in Section 4.3.2 is based on a numerical approach without approximation, which will

be shown in the rest of the steps.

The second step is to reformulate the characteristic equation for numerical pole search. By substituting $s = a + bi$ $(a, b \in \mathbb{R})$ and applying Euler's formula, ϕ_1, ϕ_2 and ϕ_3 in (4.20) can be rewritten as (4.21).

$$
\begin{aligned}
\phi_1 &= (1 - x_\delta + \Omega x_{\dot{q}}) + i(y_\delta - \Omega y_{\dot{q}}) \\
\phi_2 &= \left\{-(Z_\alpha^* + M_q^*)(1 - x_\delta) + \Omega(C_1 + C_2 + Z_\alpha^* - Z_\alpha^* x_{\dot{q}})\right\} \\
&\quad + i\left\{-(Z_\alpha^* + M_q^*)y_\delta + \Omega Z_\alpha^* y_{\dot{q}}\right\} \\
\phi_3 &= \left\{(Z_\alpha^* M_q^* - M_\alpha^*)(1 - x_\delta) + \Omega(C_1 C_2 + 1)\right\} + i(Z_\alpha^* M_q^* - M_\alpha^*)y_\delta
\end{aligned} \tag{4.21}
$$

where

$$
x_\delta = e^{-\tau_\delta a} cos(\tau_\delta b) \qquad x_{\dot{q}} = e^{-\tau_{\dot{q}} a} cos(\tau_{\dot{q}} b)
$$

$$
y_\delta = e^{-\tau_\delta a} sin(\tau_\delta b) \qquad y_{\dot{q}} = e^{-\tau_{\dot{q}} a} sin(\tau_{\dot{q}} b) \qquad \Omega = \frac{M_\delta^*}{\hat{M}_\delta^*}
$$

From (4.21) with $s = a+bi$ $(a, b \in \mathbb{R})$, the characteristic equation $\phi_1 s^2 + \phi_2 s + \phi_3 = 0$ can be re-arranged as (4.22).

$$
\phi_1 s^2 + \phi_2 s + \phi_3 = Re(a, b) + Im(a, b)i = 0
$$

where

$$
\begin{aligned}
Re(a,b) &= (a^2 - b^2)\left[1 - \left\{e^{-\tau_\delta a} cos(\tau_\delta b) - \Omega e^{-\tau_{\dot{q}} a} cos(\tau_{\dot{q}} b)\right\}\right] \\
&\quad - 2ab\left\{e^{-\tau_\delta a} sin(\tau_\delta b) - \Omega e^{-\tau_{\dot{q}} a} sin(\tau_{\dot{q}} b)\right\} \\
&\quad + a\left[-(Z_\alpha^* + M_q^*) + \Omega(C_1 + C_2 + Z_\alpha^*) + M_q^* e^{-\tau_\delta a} cos(\tau_\delta b)\right. \\
&\quad \left. + Z_\alpha^*\left\{e^{-\tau_\delta a} cos(\tau_\delta b) - \Omega e^{-\tau_{\dot{q}} a} cos(\tau_{\dot{q}} b))\right\}\right] \\
&\quad + b\left[M_q^* e^{-\tau_\delta a} sin(\tau_\delta b) + Z_\alpha^*\left\{e^{-\tau_\delta a} sin(\tau_\delta b) - \Omega e^{-\tau_{\dot{q}} a} sin(\tau_{\dot{q}} b)\right\}\right] \\
&\quad + \left\{(Z_\alpha^* M_q^* - M_\alpha^*)(1 - e^{-\tau_\delta a} cos(\tau_\delta b)) + \Omega(C_1 C_2 + 1)\right\} \\
Im(a,b) &= (a^2 - b^2)\left\{e^{-\tau_\delta a} sin(\tau_\delta b) - \Omega e^{-\tau_{\dot{q}} a} sin(\tau_{\dot{q}} b)\right\} \\
&\quad + 2ab\left[1 - \left\{e^{-\tau_\delta a} cos(\tau_\delta b) - \Omega e^{-\tau_{\dot{q}} a} cos(\tau_{\dot{q}} b)\right\}\right] \\
&\quad - a\left[M_q^* e^{-\tau_\delta a} sin(\tau_\delta b) + Z_\alpha^*\left\{e^{-\tau_\delta a} sin(\tau_\delta b) - \Omega e^{-\tau_{\dot{q}} a} sin(\tau_{\dot{q}} b)\right\}\right] \\
&\quad + b\left[-(Z_\alpha^* + M_q^*) + \Omega(C_1 + C_2 + Z_\alpha^*) + M_q^* e^{-\tau_\delta a} cos(\tau_\delta b)\right. \\
&\quad \left. + Z_\alpha^*\left\{e^{-\tau_\delta a} cos(\tau_\delta b) - \Omega e^{-\tau_{\dot{q}} a} cos(\tau_{\dot{q}} b)\right\}\right] \\
&\quad + (Z_\alpha^* M_q^* - M_\alpha^*) e^{-\tau_\delta a} sin(\tau_\delta b)
\end{aligned} \tag{4.22}
$$

The last step is to find poles by searching a and b which make $f(a,b)$ in (4.23) zero, because both $Re(a,b)$ and $Im(a,b)$ should be zeros to have zero $f(a,b)$.

$$f(a,b) \triangleq |Re(a,b)| + |Im(a,b)| \tag{4.23}$$

If $\exists a > 0$ *s.t.* $f(a,b) = 0$, the system is unstable. If not, it is stable. By utilizing this property, Chapter 4 suggests a numerical analysis framework to judge absolute stability for the system with IBKS considering $\tau_{\dot{q}}$ and τ_δ along with $\Delta_{M_\delta^*}$, which is summarized in Table 4.1.

Table 4.1: Stability Test Algorithm for Nonlinear Characteristic Equations

Algorithm 1. Stability Test Algorithm
count $\leftarrow 0$
for $a_{GRID} = 0$ to a_{max} with Δa
for $b_{GRID} = b_{min}$ to b_{max} with Δb
if $f\left(a_{GRID}, b_{GRID}\right) < f_{TH}$
$a^*, b^* \leftarrow \arg\min_{a,b\in\mathbb{R}} f\left(a,b\right)$
with $a_0, b_0 \leftarrow a_{GRID}, b_{GRID}$
$f^* \leftarrow f\left(a^*, b^*\right)$
if $f^* < \epsilon$ and $a^* > 0$
count $\leftarrow$ *count* $+ 1$
end if
end if
end for
end for
if *count* > 0
return Unstable
else
return Stable
end if

First, grid points (a_{GRID}, b_{GRID}) are determined by sparsely dividing the area of interest, $0 \leq a_{GRID} < a_{max}$ and $b_{min} \leq b_{GRID} < b_{max}$, with grid sizes Δa and Δb. The grid points (a_{GRID}, b_{GRID}), whose function values $f(a_{GRID}, b_{GRID})$ are less than a certain threshold value f_{TH}, are selected as points for the initial guess. Second, optimizations are conducted with each initial guess points, resulting in a set of local minimum points (a^*, b^*). The local optimal points, where $f(a^*, b^*)$ are less than a threshold value $\epsilon \simeq 0$, are regarded as poles. *count* indicates the number of unstable poles.

As shown in Table 4.1, the proposed framework utilizes an optimization concept to

examine the existence of the poles in the right half plane in systematic and efficient way, even for the highly nonlinear metric function (4.23) with (4.22). Note that under the heuristic approach as in [33], reliable pole search can not be guaranteed even with the reduced grid size which elevates the computation load.

4.3.3 Closed-loop characteristics : Stability

In Section 4.3.3, closed loop characteristics under measurement delays along with model uncertainties especially in stability point of view are presented, which are identified by applying the suggested numerical framework in Section 4.3.2. Simulations are performed for verification and validation of the obtained properties from the framework. As illustrative examples, four different types of aircraft models are considered for analysis and simulation, and their aerodynamic derivatives at certain flight conditions [36] are provided in Appendix B. The design parameters C_1 and C_2 for the control algorithm are set to be 1.5 respectively. An extensive range of $\tau_{\dot{q}}$ and τ_δ together with $\Delta_{M_\delta^*}$ is introduced to obtain critical insights about the effects of measurement delays along with a model uncertainty on the system. Note that considering the page limit, this paper shows some parts of the results that are representative. The presented cases are with $\tau_{\dot{q}}$ and τ_δ from $0s$ to $0.1s$ with $0.01s$ increment and from $0.1s$ to $0.2s$ with $0.02s$ increment (i.e. $\big[\{0s : 0.01s : 0.1s\} \cup \{0.1s : 0.02s : 0.2s\}\big]$) along with $\Delta_{M_\delta^*} = \big[-50\%,\ -35\%,\ -20\%,\ 0\%,\ 25\%,\ 100\%,\ 200\%,\ 300\%\big]$. Initial values for the state variables α and q, and the α-command α_c, are set to be $0°$, $0°/s$ and $1.5°$ respectively. Remaining parameters especially for the framework are listed in Table 4.2.

Table 4.2: Framework Parameters

Parameter	Value
a_{max}	1000
Δa	10
b_{min}	-1000
Δb	10
b_{max}	1000
f_{TH}	10^6
ϵ	10^{-3}

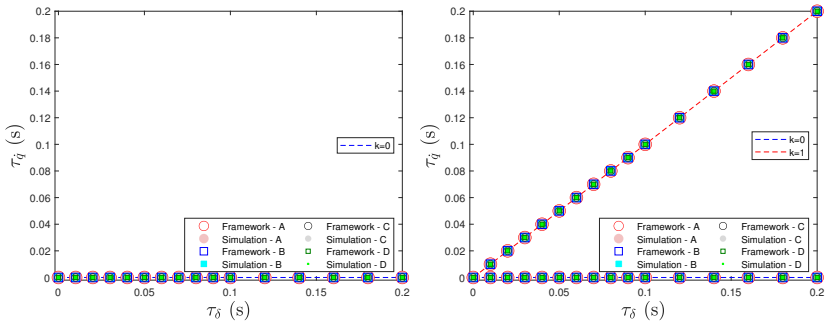

(a) With $\Delta_{M_\delta^*} = -50\%$

(b) With $\Delta_{M_\delta^*} = -35\%$

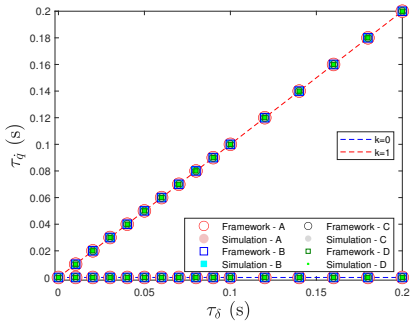

(c) With $\Delta_{M_\delta^*} = -20\%$

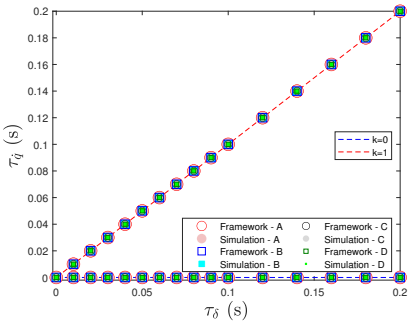

(d) With $\Delta_{M_\delta^*} = 0\%$

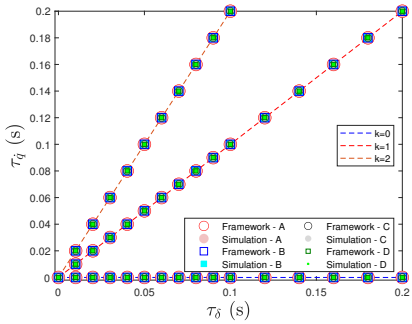

(e) With $\Delta_{M_\delta^*} = 25\%$

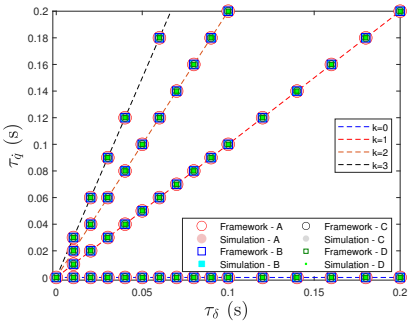

(f) With $\Delta_{M_\delta^*} = 100\%$

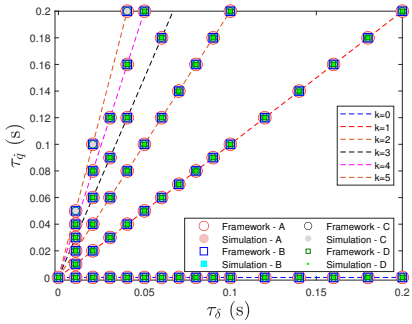

(g) With $\Delta_{M_\delta^*} = 200\%$

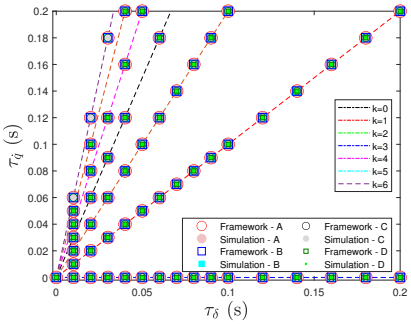

(h) With $\Delta_{M_\delta^*} = 300\%$

Figure 4.1: Relationships between $\tau_{\dot{q}}$ and τ_δ for system stability under $\Delta_{\hat{M}_\delta^*}$

$\tau_{\dot{q}}$ and τ_δ cases examined to be stable by the framework are illustrated for each $\Delta_{M_\delta^*}$ in Fig. 4.1. Note that the markers ◯, □, ○ and □ in Fig. 4.1 denote the framework results of aircraft A, B, C and D, respectively. Fig. 4.1 shows that the closed loop system is stable if $\tau_{\dot{q}} = k\tau_\delta$ and the non-negative k has an upper bound k_{max} which varies with $\Delta_{\hat{M}_\delta^*}$. k_{max} values in Fig. 4.1 are summarized as Table 4.3 which provides following observations. For $\Delta_{\hat{M}_\delta^*} = 0$, k_{max} is 1, indicating the system becomes stable when there is no delay on $\dot{q}_0$ measurement (i.e. $\tau_{\dot{q}} = 0$) or when the additional measurements $\dot{q}_0$ and δ_0 are synchronized with the same amount of delay (i.e. $\tau_{\dot{q}} = \tau_\delta$). If $\hat{M}_\delta^*$ is under-estimated(i.e. $\Delta_{\hat{M}_\delta^*} < 0$), k_{max} gets smaller, resulting in reduced number of stable points. On contrary, if $\hat{M}_\delta^*$ is over-estimated (i.e. $\Delta_{\hat{M}_\delta^*} > 0$), k_{max} becomes larger, resulting in increased number of stable points.

Table 4.3: k_{max} for each $\Delta_{\hat{M}_\delta^*}$

	k_{max}			
$\Delta_{\hat{M}_\delta^*}$	Airplane A	Airplane B	Airplane C	Airplane D
-0.5	0	0	0	0
-0.35	1	1	1	1
-0.2	1	1	1	1
0	1	1	1	1
0.25	2	2	2	2
1	3	3	3	3
2	5	5	5	4
3	6	6	6	5

The simulation results appear to coincide with the framework results, as can be seen in Fig. 4.1. Note that the simulation results are given with markers ●, ■, ● and ■ for each aircraft A, B, C and D in Fig. 4.1. For some representative cases with Aircraft A, time responses are presented in Fig. 4.2. It is shown in Fig. 4.2 that the closed-loop system is unstable if $\tau_{\dot{q}}$ and τ_δ do not satisfy $\tau_{\dot{q}} = k\tau_\delta$ ($k \leq k_{max}$) even with small deviation.

For better understandings on stability and robustness of the closed loop systems, gain margins under $\tau_{\dot{q}}$ and τ_δ together with $\Delta_{\hat{M}_\delta^*}$ are examined through simulations. For illustrative purpose, a part of results with Aircraft A under $\tau_\delta = \{0s : 0.01s : 0.05s\}$ are given as Fig. 4.3, but the trend of all results is the same. Fig. 4.3 indicates that the gain margin increases as $\Delta_{\hat{M}_\delta^*}$ increases under the same $\tau_{\dot{q}}$ and τ_δ. For the same $\Delta_{\hat{M}_\delta^*}$, the gain margin decreases when k approaches to its upper bound k_{max}.

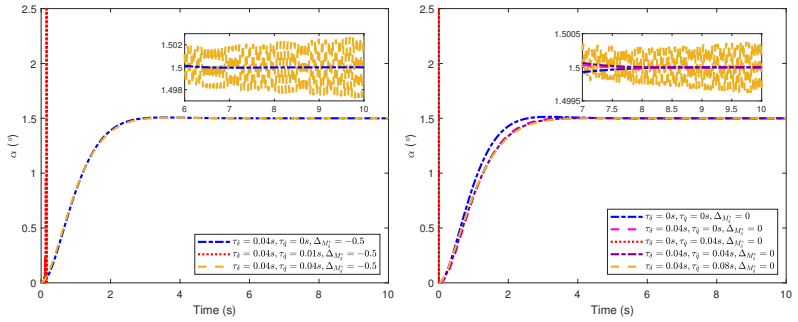

(a) $\Delta_{\hat{M}_\delta^*} = -0.5$ (b) $\Delta_{\hat{M}_\delta^*} = 0$

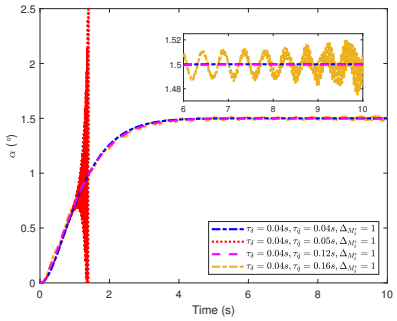

(c) $\Delta_{\hat{M}_\delta^*} = 1$

Figure 4.2: Time response graphs for Aircraft A

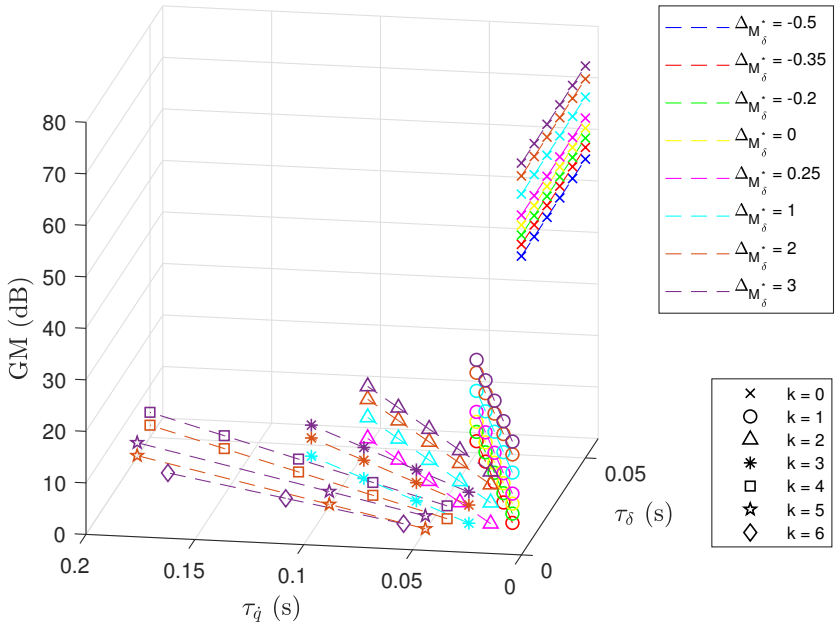

Figure 4.3: Gain margin(GM) for stable closed-loop system under $\tau_{\dot{q}}$ and τ_δ together with $\Delta_{\hat{M}_\delta^*}$

The important findings from the framework results can be summarized as Observation 4.1 and 4.2.

Observation 4.1. *(Stability condition with $\tau_{\dot{q}}$ and τ_δ) : The system with IBKS is stable only when $\tau_{\dot{q}} = k\tau_\delta$ with a non-negative integer k which has an upper bound k_{max}. Otherwise, the closed loop system becomes unstable.*

Observation 4.2. *(Effect of $\Delta_{\hat{M}_\delta^*}$ to stability condition) : k_{max} becomes smaller as the model uncertainty on control effectiveness information $\Delta_{\hat{M}_\delta^*}$ decreases.*

Observation 4.1 and 4.2 can be understood as follows. $\dot{q}_0$ measurement has critical influences on the system with IBKS because it contains the model information about M_α^* and M_q^* to be replaced. If there is no delay on this measurement (i.e. $\tau_{\dot{q}} = 0$ with $k = 0$), the system with IBKS becomes stable. If $\dot{q}_0$ signal is delayed, the relationship between delays on $\dot{q}_0$ and δ_0 becomes important for the system stability due to the following reason. Due to the considered delays on $\dot{q}_0$ and δ_0, trigonometric functions whose frequencies are $\tau_{\dot{q}}$ and τ_δ appear in the characteristic equation (4.22). The differences between trigonometric terms with frequencies of $\tau_{\dot{q}}$ and τ_δ are repeatedly shown in (4.22) and they have significant impacts to the closed-loop system stability with IBKS. When $\tau_{\dot{q}} = k\tau_\delta$ with a positive integer k, these differences shows a periodic pattern with the frequency of τ_δ like the case without $\tau_{\dot{q}}$, resulting in the stable closed-loop response. k has its upper bound k_{max} determined by the model uncertainty on control effectiveness information $\Delta_{\hat{M}_\delta^*}$, which can be explained as follows. k indicates how many times the cycle of the trigonometric term with $\tau_{\dot{q}}$ is repeated during one period of that with τ_δ. $\Delta_{\hat{M}_\delta^*}$ affects the amplitude of the trigonometric term with $\tau_{\dot{q}}$, as can be seen in (4.22). The maximum magnitude of the differences between trigonometric terms with frequencies of $\tau_{\dot{q}}$ and τ_δ can be more amplified as k increases, and $\Delta_{\hat{M}_\delta^*}$ has an impact on the magnitude of this amplification. This implies that there exists an upper bound k_{max} which makes the amplification to be within the range where the system is stable and this k_{max} is affected by $\Delta_{\hat{M}_\delta^*}$. The reason why k_{max} decreases as $\Delta_{\hat{M}_\delta^*}$ gets smaller can be explained with loop gain point of view. In the derived control command (4.14), there exists a reciprocal of $\hat{M}_\delta^*$. This implies that a loop gain becomes smaller with over-estimated $\hat{M}_\delta^*$ (i.e. $\Delta_{\hat{M}_\delta^*} > 0$), while it gets larger with under-estimated $\hat{M}_\delta^*$ (i.e. $\Delta_{\hat{M}_\delta^*} < 0$). Thus, the closed-loop system becomes less robust against the defects as $\Delta_{\hat{M}_\delta^*}$ reduces, resulting in smaller k_{max}. Instead, the time domain response of the system becomes faster as $\Delta_{\hat{M}_\delta^*}$ gets smaller since the loop gain increases.

The comparative study between the closed loop systems with and without measurement delays under model uncertainties is provided as follows. Note that critical understandings about individual and integrated effects of measurement delays and model uncertainties to the system with IBKS can be facilitated by this comparative

study. For the closed loop system with model uncertainties and without measurement delays, the previous study in [16] shows that the system with IBKS is not affected by any model uncertainty even in $\hat{M}_\delta^*$ and always stable with uniform performance. When the closed loop system is under both measurement delays and model uncertainties, the relationship between $\tau_{\dot{q}}$ and τ_δ for the system stability is provided, which is affected by $\Delta_{\hat{M}_\delta^*}$. The framework result with $\Delta_{\hat{M}_\delta^*} = 0$ indicates the case when $\tau_{\dot{q}}$ and τ_δ are only considered. In this case, the system is stable only if $\tau_{\dot{q}} = 0$ or $\tau_{\dot{q}} = \tau_\delta$ (i.e. $k_{max} = 1$). If $\Delta_{\hat{M}_\delta^*}$ is additionally considered, the number of stable points tends to decrease with $0 \leq k_{max} \leq 1$ for under-estimated $\hat{M}_\delta^*$ and increase with $k_{max} \geq 1$ for over-estimated $\hat{M}_\delta^*$.

4.3.4 Closed-loop characteristics : Performance

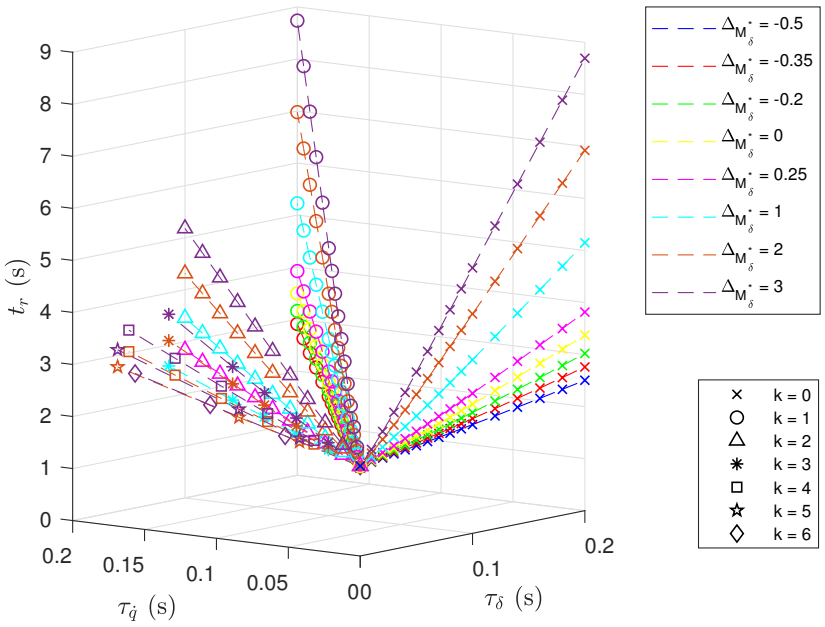

Figure 4.4: Rising time(t_r) for the stable points

Section 4.3.4 suggests closed-loop characteristics about system performance investigated from the simulation results. One of the system stability related properties mentioned in Section 4.3.3 is that the number of stable points increases with improved gain margin as $\Delta_{\hat{M}_\delta^*}$ gets bigger in the positive direction. However, large $\Delta_{\hat{M}_\delta^*}$ has a negative impact on the system performance, especially about fast response. As can be seen in Fig. 4.4, rising time t_r gets larger as $\Delta_{\hat{M}_\delta^*}$ increases for the same amount of delays on $\dot{q}_0$ and δ_0. For the same $\Delta_{\hat{M}_\delta^*}$, t_r increases with larger $\tau_{\dot{q}}$ and τ_δ. The time response graph for the representative cases, Fig. 4.5, shows that the

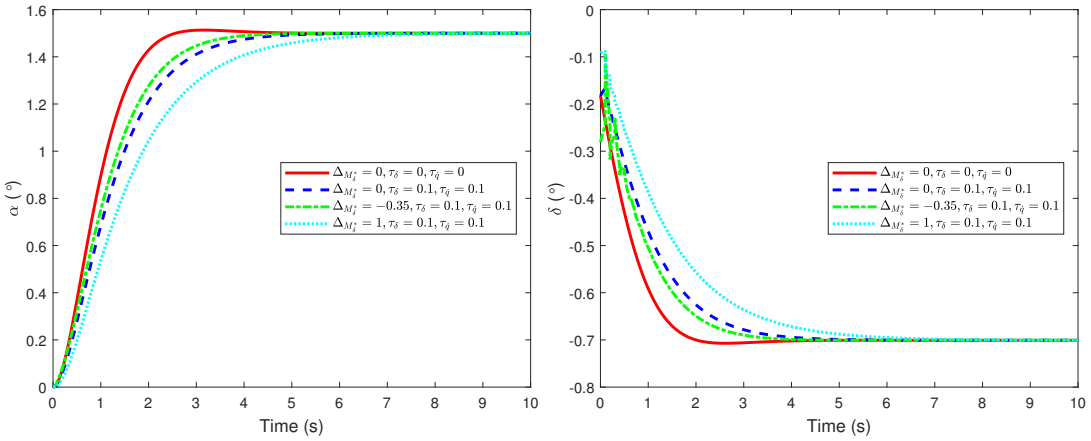

(a) System Output (b) Control Input

Figure 4.5: Time response graphs for the representative cases

steady state error always becomes zero. Steady state error can be also obtained in analytic way by applying (4.20) and (4.18) to (4.17), resulting in zero value.

4.4 Conclusion

Chapter 4 suggests closed loop characteristics with IBKS obtained from the proposed analysis framework, especially with consideration of measurement delays along with model uncertainties. A numerical framework is proposed to judge absolute stability for the closed loop system with IBKS under the measurement delays and the model uncertainties. The suggested framework with an optimization concept efficiently and systematically examines the existence of the poles in the right half plane, even for the highly nonlinear metric function due to the considered measurement delays. Chapter 4 also suggests critical understandings about the closed loop characteristics with IBKS considering both measurement delays and model uncertainty. By applying the proposed numerical framework, a stability condition about the relationship between delays on state derivative and control surface deflection angle measurements is found. It is shown that this condition is affected by the model uncertainty on control effectiveness information. The comparative study are conducted to suggest important insights about individual and integrated effects of the measurement delays and the model uncertainties to the closed loop system. The obtained properties about the absolute stability are verified through the simulation. From the simulation results, robustness and performance under the measurement delays and the model uncertainty are additionally investigated.

Appendix

A Derivation of Transfer Function for the System with IBKS under Measurement Delays and Model Uncertainties

Dynamics (4.2) can be expressed as a state space equation (4.24).

$$\begin{aligned}
&\dot{\mathbf{x}} = \mathbf{A}\mathbf{x} + \mathbf{B}\mathbf{u} \qquad \mathbf{y} = \mathbf{C}\mathbf{x} \\
&\mathbf{x} = \begin{bmatrix} \alpha & q \end{bmatrix}^T \qquad \mathbf{u} = \delta \\
&\mathbf{A} = \begin{bmatrix} Z_\alpha^* & 1 \\ M_\alpha^* & M_q^* \end{bmatrix} \quad \mathbf{B} = \begin{bmatrix} 0 \\ M_\delta^* \end{bmatrix} \quad \mathbf{C} = \begin{bmatrix} 1 & 0 \end{bmatrix}
\end{aligned} \tag{4.24}$$

Delays on $\dot{q}_0$ and δ_0 measurments are mainly considered for the analysis with IBKS in Chapter 4, and modellings of these delayed measurements are suggested for the closed loop analysis as (4.25) utilizing (4.2) for $\dot{q}_0$.

$$\begin{aligned}
\delta_0 &= \delta\left(t - \tau_\delta\right) \\
\dot{q}_0 &= \dot{q}\left(t - \tau_{\dot{q}}\right) \\
&= M_\alpha^* \alpha\left(t - \tau_{\dot{q}}\right) + M_q^* q\left(t - \tau_{\dot{q}}\right) + M_\delta^* \delta\left(t - \tau_{\dot{q}}\right)
\end{aligned} \tag{4.25}$$

Since Chapter 4 focuses on IBKS, the model uncertainty $\Delta_{M_\delta^*}$ on $\hat{M}_\delta^*$ is mainly considered in this closed loop analysis. Using (4.14) with (4.2), (4.6) and (4.25) under the assumption of constant α_c(i.e. $\dot{\alpha}_c = \ddot{\alpha}_c = 0$) and zero $\Delta_{Z_\alpha^*}$, δ can be rearranged as (4.26).

$$\begin{aligned}
\delta = &-\frac{1}{\hat{M}_\delta^*}\nu_\alpha \alpha - \frac{1}{\hat{M}_\delta^*}\nu_q q + \frac{1}{\hat{M}_\delta^*}\left(C_1 C_2 + 1\right)\alpha_c \\
&- \frac{M_\alpha^*}{\hat{M}_\delta^*}\alpha\left(t - \tau_{\dot{q}}\right) - \frac{M_q^*}{\hat{M}_\delta^*} q\left(t - \tau_{\dot{q}}\right) \\
&+ \left\{\delta\left(t - \tau_\delta\right) - \frac{M_\delta^*}{\hat{M}_\delta^*}\delta\left(t - \tau_{\dot{q}}\right)\right\}
\end{aligned} \tag{4.26}$$

where

$$\nu_\alpha = \left\{\left(C_1 + Z_\alpha^*\right)\left(C_2 + Z_\alpha^*\right) + 1\right\}$$

$$\nu_q = \left(C_1 + C_2 + Z_\alpha^*\right)$$

Applying Laplace transform to (4.26) and rearranging the equation with respect to δ,

$$\begin{aligned}\delta(s) = &\left[-\tfrac{1}{\hat{M}_\delta^* \phi_1(s)}\mu_\alpha(s) \quad -\tfrac{1}{\hat{M}_\delta^* \phi_1(s)}\mu_q(s) \right] \mathbf{X}(s) \\ &+ \frac{1}{\hat{M}_\delta^* \phi_1(s)} \left(C_1 C_2 + 1\right) \alpha_c(s) \\ &\text{where} \\ &\phi_1(s) = 1 - e^{-\tau_\delta s} + \frac{M_\delta^*}{\hat{M}_\delta^*} e^{-\tau_{\dot{q}} s} \\ &\mu_\alpha(s) = \nu_\alpha + M_\alpha^* e^{-\tau_{\dot{q}} s} \\ &\mu_q(s) = \nu_q + M_q^* e^{-\tau_{\dot{q}} s}\end{aligned} \tag{4.27}$$

If Laplace transform is applied to (4.24) and $\delta(s)$ in (4.27) is substituted into that equation, the closed loop system can be derived as (4.28).

$$\begin{aligned}&s\mathbf{X}(s) = \mathbf{A}(s)\mathbf{X}(s) + \mathbf{B}(s)\alpha_c(s) \qquad \mathbf{Y} = \mathbf{C}(s)\mathbf{X}(s) \\ &\mathbf{A}(s) = \begin{bmatrix} a_{11}(s) & a_{12}(s) \\ a_{21}(s) & a_{22}(s) \end{bmatrix} = \begin{bmatrix} Z_\alpha^* & 1 \\ M_\alpha^* - \frac{M_\delta^*}{\hat{M}_\delta^* \phi_1(s)}\mu_\alpha(s) & M_q^* - \frac{M_\delta^*}{\hat{M}_\delta^* \phi_1(s)}\mu_q(s) \end{bmatrix} \\ &\mathbf{B}(s) = \begin{bmatrix} 0 \\ \frac{M_\delta^*}{\hat{M}_\delta^* \phi_1(s)} \left(C_1 C_2 + 1\right) \end{bmatrix} \\ &\mathbf{C}(s) = \begin{bmatrix} 1 & 0 \end{bmatrix}\end{aligned} \tag{4.28}$$

From (4.28), transfer function can be derived as (4.29).

$$\begin{aligned}\frac{\alpha(s)}{\alpha_c(s)} &= \mathbf{C}(s)\left(s\mathbf{I} - \mathbf{A}(s)\right)^{-1}\mathbf{B}(s) \\ &= \frac{a_{12}\frac{M_\delta^*}{\hat{M}_\delta^* \phi_1(s)}\left(C_1 C_2 + 1\right)}{s^2 - \left(a_{11} + a_{22}\right)s + \left(a_{11}a_{22} - a_{12}a_{21}\right)} = \frac{\frac{M_\delta^*}{\hat{M}_\delta^*}(C_1 C_2 + 1)}{\phi_1(s)s^2 + \phi_2(s)s + \phi_3} \\ &\text{where} \\ &\phi_1(s) = 1 - e^{-\tau_\delta s} + \frac{M_\delta^*}{\hat{M}_\delta^*} e^{-\tau_{\dot{q}} s} \\ &\phi_2(s) = -(Z_\alpha^* + M_q^*)(1 - e^{-\tau_\delta s}) + \frac{M_\delta^*}{\hat{M}_\delta^*}(C_1 + C_2 + Z_\alpha^* - Z_\alpha^* e^{-\tau_{\dot{q}} s}) \\ &\phi_3(s) = (Z_\alpha^* M_q^* - M_\alpha^*)(1 - e^{-\tau_\delta s}) + \frac{M_\delta^*}{\hat{M}_\delta^*}\left(C_1 C_2 + 1\right)\end{aligned} \tag{4.29}$$

B Aerodynamic Derivatives

Table 4.4: Aerodynamic Derivatives of Aircraft

Parameters	Airplane A	Airplane B	Airplane C	Airplane D
$h\ (km)$	7.6200	1.5240	1.5240	6.0960
$U_0\ (m/s)$	185.9280	67.0865	103.6320	205.1304
Z^*_α	-1.9626	-0.8222	-2.4660	-0.5249
M^*_α	-4.7488	-17.1690	-23.8147	-1.2473
M^*_q	-3.9326	-6.8791	-5.8557	-0.6474
M^*_δ	-26.6845	-35.2513	-28.4270	-1.6937

References

[1] Petar V Kokotovic. The joy of feedback: nonlinear and adaptive. *IEEE Control Systems Magazine*, 12(3):7–17, 1992.

[2] Taeyoung Lee and Youdan Kim. Nonlinear adaptive flight control using backstepping and neural networks controller. *Journal of Guidance, Control, and Dynamics*, 24(4):675–682, 2001.

[3] Jay Farrell, Manu Sharma, and Marios Polycarpou. Backstepping-based flight control with adaptive function approximation. *Journal of Guidance, Control, and Dynamics*, 28(6):1089–1102, 2005.

[4] Hann-Shing Ju and Ching-Chih Tsai. Longitudinal axis flight control law design by adaptive backstepping. *IEEE Transactions on Aerospace and Electronic Systems*, 43(1):311–329, 2007.

[5] LR García Carrillo, Alejandro Dzul, and Rogelio Lozano. Hovering quad-rotor control: A comparison of nonlinear controllers using visual feedback. *IEEE Transactions on Aerospace and Electronic Systems*, 48(4):3159–3170, 2012.

[6] Lars Sonneveldt, QP Chu, and JA Mulder. Nonlinear flight control design using constrained adaptive backstepping. *Journal of Guidance, Control, and Dynamics*, 30(2):322–336, 2007.

[7] Baohua Lian and Hyochoong Bang. Momentum transfer-based attitude control of spacecraft with backstepping. *IEEE transactions on aerospace and electronic systems*, 42(2):453–463, 2006.

[8] Yang Zhang, Sheng-hai Wang, Bin Chang, and Wen-hai Wu. Adaptive constrained backstepping controller with prescribed performance methodology for carrier-based uav. *Aerospace Science and Technology*, 92:55–65, 2019.

[9] Mihai Lungu. Auto-landing of uavs with variable centre of mass using the backstepping and dynamic inversion control. *Aerospace Science and Technology*, page 105912, 2020.

[10] Mihai Lungu. Backstepping and dynamic inversion combined controller for auto-landing of fixed wing uavs. *Aerospace Science and Technology*, 96:105526, 2020.

[11] Pieter van Gils, Erik-Jan Van Kampen, Coen C de Visser, and Q Ping Chu. Adaptive incremental backstepping flight control for a high-performance aircraft with uncertainties. In *AIAA Guidance, Navigation, and Control Conference*, 2016.

[12] Abdelouahed Ait Haddou Ali, Q Ping Chu, Erik-Jan Van Kampen, and Coen C de Visser. Exploring adaptive incremental backstepping using immersion and invariance for an f-16 aircraft. In *AIAA Guidance, Navigation, and Control Conference*, 2014.

[13] Paul Acquatella, E van Kampen, and Qi Ping Chu. Incremental backstepping for robust nonlinear flight control. In *Proceedings of the EuroGNC 2013, 2nd CEAS Specialist Conference on Guidance, Navigation and Control*, pages 1444–1463, 2013.

[14] Guillermo P Falconí, Valentin A Marvakov, and Florian Holzapfel. Fault tolerant control for a hexarotor system using incremental backstepping. In *2016 IEEE Conference on Control Applications (CCA)*, pages 237–242. IEEE, 2016.

[15] Byoung-Ju Jeon, Min-Guk Seo, Hyo-Sang Shin, and Antonios Tsourdos. Understandings of the incremental backstepping control through theoretical analysis under the model uncertainties. In *2018 IEEE Conference on Control Technology and Applications (CCTA)*, pages 318–323. IEEE, 2018.

[16] B. Jeon, M. Seo, H. Shin, and A. Tsourdos. Understandings of classical and incremental backstepping controllers with model uncertainties. *IEEE Transactions on Aerospace and Electronic Systems*, 56(4):2628–2641, 2020.

[17] Byoung-Ju Jeon, Min-Guk Seo, Hyo-Sang Shin, and Antonios Tsourdos. Closed-loop analysis with incremental backstepping controller considering measurement bias. *IFAC-PapersOnLine*, 52(12):405–410, 2019.

[18] Dmitry I Ignatyev, Hyo-Sang Shin, and Antonios Tsourdos. Two-layer adaptive augmentation for incremental backstepping flight control of transport aircraft in uncertain conditions. *Aerospace Science and Technology*, page 106051, 2020.

[19] Lijia Cao, Xiaofeng Li, Yu Hu, Mingtao Liu, and Jiefu Li. Discrete-time incremental backstepping controller for unmanned aircrafts subject to actuator constraints. *Aerospace Science and Technology*, 96:105530, 2020.

[20] S Sieberling, QP Chu, and JA Mulder. Robust flight control using incremental nonlinear dynamic inversion and angular acceleration prediction. *Journal of guidance, control, and dynamics*, 33(6):1732–1742, 2010.

[21] Ewoud JJ Smeur, Qiping Chu, and Guido CHE de Croon. Adaptive incremental nonlinear dynamic inversion for attitude control of micro air vehicles. *Journal of Guidance, Control, and Dynamics*, 38(12):450–461, 2015.

[22] Fabian Grondman, Gertjan Looye, Richard O Kuchar, Q Ping Chu, and Erik-Jan Van Kampen. Design and flight testing of incremental nonlinear dynamic inversion-based control laws for a passenger aircraft. In *2018 AIAA Guidance, Navigation, and Control Conference*, page 0385, 2018.

[23] Paul Acquatella, Wouter Falkena, Erik-Jan van Kampen, and Q Ping Chu. Robust nonlinear spacecraft attitude control using incremental nonlinear dynamic inversion. In *AIAA Guidance, Navigation, and Control Conference*, 2012.

[24] P Simplício, MD Pavel, E Van Kampen, and QP Chu. An acceleration measurements-based approach for helicopter nonlinear flight control using incremental nonlinear dynamic inversion. *Control Engineering Practice*, 21(8):1065–1077, 2013.

[25] Xuerui Wang, Erik-Jan Van Kampen, Qiping Chu, and Peng Lu. Stability analysis for incremental nonlinear dynamic inversion control. *Journal of Guidance, Control, and Dynamics*, 42(5):1116–1129, 2019.

[26] Stephen H Lane and Robert F Stengel. Flight control design using non-linear inverse dynamics. *Automatica*, 24(4):471–483, 1988.

[27] RD Driver, DW Sasser, and ML Slater. The equation x'(t)= ax (t)+ bx (t- τ) with "small" delay. *The American Mathematical Monthly*, 80(9):990–995, 1973.

[28] Steve Guillouzic, Ivan L'Heureux, and André Longtin. Small delay approximation of stochastic delay differential equations. *Physical Review E*, 59(4):3970, 1999.

[29] Tamas Insperger. On the approximation of delayed systems by taylor series expansion. *Journal of Computational and Nonlinear Dynamics*, 10(2):024503, 2015.

[30] A Bahill. A simple adaptive smith-predictor for controlling time-delay systems: A tutorial. *IEEE Control systems magazine*, 3(2):16–22, 1983.

[31] Nejat Olgac and Rifat Sipahi. An exact method for the stability analysis of time-delayed linear time-invariant (lti) systems. *IEEE Transactions on Automatic Control*, 47(5):793–797, 2002.

[32] ZV Rekasius. A stability test for systems with delays. In *Joint Automatic Control Conference*, number 17, page 39, 1980.

[33] Maxime Doublet, Cédric Join, and Frederic Hamelin. Stability analysis for unknown delayed systems controlled by model-free control. In *2017 21st International Conference on System Theory, Control and Computing (ICSTCC)*, pages 441–446. IEEE, 2017.

[34] Donald McLean. *Automatic flight control systems*. Prentice Hall, New York, 1990.

[35] Chang-Hun Lee, Byung-Eul Jun, and Jin-Ik Lee. Connections between linear and nonlinear missile autopilots via three-loop topology. *Journal of Guidance, Control, and Dynamics*, pages 1426–1432, 2016.

[36] Jan Roskam. *Airplane flight dynamics and automatic flight controls*. DARcorporation, 1998.

[37] Hassan K Khalil. *Nonlinear systems*. Upper Saddle River, 1996.

[38] Jean-Jacques E Slotine, Weiping Li, et al. *Applied nonlinear control*. Prentice hall Englewood Cliffs, NJ, 1991.

[39] I. Kanellakopoulos M. Krstic and P. Kokotovic. *Nonlinear and Adaptive Control*. John Wiley and Sons, Inc., New York, 1995.

[40] B. Kim et al. *Flight Dynamics and Control*. Kyung Moon Sa, 2004.

[41] Farid Golnaraghi and Benjamin C Kuo. *Automatic Control Systems*. John Wiley and Sons Ltd, 2009.

Chapter 5

Composite Adaptive Backstepping Control

5.1 Introduction

Backstepping(BKS) control is one of the most widely and successfully applied nonlinear flight control methods [1–3]. BKS has a cascade control structure, where a state for an inner loop acts on an outer loop as a pseudo input driving a state for an outer loop to its desired value. This implies that a control law design for a system with large dimension can be split into several control law designs for simple systems with smaller dimension in recursive way. The closed-loop system with BKS fulfills a desired system response with known stability and convergence properties under Lyapunov framework. One of the critical issues about BKS is that it is sensitive to model uncertainties, because it requires full model information for implementation of the algorithm. Since it is difficult to get accurate model information in general, it is important to make BKS less dependent on model information.

In Chapter 5, a composite adaptive control approach [4–10] is introduced to BKS in order to reduce its model dependency by estimating part of model parameters online and utilizing the estimates for controller implementation. Note that the composite adaptive control scheme has been widely utilized in previous studies, resulting in advanced algorithms like composite model reference adaptive control (MRAC) [9] and composite adaptive neural network-based control [11]. A composite adaptation law has an advantage of improved estimation performance, which is achieved by introducing an estimation error based term to a tracking error based adaptation

law [4]. While a tracking error based adaptation law can be interpreted as a simple integration of a tracking error signal, a composite adaptation law appears to be a low pass filter on a tracking error signal due to the additionally introduced estimation error based term. This implies that, when adaptation gains are increased to enhance estimation speed, oscillations on estimation and tracking response in transient phase can be amplified with a tracking error based adaptation law. On the other hand, increase of adaptation gains enlarges a bandwidth of a composite adaptation law without excessive amplifications of oscillatory behaviors in estimation and tracking response in transient phase. Thus, a composite adaptation law achieves smoother transient response than a tracking error based adaptation law, resulting in enhanced tracking performance and system robustness. Note that robust adaptation laws have been developed to enhance system robustness by introducing modification terms like σ-modification[12], e-modification[13] and low-frequency learning[14], or suggesting architectures like $\mathcal{L}_1$ adaptation law[15] and derivative-free adaptation law[16], but only boundedness of parameter estimation error is guaranteed with those algorithms.

The parameter convergence can be guaranteed with the composite adaptation law, but one of the main issues is that persistent excitation (PE) is required for the convergence. This PE condition results in persistent oscillations of state and control input signals, which is unrealistic for practical applications. There have been previous studies [17–20] on relaxation of PE condition to finite excitation (FE) condition for composite adaptation laws. To achieve convergence of parameter estimation only with FE, they utilize a similar approach as follows. An information matrix is obtained by accumulating regressor data and algorithms to make use of richer regressor signals for the information matrix are introduced. This results in full rank of the information matrix after a certain time, only with FE. Besides, speed in the slowest adaptation direction is maximized since the information matrix which maximizes its minimum eigenvalue is selected. The approaches in [17–19] require larger memory than [20], since they store all regressor matrices for the information matrix calculation. To the best of our knowledge, relaxation of PE condition has not been discussed for the composite ABKS [21]. [17] and [20] are based on full-state feedback control, and [18] and [19] utilize dynamic inversion control scheme.

For successful design of an adaptation law, it is also important to consider practical issues related to computational complexity induced from the adaptation law structure. A structure of an adaptation law is highly dependent on a structure of a baseline control algorithm. If the baseline control law has a cascade control structure, it is possible to design the adaptation law for each loop of the control system.

In previous studies [17–20], baseline control algorithms do not have cascade control structures. Even in [21] with ABKS, an adaptation law design does not fully take advantage of the structural characteristics of BKS. As a result, adaptation laws in relevant literature [17–21] are designed to estimate all the uncertain parameters in the dynamic system at once. Since a dimension of an augmented parameter estimation problem enlarges as the number of dynamic equations and uncertain parameters increases, matrix operations with excessively large matrices are required, resulting in high computational complexity. Thus, a structure of the proposed adaptation law needs to be designed in a way to decrease the estimation problem dimension.

In Chapter 5, a composite ABKS control algorithm is designed, where its estimation problem dimension is reduced and PE requirement is relaxed. The composite adaptation law which enhances both estimation and tracking performance is utilized. The relaxation of PE requirement to FE for parameter convergence is accomplished by utilizing information matrix construction and selection methods based on [20]. One of the main contributions of Chapter 5 is that the adaptation problem for the overall dynamic system is divided into smaller estimation problems with the new composite ABKS. By taking advantages from a cascade control structure of BKS, the proposed adaptation law estimates model parameters in each loop separately, rather than estimates whole parameters of the system at once. This results in decreased computational complexity from reduced estimation problem dimension.

Chapter 5 is organized as follows. System dynamics with model uncertainty is defined in Section 5.2. Derivation and stability analysis of the proposed composite ABKS are addressed in Section 5.3. In Section 5.4, simulations are conducted to show performance and characteristics of the new composite ABKS. The overall concluding remarks are stated in Section 5.5.

5.2 System Dynamics

In Chapter 5, system dynamics with model uncertainty is considered as follows.

$$\dot{\boldsymbol{x}} = \boldsymbol{f}(\boldsymbol{x}) + \boldsymbol{g}(\boldsymbol{x})\boldsymbol{u} + \boldsymbol{\Delta}(\boldsymbol{x})$$

where

$$\begin{aligned}
&\boldsymbol{x} = [x_1, x_2, \cdots, x_n]^T \\
&\boldsymbol{x_i'} = [x_1, x_2, \cdots, x_i]^T \quad (i = 1, \cdots, n) \\
&\boldsymbol{f}(\boldsymbol{x}) = \left[f_1(\boldsymbol{x_1'}), f_2(\boldsymbol{x_2'}), \cdots, f_n(\boldsymbol{x_n'})\right]^T \\
&\boldsymbol{g}(\boldsymbol{x}) = \text{diag}\left[g_1(\boldsymbol{x_1'}), g_2(\boldsymbol{x_2'}), \cdots, g_n(\boldsymbol{x_n'})\right] \\
&\boldsymbol{u} = [u_1, u_2, \cdots, u_n]^T \text{ with } u_i = \begin{cases} x_{i+1} & (i = 1, \cdots, n-1) \\ \delta & (i = n) \end{cases} \\
&\boldsymbol{\Delta}(\boldsymbol{x}) = \left[\Delta_1(\boldsymbol{x_1'}), \Delta_2(\boldsymbol{x_2'}), \cdots, \Delta_n(\boldsymbol{x_n'})\right]^T
\end{aligned} \tag{5.1}$$

$\boldsymbol{x} \in \mathbb{R}^{n\times 1}$ indicates a state vector and $\boldsymbol{x_i'} \in \mathbb{R}^{i\times 1}$ is a subset of the state vector $\boldsymbol{x}$. $\boldsymbol{f}(\boldsymbol{x}) \in \mathbb{R}^{n\times 1}$ and $\boldsymbol{g}(\boldsymbol{x}) \in \mathbb{R}^{n\times n}$ represent known model information. $\boldsymbol{u} \in \mathbb{R}^{n\times 1}$ denotes a control input vector. Model uncertainty is expressed as $\boldsymbol{\Delta}(\boldsymbol{x}) \in \mathbb{R}^{n\times 1}$, which satisfies the matching condition in [22]. Since a control algorithm based on the backstepping methodology will be proposed, the system dynamics (5.1) is suggested in a strict-feedback form. First, $f_i(\boldsymbol{x_i'})$ and $g_i(\boldsymbol{x_i'})$ in $\boldsymbol{f}(\boldsymbol{x})$ and a diagonal matrix $\boldsymbol{g}(\boldsymbol{x})$ only depend on $\boldsymbol{x_i'}$. Second, a real control input δ is applied for the innermost loop and a state becomes a pseudo input for the next outer-loop in recursive way, constructing the control input vector $\boldsymbol{u}$ as (5.1).

A structured model uncertainty $\boldsymbol{\Delta}(\boldsymbol{x})$ which is linearly parameterized, is utilized in Chapter 5 as below.

$$\begin{aligned}
&\Delta_i(\boldsymbol{x_i'}) = \boldsymbol{\theta_i}^T \boldsymbol{\phi_i}(\boldsymbol{x_i'}) \qquad (i = 1, \cdots, n) \\
&\text{where} \\
&\boldsymbol{\theta_i} = \left[\theta_{i_1}, \theta_{i_2} \cdots \theta_{i_{m_i}}\right]^T \\
&\boldsymbol{\phi_i}(\boldsymbol{x_i'}) = \left[\phi_{i_1}(\boldsymbol{x_i'}), \phi_{i_2}(\boldsymbol{x_i'}) \cdots \phi_{i_{m_i}}(\boldsymbol{x_i'})\right]^T
\end{aligned} \tag{5.2}$$

$\boldsymbol{\theta_i} \in \mathbb{R}^{m_i\times 1}$ is a vector of unique constant true parameters, which is unknown. $\boldsymbol{\phi_i}(\boldsymbol{x_i'}) \in \mathbb{R}^{m_i\times 1}$ represents a known regressor vector which is continuously differentiable.

5.3 Composite Adaptive Backstepping Control

5.3.1 Derivation

A control command vector $\boldsymbol{u_c} \in \mathbb{R}^{n\times 1}$ is defined as (5.3) from (5.1). Subscript c indicates a command.

$$\begin{aligned} &\boldsymbol{u_c} = [u_{1_c}, u_{2_c}, \cdots, u_{n_c}]^T \\ &\text{with } u_{i_c} = \begin{cases} x_{i+1_c} & (i = 1, \cdots, n-1) \\ \delta_c & (i = n) \end{cases} \end{aligned} \tag{5.3}$$

u_{i_c} is a command which u_i should follow in order to drive x_i to x_{i_c}. Under the assumption of ideal actuator, $u_{n_c} = \delta_c = \delta$.

A tracking error $\boldsymbol{z} \in \mathbb{R}^{n\times 1}$ is given as below.

$$\begin{aligned} &\boldsymbol{z} = [z_1, z_2, \cdots, z_n]^T \\ &\text{where } z_i = x_i - x_{ic} \end{aligned} \tag{5.4}$$

The unknown vector $\boldsymbol{\theta_i}$ of true parameters will be estimated as $\hat{\boldsymbol{\theta}}_{\boldsymbol{i}}$ by the adaptation law (5.7). A vector of parameter estimation errors is given as (5.5).

$$\hat{\boldsymbol{\theta}}_{\boldsymbol{i}} - \boldsymbol{\theta}_i = \left[\hat{\theta}_{i_1} - \theta_{i_1}, \hat{\theta}_{i_2} - \theta_{i_2}, \cdots, \hat{\theta}_{i_{m_i}} - \theta_{i_{m_i}}\right]^T \tag{5.5}$$

A recursive design methodology for the control command $\boldsymbol{u_c}$ with an adaptation law is utilized under Lyapunov framework, resulting in (5.6) with (5.7). Asymptotic stability is achieved for the closed loop system with (5.6) and (5.7), which will be proved under Lyapunov stability analysis framework in following Section 5.3.2.

A derived control command u_{i_c} is suggested as follows.

$$\begin{aligned} &u_{ic} = \frac{1}{g_i}\left[-C_i z_i - g_{i-1} z_{i-1} - f_i - \hat{\boldsymbol{\theta}}_{\boldsymbol{i}}^T \boldsymbol{\phi_i} + \dot{x}_{ic}\right] \\ &\text{where } g_0 z_0 \triangleq 0 \end{aligned} \tag{5.6}$$

C_i is a constant and positive design parameter for the control law to achieve a desired closed-loop response.

$\hat{\boldsymbol{\theta}}_{\boldsymbol{i}}$ in (5.6) can be obtained from the adaptation law (5.7).

$$\frac{d}{dt}\hat{\boldsymbol{\theta}}_{\boldsymbol{i}} = z_i \boldsymbol{\Gamma_i} \boldsymbol{\phi_i} - \lambda_i \boldsymbol{\Gamma_i} \left(\boldsymbol{\Omega_i} \hat{\boldsymbol{\theta}}_{\boldsymbol{i}} - \boldsymbol{\eta_i} \right) \tag{5.7}$$

$\boldsymbol{\Gamma_i} = \text{diag}\left[\gamma_{i_1}, \gamma_{i_2}, \cdots, \gamma_{i_{m_i}}\right] \in \mathbb{R}^{m_i \times m_i}$ is a matrix of constant and positive design parameters for the adaptation law. Constant and positive λ_i is a relative weight factor on the estimation error based term to the tracking error based term. $\boldsymbol{\Omega_i} \in \mathbb{R}^{m_i \times m_i}$ denotes an information matrix to be designed. $\boldsymbol{\eta_i} \in \mathbb{R}^{m_i \times 1}$ denotes an auxiliary vector, which can be expressed as $\boldsymbol{\eta_i} = \boldsymbol{\Omega_i} \boldsymbol{\theta}_i$. Since $\boldsymbol{\theta}_i$ is unknown, $\boldsymbol{\eta_i}$ should be calculated from known signals in another way, which will be discussed in later part related to a regressor filtering scheme. The estimation error based term in the composite adaptation law (5.7) leads to smoother transient estimation and tracking response, resulting in enhanced system performance.

Regressor filtering scheme is utilized to compute the auxiliary vector without state derivative information. For the i-th loop, (5.1) can be rewritten as (5.8) with $g_i' \triangleq g_i u_i$.

$$\dot{x}_i = f_i + g_i' + \boldsymbol{\theta}_{\boldsymbol{i}}^T \boldsymbol{\phi_i} \tag{5.8}$$

By applying Laplace transform to (5.8),

$$s x_i(s) = f_i(s) + g_i'(s) + \boldsymbol{\theta}_{\boldsymbol{i}}^T \boldsymbol{\phi_i}(s) \tag{5.9}$$

Filtered dynamics (5.10) can be obtained by multiplying a first order filter $F(s) = \frac{1}{ks+1}$ with the filter parameter k for both sides.

$$s F(s) x_i(s) = F(s) \left\{ f_i(s) + g_i'(s) + \boldsymbol{\theta}_{\boldsymbol{i}}^T \boldsymbol{\phi_i}(s) \right\} \tag{5.10}$$

Using $sF(s) = \frac{1}{k}(1 - F(s))$, (5.10) can be rearranged as (5.11).

$$\begin{aligned} &\frac{1}{k} \left\{ x_i(s) - F(s) x_i(s) \right\} \\ &= F(s) f_i(s) + F(s) g_i'(s) + \boldsymbol{\theta}_{\boldsymbol{i}}^T \left\{ F(s) \boldsymbol{\phi_i}(s) \right\} \end{aligned} \tag{5.11}$$

Filtered dynamics in the time domain (5.12) is obtained by applying inverse Laplace

tranform to (5.11).

$$\frac{1}{k}\left(x_i - x_{if}\right) = f_{if} + g'_{if} + \boldsymbol{\theta_i}^T \boldsymbol{\phi_{if}} \tag{5.12}$$

where $(\cdot)_f$ represents a filtered signal by $F(s)$.

Let

$$\zeta_{if} \triangleq \frac{1}{k} x_{if} + f_{if} + g'_{if} \tag{5.13}$$

(5.14) is obtained by rearranging (5.12) in terms of $\boldsymbol{\theta_i}^T \boldsymbol{\phi_{if}}$ and substituting (5.13) into the rearranged equation.

$$\begin{aligned} &\boldsymbol{\theta_i}^T \boldsymbol{\phi_{if}} = \frac{1}{k} x_i - \zeta_{if} \\ &\text{where} \\ &\dot{\boldsymbol{\phi}}_{\boldsymbol{if}} = \frac{1}{k}\left(\boldsymbol{\phi_i} - \boldsymbol{\phi_{if}}\right) \\ &\dot{\zeta}_{if} = \frac{1}{k}\left(\frac{1}{k} x_i + f_i + g'_i - \zeta_{if}\right) \end{aligned} \tag{5.14}$$

$\boldsymbol{\theta_i}^T \boldsymbol{\phi_{if}}$ information in (5.14) will be utilized to calculate the auxiliary vector in (5.15). Without regressor filtering scheme, $\boldsymbol{\theta_i}^T \boldsymbol{\phi_i}$ information is required to calculate the auxiliary vector instead of $\boldsymbol{\theta_i}^T \boldsymbol{\phi_{if}}$ information, and $\boldsymbol{\theta_i}^T \boldsymbol{\phi_i}$ information can be obtained from (5.8), resulting in usage of the state derivative information. In general, state derivatives are difficult to be measured, and noise in state measurement signals can be amplified if the state derivatives are calculated via differentiation of the state measurements. Hence, it is advantageous to utilize regressor filtering scheme and prevent usage of the state derivative information in auxiliary vector calculation.

Update laws for the information matrix $\boldsymbol{\Omega_i}$ and the auxiliary vector $\boldsymbol{\eta_i}$ are designed as (5.15).

$$\begin{aligned} \dot{\boldsymbol{\Omega}}_{\boldsymbol{i}}(t) &= -K(t)\boldsymbol{\Omega_i}(t) + \boldsymbol{\phi_{if}}(t)\boldsymbol{\phi_{if}}^T(t) \\ \dot{\boldsymbol{\eta}}_{\boldsymbol{i}}(t) &= -K(t)\boldsymbol{\eta_i}(t) + \boldsymbol{\phi_{if}}(t)\left(\frac{1}{k} x_i(t) - \zeta_{if}(t)\right)^T \end{aligned} \tag{5.15}$$

with $\boldsymbol{\Omega_i}(t_0) = 0_{m_i \times m_i}$ and $\boldsymbol{\eta_i}(t_0) = 0_{m_i \times 1}$. $K(t)$ is a forgetting factor to be designed, which is positive and bounded. The information matrix update law in (5.15) consists

of two terms. The first term is defined by introducing the forgetting factor (5.17) to the current information matrix obtained from accumulated regressor data for previous time interval. The second term represents the effects of the current filtered regressor $\boldsymbol{\phi_{if}}$ on the information matrix update.

$\boldsymbol{\Omega_i}$ and $\boldsymbol{\eta_i}$ are derived by integrating the update laws (5.15).

$$\begin{aligned}\boldsymbol{\Omega_i}(t) &= \int_{t_0}^{t} e^{-\int_{\tau}^{t} K(\nu)d\nu} \boldsymbol{\phi_{if}}(\tau)\boldsymbol{\phi_{if}}^{T}(\tau)d\tau \\ \boldsymbol{\eta_i}(t) &= \int_{t_0}^{t} e^{-\int_{\tau}^{t} K(\nu)d\nu} \boldsymbol{\phi_{if}}(\tau)\left(\frac{1}{k}x_i(\tau) - \zeta_{if}(\tau)\right)^{T} d\tau \\ &= \boldsymbol{\Omega_i}(t)\boldsymbol{\theta}_i\end{aligned} \tag{5.16}$$

It can be observed from (5.16) that the information matrix $\boldsymbol{\Omega_i}$ is positive semi-definite. Besides, (5.16) implies that the information matrix can have full rank and become positive definite matrix over time, when the regressor signal is excited.

$K(t)$ is a forgetting factor, which is designed as below.

$$K(t) = k_L + (k_U - k_L)\tanh\left(\vartheta\|\dot{\boldsymbol{\phi}}_{\boldsymbol{if}}(t)\|\right) \tag{5.17}$$

k_L and k_U indicate lower and upper bounds of $K(t)$ with positive constant values, respectively. ϑ is a constant and positive design parameter for the forgetting factor.

The effects of the forgetting factor on the information matrix are addressed as follows. First, the forgetting factor enables the information matrix to be upper bounded in its norm. Second, the forgetting factor makes richer signal to be reflected more on the information matrix update (5.15). The forgetting factor (5.17) becomes larger when $\boldsymbol{\phi_{if}}$ contains richer data with large $\|\dot{\boldsymbol{\phi}}_{\boldsymbol{if}}(t)\|$. Consequently, the information matrix is updated to consider the current filtered regressor signal more and the accumulated data less. On the other hand, when $\boldsymbol{\phi_{if}}$ does not contain rich data with small $\|\dot{\boldsymbol{\phi}}_{\boldsymbol{if}}(t)\|$, the forgetting factor (5.17) gets smaller. As a result, the current filtered regressor signal is reflected less and the accumulated data affects more to the information matrix update.

After the excitation is finished, the information matrix will be degenerated due to the forgetting design and the incoming filtered regressor signal which is not rich. In

order to prevent this phenomena, information matrix selection method is introduced.

$$\begin{aligned} &\boldsymbol{\Omega_{ib}}(t) \triangleq \boldsymbol{\Omega_i}(t_b), \quad \boldsymbol{\eta_{ib}}(t) \triangleq \boldsymbol{\eta_i}(t_b) \\ &t_b \triangleq \max \left\{ \underset{\tau \in (t_0, t)}{\operatorname{argmax}} \mathcal{F}(\Omega(\tau)) \right\} \\ &\text{where } \mathcal{F}(\Omega(\tau)) = \sigma_{min}(\tau) \end{aligned} \tag{5.18}$$

$\mathcal{F}(\Omega(\tau))$ is selected as a minimum eigenvalue of the information matrix. Eigenvalues of the information matrix are related to speed for the estimation error based term of the adaptation law in corresponding eigenvector directions. This means that maximizing the minimum eigenvalue can be interpreted as maximizing the adaptation speed of the slowest direction. Information matrix becomes positive definite during excitation, but after FE it might become positive semi-definite again with rank deficiency. The selection method (5.18) has an effect which automatically excludes positive semi-definite matrices with zero eigenvalues. Hence, the condition to guarantee parameter convergence is relaxed from PE to FE through accumulation and selection procedures.

A final adaptation law is suggested as (5.19), with best information matrix and auxiliary vector from (5.18).

$$\frac{d}{dt}\hat{\boldsymbol{\theta}}_{\boldsymbol{i}} = z_i \boldsymbol{\Gamma_i} \boldsymbol{\phi_i} - \lambda_i \boldsymbol{\Gamma_i} \left(\boldsymbol{\Omega_{ib}} \hat{\boldsymbol{\theta}}_{\boldsymbol{i}} - \boldsymbol{\eta_{ib}} \right) \tag{5.19}$$

Note that the adaptation law (5.19) is designed to estimate $\boldsymbol{\theta_i}$ for each loop separately. If all $\boldsymbol{\theta_i}$ are augmented into one parameter estimation problem for whole system, the size of this augmented matrix for the unknown parameters is $\sum_{i=1}^{n} m_i \times n$, and the size of the corresponding information matrix becomes $\sum_{i=1}^{n} m_i \times \sum_{i=1}^{n} m_i$ in maximum. This implies that complex matrix operations, like matrix multiplication and eigenvalue calculation for matrix selection, should be conducted with an excessively large size of a matrix. Since the computational complexity of those matrix operations dramatically increases as the matrix size enlarges, it is beneficial to divide the adaptation problem into smaller ones and conduct estimation for parameters in each loop, as addressed in (5.19).

5.3.2 Stability Proof

A Lyapunov candidate function V_n considering both tracking and parameter estimation errors, is selected as below.

$$V_n = \frac{1}{2}\sum_{i=1}^{n} z_i^2 + \frac{1}{2}\sum_{i=1}^{n}\sum_{j=1}^{m_i}\frac{1}{\gamma_{i_j}}\Big(\hat{\theta}_{i_j} - \theta_{i_j}\Big)^2 \tag{5.20}$$

V_n is positive definite for all tracking and parameter estimation errors except the origin. $\dot{V}_n$, derivative of V_n, can be derived as (5.21).

$$\begin{aligned}
\dot{V}_n =& \sum_{i=1}^{n} z_i \dot{z}_i + \sum_{i=1}^{n}\sum_{j=1}^{m_i}\frac{1}{\gamma_{i_j}}\left(\hat{\theta}_{i_j} - \theta_{i_j}\right)\dot{\hat{\theta}}_{ij} \\
=& \Bigg[z_1\left\{-C_1 z_1 + g_1 z_2 - \tilde{\boldsymbol{\theta}}_1^T \boldsymbol{\phi}_1\right\} \\
&+ \sum_{i=2}^{n-1} z_i\left\{-C_i z_i - g_{i-1} z_{i-1} + g_i z_{i+1} - \tilde{\boldsymbol{\theta}}_i^T \boldsymbol{\phi}_i\right\} \\
&+ z_n\left\{-C_n z_n + g_{n-1} z_{n-1} - \tilde{\boldsymbol{\theta}}_n^T \boldsymbol{\phi}_n\right\}\Bigg] \\
&+ \sum_{i=1}^{n}\sum_{j=1}^{m_i}\frac{1}{\gamma_{i_j}}\left(\hat{\theta}_{i_j} - \theta_{i_j}\right)\dot{\hat{\theta}}_{i_j} \\
=& -\sum_{i=1}^{n} C_i z_i^2 - \sum_{i=1}^{n}\sum_{j=1}^{m_i}\left(\hat{\theta}_{i_j} - \theta_{i_j}\right)\phi_{i_j} z_i \\
&+ \sum_{i=1}^{i}\sum_{j=1}^{m_i}\frac{1}{\gamma_{i_j}}\left(\hat{\theta}_{i_j} - \theta_{i_j}\right)\dot{\hat{\theta}}_{i_j} \\
=& -\sum_{i=1}^{n} C_i z_i^2 - \sum_{i=1}^{n}\lambda_i\Big(\hat{\boldsymbol{\theta}}_{\boldsymbol{i}} - \boldsymbol{\theta}_{\boldsymbol{i}}\Big)^T\Big(\boldsymbol{\Omega}_{\boldsymbol{i}b}\hat{\boldsymbol{\theta}}_{\boldsymbol{i}} - \boldsymbol{\eta}_{\boldsymbol{i}b}\Big) \\
=& -\sum_{i=1}^{n} C_i z_i^2 - \sum_{i=1}^{n}\lambda_i\Big(\hat{\boldsymbol{\theta}}_{\boldsymbol{i}} - \boldsymbol{\theta}_{\boldsymbol{i}}\Big)^T\boldsymbol{\Omega}_{\boldsymbol{i}b}\Big(\hat{\boldsymbol{\theta}}_{\boldsymbol{i}} - \boldsymbol{\theta}_{\boldsymbol{i}}\Big)
\end{aligned} \tag{5.21}$$

Since $\boldsymbol{\Omega}_{\boldsymbol{i}b}$ becomes positive definite under FE, $\dot{V}_n$ becomes negative definite for all tracking and parameter estimation errors except the origin. To this end, the asymptotic stability for the closed-loop system is guaranteed.

5.4 Simulation

Simulations are carried out to check performance of the proposed composite ABKS. As an illustrative example, simulation results with short period mode dynamics for an aircraft will be suggested in Section 5.4.

A short period mode dynamics is considered in this simulation as follows.

$$\begin{bmatrix} \dot{\alpha} \\ \dot{q} \end{bmatrix} = \begin{bmatrix} Z_\alpha^* & 1 \\ M_\alpha^* & M_q^* \end{bmatrix} \begin{bmatrix} \alpha \\ q \end{bmatrix} + \begin{bmatrix} Z_\delta^* \\ M_\delta^* \end{bmatrix} \delta \tag{5.22}$$

State variables α and q represent an angle of attack and a pitch rate, respectively. δ denotes a deflection angle of an elevator. Z_α^*, M_α^*, M_q^*, Z_δ^* and M_δ^* are aerodynamic derivatives.

(5.22) is rewritten in the strict-feedback form in (5.1) with (5.2) under the assumption that the effect of Z_δ^* is negligible [23].

$$\begin{aligned}
&\boldsymbol{x} = [\alpha, q]^T \\
&\boldsymbol{f}(\boldsymbol{x}) = [0, 0]^T \\
&\boldsymbol{g}(\boldsymbol{x}) = \mathrm{diag}\,[1, M_\delta^*] \\
&\boldsymbol{u} = [q, \delta]^T \\
&\boldsymbol{\Delta}(\boldsymbol{x}) = \left[\Delta_1(\boldsymbol{x_1'}), \Delta_2(\boldsymbol{x_2'})\right]^T \\
&\qquad = \left[\boldsymbol{\theta_1}^T \boldsymbol{\phi_1}(\boldsymbol{x_1'}), \boldsymbol{\theta_2}^T \boldsymbol{\phi_2}(\boldsymbol{x_2'})\right]^T \\
&\text{where} \\
&\boldsymbol{\theta_1} = [Z_\alpha^*] \\
&\boldsymbol{\phi_1}(\boldsymbol{x_1'}) = [\alpha] \\
&\boldsymbol{\theta_2} = \left[M_\alpha^*, M_q^*\right]^T \\
&\boldsymbol{\phi_2}(\boldsymbol{x_2'}) = [\alpha, q]^T
\end{aligned} \tag{5.23}$$

Note that Z_α^*, M_α^* and M_q^* are considered as unknown model parameters to be estimated as $\hat{\boldsymbol{\theta}}_{\mathbf{1}} = \left[\hat{Z}_\alpha^*\right]$ and $\hat{\boldsymbol{\theta}}_{\mathbf{2}} = \left[\hat{M}_\alpha^*, \hat{M}_q^*\right]^T$ with the proposed composite ABKS. The estimate $\hat{(\cdot)}$ of the parameter $(\cdot)$ is defined as $\hat{(\cdot)} = (\cdot)(1 + D_{(\cdot)})$, where $D_{(\cdot)}$ is a parameter uncertainty level on $(\cdot)$ in percentage. True values for the model parameters are set to be $\boldsymbol{\theta_1} = [-1.963]$ and $\boldsymbol{\theta_2} = [-4.749, -3.933]^T$ and $M_\delta^* =$

-26.685.

To have critical understandings about closed-loop characteristics with the proposed composite ABKS, simulation results with BKS will be additionally suggested and investigated for cases with and without $D_{(\cdot)}$, as references. For BKS and the proposed composite ABKS, C_1 and C_2 are set to be 1.5, and angle of attack command α_c is given as low pass filtered $0^\circ \rightarrow 1.5^\circ \rightarrow 0^\circ \rightarrow -1.5^\circ \rightarrow 0^\circ$ with $\frac{1}{s+1}$. Simulation parameters for the proposed composite ABKS can be summarized as Table. 5.1.

Table 5.1: Simulation parameters for ABKS

$\mathbf{\Gamma_1}$	λ_1	$\mathbf{\Gamma_2}$	λ_2	k	k_L	k_U	ϑ
10^4	0.5	diag $\left[10^4, 10^4\right]$	0.5	10^{-3}	0.1	10	1

Figure. 5.1 shows each α response for nominal BKS, BKS with $D_{(\cdot)} = 5\%$ and ABKS.

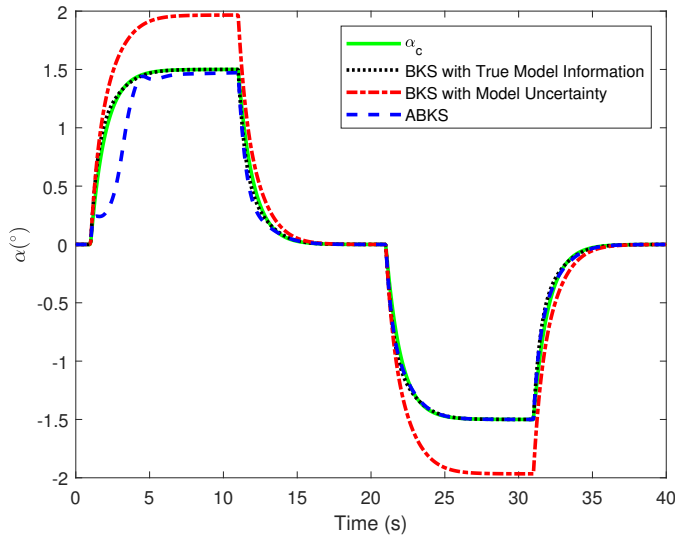

Figure 5.1: α Response

Magnitudes of tracking errors for each case and estimation errors with the proposed composite ABKS are suggested in Figure. 5.2.

It is shown in Fig. 5.1 that the closed-loop system with BKS under true model information tracks a desired response determined by C_1 and C_2 without any steady state error. However, for BKS, 5% error on model information results in about 30% steady state error. The angle of attack response with new composite ABKS converges to the command without any prior knowledge on model parameters. At

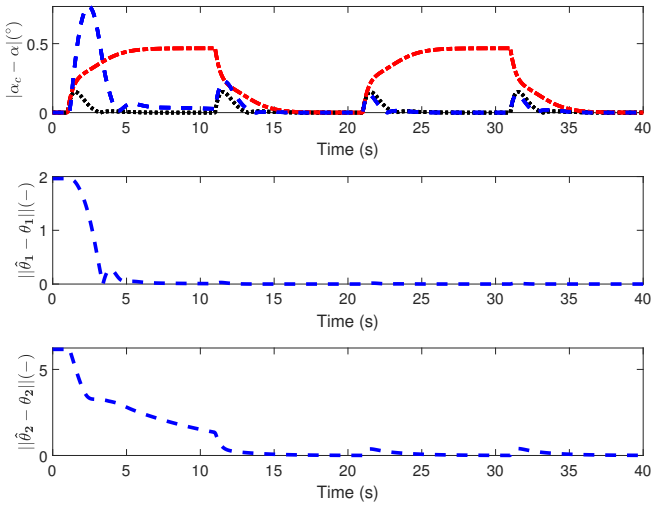

Figure 5.2: Tracking and Estimation Error

the early stage, since the parameter estimation is not converged yet, it is observed in Fig. 5.1 and Fig. 5.2 that the tracking performance with the proposed composite ABKS is worse than with BKS for the nominal case. As the parameter estimation converges, the tracking performance of the system with new composite ABKS is enhanced, showing similar performance with nominal BKS, as addressed in Fig. 5.1 and Fig. 5.2. These simulation results imply that the information matrix becomes full rank with the finite excitation and the information matrix is maintained to be full rank after the finite excitation. The proposed composite ABKS shows high estimation and tracking performance without persistent excitation.

5.5 Conclusion

A new composite ABKS control is successfully suggested with relaxation of PE requirement to FE for parameter convergence and reduction of computational complexity from decreased estimation problem dimension. A composite adaptation method is applied for enhanced estimation and tracking performance. Parameter convergence is accomplished without PE by making the information matrix full rank only with FE. The adaptation law of the proposed composite ABKS is designed by taking advantage of a cascade control structure of BKS. As a result, this adaptation law estimates uncertain model parameters of each loop separately and computational complexity is decreased from the reduced estimation problem dimension. Simulation results are provided to show performance with the proposed composite ABKS under FE.

References

[1] Petar V Kokotovic. The joy of feedback: nonlinear and adaptive. *IEEE Control Systems Magazine*, 12(3):7–17, 1992.

[2] Yoonsoo Kim and Byoung Soo Kim. Pitch autopilot design for agile missiles with uncertain aerodynamic coefficients. *IEEE Transactions on Aerospace and Electronic Systems*, 49(2):907–914, 2013.

[3] Jawhar Ghommam and Maarouf Saad. Autonomous landing of a quadrotor on a moving platform. *IEEE Transactions on Aerospace and Electronic Systems*, 53(3):1504–1519, 2017.

[4] Jean-Jacques E Slotine, Weiping Li, et al. *Applied nonlinear control*. Prentice hall Englewood Cliffs, NJ, 1991.

[5] Manuel A Duarte and Kumpati S Narendra. Combined direct and indirect approach to adaptive control. *IEEE Transactions on Automatic Control*, 34(10):1071–1075, 1989.

[6] M Kemal Ciliz. Combined direct and indirect adaptive control for a class of nonlinear systems. *IET Control Theory & Applications*, 3(1):151–159, 2009.

[7] Kumpati S Narendra and Manuel A Duarte. Application of robust adaptive control using combined direct and indirect methods. *International Journal of Adaptive Control and Signal Processing*, 3(2):131–142, 1989.

[8] Jean-Jacques E Slotine and Weiping Li. Composite adaptive control of robot manipulators. *Automatica*, 25(4):509–519, 1989.

[9] Eugene Lavretsky. Combined/composite model reference adaptive control. *IEEE Transactions on Automatic Control*, 54(11):2692–2697, 2009.

[10] Parag M Patre, William MacKunis, Marcus Johnson, and Warren E Dixon. Composite adaptive control for euler–lagrange systems with additive disturbances. *Automatica*, 46(1):140–147, 2010.

[11] Parag M Patre, Shubhendu Bhasin, Zachary D Wilcox, and Warren E Dixon. Composite adaptation for neural network-based controllers. *IEEE Transactions on Automatic Control*, 55(4):944–950, 2010.

[12] Petros A Ioannou and Petar V Kokotovic. Instability analysis and improvement of robustness of adaptive control. *Automatica*, 20(5):583–594, 1984.

[13] Kumpatis Narendra and Anuradham Annaswamy. A new adaptive law for robust adaptation without persistent excitation. *IEEE Transactions on Automatic control*, 32(2):134–145, 1987.

[14] Tansel Yucelen and Wassim M Haddad. Low-frequency learning and fast adaptation in model reference adaptive control. *IEEE Transactions on Automatic Control*, 58(4):1080–1085, 2012.

[15] Chengyu Cao and Naira Hovakimyan. Design and analysis of a novel L_1 adaptive control architecture with guaranteed transient performance. *IEEE Transactions on Automatic Control*, 53(2):586–591, 2008.

[16] Tansel Yucelen and Anthony J Calise. Derivative-free model reference adaptive control. *Journal of Guidance, Control, and Dynamics*, 34(4):933–950, 2011.

[17] Girish Chowdhary, Tansel Yucelen, Maximillian Mühlegg, and Eric N Johnson. Concurrent learning adaptive control of linear systems with exponentially convergent bounds. *International Journal of Adaptive Control and Signal Processing*, 27(4):280–301, 2013.

[18] Girish Chowdhary, Maximilian Mühlegg, and Eric Johnson. Exponential parameter and tracking error convergence guarantees for adaptive controllers without persistency of excitation. *International Journal of Control*, 87(8):1583–1603, 2014.

[19] Anup Parikh, Rushikesh Kamalapurkar, and Warren E Dixon. Integral concurrent learning: Adaptive control with parameter convergence using finite excitation. *International Journal of Adaptive Control and Signal Processing*, 2018.

[20] Namhoon Cho, Hyo-Sang Shin, Youdan Kim, and Antonios Tsourdos. Composite model reference adaptive control with parameter convergence under finite excitation. *IEEE Transactions on Automatic Control*, 63(3):811–818, 2017.

[21] MK Ciliz. Adaptive backstepping control using combined direct and indirect adaptation. *Circuits, Systems & Signal Processing*, 26(6):911–939, 2007.

[22] G Leitmann. Guaranteed asymptotic stability for some linear systems with bounded uncertainties. *Journal of Dynamic Systems, Measurement, and Control*, 101(3):212–216, 1979.

[23] Donald McLean. *Automatic flight control systems*. Prentice Hall, New York, 1990.

[24] Hassan K Khalil. *Nonlinear systems*. Upper Saddle River, 1996.

[25] I. Kanellakopoulos M. Krstic and P. Kokotovic. *Nonlinear and Adaptive Control*. John Wiley and Sons, Inc., New York, 1995.

Chapter 6

Composite Adaptive Backstepping Control with New Information Matrix

6.1 Introduction

Adaptive control is one of the most widely and successfully applied control methodologies for dynamic systems with uncertain model parameters [1–5]. Uncertainty or unknown variation in model parameters frequently occurs in many practical applications e.g. ship steering [1, 6], aircraft control [2, 7, 8], process control [9, 10], power system control [3, 11] and robot manipulation [4, 5, 12]. The overall aim in adaptive control algorithms is to maintain consistent performance of the closed loop system under the model uncertainty. The basic idea for the adaptive control methodologies to achieve this aim can be summarized as follows; uncertain model parameters or corresponding controller parameters are estimated online via an adaptation law and these estimates are utilized in a control command calculation.

Chapter 6 considers a composite adaptation law [12–24], which is designed by introducing a linear regression term to a tracking error based adaptation law. Note that the composite adaptation law achieves faster estimation with smoother transient response than the tracking error based adaptation law, resulting in enhanced estimation and tracking performance with improved system robustness [25]. The linear regression term consists of the information matrix and the corresponding auxiliary vector. The information matrix appears to be positive semi-definite with rank-1 as

shown in [12, 25] with its fundamental design. Consequently, persistent excitation (PE) is required to guarantee the convergence of the parameter estimation. If parameter estimates do not converge to their true values, parameter drift can occur especially under the existence of non-parametric uncertainties such as noise and unmodeled dynamics, resulting in instability phenomena with sudden bursting [25]. Hence, the convergence of the parameter estimation should be guaranteed, but PE requirement is undesirable for practical applications since this leads to continuous oscillations of state and control input signals. The leading principle to relax the PE requirement is to design positive definite information matrix under finite excitation (FE) by modifying its fundamental form with positive semi-definiteness to be full rank.

There have been extensive studies [26–30] which attempt to design positive definite information matrix under FE by accumulating rank-1 matrices over time. Note that the information matrix is populated to be full rank with rank-1 matrices obtained from sufficiently excited regressor signals. Since this accumulation based approach can lead to unboundedness of the information matrix and low tracking capability against sudden parameter changes, a forgetting algorithm is introduced to this approach. The forgetting algorithm can make the information matrix become rank deficient after FE, but this is prevented by additionally introduced selective update scheme. Despite those measures in the previous researches, limitations from the nature of accumulation over time still remain as follows. First, uncertain amount of time is required to obtain sufficient number of linearly independent regressor signals to make the information matrix full rank. Note that adaptation speed is degenerated and asymptotic stability is not guaranteed before the information matrix becomes full rank. Second, the eigenvalues of the information matrix constructed by accumulating the rank-1 matrices from the regressor vectors with uncertain directions can show undesirable pattern. For example, when obtained regressors are independent but on a similar direction over time, the information matrix has an excessively large principal eigenvalue and the others with extremely small values, resulting in lack of system robustness and adaptation speed degeneration, respectively. These issues do not appear if positive definite information matrix can be achieved under FE without accumulation over time.

In Chapter 6, a new paradigm for the information matrix design is proposed to accomplish full rank under FE for parameter convergence by developing a modulation-based approach. Since the modulation effects of the multiple filters on a regressor signal are different from each other especially in its transient phase, a sufficient

number of filtered regressor signals which are linearly independent with each other can be obtained at each time step during excitation. These filtered regressor vectors are modified to be orthogonal from each other while maintaining their original magnitudes, and the information matrix is constructed from the set of these modified regressor vectors. The information matrix is updated to maximize its minimum eigenvalue to enhance the adaptation speed and prevent a possible impacts from linear dependency between filtered regressor vectors after excitation. This information matrix is guaranteed to be full rank for all the time from the beginning under FE, while achieving bounded information matrix and enhanced tracking capability. Besides, adaptation speed and system robustness can be improved with a moderate level of eigenvalues of the information matrix from the modified filtered regressors.

The rest of Chapter 6 is organized as follows. Preliminaries with mathematical definitions are given in Section 6.2 and Section 6.3 provides system dynamics with model uncertainties. In Section 6.4, a composite adaptive control with new information matrix is proposed to guarantee parameter convergence under FE. The fundamental structure of the composite adaptive control is addressed in Section 6.4.1, and Section 6.4.2 suggests new information matrix from new modulation based design approach and corresponding composite adaptation law. Section 6.5 presents key properties of new information matrix including its positive definiteness and boundedness under FE with theoretical proofs. In Section 6.6, it is proven that the closed-loop system with the proposed algorithm is globally exponentially stable. Numerical simulations in Section 6.7 are performed to examine the characteristics illustrated in Section 6.4, 6.5 and 6.6. The overall concluding remarks are addressed in Section 6.8.

6.2 Preliminaries

The main objective of this research is to propose new composite adaptive control algorithm with relaxed requirement for parameter convergence from PE to FE. In Section 6.2, definitions of persistent excitation (PE) and finite excitation (FE) in [25, 31] are addressed as preliminaries.

Definition 6.1. *(Persistent Excitation) : A bounded vector signal $\boldsymbol{\psi}(t)$ is persistently exciting, if $\forall t \geq t_0$ there exist $T > 0$ and $\gamma > 0$ s.t.*

$$\int_t^{t+T} \boldsymbol{\psi}(\tau)\boldsymbol{\psi}^T(\tau)d\tau \geq \gamma \boldsymbol{I} \tag{6.1}$$

Definition 6.2. *(Finite Excitation) : A bounded vector signal $\boldsymbol{\psi}(t)$ is finitely exciting over a time interval $[t_s, t_s + T]$, if there exist $T > 0$, $t_s \geq t_0$ and $\gamma > 0$ s.t.*

$$\int_{t_s}^{t_s+T} \boldsymbol{\psi}(\tau)\boldsymbol{\psi}^T(\tau)d\tau \geq \gamma \boldsymbol{I} \tag{6.2}$$

6.3 System dynamics

In Chapter 6, system dynamics with model uncertainty is considered in strict feedback form as (6.3), since backstepping control is introduced in Section 6.4.1 as a representative example of baseline control algorithms to apply new composite adaptation law in Section 6.4.2. Note that the proposed adaptation law is compatible with any stabilizable system and baseline control algorithm.

$$\dot{\boldsymbol{x}} = \boldsymbol{f}(\boldsymbol{x}) + \boldsymbol{G}(\boldsymbol{x})\left[\boldsymbol{u} + \boldsymbol{\Delta}(\boldsymbol{x})\right]$$

where

$$\begin{aligned}
&\boldsymbol{x} = [x_1, x_2, \cdots, x_n]^T \\
&\boldsymbol{x}_i' = [x_1, x_2, \cdots, x_i]^T \quad (i = 1, \cdots, n) \\
&\boldsymbol{f}(\boldsymbol{x}) = \left[f_1(\boldsymbol{x}_1'), f_2(\boldsymbol{x}_2'), \cdots, f_n(\boldsymbol{x}_n')\right]^T \\
&\boldsymbol{G}(\boldsymbol{x}) = \text{diag}\left[g_1(\boldsymbol{x}_1'), g_2(\boldsymbol{x}_2'), \cdots, g_n(\boldsymbol{x}_n')\right] \\
&\boldsymbol{u} = [u_1, u_2, \cdots, u_n]^T \text{ with } u_i = \begin{cases} x_{i+1} & (i = 1, \cdots, n-1) \\ u & (i = n) \end{cases} \\
&\boldsymbol{\Delta}(\boldsymbol{x}) = \left[\Delta_1(\boldsymbol{x}_1'), \Delta_2(\boldsymbol{x}_2'), \cdots, \Delta_n(\boldsymbol{x}_n')\right]^T
\end{aligned} \tag{6.3}$$

$\boldsymbol{x} \in \mathbb{R}^{n\times 1}$ denotes a state vector and $\boldsymbol{x}_i' \in \mathbb{R}^{i\times 1}$ are subsets of the state vector. $\boldsymbol{f}(\boldsymbol{x}) \in \mathbb{R}^{n\times 1}$ and $\boldsymbol{G}(\boldsymbol{x}) \in \mathbb{R}^{n\times m}$ are known model information, and all elements in the control effectiveness information are not zeros (i.e. $g_i(\boldsymbol{x}_i') \neq 0$). $\boldsymbol{u} \in \mathbb{R}^{m\times 1}$ is a control input vector; a real control input u is applied for the innermost loop and a state becomes a pseudo input for the next outer-loop in recursive way. Matched model uncertainty is represented as $\boldsymbol{\Delta}(\boldsymbol{x}) \in \mathbb{R}^{n\times 1}$.

It is assumed that the model uncertainty in (6.3) has a linearly parameterized structure, resulting in (6.4).

$$
\begin{aligned}
&\Delta_i(\boldsymbol{x}_i') = \boldsymbol{\theta}_i^T \boldsymbol{\phi}_i(\boldsymbol{x}_i') \qquad (i = 1, \cdots, n) \\
&\text{where} \\
&\boldsymbol{\theta}_i = \left[\theta_{i1}, \theta_{i2} \cdots \theta_{im_i}\right]^T \\
&\boldsymbol{\phi}_i(\boldsymbol{x}_i') = \left[\phi_{i1}(\boldsymbol{x}_i'), \phi_{i2}(\boldsymbol{x}_i') \cdots \phi_{im_i}(\boldsymbol{x}_i')\right]^T
\end{aligned} \tag{6.4}
$$

$\boldsymbol{\theta}_i \in \mathbb{R}^{m_i \times 1}$ represents a vector of unique and constant true parameters for the i-th loop, which is unknown. $\boldsymbol{\phi}_i(\boldsymbol{x}_i') \in \mathbb{R}^{m_i \times 1}$ indicates a known regressor vector for the i-th loop, where its components $\phi_{ij}(\boldsymbol{x}_i')$ are linearly independent functions from each other.

6.4 Composite Adaptive Control with New Information Matrix

6.4.1 Structure of Composite Adaptive Control

As a representative example, composite adaptive backstepping control is introduced in Chapter 6. Note that the composite adaptation law with new information matrix proposed in Section 6.4.2 is compatible with various baseline control algorithms, whose application is not restricted to backstepping control. With the backstepping algorithm, the adaptive control system in Chapter 6 can be designed for each loop in a recursive way by taking advantage of its cascade structure [28, 32].

The control input command u_{ic} based on the backstepping algorithm is derived as (6.5).

$$
u_{ic} = \begin{cases}
\dfrac{1}{g_i}\left[-C_i z_i - f_i + \dot{x}_{ic}\right] - \hat{\boldsymbol{\theta}}_i^T \boldsymbol{\phi}_i & (i = 1) \\
\dfrac{1}{g_i}\left[-C_i z_i - f_i + \dot{x}_{ic} - g_{i-1} z_{i-1}\right] - \hat{\boldsymbol{\theta}}_i^T \boldsymbol{\phi}_i & (i = 2, \cdots, n)
\end{cases} \tag{6.5}
$$

C_i is a constant and positive design parameter for u_{ic} to achieve a desired i-th closed-loop response. z_i is the i-th component of a tracking error vector $\boldsymbol{z} \triangleq \boldsymbol{x} - \boldsymbol{x}_c \in \mathbb{R}^{n \times 1}$. $\hat{\boldsymbol{\theta}}_i \in \mathbb{R}^{m_i \times 1}$ denotes an estimate of the unknown parameter vector in the i-th loop $\boldsymbol{\theta}_i$, obtained by the composite adaptation law (6.6). Note that subscript c represents a

command to follow.

A fundamental structure of the composite adaptation law to provide perfect estimation for u_{ic} in (6.5) is derived as (6.6) with $\boldsymbol{\phi}_i' \triangleq g_i \boldsymbol{\phi}_i$.

$$\dot{\hat{\boldsymbol{\theta}}}_i = z_i \boldsymbol{\Gamma}_i \boldsymbol{\phi}_i' - \lambda_i \boldsymbol{\Gamma}_i \left(\boldsymbol{\Omega}_i \hat{\boldsymbol{\theta}}_i - \boldsymbol{\eta}_i \right) \quad (i = 1, \cdots, n) \tag{6.6}$$

$\boldsymbol{\Gamma}_i \in \mathbb{R}^{m_i \times m_i}$ is a constant and positive definite matrix with design parameters of the adaptation law for the i-th loop. λ_i represents a relative weight factor on the linear regression term to the tracking error based term in the adaptation law for the i-th loop, which is constant and positive. $\boldsymbol{\Omega}_i \in \mathbb{R}^{m_i \times m_i}$ denotes an information matrix for the i-th loop, which is designed in Section 6.4.2 to be positive definite. An auxiliary vector for the i-th loop $\boldsymbol{\eta}_i \in \mathbb{R}^{m_i \times 1}$ is designed to satisfy $\boldsymbol{\eta}_i = \boldsymbol{\Omega}_i \boldsymbol{\theta}_i$ in Section 6.4.2 to make linear regression term for the composite adaptation law (6.6).

Comparing to the tracking error based adaptation laws, the composite adaptation law (6.6) shows improved estimation and tracking performance with enhanced system robustness because of the additionally introduced linear regression term [25]. The most fundamental way to design $\boldsymbol{\eta}_i = \boldsymbol{\Omega}_i \boldsymbol{\theta}_i$ from known information in dynamics with $\Delta_i(\boldsymbol{x}_i') = \boldsymbol{\theta}_i^T \boldsymbol{\phi}_i(\boldsymbol{x}_i')$ is to design corresponding information matrix as $\boldsymbol{\Omega}_i = \boldsymbol{\phi}_i' \boldsymbol{\phi}_i'^T$ [12, 25]. In this case, $\boldsymbol{\Omega}_i$ is positive semi-definite always with rank-1, resulting in PE requirement to make parameter estimates converge to their true values. This PE requirement can be relaxed by designing a positive definite information matrix under FE with consideration of rank deficiency issue in $\boldsymbol{\Omega}_i = \boldsymbol{\phi}_i' \boldsymbol{\phi}_i'^T$. Previous studies [26–30] utilize the property that rank of $\boldsymbol{\Omega}_i$ can be populated to full rank by accumulating $\boldsymbol{\phi}_i' \boldsymbol{\phi}_i'^T$ over time if direction of $\boldsymbol{\phi}_i'$ changes sufficiently, not persistently. In Chapter 6, a novel idea to design the information matrix with full rank under FE is suggested in Section 6.4.2; a modulation-based approach is developed which utilizes linear independency between multiple filtered regressor signals generated from $\boldsymbol{\phi}_i'$ at each time instance.

6.4.2 New Information Matrix and Composite Adaptation Law

To achieve parameter convergence without PE, new information matrix design framework is proposed in Section 6.4.2, which guarantees its positive definiteness under FE. The final composite adaption law is suggested by combining new information matrix with the fundamental structure of the composite adaptation law introduced

in Section 6.4.1.

The information matrix $\boldsymbol{\Omega}_i$ in the adaptation law for the i-th loop is defined as (6.7).

$$\boldsymbol{\Omega}_i \triangleq \boldsymbol{\Omega}_{iH}^T \boldsymbol{\Omega}_{iH} \tag{6.7}$$

where $\boldsymbol{\Omega}_{iH} \in \mathbb{R}^{m_i \times m_i}$ is a matrix to be designed. Positive semi-definite $\boldsymbol{\Omega}_i$ in (6.7) can become positive definite if $\boldsymbol{\Omega}_i$ is designed to be full rank. Since ranks of $\boldsymbol{\Omega}_i$ and $\boldsymbol{\Omega}_{iH}$ are the same, full rank of $\boldsymbol{\Omega}_i$ can be achieved by designing $\boldsymbol{\Omega}_{iH}$ to be full rank. Chapter 6 proposes a new paradigm for the information matrix design based on modulated regressor vectors $\boldsymbol{\phi}'_{iF_{ij}}$ via multiple filters F_{ij} which are shown to be linearly independent with each other in Section 6.5.1.

$$\begin{aligned} &\boldsymbol{\phi}'_{iF_{ij}} = F_{ij}(s)\boldsymbol{\phi}'_i \\ &\text{where } F_{ij}(s) = \frac{1}{k_{ij}s+1} \end{aligned} \tag{6.8}$$

k_{ij} $(j = 1, \cdots, m_i)$ denote multiple filter parameters with different values for the i-th loop. The fundamental design methodology for $\boldsymbol{\Omega}_{iH}$ with full rank based on the new paradigm is to simply augment $\boldsymbol{\phi}'^T_{iF_{ij}}$. In this case, $\boldsymbol{\Omega}_i$ appears to have an extremely large principal eigenvalue and the others with excessively small values. This is because $\boldsymbol{\phi}'_{iF_{ij}}$ which are obtained from modulations of the same $\boldsymbol{\phi}'_i$ tend to have large parallel component but small orthogonal components with each other. Note that excessively small or large eigenvalues of the information matrix can be problematic for the estimation performance and system robustness since they work as adaptation gains for the corresponding components of the estimation error vector. To this end, Chapter 6 proposes $\boldsymbol{\Omega}_{iH}$ to be designed as (6.9) by augmenting the vectors $\boldsymbol{\phi}^{*T}_{i\,F_{ij}}$.

$$\boldsymbol{\Omega}_{iH} \triangleq \begin{bmatrix} \boldsymbol{\phi}^*_{i\,F_{i1}} & \boldsymbol{\phi}^*_{i\,F_{i2}} & \cdots & \boldsymbol{\phi}^*_{i\,F_{im_i}} \end{bmatrix}^T$$

where

$$\begin{cases} \boldsymbol{\phi}^*_{i\,F_{ij}} = \boldsymbol{\phi}'_{iF_{ij}} & (j=1) \\ \boldsymbol{\phi}^*_{i\,F_{ij}} = \dfrac{\left\|\boldsymbol{\phi}'_{iF_{ij}}\right\|}{\left\|\boldsymbol{\varphi}_{iF_{ij}}\right\|}\boldsymbol{\varphi}_{iF_{ij}}, \quad \boldsymbol{\varphi}_{iF_{ij}} = \boldsymbol{\phi}'_{iF_{ij}} - \displaystyle\sum_{\xi=1}^{j-1} \frac{\boldsymbol{\phi}'_{iF_{ij}} \cdot \boldsymbol{\phi}^*_{i\,F_{i\xi}}}{\left\|\boldsymbol{\phi}^*_{i\,F_{i\xi}}\right\|^2}\boldsymbol{\phi}^*_{i\,F_{i\xi}} & (j=2,\cdots,m_i) \end{cases} \tag{6.9}$$

In (6.9), $\boldsymbol{\phi}^*_{i\,F_{ij}}$ are obtained by conducting following procedures recursively from $j = 2$ to $j = m_i$ with $\boldsymbol{\phi}^*_{i\,F_{i1}} = \boldsymbol{\phi}'_{iF_{i1}}$. First, components of $\boldsymbol{\phi}'_{iF_{ij}}$ parallel to $\boldsymbol{\phi}^*_{i\,F_{ij'}}$ ($j' = 1, \cdots, j-1$) are subtracted from $\boldsymbol{\phi}'_{iF_{ij}}$, resulting in a vector $\boldsymbol{\varphi}_{iF_{ij}}$ orthogonal to $\boldsymbol{\phi}^*_{i\,F_{ij'}}$. Second, $\boldsymbol{\phi}^*_{i\,F_{ij}}$ is obtained by scaling up $\boldsymbol{\varphi}_{iF_{ij}}$ to have the same magnitude with the original $\boldsymbol{\phi}'_{iF_{ij}}$. Note that it is proven in Section 6.5.1 that the proposed $\boldsymbol{\Omega}_{iH}$ is full rank from the orthogonality among $\boldsymbol{\phi}^*_{i\,F_{ij}}$. For detailed discussion on the auxiliary vector design, $\boldsymbol{\Omega}_{iH}$ in (6.9) is rewritten as a multiplication of $\boldsymbol{O}_i \in \mathbb{R}^{m_i \times m_i}$ and $\boldsymbol{H}_i \in \mathbb{R}^{m_i \times m_i}$ in (6.10), which represents an operation to transform $\boldsymbol{\phi}'^T_{iF_{ij}}$ into $\boldsymbol{\phi}^{*T}_{i\,F_{ij}}$ and a set of $\boldsymbol{\phi}'^T_{iF_{ij}}$, respectively.

$$
\begin{aligned}
&\boldsymbol{\Omega}_{iH} = \boldsymbol{O}_i \boldsymbol{H}_i \\
&\text{where} \\
&\boldsymbol{O}_i = \boldsymbol{P}_{im_i} \boldsymbol{P}_{i(m_i-1)} \cdots \boldsymbol{P}_{i1} \\
&\boldsymbol{P}_{ir}(j,l) = \begin{cases}
-\dfrac{\left\|\boldsymbol{\phi}'_{iF_{ij}}\right\|}{\left\|\boldsymbol{\varphi}_{iF_{ij}}\right\|} \dfrac{\boldsymbol{\phi}'_{iF_{ij}} \cdot \boldsymbol{\phi}^*_{i\,F_{il}}}{\left\|\boldsymbol{\phi}^*_{i\,F_{il}}\right\|^2}, & l < j = r \\
\dfrac{\left\|\boldsymbol{\phi}'_{iF_{ij}}\right\|}{\left\|\boldsymbol{\varphi}_{iF_{ij}}\right\|}, & l = j = r \\
1, & l = j \neq r \\
0, & \text{Otherwise}
\end{cases} \\
&\boldsymbol{H}_i \triangleq \begin{bmatrix} \boldsymbol{\phi}'_{iF_{i1}} & \boldsymbol{\phi}'_{iF_{i2}} & \cdots & \boldsymbol{\phi}'_{iF_{im_i}} \end{bmatrix}^T
\end{aligned}
\tag{6.10}
$$

The auxiliary vector $\boldsymbol{\eta}_i$ in the adaptation law for the i-th loop can be suggested as (6.11) with (6.7) and (6.10).

$$
\boldsymbol{\eta}_i \triangleq \boldsymbol{\Omega}_i \boldsymbol{\theta}_i = \boldsymbol{\Omega}_{iH}^T \boldsymbol{\Omega}_{iH} \boldsymbol{\theta}_i = \boldsymbol{\Omega}_{iH}^T \boldsymbol{O}_i \boldsymbol{H}_i \boldsymbol{\theta}_i \tag{6.11}
$$

$\boldsymbol{H}_i \boldsymbol{\theta}_i$, which is a set of filtered uncertainties for the i-th loop $\boldsymbol{\theta}_i^T \boldsymbol{\phi}'_{iF_{ij}}$, can be derived from known information in a set of filtered dynamics for the i-th loop as follows. First, a set of filtered dynamics for the i-th loop is obtained as (6.12) by applying multiple filters $F_{ij}(s)$ in (6.8) to the dynamics (6.3) for the i-th loop in s-domain and taking inverse Laplace transform of this filtered dynamics in s-domain.

$$
\frac{1}{k_{ij}} \left(x_i - x_{iF_{ij}} \right) = f_{iF_{ij}} + g_{uiF_{ij}} + \boldsymbol{\theta}_i{}^T \boldsymbol{\phi}'_{iF_{ij}} \tag{6.12}
$$

where $g_{ui} \triangleq g_i u_i$ and $(\cdot)_{F_{ij}}$ indicates a filtered signal by $F_{ij}(s)$. Second, a set of filtered uncertainties for the i-th loop $\boldsymbol{\theta}_i^T \boldsymbol{\phi}'_{iF_{ij}}$ is obtained as (6.13) from known information in (6.12).

$$\begin{aligned} &\boldsymbol{\theta}_i{}^T \boldsymbol{\phi}'_{iF_{ij}} = \frac{1}{k_{ij}} x_i - \zeta_{iF_{ij}} \\ &\text{where} \\ &\dot{\zeta}_{iF_{ij}} = \frac{1}{k_{ij}} \left(\frac{1}{k_{ij}} x_i + f_i + g_{ui} - \zeta_{iF_{ij}} \right) \end{aligned} \tag{6.13}$$

From the definition of $\boldsymbol{H}_i$ in (6.10) and (6.13), $\boldsymbol{H}_i \boldsymbol{\theta}_i$ is obtained as (6.14).

$$\boldsymbol{H}_i \boldsymbol{\theta}_i = \begin{bmatrix} \frac{1}{k_{i1}} x_i - \zeta_{iF_{i1}} \\ \frac{1}{k_{i2}} x_i - \zeta_{iF_{i2}} \\ \vdots \\ \frac{1}{k_{im_i}} x_i - \zeta_{iF_{im_i}} \end{bmatrix} \tag{6.14}$$

By substituting (6.14) into (6.11), $\boldsymbol{\eta}_i$ is derived as (6.15).

$$\boldsymbol{\eta}_i = \boldsymbol{\Omega}_{iH}^T \boldsymbol{O}_i \begin{bmatrix} \frac{1}{k_{i1}} x_i - \zeta_{iF_{i1}} \\ \frac{1}{k_{i2}} x_i - \zeta_{iF_{i2}} \\ \vdots \\ \frac{1}{k_{im_i}} x_i - \zeta_{iF_{im_i}} \end{bmatrix} \tag{6.15}$$

The new composite adaptation law is obtained as (6.16) by utilizing $\boldsymbol{\Omega}_i$ in (6.7) with (6.9) and $\boldsymbol{\eta}_i$ in (6.15) with the maximum $\mathcal{F}(\boldsymbol{\Omega}_i)$.

$$\begin{aligned} &\dot{\hat{\boldsymbol{\theta}}}_i = z_i \boldsymbol{\Gamma}_i \boldsymbol{\phi}'_i - \lambda_i \boldsymbol{\Gamma}_i \left(\boldsymbol{\Omega}_{ib} \hat{\boldsymbol{\theta}}_i - \boldsymbol{\eta}_{ib} \right) \quad (i = 1, \cdots, n) \\ &\text{where} \\ &\boldsymbol{\Omega}_{ib}(t) \triangleq \boldsymbol{\Omega}_i(t_b), \quad \boldsymbol{\eta}_{ib}(t) \triangleq \boldsymbol{\eta}_i(t_b) \\ &t_b \triangleq \max \left\{ \underset{\tau \in (t_0, t)}{\operatorname{argmax}} \mathcal{F}(\boldsymbol{\Omega}_i(\tau)) \right\} \end{aligned} \tag{6.16}$$

(6.16) implies that $\boldsymbol{\Omega}_{ib}$ and $\boldsymbol{\eta}_{ib}$ are updated only when a newly acquired $\boldsymbol{\Omega}_i$ increases $\mathcal{F}(\boldsymbol{\Omega}_i)$. Minimum eigenvalue of $\boldsymbol{\Omega}_i$ is considered for the metric function $\mathcal{F}(\boldsymbol{\Omega}_i)$ as

(6.17), resulting in adaptation speed maximization in the slowest direction.

$$\mathcal{F}(\mathbf{\Omega}_i) = \min_q \sigma_{\mathbf{\Omega}_i q} \tag{6.17}$$

where $\sigma_{\mathbf{\Omega}_i q}$ $(q = 1, \cdots, m_i)$ denote eigenvalues of $\mathbf{\Omega}_i$. The proposed composite adaptation law accomplishes parameter convergence with positive definite $\mathbf{\Omega}_{ib}$ under FE, which is proven in Section 6.5.1. Note that key design considerations such as linear independency of $\boldsymbol{\phi}'_{iF_{ij}}$, orthogonality of $\boldsymbol{\phi}^*_{\boldsymbol{i}\,F_{ij}}$, and selective update to maximize minimum eigenvalue of $\mathbf{\Omega}_{ib}$, are discussed to show positive definiteness of $\mathbf{\Omega}_{ib}$ in Section 6.5.1.

6.5 Properties of New Information Matrix

6.5.1 Positive Definiteness

The parameter estimates converge to their true values if the information matrix in the composite adaptation law is positive definite. In order to show positive definiteness of the proposed $\mathbf{\Omega}_{ib}$ under FE, the first step is to address linear independency between $\boldsymbol{\phi}'_{iF_{ij}}$ during excitation in Remark 6.1. From Remark 6.1 and the orthogonality between $\boldsymbol{\phi}^*_{i\,F_{ij}}$, the second step is to prove that $\mathbf{\Omega}_{iH}$ is full rank while excited in Lemma 6.1. Based on Lemma 6.1 and the selective update scheme, $\mathbf{\Omega}_{ib}$ is shown to be positive definite for all the time during and after excitation in Theorem 6.1, as the final step.

Remark 6.1. *(Linear Independency between Filtered Regressor Vectors) :* $\boldsymbol{\phi}'_{iF_{ij}}$ *are linearly independent while excited.*

$\boldsymbol{\phi}'_{iF_{ij}} = \left[\phi'_{i1F_{ij}}, \cdots, \phi'_{im_iF_{ij}}\right]^T$ $(j = 1, \cdots, m_i)$ are linearly independent with each other if and only if there exist l^* and l' $(l^* \neq l')$ with any set of β_{ij} which satisfy (6.18) for any j^*.

$$\begin{cases} \phi'_{il^*F_{ij^*}}(t) = \sum_{\substack{j=1 \\ j\neq j^*}}^{m_i} \beta_{ij}\phi'_{il^*F_{ij}}(t) \\ \\ \phi'_{il'F_{ij^*}}(t) \neq \sum_{\substack{j=1 \\ j\neq j^*}}^{m_i} \beta_{ij}\phi'_{il'F_{ij}}(t) \end{cases} \tag{6.18}$$

From (6.8), the dynamics of $\phi'_{il\,F_{ij}}(t)$ can be given as (6.19).

$$k_{ij}\dot{\phi}'_{il\,F_{ij}}(t) = -\phi'_{il\,F_{ij}}(t) + \phi'_{il}(t) \quad (l = 1, \cdots, m_i) \tag{6.19}$$

$\phi'_{il\,F_{ij}}(t)$ is obtained as (6.20) by integrating (6.19) with an initial condition $\phi'_{il\,F_{ij}}(0) = 0$.

$$\phi'_{il\,F_{ij}}(t) = \frac{1}{k_{ij}} \int_0^t e^{-\frac{t-\tau}{k_{ij}}} \phi'_{il}(\tau) d\tau \tag{6.20}$$

By substituting (6.20) and $\phi'_{il} \triangleq g_i \phi_{il}$ into (6.18), (6.18) can be rewritten as (6.21).

$$\begin{cases} \displaystyle\int_0^t e^{-\frac{t-\tau}{k_{ij^*}}} g_i(\tau)\phi_{il^*}(\tau) d\tau = \sum_{\substack{j=1 \\ j\neq j^*}}^{m_i} \beta_{ij} \int_0^t e^{-\frac{t-\tau}{k_{ij}}} g_i(\tau)\phi_{il^*}(\tau) d\tau \\ \displaystyle\int_0^t e^{-\frac{t-\tau}{k_{ij^*}}} g_i(\tau)\phi_{il'}(\tau) d\tau \neq \sum_{\substack{j=1 \\ j\neq j^*}}^{m_i} \beta_{ij} \int_0^t e^{-\frac{t-\tau}{k_{ij}}} g_i(\tau)\phi_{il'}(\tau) d\tau \end{cases} \tag{6.21}$$

Since k_{ij} $(j = 1, \cdots, m_i)$ are defined to be different from each other and ϕ_{il} $(l = 1, \cdots, m_i)$ are linearly independent functions of state variables, a set of β_{ij} which makes both conditions in (6.21) to become equality for all pairs of l^* and l' $(l^* \neq l')$ with any j^* does not exist while ϕ_{il} are excited. This implies that $\boldsymbol{\phi}'_{i\,F_{ij}}$ are linearly independent during the excitation.

Lemma 6.1. *($\boldsymbol{\Omega}_{iH}$ with Full Rank) : $\boldsymbol{\Omega}_{iH}$ is full rank during excitation.*

Proof. $\boldsymbol{\Omega}_{iH}$ is shown to be full rank during excitation by proving that all of its row vectors, $\boldsymbol{\phi}^{*T}_{i\,F_{ij}}$ $(j = 1, \cdots, m_i)$, are non-zero and orthogonal to each other while excited.

First, all $\boldsymbol{\phi}^*_{i\,F_{ij}}$ are shown to be non-zero by utilizing Remark 6.1. From (6.10), $\boldsymbol{\phi}^*_{i\,F_{ij}}$ can be expressed for any j as (6.22).

$$\boldsymbol{\phi}^*_{i\,F_{ij}} = \sum_{\xi=1}^{m_i} \boldsymbol{O}_i(j,\xi) \boldsymbol{\phi}'_{i F_{i\xi}} \tag{6.22}$$

Since $\boldsymbol{\phi}'_{i F_{ij}}$ are linearly independent while excited as described in Remark 6.1, $\boldsymbol{\phi}^*_{i\,F_{ij}}$ in (6.22) equals to $\mathbf{0}_{m_i \times 1}$ during excitation only when $\boldsymbol{O}_i(j,\xi) = 0$ for all $\xi = 1, \cdots, m_i$. However, as shown in (6.10), $\boldsymbol{O}_i(j,j)$ is non-zero with linearly

independent $\boldsymbol{\phi}'_{iF_{ij}}$. This implies that at least one of $\boldsymbol{O}_i(j,\xi)$ is non-zero. Thus, $\boldsymbol{\phi}^*_{i\,F_{ij}} \neq \mathbf{0}_{m_i\times 1}$ $(j=1,\cdots,m_i)$ holds.

Second, orthogonality between non-zero $\boldsymbol{\phi}^*_{i\,F_{ij^*}}$ and $\boldsymbol{\phi}^*_{i\,F_{ij'}}$ for all $j^*, j' \leq m_i (j^* \neq j')$ is proven from a mathematical induction to show that the inner product between $\boldsymbol{\phi}^*_{i\,F_{ij^*}}$ and $\boldsymbol{\phi}^*_{i\,F_{ij'}}$ equals to 0.

The base step shows that $\boldsymbol{\phi}^*_{i\,F_{ij^*}} \cdot \boldsymbol{\phi}^*_{i\,F_{ij'}} = 0$ for all j' and j^* $(1 \leq j^* < j' \leq j^{\#})$ holds with $j^{\#} = 2$. The dot product between $\boldsymbol{\phi}^*_{i\,F_{i2}}$ and $\boldsymbol{\phi}^*_{i\,F_{i1}}$ is calculated from (6.9) as (6.23).

$$\boldsymbol{\phi}^*_{i\,F_{i1}} \cdot \boldsymbol{\phi}^*_{i\,F_{i2}} = \frac{\left\|\boldsymbol{\phi}'_{iF_{i2}}\right\|}{\left\|\boldsymbol{\varphi}_{iF_{i2}}\right\|}\left[\boldsymbol{\phi}^*_{i\,F_{i1}} \cdot \boldsymbol{\phi}'_{iF_{i2}} - \frac{\boldsymbol{\phi}'_{iF_{i2}} \cdot \boldsymbol{\phi}^*_{i\,F_{i1}}}{\left\|\boldsymbol{\phi}^*_{i\,F_{i1}}\right\|^2}\boldsymbol{\phi}^*_{i\,F_{i1}} \cdot \boldsymbol{\phi}^*_{i\,F_{i1}}\right] = 0 \tag{6.23}$$

The inductive step shows that $\boldsymbol{\phi}^*_{i\,F_{ij^*}} \cdot \boldsymbol{\phi}^*_{i\,F_{ij'}} = 0$ for all j' and j^* $(1 \leq j^* < j' \leq j^{\#})$ holds for an arbitrary $j^{\#} = j^+$ $(j^+ \geq 3)$ under the assumption that the relationship is satisfied for $j^{\#} = j^+ - 1$ case. The dot product between $\boldsymbol{\phi}^*_{i\,F_{ij^*}}$ and $\boldsymbol{\phi}^*_{i\,F_{ij'}}$ for any j' and j^* $(1 \leq j^* < j' \leq j^+)$ is calculated as (6.24).

$$\boldsymbol{\phi}^*_{i\,F_{ij^*}} \cdot \boldsymbol{\phi}^*_{i\,F_{ij'}} = \frac{\left\|\boldsymbol{\phi}'_{iF_{ij'}}\right\|}{\left\|\boldsymbol{\varphi}_{iF_{ij'}}\right\|}\left[\boldsymbol{\phi}^*_{i\,F_{ij^*}} \cdot \boldsymbol{\phi}'_{iF_{ij'}} - \sum_{\xi=1}^{j'-1}\frac{\boldsymbol{\phi}'_{iF_{ij'}} \cdot \boldsymbol{\phi}^*_{i\,F_{i\xi}}}{\left\|\boldsymbol{\phi}^*_{i\,F_{i\xi}}\right\|^2}\boldsymbol{\phi}^*_{i\,F_{ij^*}} \cdot \boldsymbol{\phi}^*_{i\,F_{i\xi}}\right] \tag{6.24}$$

If $j' \leq j^+ - 1$, it is given from the assumption that $\boldsymbol{\phi}^*_{i\,F_{ij^*}} \cdot \boldsymbol{\phi}^*_{i\,F_{ij'}}$ in (6.24) equals to 0. If $j' = j^+$, (6.24) is rewritten as (6.25).

$$\boldsymbol{\phi}^*_{i\,F_{ij^*}} \cdot \boldsymbol{\phi}^*_{i\,F_{ij'}} = \frac{\left\|\boldsymbol{\phi}'_{iF_{ij+}}\right\|}{\left\|\boldsymbol{\varphi}_{iF_{ij+}}\right\|}\left[\boldsymbol{\phi}^*_{i\,F_{ij^*}} \cdot \boldsymbol{\phi}'_{iF_{ij+}} - \sum_{\xi=1}^{j^+-1}\frac{\boldsymbol{\phi}'_{iF_{ij+}} \cdot \boldsymbol{\phi}^*_{i\,F_{i\xi}}}{\left\|\boldsymbol{\phi}^*_{i\,F_{i\xi}}\right\|^2}\boldsymbol{\phi}^*_{i\,F_{ij^*}} \cdot \boldsymbol{\phi}^*_{i\,F_{i\xi}}\right] \tag{6.25}$$

Since the assumption indicates that $\boldsymbol{\phi}^*_{i\,F_{ij^*}} \cdot \boldsymbol{\phi}^*_{i\,F_{i\xi}} = 0$ for all $\xi \neq j^*$ $(\xi \leq j^+ - 1)$, (6.26) is derived from (6.25).

$$\begin{aligned}\boldsymbol{\phi}^*_{i\,F_{ij^*}} \cdot \boldsymbol{\phi}^*_{i\,F_{ij'}} &= \frac{\left\|\boldsymbol{\phi}'_{iF_{ij+}}\right\|}{\left\|\boldsymbol{\varphi}_{iF_{ij+}}\right\|}\left[\boldsymbol{\phi}^*_{i\,F_{ij^*}} \cdot \boldsymbol{\phi}'_{iF_{ij+}} - \frac{\boldsymbol{\phi}'_{iF_{ij+}} \cdot \boldsymbol{\phi}^*_{i\,F_{ij^*}}}{\left\|\boldsymbol{\phi}^*_{i\,F_{ij^*}}\right\|^2}\boldsymbol{\phi}^*_{i\,F_{ij^*}} \cdot \boldsymbol{\phi}^*_{i\,F_{ij^*}}\right] \\ &= 0\end{aligned} \tag{6.26}$$

Thus, $\boldsymbol{\phi}^*_{i\,F_{ij^*}}$ is orthogonal to $\boldsymbol{\phi}^*_{i\,F_{ij'}}$ for all j' and j^* $(1 \leq j^* < j' \leq j^{\#})$ with an

arbitrary $j^{\#} = j^{+}$ ($j^{+} \geq 3$) if this statement holds for $j^{\#} = j^{+} - 1$. From the base and the inductive steps, the orthogonality between non-zero $\boldsymbol{\phi}^{*}_{i\,F_{ij^*}}$ and $\boldsymbol{\phi}^{*}_{i\,F_{ij'}}$ for all $j^{*}, j' \leq j^{\#}$ ($j^{*} \neq j'$) is proven.

The first and the second steps imply that all $\boldsymbol{\phi}^{*T}_{i\,F_{ij}}$ are non-zero and orthogonal to each other with $j^{\#} = m_i$ while excited. Thus, $\boldsymbol{\Omega}_{iH}$ is full rank during excitation. □

Theorem 6.1. *(Positive Definiteness of New Information Matrix) :* $\boldsymbol{\Omega}_{ib}(t)$ ($i = 1, \cdots, n$) *is positive definite for all* $t > t_0$ *if* $\boldsymbol{\phi}'_i(t)$ *is finitely exciting over* $t \in [t_0, t_1]$.

Proof. Lemma 6.1 implies that $\boldsymbol{\Omega}_i(t)$ in (6.7) becomes full rank during excitation, resulting in positive definite $\boldsymbol{\Omega}_i(t)$ for $t \in (t_0, t_1]$. Since $\boldsymbol{\Omega}_{ib}(t)$ is selected among $\boldsymbol{\Omega}_i(t)$, $\boldsymbol{\Omega}_{ib}(t)$ is positive definite for $t \in (t_0, t_1]$.

For $t > t_1$, rank deficiency issue for $\boldsymbol{\Omega}_i(t)$ can be arised as $\boldsymbol{\phi}'_{i\,F_{ij}}(t)$ from multiple filters converge to a steady-state value of $\boldsymbol{\phi}'_i(t)$. Although one or more eigenvalues of $\boldsymbol{\Omega}_i(t)$ diminish to 0 and $\boldsymbol{\Omega}_i(t)$ becomes positive semi-definite after excitation, $\boldsymbol{\Omega}_{ib}(t)$ remains to be positive definite for $t > t_1$ as follows. $\boldsymbol{\Omega}_{ib}(t)$ is obtained from $\boldsymbol{\Omega}_i(t)$ with the selective update scheme; $\boldsymbol{\Omega}_{ib}(t)$ is designed to be updated only when $\min_q \sigma_{\boldsymbol{\Omega}_{iq}}$ is increased. Hence, $\boldsymbol{\Omega}_{ib}(t)$ is not updated for the case when $\boldsymbol{\Omega}_i(t)$ becomes rank deficient after excitation, since all eigenvalues of $\boldsymbol{\Omega}_i(t)$ are always positive during excitation.

From the analyses on positive definiteness of $\boldsymbol{\Omega}_{ib}(t)$ for $t \in (t_0, t_1]$ and for $t > t_1$, $\boldsymbol{\Omega}_{ib}(t)$ is shown to be positive definite for all $t > t_0$. □

6.5.2 Boundedness

Since the information matrix works as a time-varying gain for the linear regression term of the composite adaptation law, boundedness of the information matrix is inevitably related to estimation performance of the composite adaptation law and stability of the closed-loop system. In Section 6.5.2, $\boldsymbol{\Omega}_{ib}$ is shown to have lower and upper bounds in Theorem 6.2 and 6.3, respectively.

Theorem 6.2. *(Lower Bound of New Information Matrix) : If* $\boldsymbol{\phi}'_i$ *is exciting over finite time* $[t_0, t_1]$*, there exists a constant* $K_L > 0$ *where* $\boldsymbol{\Omega}_{ib} \geq K_L \boldsymbol{I}_{m_i \times m_i}$ *for all* $t > t_0$.

Proof. In Theorem 6.1, $\boldsymbol{\Omega}_{ib}$ is shown to be positive definite for all $t > t_0$ if $\boldsymbol{\phi}'_i$ is

exciting over $[t_0, t_1]$. $\boldsymbol{\Omega}_{ib} > 0$ indicates that $\min_q \sigma_{\boldsymbol{\Omega}_{ibq}}$ is greater than 0. As a result, there exists $K_L > 0$ where $\boldsymbol{\Omega}_{ib} \geq K_L \boldsymbol{I}_{m_i \times m_i}$ for all $t > t_0$. □

Theorem 6.3. *(Upper Bound of New Information Matrix) : If $\boldsymbol{\phi}_i'$ is bounded i.e. $\left\|\boldsymbol{\phi}_i'\right\| \leq \delta_{\boldsymbol{\phi}_i'}$, there exists a constant $K_U > 0$ where $\boldsymbol{\Omega}_{ib} \leq K_U \boldsymbol{I}_{m_i \times m_i}$ for all $t > t_0$.*

Proof. The sum of the eigenvalues of $\boldsymbol{\Omega}_{ib}$ is obtained as (6.27) from (6.7), (6.9) and (6.16).

$$\sum_{q=1}^{m_i} \sigma_{\boldsymbol{\Omega}_{ibq}} = \mathrm{tr}\left(\boldsymbol{\Omega}_i\right) = \sum_{j=1}^{m_i} \left\| \boldsymbol{\phi}^*_{i\,F_{ij}}(t_b) \right\|^2 \tag{6.27}$$

Since $\left\|\boldsymbol{\phi}'_{iF_{ij}}\right\| \leq \left\|\boldsymbol{\phi}_i'\right\|$ and (6.9) implies $\left\|\boldsymbol{\phi}^*_{i\,F_{ij}}\right\| = \left\|\boldsymbol{\phi}'_{iF_{ij}}\right\|$, (6.27) results in the inequality (6.28).

$$\sum_{q=1}^{m_i} \sigma_{\boldsymbol{\Omega}_{ibq}} \leq m_i \delta^2_{\boldsymbol{\phi}_i'} \tag{6.28}$$

Since $\sigma_{\boldsymbol{\Omega}_{ibq}}$ are all positive for all $t > t_0$ from Theorem 6.1, the upper bound of $\sigma_{\boldsymbol{\Omega}_{ibq}}$ can be suggested as (6.29) from (6.28).

$$\max_q \sigma_{\boldsymbol{\Omega}_{ibq}} < m_i \delta^2_{\boldsymbol{\phi}_i'} \tag{6.29}$$

(6.29) indicates that there exists a constant $K_U > 0$ where $\boldsymbol{\Omega}_{ib} \leq K_U \boldsymbol{I}_{m_i \times m_i}$. □

6.6 Stability Analysis

The stability of the closed-loop system with the proposed composite adaptive control utilizing new information matrix is analyzed in Section 6.6. The closed-loop error dynamics is derived as (6.30) by substituting (6.5) into (6.3).

$$\dot{z}_i = \begin{cases} -C_i z_i + g_i z_{i+1} - \tilde{\boldsymbol{\theta}}_i^T \boldsymbol{\phi}_i' & (i = 1) \\ -C_i z_i - g_{i-1} z_{i-1} + g_i z_{i+1} - \tilde{\boldsymbol{\theta}}_i^T \boldsymbol{\phi}_i' & (i = 2, \cdots, n-1) \\ -C_i z_i - g_{i-1} z_{i-1} - \tilde{\boldsymbol{\theta}}_i^T \boldsymbol{\phi}_i' & (i = n) \end{cases} \tag{6.30}$$

The estimation error dynamics is obtained as (6.31) by rearranging (6.16) with respect to $\tilde{\boldsymbol{\theta}}_i$.

$$\dot{\tilde{\boldsymbol{\theta}}}_i = z_i \boldsymbol{\Gamma}_i \boldsymbol{\phi}_i' - \lambda_i \boldsymbol{\Gamma}_i \boldsymbol{\Omega}_{ib} \tilde{\boldsymbol{\theta}}_i \quad (i = 1, \cdots, n) \tag{6.31}$$

The equilibrium points for the system with (6.30) and (6.31) are $\boldsymbol{z} = \mathbf{0}$ and $\tilde{\boldsymbol{\theta}}_i = \mathbf{0}$ $(i = 1, \cdots, n)$. The global exponential stability of the closed-loop system with (6.30) and (6.31) is shown in Theorem 6.4 based on Lyapunov stability theory.

Theorem 6.4. *(Global Exponential Stability of Closed-loop system) : The closed-loop system with the proposed composite adaptive control utilizing new information matrix is globally exponentially stable under FE for all $t > t_0$.*

Proof. The Lyapunov candidate function V_n is defined as (6.32).

$$V_n = \frac{1}{2} \boldsymbol{z}^T \boldsymbol{z} + \frac{1}{2} \sum_{i=1}^{n} \tilde{\boldsymbol{\theta}}_i^T \boldsymbol{\Gamma}_i^{-1} \tilde{\boldsymbol{\theta}}_i \tag{6.32}$$

(6.32) indicates that $V_n = 0$ if and only if $\boldsymbol{z}$ and $\tilde{\boldsymbol{\theta}}_i$ $(i = 1, \cdots, n)$ are $\mathbf{0}$, and $V_n > 0$ if and only if $\boldsymbol{z}$ or $\tilde{\boldsymbol{\theta}}_i$ $(i = 1, \cdots, n)$ is not $\mathbf{0}$. (6.32) implies that V_n is bounded as in (6.33).

$$\frac{1}{2} \min \left\{ 1, \min_q \sigma_{\boldsymbol{\Gamma}_i^{-1} q} \right\} \|\boldsymbol{\nu}\|^2 \leq V_n \leq \frac{1}{2} \max \left\{ 1, \max_q \sigma_{\boldsymbol{\Gamma}_i^{-1} q} \right\} \|\boldsymbol{\nu}\|^2 \tag{6.33}$$

where $\boldsymbol{\nu} \triangleq \left[\boldsymbol{z}^T \ \tilde{\boldsymbol{\theta}}_1^T \ \cdots \ \tilde{\boldsymbol{\theta}}_{m_i}^T \right]^T$. The derivative of V_n is obtained as (6.34) from (6.32) with (6.30) and (6.31).

$$\begin{aligned}
\dot{V}_n =& \sum_{i=1}^{n} z_i \dot{z}_i + \sum_{i=1}^{n} \tilde{\boldsymbol{\theta}}_i^T \boldsymbol{\Gamma}_i^{-1} \dot{\tilde{\boldsymbol{\theta}}}_i \\
=& \Bigg[z_1 \left\{ -C_1 z_1 + g_1 z_2 - \tilde{\boldsymbol{\theta}}_1^T \boldsymbol{\phi}_1' \right\} + \sum_{i=2}^{n-1} z_i \left\{ -C_i z_i - g_{i-1} z_{i-1} + g_i z_{i+1} - \tilde{\boldsymbol{\theta}}_i^T \boldsymbol{\phi}_i' \right\} \\
& + z_n \left\{ -C_n z_n + g_{n-1} z_{n-1} - \tilde{\boldsymbol{\theta}}_n^T \boldsymbol{\phi}_n' \right\} \Bigg] \\
& + \sum_{i=1}^{n} \tilde{\boldsymbol{\theta}}_i^T \left\{ z_i \boldsymbol{\phi}_{\boldsymbol{i}}' - \lambda_i \boldsymbol{\Omega}_{ib} \tilde{\boldsymbol{\theta}}_i \right\} \\
=& - \sum_{i=1}^{n} C_i z_i^2 - \sum_{i=1}^{n} \lambda_i \tilde{\boldsymbol{\theta}}_i^T \boldsymbol{\Omega}_{ib} \tilde{\boldsymbol{\theta}}_i
\end{aligned} \tag{6.34}$$

The boundary of $\dot{V}_n$ is derived from (6.34) as (6.35).

$$\begin{aligned}\dot{V}_n &\leq -\min_i C_i\|\boldsymbol{z}\|^2 - \sum_{i=1}^{n}\min_{i,q}\left(\lambda_i\sigma_{\boldsymbol{\Omega}_{ibq}}\right)\left\|\tilde{\boldsymbol{\theta}}_i\right\|^2 \\ &\leq -\min\left\{\min_i C_i, \min_{i,q}\left(\lambda_i\sigma_{\boldsymbol{\Omega}_{ibq}}\right)\right\}\|\boldsymbol{\nu}\|^2\end{aligned} \tag{6.35}$$

To this end, (6.36) is obtained from (6.33) and (6.35).

$$\begin{aligned}&\dot{V}_n \leq -aV_n \\ &\text{where} \\ &a = \frac{2\min\left\{\min_i C_i, \min_{i,q}\left(\lambda_i\sigma_{\boldsymbol{\Omega}_{ibq}}\right)\right\}}{\max\left\{1, \max_q \sigma_{\boldsymbol{\Gamma}_i^{-1}q}\right\}}\end{aligned} \tag{6.36}$$

Since $\sigma_{\boldsymbol{\Omega}_{ibq}} > 0$ under FE, $a > 0$ which implies that V_n converges to 0 exponentially fast. Thus, the equilibrium point $\boldsymbol{\nu} = \left[\boldsymbol{z}^T\ \tilde{\boldsymbol{\theta}}_1^T\ \cdots\ \tilde{\boldsymbol{\theta}}_{m_i}^T\right]^T = \mathbf{0}$ is globally exponentially stable. □

6.7 Numerical Simulation

6.7.1 Simulation Setup

As an illustrative example, system dynamics for numerical simulation is defined as (6.37).

$$\dot{\boldsymbol{x}} = \boldsymbol{f}(\boldsymbol{x}) + \boldsymbol{G}(\boldsymbol{x})\left[\boldsymbol{u} + \boldsymbol{\Delta}(\boldsymbol{x})\right]$$

where

$$\begin{aligned}&\boldsymbol{x} = [x_1,\ x_2]^T \\ &\boldsymbol{f}(\boldsymbol{x}) = \left[f_1(x_1),\ f_2(x_1,x_2)\right]^T = \left[x_1|x_1|,\ x_1\sin(x_2) + x_2^3\right]^T \\ &\boldsymbol{G}(\boldsymbol{x}) = \mathrm{diag}\left[g_1(x_1),\ g_2(x_1,x_2)\right] \\ &\qquad = \mathrm{diag}\left[x_1^4|x_1| + 1,\ |x_1| + |x_2| + 1\right] \\ &\boldsymbol{u} = [x_2,\ u]^T \\ &\boldsymbol{\Delta}(\boldsymbol{x}) = \left[\Delta_1(x_1),\ \Delta_2(x_1,x_2)\right]^T\end{aligned} \tag{6.37}$$

The initial value for the state vector $\boldsymbol{x}$ is set to be $[0,\ 0]^T$. Δ_i $(i = 1, 2)$ in (6.37) are modeled as (6.38).

$$\begin{aligned}
&\Delta_1(x_1) = \boldsymbol{\theta}_1^T \boldsymbol{\phi}_1(x_1) \qquad \Delta_2(x_1, x_2) = \boldsymbol{\theta}_2^T \boldsymbol{\phi}_2(x_1, x_2) \\
&\text{where} \\
&\boldsymbol{\theta}_1 = [\theta_{11},\ \theta_{12}]^T \qquad\qquad \boldsymbol{\phi}_1'(x_1) = \left[x_1^2,\ \sqrt{|x_1|}\right]^T \\
&\boldsymbol{\theta}_2 = [\theta_{21},\ \theta_{22},\ \theta_{23},\ \theta_{24}]^T \qquad \boldsymbol{\phi}_2'(x_1, x_2) = \left[x_1^2,\ |x_1|\, x_2,\ x_1 + x_2^2,\ \log\left(|x_1| + 1\right)\right]^T
\end{aligned} \tag{6.38}$$

The true values of the model parameters are defined as $\boldsymbol{\theta}_1 = [1.2,\ 2.5]^T$ and $\boldsymbol{\theta}_2 = [2.3,\ 1.7,\ 1.2,\ 3.1]^T$. The initial values for their estimates $\hat{\boldsymbol{\theta}}_1$ and $\hat{\boldsymbol{\theta}}_2$ are set to be $[0,\ 0]^T$ and $[0,\ 0,\ 0,\ 0]^T$, respectively.

Simulations are performed to verify the composite adaptive control with new information matrix proposed in Section 6.4.2. As discussed in Section 6.4.1, the backstepping algorithm is applied for simulations as a representative example of baseline control algorithms. To clearly show the characteristics of the new information matrix investigated in Section 6.4, 6.5 and 6.6 via simulations, the proposed algorithm is compared to the composite adaptive backstepping control algorithms with the rank-1 information matrix $\boldsymbol{\Omega}_i^+$ as in [12, 25] and with the accumulation based $\boldsymbol{\Omega}_{i\,b}^*$ in [29]. The rank-1 information matrix $\boldsymbol{\Omega}_i^+$ is provided as (6.39).

$$\begin{aligned}
\boldsymbol{\Omega}_i^+ &= \boldsymbol{\phi}_{iF_i}' \boldsymbol{\phi}_{iF_i}'^T \\
\boldsymbol{\eta}_i^+ &= \boldsymbol{\phi}_{iF_i}' \left\{ \frac{1}{k} x_i - \zeta_{iF_i} \right\}
\end{aligned} \tag{6.39}$$

In [29], $\boldsymbol{\Omega}_{i\,b}^*$ is obtained from $\boldsymbol{\Omega}_i^*$ in (6.40) by applying the selective update scheme given in (6.16) and (6.17) to prevent rank deficiency after FE due to the forgetting design.

$$\begin{aligned}
\dot{\boldsymbol{\Omega}}_i^* &= -\kappa_i \boldsymbol{\Omega}_i^* + \boldsymbol{\phi}_{iF_i}' \boldsymbol{\phi}_{iF_i}'^T \\
\dot{\boldsymbol{\eta}}_i^* &= -\kappa_i \boldsymbol{\eta}_i^* + \left\{ \frac{1}{k} x_i - \zeta_{iF_i} \right\} \boldsymbol{\phi}_{iF_i}' \\
&\text{where} \\
\kappa_i &= \kappa_{iL} + (\kappa_{iU} - \kappa_{iL}) \tanh\left(\vartheta_i \|\dot{\boldsymbol{\eta}}_i^*\|\right)
\end{aligned} \tag{6.40}$$

κ_{iL}, κ_{iU} and ϑ_i are design parameters for the forgetting factor κ_i where $0 < \kappa_{iL} \leq \kappa_i \leq \kappa_{iU}$. Note that the subscript F_i in (6.39) and (6.40) denotes a filter with a single

parameter k_i which is applied not to use state derivative information for $\boldsymbol{\eta}_i$. Since the information matrix designs in the previous researches have different principles and parameters with the one in this research, simulations are conducted with various parameter sets for each algorithm and the results with the set which show the best adaptation performance with each algorithm are provided in Chapter 6 for fair comparison. Common design parameters are listed in Table 6.1 and individual design parameters for each information matrix with the values for the best adaptation performance are provided in Table 6.2. The state command to follow is given as a step function with $x_{1c} = 1.5$ and the step size for numerical simulations is set to be 10^{-4}.

Table 6.1: Common Design Parameters

Parameter	Value
C_1, C_2	1.5, 1.5
Γ_1, Γ_2	diag [10, 10], diag [10, 10, 10, 10]
λ_1, λ_2	2, 2

Table 6.2: Design Parameters for Information Matrix

Simulation Cases	Parameters and Values
$\boldsymbol{\Omega}_i^+$ with Rank 1	$k_1 = k_2 = 1.0 \times 10^{-2}$
$\boldsymbol{\Omega}_{i\,b}^*$ in [29]	$k_i = 1.0 \times 10^{-2}$, $\kappa_{iL} = 5 \times 10^{-3}$, $\kappa_{iU} = 1 \times 10^{-2}$, $\vartheta_i = 1$ $(i = 1, 2)$
New $\boldsymbol{\Omega}_{ib}$	$k_{11} = k_{21} = 1.0 \times 10^{-2}$, $k_{12} = k_{22} = 1.5 \times 10^{-2}$, $k_{23} = 2.0 \times 10^{-2}$, $k_{24} = 2.5 \times 10^{-2}$

6.7.2 Simulation Results

The simulation results under $\boldsymbol{\Omega}_i^+$ with rank-1, $\boldsymbol{\Omega}_{i\,b}^*$ in [29] and new $\boldsymbol{\Omega}_{ib}$ proposed in Chapter 6 are addressed in Fig. 6.1 to 6.4. Note that it can be inferred from Fig. 6.1 that there is no PE. Under FE, Fig. 6.1 and 6.2 show that tracking errors become zeros for all cases. It is observed from Fig. 6.3 and 6.4 that the information matrices of all three cases are bounded. Fig. 6.2 clearly indicates that $\hat{\boldsymbol{\theta}}_1$ and $\hat{\boldsymbol{\theta}}_2$ do not converge to their true values $\boldsymbol{\theta}_1$ and $\boldsymbol{\theta}_2$ without PE for the case under the $\boldsymbol{\Omega}_i^+$ with rank-1. This is because $\boldsymbol{\Omega}_i^+$ is rank deficient in the outer loop $(i = 1)$ and the

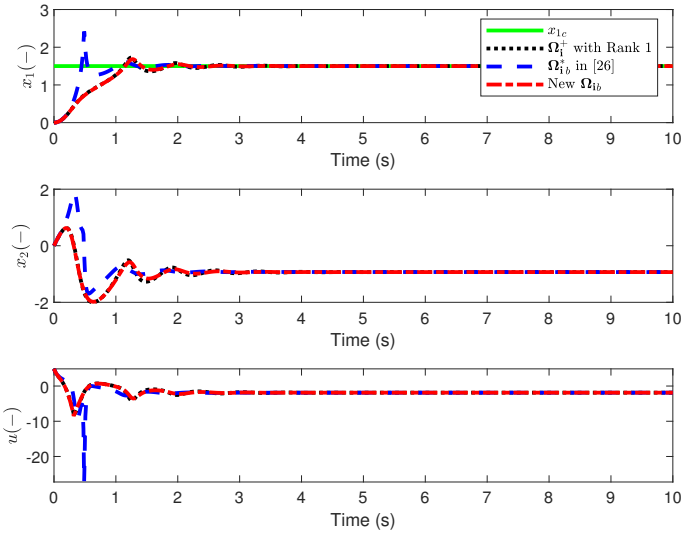

Figure 6.1: State Response and Control Input

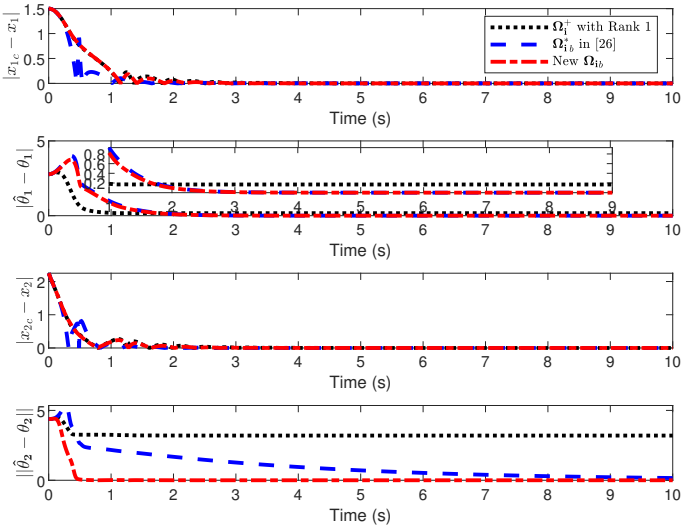

Figure 6.2: Tracking and Estimation Error

inner loop ($i = 2$) where the number of unknown parameters are set to be 2 and 4 respectively, which is confirmed in Fig. 6.3 and 6.4 with 0 eigenvalues. Note that instability phenomena can occur under the existence of non-parametric uncertainties such as measurement noise and unmodeled dynamics if parameter convergence is not accomplished even for the nominal circumstances [25]. $\hat{\boldsymbol{\theta}}_1$ and $\hat{\boldsymbol{\theta}}_2$ converge to $\boldsymbol{\theta}_1$ and $\boldsymbol{\theta}_2$ for both cases under $\boldsymbol{\Omega}_{i\,b}^*$ in [29] and new $\boldsymbol{\Omega}_{ib}$ proposed in Chapter 6. Fig. 6.3 and 6.4 show that both $\boldsymbol{\Omega}_{i\,b}^*$ and $\boldsymbol{\Omega}_{ib}$ become full rank with all positive eigenvalues but have different patterns in these eigenvalues. The principal eigenvalue of $\boldsymbol{\Omega}_{i\,b}^*$ is excessively large while the others are extremely small. For $\boldsymbol{\Omega}_{ib}$, all eigenvalues have similar and moderate values. These observations imply that the adaptation speeds in all directions, including the slowest direction, are evenly high with $\boldsymbol{\Omega}_{ib}$. As a

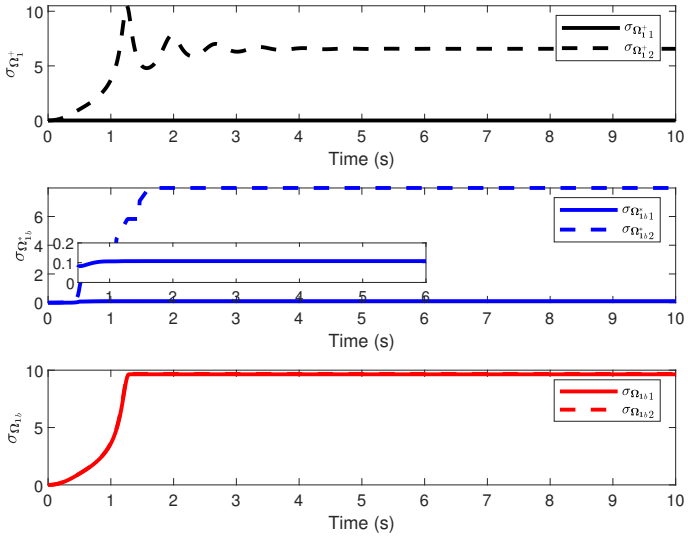

Figure 6.3: Eigenvalues of Information Matrix (Outer Loop)

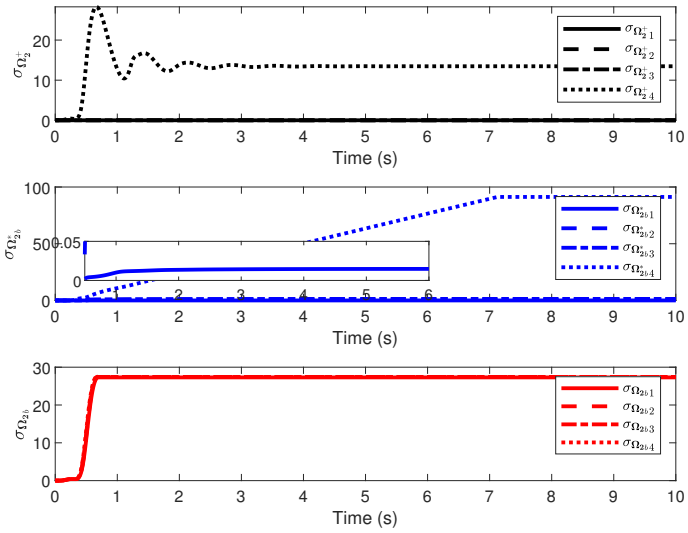

Figure 6.4: Eigenvalues of Information Matrix (Inner Loop)

result, the overall adaptation speed with $\mathbf{\Omega}_{ib}$ is higher than with $\mathbf{\Omega}^*_{i\,b}$ as can be seen in Fig. 6.2.

6.8 Conclusion

A composite adaptive control with new information matrix is successfully suggested in Chapter 6 which guarantees convergence of parameter estimation under FE. The novelty of this research is in the modulation based information matrix design framework which achieves its positive definiteness for all the time only with FE. Based on

the key design considerations such as linear independency between the filtered regressor signals, orthogonality between the modified filtered regressor vectors and the selective update for the information matrix, the new information matrix is proven to be positive definite for all time from the beginning under FE. Besides, the new information matrix is shown to be lower and upper bounded. Note that the proposed information matrix appears to have eigenvalues with moderate level of magnitudes, which is advantageous for adaptation speed and system robustness. The global exponential stability of the closed-loop system with the proposed composite adaptation control utilizing new information matrix is addressed via stability analysis based on Lyapunov theory. Numerical simulations are conducted to verify the proposed algorithm and related theoretical findings.

References

[1] Nazli E Kahveci and Petros A Ioannou. Adaptive steering control for uncertain ship dynamics and stability analysis. *Automatica*, 49(3):685–697, 2013.

[2] Ye Zhou, Erik-Jan van Kampen, and QiPing Chu. Nonlinear adaptive flight control using incremental approximate dynamic programming and output feedback. *Journal of Guidance, Control, and Dynamics*, 40(2):493–496, 2016.

[3] Chengshuai Wu, Jian Chen, Chenfeng Xu, and Zhiyang Liu. Real-time adaptive control of a fuel cell/battery hybrid power system with guaranteed stability. *IEEE Transactions on Control Systems Technology*, 25(4):1394–1405, 2016.

[4] Hanlei Wang. Adaptive control of robot manipulators with uncertain kinematics and dynamics. *IEEE Transactions on Automatic Control*, 62(2):948–954, 2016.

[5] Jean-Jacques E Slotine and Weiping Li. On the adaptive control of robot manipulators. *The international journal of robotics research*, 6(3):49–59, 1987.

[6] J Van Amerongen. Model reference adaptive control applied to steering of ships. In *Methods and applications in adaptive control*, pages 199–208. Springer, 1980.

[7] HJ Tol, CC De Visser, LG Sun, E van Kampen, and QP Chu. Multivariate spline-based adaptive control of high-performance aircraft with aerodynamic uncertainties. *Journal of Guidance, Control, and Dynamics*, 39(4):781–800, 2016.

[8] Nhan Nguyen, Kalmanje Krishnakumar, John Kaneshige, and Pascal Nespeca. Flight dynamics and hybrid adaptive control of damaged aircraft. *Journal of guidance, control, and dynamics*, 31(3):751–764, 2008.

[9] DE Seborg, Thomas F Edgar, and SL Shah. Adaptive control strategies for process control: a survey. *AIChE Journal*, 32(6):881–913, 1986.

[10] A Galip Ulsoy and Yoram Koren. Applications of adaptive control to machine tool process control. *IEEE Control Systems Magazine*, 9(4):33–37, 1989.

[11] Dezhi Xu, Jianxing Liu, Xing-Gang Yan, and Wenxu Yan. A novel adaptive neural network constrained control for a multi-area interconnected power system with hybrid energy storage. *IEEE Transactions on Industrial Electronics*, 65(8):6625–6634, 2017.

[12] Jean-Jacques E Slotine and Weiping Li. Composite adaptive control of robot manipulators. *Automatica*, 25(4):509–519, 1989.

[13] Yongping Pan and Haoyong Yu. Composite learning from adaptive dynamic surface control. *IEEE Transactions on Automatic Control*, 61(9):2603–2609, 2015.

[14] Parag M Patre, William MacKunis, Marcus Johnson, and Warren E Dixon. Composite adaptive control for euler–lagrange systems with additive disturbances. *Automatica*, 46(1):140–147, 2010.

[15] Zachary T Dydek, Anuradha M Annaswamy, Jean-Jacques E Slotine, and Eugene Lavretsky. Composite adaptive posicast control for a class of lti plants with known delay. *Automatica*, 49(6):1914–1924, 2013.

[16] Yongping Pan and Haoyong Yu. Composite learning robot control with guaranteed parameter convergence. *Automatica*, 89:398–406, 2018.

[17] Manuel A Duarte and Kumpati S Narendra. Combined direct and indirect approach to adaptive control. *IEEE Transactions on Automatic Control*, 34(10):1071–1075, 1989.

[18] Manuel A Duarte and Kumpati S Narendra. A new approach to model reference adaptive control. *International Journal of Adaptive Control and Signal Processing*, 3(1):53–73, 1989.

[19] Kumpati S Narendra and Manuel A Duarte. Application of robust adaptive control using combined direct and indirect methods. *International Journal of Adaptive Control and Signal Processing*, 3(2):131–142, 1989.

[20] Eugene Lavretsky. Combined/composite model reference adaptive control. *IEEE Transactions on Automatic Control*, 54(11):2692–2697, 2009.

[21] M Kemal Ciliz. Combined direct and indirect adaptive control for a class of nonlinear systems. *IET Control Theory & Applications*, 3(1):151–159, 2009.

[22] MK Ciliz. Adaptive backstepping control using combined direct and indirect adaptation. *Circuits, Systems & Signal Processing*, 26(6):911–939, 2007.

[23] Parag M Patre, Shubhendu Bhasin, Zachary D Wilcox, and Warren E Dixon. Composite adaptation for neural network-based controllers. *IEEE Transactions on Automatic Control*, 55(4):944–950, 2010.

[24] Yongping Pan, Yiqi Liu, and Haoyong Yu. Online data-driven composite adaptive backstepping control with exact differentiators. *International Journal of Adaptive Control and Signal Processing*, 30(5):779–789, 2016.

[25] Jean-Jacques E Slotine, Weiping Li, et al. *Applied nonlinear control*. Prentice hall Englewood Cliffs, NJ, 1991.

[26] Girish Chowdhary, Tansel Yucelen, Maximillian Mühlegg, and Eric N Johnson. Concurrent learning adaptive control of linear systems with exponentially convergent bounds. *International Journal of Adaptive Control and Signal Processing*, 27(4):280–301, 2013.

[27] Girish Chowdhary, Maximilian Mühlegg, and Eric Johnson. Exponential parameter and tracking error convergence guarantees for adaptive controllers without persistency of excitation. *International Journal of Control*, 87(8):1583–1603, 2014.

[28] Byoung-Ju Jeon, Hyo-Sang Shin, and Antonios Tsourdos. Composite adaptive backstepping control considering computational complexity and relaxation of persistent excitation. In *21st IFAC World Congress*. IEEE, 2020.

[29] Namhoon Cho, Hyo-Sang Shin, Youdan Kim, and Antonios Tsourdos. Composite model reference adaptive control with parameter convergence under finite excitation. *IEEE Transactions on Automatic Control*, 63(3):811–818, 2017.

[30] Hae-In Lee, Hyo-Sang Shin, and Antonios Tsourdos. Concurrent learning adaptive control with directional forgetting. *IEEE Transactions on Automatic Control*, 64(12):5164–5170, 2019.

[31] Gang Tao. *Adaptive control design and analysis*, volume 37. John Wiley & Sons, 2003.

[32] Petar V Kokotovic. The joy of feedback: nonlinear and adaptive. *IEEE Control Systems Magazine*, 12(3):7–17, 1992.

Chapter 7

Logarithmic Regression based Composite Adaptive Backstepping Control with New Information Matrix

7.1 Introduction

Adaptive control has been extensively studied and utilized for various dynamic systems with uncertainties from robot manipulators to aircraft systems [1–15]. Since an adaptive control algorithm estimates uncertain model parameters on-line and then calculates a control input command from these estimates, stability and performance of the closed-loop system are highly dependent on estimation performance of the adaptation law. In order to achieve fast tracking performance of the closed loop system, the parameter estimates should converge fast to their true values, which is essential especially for fast dynamic systems like fighters [12] and missiles [13].

Composite adaptive control [14–28] is designed to achieve fast parameter convergence by introducing a linear regression term to a tracking error based adaptation law. This results in enhanced estimation and tracking performance with improved system robustness comparing to the tracking error based adaptation law. Since the linear regression term is simply proportional to the estimation error, the adaptation speed is sufficiently high at the early stage with large estimation error, but it decreases as the estimation error becomes small. If the adaptation gain increases to

relax this parameter convergence speed degeneration, the system robustness might be reduced with the high adaptation gain. To the best of our knowledge, there has been no relevant studies on the learning rate enhancement without excessive increase of the adaptation gain for composite adaptive control.

In Chapter 7, a new paradigm for composite adaptation law design with regression pattern shaping is proposed to achieve fast parameter convergence. The proposed regression term is designed to be a logarithmic function of a signal containing estimation error information, resulting in a high learning rate with reduced necessity of a large adaptation gain. Since a logarithm is a concave and monotonically increasing function, the new regression term diminishes slowly comparing to the linear regression term in the existing composite adaptation law. Chapter 7 suggests detailed analysis about the condition on the design parameters of the logarithmic regression-based composite adaptation law to guarantee faster parameter convergence than the linear regression-based approach for the same adaptation gain within the system boundary. If this condition is accomplished, it is examined for the linear regression-based approach how much its adaptation gain is required to be increased for higher adaptation speed than that of the logarithmic regression-based approach. Note that the logarithmic regression-based composite adaptation law can provide improved system robustness since lower adaptation gain can be utilized for the similar adaptation speed with the linear regression-based approach. The proposed logarithmic regression-based composite adaptation law is designed to guarantee the asymptotic stability of the closed-loop system and it is proven under the Lyapunov stability theory. Note that the signal containing estimation error information is obtained by utilizing the information matrix design in [28] which achieves positive definiteness all the time under FE.

The rest of Chapter 7 is organized as follows. System dynamics with model uncertainty and a baseline controller are provided in Section 7.2. In Section 7.3, the new logarithmic regression-based composite adaptation law is proposed to enhance the parameter convergence speed via regression pattern shaping instead of adaptation gain increase. The asymptotic stability of the closed-loop system with the proposed logarithmic regression-based composite adaptation law is proven under the Lyapunov stability theory in Section 7.4. Section 7.5 provides comparative study between the existing linear regression based approach and the proposed logarithmic regression-based approach in adaptation speed and system robustness point of view. Numerical simulations are conducted in Section 7.6 for verification and Section 7.7 addresses the overall concluding remarks of Chapter 7.

7.2 Preliminaries and Problem Formulation

7.2.1 Preliminaries

In Chapter 7, a new composite adaptive control algorithm for fast adaptation is proposed, which is basically designed to achieve parameter convergence under finite excitation. Note that the requirement for parameter convergence is relaxed from persistent excitation to finite excitation based on the information matrix design in [28]. Section 7.2.1 suggests definitions of persistent excitation (PE) and finite excitation (FE) in [16, 29] as preliminaries.

Definition 7.1. *(Persistent Excitation) : A bounded vector signal $\boldsymbol{\psi}(t)$ is persistently exciting, if $\forall t \geq t_0$ there exist $T > 0$ and $\gamma > 0$ s.t.*

$$\int_{t}^{t+T} \boldsymbol{\psi}(\tau)\boldsymbol{\psi}^T(\tau)d\tau \geq \gamma \boldsymbol{I} \tag{7.1}$$

Definition 7.2. *(Finite Excitation) : A bounded vector signal $\boldsymbol{\psi}(t)$ is finitely exciting over a time interval $[t_s, t_s + T]$, if there exist $T > 0$, $t_s \geq t_0$ and $\gamma > 0$ s.t.*

$$\int_{t_s}^{t_s+T} \boldsymbol{\psi}(\tau)\boldsymbol{\psi}^T(\tau)d\tau \geq \gamma \boldsymbol{I} \tag{7.2}$$

7.2.2 Problem Formulation

A backstepping control algorithm is introduced in Section 7.2.2.2 as a representative example of the baseline controller for the adaptive control system with the new logarithmic regression-based composite adaptation law in Section 7.3. Consequently, system dynamics in a strict-feedback form is considered in Section 7.2.2.1 as a representative example to apply the proposed method. Note that the new logarithmic regression-based composite adaptation law in Section 7.3 is compatible with any stabilizable system and baseline control algorithm.

7.2.2.1 System dynamics

Consider system dynamics with model uncertainty as (7.3).

$$\dot{\boldsymbol{x}} = \boldsymbol{f}(\boldsymbol{x}) + \boldsymbol{G}(\boldsymbol{x})\left[\boldsymbol{u} + \boldsymbol{\Delta}(\boldsymbol{x})\right]$$

where

$$\begin{aligned}
&\boldsymbol{x} = [x_1, x_2, \cdots, x_n]^T \\
&\boldsymbol{x}_i' = [x_1, x_2, \cdots, x_i]^T \quad (i = 1, \cdots, n) \\
&\boldsymbol{f}(\boldsymbol{x}) = \left[f_1(\boldsymbol{x}_1'), f_2(\boldsymbol{x}_2'), \cdots, f_n(\boldsymbol{x}_n')\right]^T \\
&\boldsymbol{G}(\boldsymbol{x}) = \mathrm{diag}\left[g_1(\boldsymbol{x}_1'), g_2(\boldsymbol{x}_2'), \cdots, g_n(\boldsymbol{x}_n')\right] \\
&\boldsymbol{u} = [u_1, u_2, \cdots, u_n]^T \text{ with } u_i = \begin{cases} x_{i+1} & (i = 1, \cdots, n-1) \\ u & (i = n) \end{cases} \\
&\boldsymbol{\Delta}(\boldsymbol{x}) = \left[\Delta_1(\boldsymbol{x}_1'), \Delta_2(\boldsymbol{x}_2'), \cdots, \Delta_n(\boldsymbol{x}_n')\right]^T
\end{aligned} \tag{7.3}$$

$\boldsymbol{x} \in \mathbb{R}^{n\times 1}$ represents a state vector and $\boldsymbol{x}_i' \in \mathbb{R}^{i\times 1}$ indicate subsets of $\boldsymbol{x}$. $\boldsymbol{f}(\boldsymbol{x}) \in \mathbb{R}^{n\times 1}$ and $\boldsymbol{G}(\boldsymbol{x}) \in \mathbb{R}^{n\times m}$ with $g_i(\boldsymbol{x}_i') \neq 0$ are defined as known model information. $\boldsymbol{u} \in \mathbb{R}^{m\times 1}$ indicates a control input vector; u is an actual control input exerted on the innermost loop, and a state variable works as a pseudo control input on the next outer loop recursively. $\boldsymbol{\Delta}(\boldsymbol{x}) \in \mathbb{R}^{n\times 1}$ stands for a matched model uncertainty.

The model uncertainty in (7.3) is assumed to be linearly structured as shown in (7.4).

$$\begin{aligned}
&\Delta_i(\boldsymbol{x}_i') = \boldsymbol{\theta}_i^T \boldsymbol{\phi}_i(\boldsymbol{x}_i') \qquad (i = 1, \cdots, n) \\
&\text{where} \\
&\boldsymbol{\theta}_i = \left[\theta_{i1}, \theta_{i2} \cdots \theta_{im_i}\right]^T \\
&\boldsymbol{\phi}_i(\boldsymbol{x}_i') = \left[\phi_{i1}(\boldsymbol{x}_i'), \phi_{i2}(\boldsymbol{x}_i') \cdots \phi_{im_i}(\boldsymbol{x}_i')\right]^T
\end{aligned} \tag{7.4}$$

$\boldsymbol{\theta}_i \in \mathbb{R}^{m_i\times 1}$ is a vector of true model parameters for the i-th loop, which is unique, constant and unknown. $\boldsymbol{\phi}_i(\boldsymbol{x}_i') \in \mathbb{R}^{m_i\times 1}$ denotes a known regressor vector for the i-th loop, and $\phi_{ij}(\boldsymbol{x}_i')$ are linearly independent from each other.

7.2.2.2 Baseline Controller and Tracking Error Dynamics

The control input command for the i-th loop u_{ic} is derived with the backstepping algorithm as (7.5). Note that the adaptive control system design can be conducted

for each loop in a recursive way by taking advantage from the cascade structure of the backstepping algorithm [27, 28, 30].

$$u_{ic} = \begin{cases} \dfrac{1}{g_i}\left[-C_i z_i - f_i + \dot{x}_{ic}\right] - \hat{\boldsymbol{\theta}}_i^T \boldsymbol{\phi}_i & (i = 1) \\ \dfrac{1}{g_i}\left[-C_i z_i - f_i + \dot{x}_{ic} - g_{i-1} z_{i-1}\right] - \hat{\boldsymbol{\theta}}_i^T \boldsymbol{\phi}_i & (i = 2, \cdots, n) \end{cases} \tag{7.5}$$

A subscript i denotes the i-th loop and $(\cdot)_c$ represents a command for $(\cdot)$. C_i represents a positive and constant design parameter for u_{ic} to accomplish a desired response of the i-th closed-loop. $\boldsymbol{z} \triangleq \boldsymbol{x} - \boldsymbol{x}_c \in \mathbb{R}^{n\times 1}$ is a tracking error vector and z_i denotes the i-th component of $\boldsymbol{z}$. $\hat{\boldsymbol{\theta}}_i \in \mathbb{R}^{m_i \times 1}$ represents an estimate of $\boldsymbol{\theta}_i$ and it is obtained from the adaptation law discussed in Section 7.3.

Tracking error dynamics of the closed-loop system is obtained by applying the control input command in (7.5) to the system dynamics in (7.3).

$$\dot{z}_i = \begin{cases} -C_i z_i + g_i z_{i+1} - \tilde{\boldsymbol{\theta}}_i^T \boldsymbol{\phi}_i' & (i = 1) \\ -C_i z_i - g_{i-1} z_{i-1} + g_i z_{i+1} - \tilde{\boldsymbol{\theta}}_i^T \boldsymbol{\phi}_i' & (i = 2, \cdots, n-1) \\ -C_i z_i - g_{i-1} z_{i-1} - \tilde{\boldsymbol{\theta}}_i^T \boldsymbol{\phi}_i' & (i = n) \end{cases} \tag{7.6}$$

7.3 Logarithmic Regression-based Composite Adaptation Law

In Section 7.3, a new composite adaptation law with logarithmic regression is proposed for fast adaptation via parameter convergence pattern shaping. A fundamental structure of the composite adaptation law is represented as (7.7) with $\boldsymbol{\phi}_i' \triangleq g_i \boldsymbol{\phi}_i$, which is constructed by introducing a regression term to a tracking error based adaptation law. Note that the regression term provides enhanced estimation and tracking performance with improved system robustness [16].

$$\dot{\hat{\boldsymbol{\theta}}}_i = z_i \boldsymbol{\Gamma}_i \boldsymbol{\phi}_i' - \lambda_i \boldsymbol{\Gamma}_i \boldsymbol{\Xi}_i \quad (i = 1, \cdots, n) \tag{7.7}$$

$\boldsymbol{\Gamma}_i \in \mathbb{R}^{m_i \times m_i}$ is a design parameter of the adaptation law which is defined as a constant and positive definite matrix. λ_i is a constant and positive design parameter representing a relative weight factor on the regression term to the tracking error

based term. $\boldsymbol{\Xi}_i = \boldsymbol{\Xi}_i(\tilde{\boldsymbol{\theta}}_i) \in \mathbb{R}^{m_i \times 1}$ is designed to be a function of a parameter estimation error $\tilde{\boldsymbol{\theta}}_i \in \mathbb{R}^{m_i \times 1}$. Since the unknown parameter $\boldsymbol{\theta}_i$ is assumed to be constant, estimation error dynamics is derived as (7.8) from (7.7).

$$\dot{\tilde{\boldsymbol{\theta}}}_i = z_i \boldsymbol{\Gamma}_i \boldsymbol{\phi}_i' - \lambda_i \boldsymbol{\Gamma}_i \boldsymbol{\Xi}_i \tag{7.8}$$

A composite adaptation law is designed by introducing an appropriate $\boldsymbol{\Xi}_i$ to its fundamental structure in (7.7). The main consideration in $\boldsymbol{\Xi}_i$ design is that desired estimation performance should be accomplished with proper $\boldsymbol{\Xi}_i$ while stability of the closed loop system is still guaranteed. A design requirement on $\boldsymbol{\Xi}_i$ in stability point of view is derived from Lyapunov stability condition as follows. First, a Lyapunov candidate function considering both state tracking and parameter estimation errors is defined as (7.9).

$$V_n = \frac{1}{2}\boldsymbol{z}^T\boldsymbol{z} + \frac{1}{2}\sum_{i=1}^{n} \tilde{\boldsymbol{\theta}}_i^T \boldsymbol{\Gamma}_i^{-1} \tilde{\boldsymbol{\theta}}_i \tag{7.9}$$

Note that V_n in (7.9) is positive definite except for the equilibrium point $\boldsymbol{z} = \mathbf{0}$ and $\tilde{\boldsymbol{\theta}}_i = \mathbf{0}$ $(i = 1, \cdots, n)$ where $V_n = 0$. Derivative of V_n is derived as (7.10) from (7.9) with (7.6) and (7.8).

$$\begin{aligned}
\dot{V}_n =& \sum_{i=1}^{n} z_i \dot{z}_i + \sum_{i=1}^{n} \tilde{\boldsymbol{\theta}}_i^T \boldsymbol{\Gamma}_i^{-1} \dot{\tilde{\boldsymbol{\theta}}}_i \\
=& \Bigg[z_1 \left\{ -C_1 z_1 + g_1 z_2 - \tilde{\boldsymbol{\theta}}_1^T \boldsymbol{\phi}_1' \right\} \\
&+ \sum_{i=2}^{n-1} z_i \left\{ -C_i z_i - g_{i-1} z_{i-1} + g_i z_{i+1} - \tilde{\boldsymbol{\theta}}_i^T \boldsymbol{\phi}_i' \right\} \\
&+ z_n \left\{ -C_n z_n + g_{n-1} z_{n-1} - \tilde{\boldsymbol{\theta}}_n^T \boldsymbol{\phi}_n' \right\} \Bigg] \\
&+ \sum_{i=1}^{n} \left(\hat{\boldsymbol{\theta}}_{\boldsymbol{i}} - \boldsymbol{\theta}_i \right)^T \boldsymbol{\Gamma}_i{}^{-1} \left[z_i \boldsymbol{\Gamma}_i \boldsymbol{\phi}_i' - \lambda_i \boldsymbol{\Gamma}_i \boldsymbol{\Xi}_i \right] \\
=& -\sum_{i=1}^{n} C_i z_i^2 - \sum_{i=1}^{n} \lambda_i \left(\hat{\boldsymbol{\theta}}_{\boldsymbol{i}} - \boldsymbol{\theta}_i \right)^T \boldsymbol{\Xi}_i
\end{aligned} \tag{7.10}$$

Since the first term in (7.10) is negative definite for all $\boldsymbol{z}$ except $\boldsymbol{z} = \mathbf{0}$, the Lyapunov stability condition can be satisfied if the second term in (7.10) becomes negative definite for $\hat{\boldsymbol{\theta}}_{\boldsymbol{i}} \neq \boldsymbol{\theta}_i$. This results in a design requirement on $\boldsymbol{\Xi}_i$ for the closed-loop

system stability as (7.11).

$$\left(\hat{\boldsymbol{\theta}}_{\boldsymbol{i}} - \boldsymbol{\theta}_i\right)^T \boldsymbol{\Xi}_i > 0 \qquad \text{for} \quad \hat{\boldsymbol{\theta}}_{\boldsymbol{i}} \neq \boldsymbol{\theta}_i \tag{7.11}$$

In previous studies [14–28], $\boldsymbol{\Xi}_i$ is designed to be simply proportional to $\tilde{\boldsymbol{\theta}}_i$, which satisfies (7.11). This linear regression term leads to sufficiently high adaptation speed for the initial phase with large estimation error, but the learning rate starts to diminish as the estimation error decreases. The adaptation speed can be enhanced by simply increasing adaptation gains like λ_i or $\boldsymbol{\Gamma}_i$, but this can result in lack of system robustness.

The main objective of a new composite adaptation law is to achieve fast adaptation with appropriate design of $\boldsymbol{\Xi}_i$ which makes the regression term to degenerate slowly. Chapter 7 proposes $\boldsymbol{\Xi}_i$ design with a logarithm as shown in (7.12) to accomplish this objective with a guarantee of the closed loop system stability.

$$\begin{aligned}
&\boldsymbol{\Xi}_i = \boldsymbol{\Omega}_{iH}^T \operatorname{diag}\left\{\operatorname{sgn}\left(\boldsymbol{E}_i\right)\right\} \boldsymbol{E}_i^* \\
&\text{where} \\
&\boldsymbol{E}_i = \boldsymbol{\Omega}_{iH}\hat{\boldsymbol{\theta}}_{\boldsymbol{i}} - \boldsymbol{r}_i = \left[\ E_{i1}, E_{i2}, \cdots, E_{im_i}\ \right]^T \\
&\operatorname{diag}\left\{\operatorname{sgn}\left(\boldsymbol{E}_i\right)\right\} = \begin{bmatrix} \operatorname{sgn}\left(E_{i1}\right) & \cdots & 0 \\ \vdots & \ddots & \vdots \\ 0 & \cdots & \operatorname{sgn}\left(E_{im_i}\right) \end{bmatrix} \\
&\boldsymbol{E}_i^* = \left[\ E_{i1}^*, E_{i2}^*, \cdots, E_{im_i}^*\ \right]^T \\
&E_{ij}^* = \log_{p_i}\left(q_i\left|E_{ij}\right| + 1\right) \quad (j = 1, \cdots, m_i)
\end{aligned} \tag{7.12}$$

$\boldsymbol{E}_i \in \mathbb{R}^{m_i \times 1}$ is a signal containing estimation error information with $\boldsymbol{r}_i \triangleq \boldsymbol{\Omega}_{iH}\boldsymbol{\theta}_i \in \mathbb{R}^{m_i \times 1}$. $\boldsymbol{\Omega}_{iH}$ is designed to be full rank for parameter convergence and system stability under FE. p_i and q_i in $\boldsymbol{E}_i^* \in \mathbb{R}^{m_i \times 1}$ denote constant design parameters for the logarithms. Note that $p_i > 1$ and $q_i > 0$ for system stability. The condition in (7.11) is satisfied and the detailed stability proof of the closed-loop system is suggested in Section 7.5. The new logarithmic regression-based composite adaptation law is designed as (7.13) by substituting (7.12) into (7.7).

$$\dot{\hat{\boldsymbol{\theta}}}_i = z_i \boldsymbol{\Gamma}_i \boldsymbol{\phi}_i' - \lambda_i \boldsymbol{\Gamma}_i \boldsymbol{\Omega}_{iH}^T \operatorname{diag}\left\{\operatorname{sgn}\left(\boldsymbol{E}_i\right)\right\} \boldsymbol{E}_i^* \tag{7.13}$$

In Chapter 7, $\boldsymbol{\Omega}_{iH}$ in (7.13) is constructed to be full rank for all the time under FE by considering the design principles in [28]. As shown in [28], multiple filtered dynamics are generated by applying the first-order filters $F_{ij}(s) = \frac{1}{k_{ij}s+1}$ $(j = 1, \cdots, m_i)$ with different parameters k_{ij} to dynamics of the i-th loop in (7.3) with $g_i u_i \triangleq g_{ui}$ and the multiple filtered uncertainties of the i-th loop can be obtained as (7.14) from these multiple filtered dynamics.

$$\begin{aligned}
&\boldsymbol{\theta}_i^T \boldsymbol{\phi}'_{iF_{ij}} = \frac{1}{k_{ij}} x_i - \zeta_{iF_{ij}} \quad (j = 1, \cdots, m_i) \\
&\text{where} \\
&\dot{\boldsymbol{\phi}}'_{iF_{ij}} = \frac{1}{k_{ij}} \left(\boldsymbol{\phi}'_i - \boldsymbol{\phi}'_{iF_{ij}} \right) \\
&\dot{\zeta}_{iF_{ij}} = \frac{1}{k_{ij}} \left(\frac{1}{k_{ij}} x_i + f_i + g_{ui} - \zeta_{iF_{ij}} \right)
\end{aligned} \tag{7.14}$$

$\boldsymbol{\Omega}_{iH} \in \mathbb{R}^{m_i \times m_i}$ is constructed as (7.15) by utilizing the multiple filtered regressor vectors $\boldsymbol{\phi}'_{iF_{ij}}$ in (7.14) which become linearly independent during excitation as shown in [28] based on different modulation effects of the multiple filters.

$$\boldsymbol{\Omega}_{iH} \triangleq \begin{bmatrix} \boldsymbol{\phi}^*_{i\,F_{i1}} & \boldsymbol{\phi}^*_{i\,F_{i2}} & \cdots & \boldsymbol{\phi}^*_{i\,F_{im_i}} \end{bmatrix}^T$$

where

$$\begin{cases}
\boldsymbol{\phi}^*_{i\,F_{ij}} = \boldsymbol{\phi}'_{iF_{ij}} & (j = 1) \\
\boldsymbol{\phi}^*_{i\,F_{ij}} = \dfrac{\left\| \boldsymbol{\phi}'_{iF_{ij}} \right\|}{\left\| \boldsymbol{\varphi}_{iF_{ij}} \right\|} \boldsymbol{\varphi}_{iF_{ij}}, \quad \boldsymbol{\varphi}_{iF_{ij}} = \boldsymbol{\phi}'_{iF_{ij}} - \displaystyle\sum_{\xi=1}^{j-1} \frac{\boldsymbol{\phi}'_{iF_{ij}} \cdot \boldsymbol{\phi}^*_{i\,F_{i\xi}}}{\left\| \boldsymbol{\phi}^*_{i\,F_{i\xi}} \right\|^2} \boldsymbol{\phi}^*_{i\,F_{i\xi}} & (j = 2, \cdots, m_i)
\end{cases} \tag{7.15}$$

$\boldsymbol{\Omega}_{iH}$ in (7.15) becomes full rank during excitation, and its detailed proof is provided in [28] based on the orthogonality among $\boldsymbol{\phi}^*_{i\,F_{ij}}$. For $\boldsymbol{r}_i$ design, $\boldsymbol{\Omega}_{iH}$ in (7.15) is rewritten as a multiplication of $\boldsymbol{O}_i \in \mathbb{R}^{m_i \times m_i}$ and $\boldsymbol{H}_i \in \mathbb{R}^{m_i \times m_i}$ in (7.16).

$$\boldsymbol{\Omega}_{iH} = \boldsymbol{O}_i \boldsymbol{H}_i$$

where

$$\boldsymbol{O}_i = \boldsymbol{P}_{im_i} \boldsymbol{P}_{i(m_i-1)} \cdots \boldsymbol{P}_{i1}$$

$$\boldsymbol{P}_{ir}(j,l) = \begin{cases} -\dfrac{\left\|\boldsymbol{\phi}'_{iF_{ij}}\right\|}{\left\|\boldsymbol{\varphi}_{iF_{ij}}\right\|} \dfrac{\boldsymbol{\phi}'_{iF_{ij}} \cdot \boldsymbol{\phi}^*_{i\,F_{il}}}{\left\|\boldsymbol{\phi}^*_{i\,F_{il}}\right\|^2}, & l < j = r \\ \dfrac{\left\|\boldsymbol{\phi}'_{iF_{ij}}\right\|}{\left\|\boldsymbol{\varphi}_{iF_{ij}}\right\|}, & l = j = r \\ 1, & l = j \neq r \\ 0, & \text{Otherwise} \end{cases} \tag{7.16}$$

$$\boldsymbol{H}_i \triangleq \begin{bmatrix} \boldsymbol{\phi}'_{iF_{i1}} & \boldsymbol{\phi}'_{iF_{i2}} & \cdots & \boldsymbol{\phi}'_{iF_{im_i}} \end{bmatrix}^T$$

From (7.14) and (7.16), $\boldsymbol{r}_i$ can be suggested as (7.17), which is obtained from known information.

$$\boldsymbol{r}_i \triangleq \boldsymbol{\Omega}_{iH} \boldsymbol{\theta_i} = \boldsymbol{O}_i \begin{bmatrix} \frac{1}{k_{i1}} x_i - \zeta_{iF_{i1}} \\ \frac{1}{k_{i2}} x_i - \zeta_{iF_{i2}} \\ \vdots \\ \frac{1}{k_{im_i}} x_i - \zeta_{iF_{im_i}} \end{bmatrix} \tag{7.17}$$

As can be seen in (7.18), $\boldsymbol{\Omega}_{iHb}$ is selectively updated from $\boldsymbol{\Omega}_{iH}$ when the minimum eigenvalue of $\boldsymbol{\Omega}_i \triangleq \boldsymbol{\Omega}_{iH}^T \boldsymbol{\Omega}_{iH}$ is maximized.

$$\boldsymbol{\Omega}_{ib}(t) \triangleq \boldsymbol{\Omega}_i(t_b) \quad \boldsymbol{\Omega}_{iHb}(t) \triangleq \boldsymbol{\Omega}_{iH}(t_b) \quad \boldsymbol{r}_{ib}(t) \triangleq \boldsymbol{r}_i(t_b)$$

where

$$t_b \triangleq \max \left\{ \underset{\tau \in (t_0, t)}{\operatorname{argmax}} \mathcal{F}(\boldsymbol{\Omega}_i(\tau)) \right\} \tag{7.18}$$

$$\mathcal{F}(\boldsymbol{\Omega}_i) = \min_q \sigma_{\boldsymbol{\Omega}_i q}$$

$\sigma_{\boldsymbol{\Omega}_i q}$ $(q = 1, \cdots, m_i)$ represent eigenvalues of $\boldsymbol{\Omega}_i$. From the linear independency of $\boldsymbol{\phi}'_{iF_{ij}}$, the orthogonality of $\boldsymbol{\phi}^*_{i\,F_{ij}}$ and this selective update scheme, it is proven that $\boldsymbol{\Omega}_{ib}$ is full rank for all the time under FE in [28]. Since the rank of $\boldsymbol{\Omega}_{iHb}$ is identical

with the rank of $\boldsymbol{\Omega}_{ib}$, $\boldsymbol{\Omega}_{iHb}$ is also full rank for all the time under FE.

The logarithmic regression-based composite adaptation law is finally proposed as (7.19) with guaranteed parameter convergence under FE by utilizing $\boldsymbol{\Omega}_{iHb}$ and $\boldsymbol{r}_{ib}$ in (7.18) for (7.13) with (7.12).

$$\begin{aligned}
&\dot{\hat{\boldsymbol{\theta}}}_i = z_i \boldsymbol{\Gamma}_i \boldsymbol{\phi}_i' - \lambda_i \boldsymbol{\Gamma}_i \boldsymbol{\Omega}_{iHb}^T \operatorname{diag}\left\{\operatorname{sgn}\left(\boldsymbol{E}_{ib}\right)\right\} \boldsymbol{E}_{ib}^* \\
&\text{where} \\
&\boldsymbol{E}_{ib} = \boldsymbol{\Omega}_{iHb} \hat{\boldsymbol{\theta}}_i - \boldsymbol{r}_{ib} = \left[\ E_{i1b}, E_{i2b}, \cdots, E_{im_ib}\ \right]^T \\
&\boldsymbol{E}_{ib}^* = \left[\ E_{i1b}^*, E_{i2b}^*, \cdots, E_{im_ib}^*\ \right]^T \\
&E_{ij_b}^* = \log_{p_i}\left(q_i \left| E_{ij_b} \right| + 1\right)
\end{aligned} \tag{7.19}$$

7.4 Stability Analysis

In Section 7.4, the asymptotic stability of the closed-loop system with the proposed logarithmic regression-based composite adaptive control is proven under the Lyapunov theory. In Section 7.2.3, tracking error dynamics of the closed-loop system is provided as (7.6). Since the unknown parameter $\boldsymbol{\theta}_i$ is assumed to be constant, the estimation error dynamics is derived from (7.19) as (7.20).

$$\dot{\tilde{\boldsymbol{\theta}}}_i = z_i \boldsymbol{\Gamma}_i \boldsymbol{\phi}_i' - \lambda_i \boldsymbol{\Gamma}_i \boldsymbol{\Omega}_{iHb}^T \operatorname{diag}\left\{\operatorname{sgn}\left(\boldsymbol{E}_{ib}\right)\right\} \boldsymbol{E}_{ib}^* \tag{7.20}$$

The equilibrium points of the closed-loop system dynamics in (7.6) and (7.20) are obtained as $\boldsymbol{z} = \boldsymbol{0}$ and $\tilde{\boldsymbol{\theta}}_i = \boldsymbol{0}$ $(i = 1, \cdots, n)$. The asymptotic stability of the closed-loop system is proven with Lyapunov theory in Theorem 7.1.

Theorem 7.1. *(Asymptotic Stability of Closed-Loop System) : The closed-loop system with the logarithmic regression-based composite adaptation law is asymptotically stable for all $t > t_0$ if the system is under FE over $t \in [t_0, t_1]$.*

Proof. The Lyapunov candidate function V_n is defined by considering both $\boldsymbol{z}$ and $\tilde{\boldsymbol{\theta}}_i$ $(i = 1, \cdots, n)$ as (7.21).

$$V_n = \frac{1}{2}\boldsymbol{z}^T\boldsymbol{z} + \frac{1}{2}\sum_{i=1}^{n} \tilde{\boldsymbol{\theta}}_i^T \boldsymbol{\Gamma}_i^{-1} \tilde{\boldsymbol{\theta}}_i \tag{7.21}$$

Note that V_n in (7.21) is positive definite except the equilibrium point and becomes

0 if and only if $\boldsymbol{z} = \mathbf{0}$ and $\tilde{\boldsymbol{\theta}}_i = \mathbf{0}$.

The derivative of V_n is derived as (7.22) from (7.21) with (7.6) and (7.20).

$$\begin{aligned}
\dot{V}_n =& \sum_{i=1}^{n} z_i \dot{z}_i + \sum_{i=1}^{n} \tilde{\boldsymbol{\theta}}_i^T \boldsymbol{\Gamma}_i^{-1} \dot{\tilde{\boldsymbol{\theta}}}_i \\
=& \Bigg[z_1 \left\{ -C_1 z_1 + g_1 z_2 - \tilde{\boldsymbol{\theta}}_1^T \boldsymbol{\phi}_1' \right\} \\
&+ \sum_{i=2}^{n-1} z_i \left\{ -C_i z_i - g_{i-1} z_{i-1} + g_i z_{i+1} - \tilde{\boldsymbol{\theta}}_i^T \boldsymbol{\phi}_i' \right\} \\
&+ z_n \left\{ -C_n z_n + g_{n-1} z_{n-1} - \tilde{\boldsymbol{\theta}}_n^T \boldsymbol{\phi}_n' \right\} \Bigg] \\
&+ \sum_{i=1}^{n} \left(\hat{\boldsymbol{\theta}}_{\boldsymbol{i}} - \boldsymbol{\theta}_i \right)^T {\boldsymbol{\Gamma}_i}^{-1} \left[z_i \boldsymbol{\Gamma}_i \boldsymbol{\phi}_i' - \lambda_i \boldsymbol{\Gamma}_i \boldsymbol{\Omega}_{iHb}^T \operatorname{diag}\left\{ \operatorname{sgn}\left(\boldsymbol{E}_{ib} \right) \right\} \boldsymbol{E}_{ib}^* \right] \\
=& - \sum_{i=1}^{n} C_i z_i^2 - \sum_{i=1}^{n} \lambda_i \boldsymbol{E}_{ib}^T \operatorname{diag}\left\{ \operatorname{sgn}\left(\boldsymbol{E}_{ib} \right) \right\} \boldsymbol{E}_{ib}^*
\end{aligned} \tag{7.22}$$

The first term of (7.22) is negative definite when $\boldsymbol{z} \neq \mathbf{0}$ and becomes 0 if and only if $\boldsymbol{z} = \mathbf{0}$. To examine the negative definiteness of the second term in (7.22), $\boldsymbol{E}_{ib}$ is rewritten as (7.23).

$$\boldsymbol{E}_{ib} = \begin{bmatrix} \operatorname{sgn}\left(E_{i1b} \right) & \cdots & 0 \\ \vdots & \ddots & \vdots \\ 0 & \cdots & \operatorname{sgn}\left(E_{im_ib} \right) \end{bmatrix} \begin{bmatrix} \left| E_{i1b} \right| \\ \vdots \\ \left| E_{im_ib} \right| \end{bmatrix} \tag{7.23}$$

(7.24) is obtained by substituting (7.19) and (7.23) into the second term of (7.22).

$$\begin{aligned}
& - \sum_{i=1}^{n} \lambda_i \boldsymbol{E}_{ib}^T \operatorname{diag}\left\{ \operatorname{sgn}\left(\boldsymbol{E}_{ib} \right) \right\} \boldsymbol{E}_{ib}^* \\
&= - \sum_{i=1}^{n} \lambda_i \left[\left| E_{i1b} \right|, \cdots \left| E_{im_ib} \right| \right] \\
&\qquad \times \operatorname{diag}\left\{ \operatorname{sgn}\left(\boldsymbol{E}_{ib} \right) \right\}^T \operatorname{diag}\left\{ \operatorname{sgn}\left(\boldsymbol{E}_{ib} \right) \right\} \boldsymbol{E}_{ib}^* \\
&= - \sum_{i=1}^{n} \left[\lambda_i \sum_{j=1}^{m_i} \left| E_{ij_b} \right| \log_{p_i} \left(q_i \left| E_{ij_b} \right| + 1 \right) \right]
\end{aligned} \tag{7.24}$$

Since $\boldsymbol{\Omega}_{iHb}$ is full-rank for all $t > t_0$ if the system is under FE over $t \in [t_0, t_1]$, $\boldsymbol{E}_{ib} = \boldsymbol{\Omega}_{iHb} \tilde{\boldsymbol{\theta}}_i = \mathbf{0}$ if and only if $\tilde{\boldsymbol{\theta}}_i = \mathbf{0}$. Hence, (7.24) is negative definite with

$p_i > 1$ and $q_i > 0$ except for $\tilde{\boldsymbol{\theta}}_i = \mathbf{0}$. Therefore, the asymptotic stability of the closed loop system with new logarithmic regression-based composite adaptation law under FE for $t > t_0$ is shown to be guaranteed. □

7.5 Comparative Study

7.5.1 Linear Regression-based Composite Adaptation Law

A linear regression-based composite adaptation law [14–28] can be derived as (7.25) by introducing $\boldsymbol{\Xi}_i = \boldsymbol{\Omega}_i \hat{\boldsymbol{\theta}}_i - \boldsymbol{\eta}_i$ to (7.7).

$$\dot{\hat{\boldsymbol{\theta}}}_i = z_i \boldsymbol{\Gamma}_i \boldsymbol{\phi}_i' - \lambda_i \boldsymbol{\Gamma}_i \left(\boldsymbol{\Omega}_i \hat{\boldsymbol{\theta}}_i - \boldsymbol{\eta}_i \right) \tag{7.25}$$

$\boldsymbol{\Omega}_i \in \mathbb{R}^{m_i \times m_i}$ denotes an information matrix, and $\boldsymbol{\eta}_i \triangleq \boldsymbol{\Omega}_i \boldsymbol{\theta}_i \in \mathbb{R}^{m_i \times 1}$ represents an auxiliary vector. For positive definite $\boldsymbol{\Omega}_i$, the condition in (7.11) is satisfied. If the information matrix in (7.18) is utilized for (7.25), the linear regression-based composite adaptation law is derived as (7.26) with guaranteed parameter estimation convergence under FE [28].

$$\begin{aligned} &\dot{\hat{\boldsymbol{\theta}}}_i = z_i \boldsymbol{\Gamma}_i \boldsymbol{\phi}_i' - \lambda_i \boldsymbol{\Gamma}_i \left(\boldsymbol{\Omega}_{ib} \hat{\boldsymbol{\theta}}_i - \boldsymbol{\eta}_{ib} \right) \\ &\text{where} \quad \boldsymbol{\Omega}_{ib} = \boldsymbol{\Omega}_{iH_b}^T \boldsymbol{\Omega}_{iHb} \quad \boldsymbol{\eta}_{ib} = \boldsymbol{\Omega}_{iH_b}^T \boldsymbol{r}_{ib} \end{aligned} \tag{7.26}$$

Note that it is proven in [28] that the closed loop system is stable with positive definite $\boldsymbol{\Omega}_i$ for all the time under FE. The linear regression-based composite adaptation law in (7.26) can be rewritten as (7.27) using $\boldsymbol{E}_{ib} = \text{diag}\left\{\text{sgn}\left(\boldsymbol{E}_{ib}\right)\right\} \boldsymbol{E}_{ib}^{\#}$ with $E_{ij_b}^{\#} = \left| E_{ij_b} \right|$.

$$\begin{aligned} &\dot{\hat{\boldsymbol{\theta}}}_i = z_i \boldsymbol{\Gamma}_i \boldsymbol{\phi}_i' - \lambda_i \boldsymbol{\Gamma}_i \boldsymbol{\Omega}_{iH_b}^T \text{diag}\left\{\text{sgn}\left(\boldsymbol{E}_{ib}\right)\right\} \boldsymbol{E}_{ib}^{\#} \\ &\text{where} \\ &\boldsymbol{E}_{ib} = \boldsymbol{\Omega}_{iHb} \hat{\boldsymbol{\theta}}_i - \boldsymbol{r}_{ib} = \left[\, E_{i1b}, E_{i2b}, \cdots, E_{im_ib} \, \right]^T \\ &\boldsymbol{E}_{ib}^{\#} = \left[\, E_{i1_b}^{\#}, E_{i2_b}^{\#}, \cdots, E_{im_ib}^{\#} \, \right]^T \\ &E_{ij_b}^{\#} = \left| E_{ij_b} \right| \end{aligned} \tag{7.27}$$

It is shown that the logarithmic regression term in (7.19) and the linear regression

term in (7.27) can be expressed in the same form with only difference from $\boldsymbol{E}_{ib}^{*}$ and $\boldsymbol{E}_{ib}^{\#}$; $E_{ij_b}^{*} = \log_{p_i}\left(q_i\left|E_{ij_b}\right| + 1\right)$ with $p_i > 1$ and $q_i > 0$ for the logarithmic regression term and $E_{ij_b}^{\#} = \left|E_{ij_b}\right|$ for the linear regression term. As a result, comparative studies on the two composite adaptation laws can be simply conducted with investigations on the differences between $E_{ij_b}^{*}$ and $E_{ij_b}^{\#}$ in Section 7.5.2.

7.5.2 Comparative Study between Logarithmic and Linear Regression-based Composite Adaptation Law

The logarithmic function $E_{ij_b}^{*}$ is a concave and monotonically increasing function of $\left|E_{ij_b}\right|$ and the linear function $E_{ij_b}^{\#}$ is a monotonically increasing function of $\left|E_{ij_b}\right|$ with constant slope. Considering these different regression patterns, a condition to always accomplish faster parameter convergence with the logarithmic regression based composite adaptation law than the linear regression based approach is mainly investigated within the system boundary.

Before detailed discussions, reasonable system boundary with respect to $\left|E_{ij_b}\right|$ is examined for the comparative study. With (7.15) and (7.17), $\left|E_{ij_b}\right|$ from $\boldsymbol{E}_{ib}$ in (7.19) and (7.27) is derived as (7.28).

$$\left|E_{ij_b}\right| = \left|{\boldsymbol{\phi}_{i\,bF_{ij}}^{*}}^{T}\tilde{\boldsymbol{\theta}}_i\right| \tag{7.28}$$

Under the assumption that $\boldsymbol{\phi}_i'$ is bounded as $\left\|\boldsymbol{\phi}_i'\right\| \leq \delta_{\phi_i}$ with constant δ_{ϕ_i}, $\left\|\boldsymbol{\phi}_{i\,bF_{ij}}^{*}\right\|$ can be suggested as (7.29) from $\left\|\boldsymbol{\phi}_{i\,bF_{ij}}^{*}\right\| = \left\|\boldsymbol{\phi}_{ibF_{ij}}'\right\| \leq \left\|\boldsymbol{\phi}_i'\right\|$.

$$\left\|\boldsymbol{\phi}_{i\,bF_{ij}}^{*}\right\| \leq \delta_{\phi_i} \tag{7.29}$$

The unknown parameter $\boldsymbol{\theta}_i$ is assumed to be within the range defined with constant $\delta_{\boldsymbol{\theta}_i L}$ and $\delta_{\boldsymbol{\theta}_i U}$ as in (7.30).

$$\delta_{\boldsymbol{\theta}_i L} \leq \left\|\boldsymbol{\theta}_i\right\| \leq \delta_{\boldsymbol{\theta}_i U} \tag{7.30}$$

If $\tilde{\boldsymbol{\theta}}_i = \hat{\boldsymbol{\theta}}_i - \boldsymbol{\theta}_i$ decreases with an adaptation law,

$$\left\|\hat{\boldsymbol{\theta}}_i - \boldsymbol{\theta}_i\right\| \leq \left\|\hat{\boldsymbol{\theta}}_{i_0} - \boldsymbol{\theta}_i\right\| \tag{7.31}$$

where $\hat{\boldsymbol{\theta}}_{i_0}$ represents the initial value of $\hat{\boldsymbol{\theta}}_i$. The upper bound of $\tilde{\boldsymbol{\theta}}_i$ is derived as (7.32) from (7.30) and (7.31).

$$\left\|\tilde{\boldsymbol{\theta}}_i\right\| \leq \left\|\hat{\boldsymbol{\theta}}_{i_0} - \boldsymbol{\theta}_i\right\| \leq \left\|\hat{\boldsymbol{\theta}}_{i_0}\right\| + \|\boldsymbol{\theta}_i\| \leq \left\|\hat{\boldsymbol{\theta}}_{i_0}\right\| + \delta_{\boldsymbol{\theta}_i U} \tag{7.32}$$

From (7.28), (7.29) and (7.32), the upper bound of $\left|E_{ij_b}\right|$ is obtained as (7.33).

$$\left|E_{ij_b}\right| \leq \left\|\boldsymbol{\phi}^*_{i\,bF_{ij}}\right\| \left\|\tilde{\boldsymbol{\theta}}_i\right\| \leq \delta_{\phi_i}\left(\left\|\hat{\boldsymbol{\theta}}_{i_0}\right\| + \delta_{\boldsymbol{\theta}_i U}\right) \tag{7.33}$$

Since $\left|E_{ij_b}\right| \geq 0$, the boundary of $\left|E_{ij_b}\right|$ is given as (7.34).

$$\begin{aligned} &0 \leq \left|E_{ij_b}\right| \leq \left|E_{ij_b}\right|_U \\ &\text{where } \left|E_{ij_b}\right|_U \triangleq \delta_{\phi_i}\left(\left\|\hat{\boldsymbol{\theta}}_{i_0}\right\| + \delta_{\boldsymbol{\theta}_i U}\right) \end{aligned} \tag{7.34}$$

Within the system boundary, the logarithmic regression-based approach always shows faster parameter convergence than the linear regression-based approach under the same λ_i and $\boldsymbol{\Gamma}_i$ when condition on p_i and q_i in Theorem 7.2 is satisfied.

Theorem 7.2. *(Condition on p_i and q_i for $E^*_{ij_b} > E^{\#}_{ij_b}$) : Under the assumption of the same λ_i and $\boldsymbol{\Gamma}_i$, the logarithmic regression-based composite adaptation law with $E^*_{ij_b}$ is guaranteed to achieve faster parameter convergence than the linear regression-based composite adaptation law with $E^{\#}_{ij_b}$ for $0 < \left|E_{ij_b}\right| \leq \left|E_{ij_b}\right|_U$ if $p_i > 1$ and $q_i > 0$ satisfy $p_i^{\left|E_{ij_b}\right|_U} - q_i\left|E_{ij_b}\right|_U < 1$.*

Proof. Since $E^*_{ij_b}$ with $p_i > 1$ and $q_i > 0$ for the logarithmic regression term is concave and monotonically increasing function, $\log_{p_i}\left(q_i\left|E_{ij_b}\right| + 1\right) > \left|E_{ij_b}\right|$ is always satisfied for $0 < \left|E_{ij_b}\right| \leq \left|E_{ij_b}\right|_U$ when (7.35) is satisfied.

$$\log_{p_i}\left(q_i\left|E_{ij_b}\right|_U + 1\right) > \left|E_{ij_b}\right|_U \tag{7.35}$$

The condition on p_i and q_i to make the logarithmic regression-based composite adaptation always faster than the linear regression-based composite adaptation for the same λ_i and $\boldsymbol{\Gamma}_i$ is derived by rewriting (7.35) into (7.36).

$$p_i^{\left|E_{ij_b}\right|_U} - q_i\left|E_{ij_b}\right|_U < 1 \tag{7.36}$$

□

When the logarithmic regression-based composite adaptation law has higher learning rate than the linear regression-based composite adaptation law satisfying the condition in Theorem 7.2, the required increase of λ_i to λ_i' for the linear regression-based approach is addressed in Theorem 7.3 for higher adaptation speed than the logarithmic regression-based approach with λ_i.

Theorem 7.3. *(Required increase of λ_i to λ_i' in linear regression for $\lambda_i' {E_{ij_b}}^{\#} > \lambda_i {E_{ij_b}}^{*}$) : If Theorem 7.2 is satisfied, λ_i for the linear regression-based composite adaptation law should increase to λ_i' which satisfies $\frac{\lambda_i'}{\lambda_i} > \frac{q_i}{\ln p_i}$ for higher learning rate than the logarithmic regression-base composite adaptation law with λ_i.*

Proof. $\lambda_i' {E_{ij_b}}^{\#} > \lambda_i {E_{ij_b}}^{*}$ is satisfied when the slope of the tangent line of $\lambda_i {E_{ij_b}}^{*} = \lambda_i \log_{p_i}\left(q_i\left|E_{ij_b}\right| + 1\right)$ $(p_i > 1,\ q_i > 0)$ at the origin is smaller than the slope of $\lambda_i' {E_{ij_b}}^{\#} = \lambda_i'\left|E_{ij_b}\right|$ which is λ_i'.

$$\left.\frac{\lambda_i q_i}{\ln p_i\left(q_i\left|E_{ij_b}\right| + 1\right)}\right|_{\left|E_{ij_b}\right|=0} < \lambda_i' \tag{7.37}$$

The condition on λ_i' in (7.37) can be rewritten as (7.38).

$$\frac{\lambda_i'}{\lambda_i} > \frac{q_i}{\ln p_i} \tag{7.38}$$

Since p_i and q_i are designed to satisfy Theorem 7.2, (7.39) is obtained from (7.36).

$$\left|E_{ij_b}\right|_U \ln p_i < \ln\left(q_i\left|E_{ij_b}\right|_U + 1\right) \tag{7.39}$$

(7.40) is derived from (7.39) by utilizing $\ln\left(q_i\left|E_{ij_b}\right|_U + 1\right) < q_i\left|E_{ij_b}\right|_U$ for any $\left|E_{ij_b}\right|_U > 0$

$$\frac{q_i}{\ln p_i} > 1 \tag{7.40}$$

Thus, $\lambda_i' > \frac{q_i}{\ln p_i}\lambda_i > \lambda_i$ for $\lambda_i' {E_{ij_b}}^{\#} > \lambda_i {E_{ij_b}}^{*}$ when Theorem 7.2 is satisfied, resulting in Theorem 7.3. □

Theorem 7.2 and 7.3 imply that the logarithmic regression term can be designed to utilize smaller adaptation gain than the linear regression term while accomplishing the same adaptation speed. Thus, measurement signal errors induced by various non-parametric uncertainties like delay, noise or bias, are less amplified with the logarithmic regression term than with the linear regression term. To this end, the logarithmic regression-based composite adaptation law has enhanced robustness than the linear regression-based composite adaptation law while providing the same adaptation speed.

In order to prevent the logarithmic regression-based composite adaptation law to become always slower than the linear regression-based composite adaptation law under the same λ_i and $\mathbf{\Gamma}_i$, p_i and q_i should be designed at least not to satisfy the condition in Theorem 7.4.

Theorem 7.4. *(Conditions on p_i and q_i for $E_{ij_b}^{*} < E_{ij_b}^{\#}$) : Under the assumption of the same λ_i and $\mathbf{\Gamma}_i$, the logarithmic regression-based composite adaptation law with $E_{ij_b}^{*}$ is slower than the linear regression-based composite adaptation law with $E_{ij_b}^{\#}$ if $p_i > 1$ and $q_i > 0$ satisfy $q_i > \log p_i$.*

Proof. Since $E_{ij_b}^{*}$ with $p_i > 1$ and $q_i > 0$ for the logarithmic regression term is concave and monotonically increasing function, $\log_{p_i}\left(q_i\left|E_{ij_b}\right|+1\right) < \left|E_{ij_b}\right|$ is satisfied when the slope of the tangent line of $E_{ij_b}^{*}$ at the origin is smaller than the slope of $E_{ij_b}^{\#}$ which is 1.

$$\left.\frac{q_i}{\ln p_i\left(q_i\left|E_{ij_b}\right|+1\right)}\right|_{\left|E_{ij_b}\right|=0} < 1 \tag{7.41}$$

From (7.41), the condition on p_i and q_i to make the logarithmic regression-based composite adaptation law slower than the linear regression-based composite adaptation law under the same λ_i and $\mathbf{\Gamma}_i$ is obtained as (7.42).

$$q_i > \ln p_i \tag{7.42}$$

□

7.6 Numerical Simulation

7.6.1 Simulation Setup

As an illustrative example, dynamics of an inverted pendulum on a cart is provided with consideration of uncertainties on a friction model as (7.43) for numerical simulation.

$$\dot{\boldsymbol{x}} = \boldsymbol{f}(\boldsymbol{x}) + \boldsymbol{G}(\boldsymbol{x})\left[\boldsymbol{u} + \boldsymbol{\Delta}(\boldsymbol{x})\right]$$

where

$$\begin{aligned}
&\boldsymbol{x} = [x_1,\ x_2]^T \\
&\boldsymbol{f}(\boldsymbol{x}) = \left[f_1(x_1),\ f_2(x_1, x_2)\right]^T \\
&\qquad = \left[0, \frac{(M_C + M_P)\, g \sin x_1 - L_P M_P x_2^2 \sin x_1 \cos x_1}{L_P\left[M_C + (1 - \cos^2 x_1)\, M_P\right]}\right]^T \\
&\boldsymbol{G}(\boldsymbol{x}) = \mathrm{diag}\left[g_1(x_1),\ g_2(x_1, x_2)\right] \\
&\qquad = \mathrm{diag}\left[1,\ \frac{-\cos x_1}{L_P\left[M_C + (1 - \cos^2 x_1)\, M_P\right]}\right] \\
&\boldsymbol{u} = [x_2,\ u]^T \\
&\boldsymbol{\Delta}(\boldsymbol{x}) = \left[0,\ \Delta_2(x_1, x_2)\right]^T
\end{aligned} \tag{7.43}$$

x_1 is a pendulum angle from the vertical line and x_2 is a pendulum angle rate. M_C and M_P denote mass of the cart and the pendulum, respectively. A pendulum length is given as L_P. g is gravitational acceleration. The control input u indicates lateral force exerted on the cart. The friction model Δ_2 is suggested as (7.44).

$$\begin{aligned}
&\Delta_2(x_1, x_2) = \boldsymbol{\theta}_2^T \boldsymbol{\phi}_2(x_1, x_2) \\
&\text{where} \\
&\boldsymbol{\theta}_2 = [\theta_{21},\ \theta_{22}]^T \quad \boldsymbol{\phi}_2'(x_1, x_2) = \left[\phi_{21}'(x_1, x_2),\ \phi_{22}'(x_1, x_2)\right]^T \\
&\phi_{21}'(x_1, x_2) = \frac{-(M_C + M_P)\, x_2}{L_P\left[M_C + (1 - \cos^2 x_1)\, M_P\right]} \\
&\phi_{22}'(x_1, x_2) = \frac{(M_C + M_P)\, g \cos x_1}{L_P\left[M_C + (1 - \cos^2 x_1)\, M_P\right]}
\end{aligned} \tag{7.44}$$

θ_{21} is a friction coefficient at the link between the pendulum and the cart. θ_{22} represents a friction coefficient between the cart and the ground. θ_{21} and θ_{22} are uncertainties to be estimated.

In this simulation, known model parameters are defined to be $M_C = 0.1kg$, $M_P = 0.01kg$, $L_P = 2m$ and $g = 9.81m/s^2$. The boundaries of the uncertain model parameters are given as $0.2 \leq \theta_{21} \leq 2$ and $0.2 \leq \theta_{22} \leq 2$, resulting in $\delta_{\boldsymbol{\theta}_2 L} = 0.2\sqrt{2}$ and $\delta_{\boldsymbol{\theta}_2 U} = 2\sqrt{2}$ in (7.30). The true values of the uncertain parameters to be estimated from the adaptation law are defined as $\boldsymbol{\theta}_2 = [1.2,\ 1.7]^T$. The initial conditions of the parameter estimates are set to be the minimum values of the boundaries as $\hat{\boldsymbol{\theta}}_{2_0} = [0.2,\ 0.2]^T$. The boundaries of the state variables are given as $-180^\circ \leq x_1 \leq 180^\circ$ and $-60^\circ/s \leq x_2 \leq 60^\circ/s$. The initial conditions of the state variables are defined as $[60^\circ,\ 0]$, and the desired command on the state x_1 is given as $x_{1c} = 0^\circ$ to make the pendulum stand vertically.

Simulations are conducted for verification of the logarithmic regression-based composite adaptation law proposed in Section 7.3. The backstepping controller is utilized as a representative example of the baseline controller as discussed in Section 7.2.2. The proposed algorithm is compared with the linear regression-based composite adaptation law in Section 7.5.1 to clearly show the characteristics suggested in Section 7.5.2. Design parameters for the control input command vector are defined as $C_1 = C_2 = 1.5$. The multiple filter parameters for $\boldsymbol{\Omega}_{2b}$ and $\boldsymbol{\Omega}_{2Hb}$ are set to be $k_{21} = 0.01$ and $k_{22} = 0.015$.

The design parameters for the logarithmic and the linear regression-based composite adaptation laws are selected to verify Theorem 7.2, 7.3 and 7.4 in Section 7.5.2 as follows. First, $\left|E_{2_{jb}}\right|_U$ in (7.34) can be inferred from the boundaries of the state variables and the uncertain parameters. $\left\|\hat{\boldsymbol{\theta}}_{2_0}\right\| = 0.2\sqrt{2}$ and $\delta_{\boldsymbol{\theta}_2 U} = 2\sqrt{2}$. To obtain δ_{ϕ_2}, norm of $\boldsymbol{\phi}_2'(x_1, x_2)$ is examined from (7.44) as (7.45).

$$\left\|\boldsymbol{\phi}_2'(x_1, x_2)\right\| = \frac{M_C + M_P}{L_P} \frac{\sqrt{g^2 \cos^2 x_1 + x_2^2}}{M_C + M_P - M_P \cos^2 x_1} \tag{7.45}$$

Since $\cos^2 x_1 \leq 1$ and $-\frac{\pi}{3} \leq x_2 \leq \frac{\pi}{3}$, δ_{ϕ_2} is derived as (7.46),

$$\left\|\boldsymbol{\phi}_2'(x_1, x_2)\right\| \leq \delta_{\phi_2} = \frac{M_C + M_P}{L_P} \frac{\sqrt{g^2 + x_{2\max}^2}}{M_C} \tag{7.46}$$

In this simulation, $\delta_{\phi_2} = 5.4262$ and this results in $\left|E_{2_{jb}}\right|_U = 16.8822$.

Second, design parameters are defined by considering Theorem 7.2, 7.3 and 7.4 with the obtained $\left|E_{ij_b}\right|_U$ as Table. 7.1.

Table 7.1: Design Parameters for Adaptation Laws

Case	Algorithm	$\mathbf{\Gamma}_2$	λ_2	p_2	q_2
1	Logarithmic Regression	diag [0.8, 0.8]	1.2	1.2	1.5
2	Logarithmic Regression	diag [0.8, 0.8]	1.2	1.2	0.15
A	Linear Regression	diag [0.8, 0.8]	1.2	-	-
B	Linear Regression with High λ_2 (λ_2')	diag [0.8, 0.8]	10	-	-

7.6.2 Simulation Results

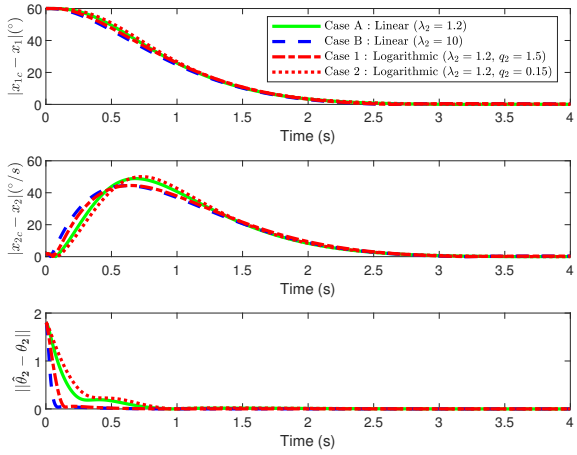

Figure 7.1: Tracking and Estimation Error under Nominal Circumstance

Under the nominal circumstance, simulation results of the logarithmic and the linear regression-based composite adaptation laws with the design parameters in Table. 7.1 are addressed in Fig. 7.1. It is shown in Fig. 7.1 that tracking and parameter estimation errors for all cases converge to 0, as expected from the analysis in Section 7.5. Theorem 7.2 is verified from the following observation with Case 1 and A in Fig. 7.1. Under the same λ_2, parameter convergence for Case 1 with the proposed logarithmic regression-based composite adaptation law is faster than the one for Case A with the existing linear regression-based composite adaptation law. Note that p_2 and q_2 of Case 1 satisfy the condition in (7.36). Simulation results with Case 1 and B in Fig. 7.1 validate Theorem 7.3. Since λ_2 increases to λ_2' which satisfies (7.38) in Case B, Case B with linear regression-based approach shows similar but slightly higher parameter estimation speed than Case 1 with the logarithmic regression-based approach. Instead, there exists a significant side-effect of the λ_2 increase in Case B on system robustness comparing to Case 1, which will be shown in Fig. 7.2 from simulations under measurement delays. Simulation results with Case 2 and A

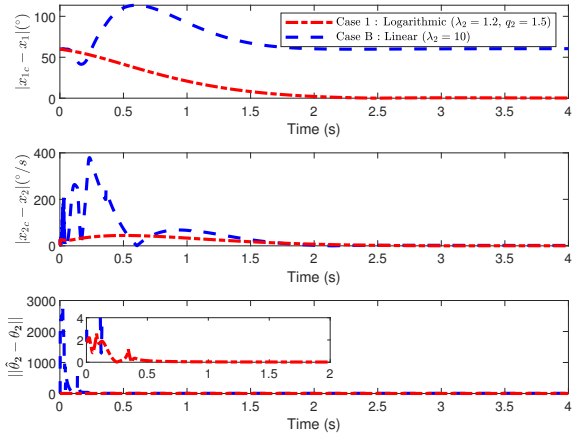

Figure 7.2: Tracking and Estimation Error with Measurement Delay

in Fig. 7.1 verify Theorem 7.3 as a design constraint for faster adaptation with the proposed algorithm.

Simulations are additionally conducted as increasing measurement delays τ on both x_1 and x_2 before system instability especially with Case 1 and Case B. The system appears to be unstable from $\tau = 0.0018s$ with Case B and from $\tau = 0.0225s$ with Case 1, which implies enhanced robustness for the logarithmic regression-based approach. As a representative example, simulation results under $\tau = 0.0017s$ are suggested in Fig. 7.2. Unlike Case 1 with the logarithmic regression-based approach, Case B with the linear regression-based approach shows undesirable parameter estimation and tracking performance in Fig. 7.2. This is because λ_2 is increased for the linear regression-based law in Case B to have similar adaptation speed with the logarithmic regression-based law in Case 1 under the nominal circumstance.

7.7 Conclusion

A new logarithmic regression-based composite adaptation law is successfully proposed in Chapter 7, which accomplishes fast parameter convergence without excessive increase of the adaptation gain. The novelty of this research is in the composite adaptation law design with regression pattern shaping based on the logarithmic function to avoid the adaptation speed degeneration. Important findings on adaptation speed and system robustness with the proposed algorithm is provided with detailed analysis, which is obtained from comparative study between the logarithmic and the linear regression-based approaches. The condition on the design parameters of the logarithmic regression-based composite adaptation law is suggested, which always

provides higher adaptation speed than the linear regression-based approach for the same adaptation gain within the system boundary. If this condition is satisfied, it is studied how much the linear regression-based approach should increase its adaptation gain to make the adaptation faster than logarithmic regression-based approach. The system robustness can be improved with the logarithmic regression-based approach comparing to the linear regression-based approach since the logarithmic approach with lower adaptation gain can accomplish similar parameter convergence speed with the linear approach. With new logarithmic regression-based composite adaptation law, the closed-loop system is proven to be globally exponentially stable. Numerical simulations are performed to verify the proposed algorithm and related theoretical findings.

References

[1] Nazli E Kahveci and Petros A Ioannou. Adaptive steering control for uncertain ship dynamics and stability analysis. *Automatica*, 49(3):685–697, 2013.

[2] J Van Amerongen. Model reference adaptive control applied to steering of ships. In *Methods and applications in adaptive control*, pages 199–208. Springer, 1980.

[3] HJ Tol, CC De Visser, LG Sun, E van Kampen, and QP Chu. Multivariate spline-based adaptive control of high-performance aircraft with aerodynamic uncertainties. *Journal of Guidance, Control, and Dynamics*, 39(4):781–800, 2016.

[4] Ye Zhou, Erik-Jan van Kampen, and QiPing Chu. Nonlinear adaptive flight control using incremental approximate dynamic programming and output feedback. *Journal of Guidance, Control, and Dynamics*, 40(2):493–496, 2016.

[5] Nhan Nguyen, Kalmanje Krishnakumar, John Kaneshige, and Pascal Nespeca. Flight dynamics and hybrid adaptive control of damaged aircraft. *Journal of guidance, control, and dynamics*, 31(3):751–764, 2008.

[6] DE Seborg, Thomas F Edgar, and SL Shah. Adaptive control strategies for process control: a survey. *AIChE Journal*, 32(6):881–913, 1986.

[7] A Galip Ulsoy and Yoram Koren. Applications of adaptive control to machine tool process control. *IEEE Control Systems Magazine*, 9(4):33–37, 1989.

[8] Chengshuai Wu, Jian Chen, Chenfeng Xu, and Zhiyang Liu. Real-time adaptive control of a fuel cell/battery hybrid power system with guaranteed stability. *IEEE Transactions on Control Systems Technology*, 25(4):1394–1405, 2016.

[9] Dezhi Xu, Jianxing Liu, Xing-Gang Yan, and Wenxu Yan. A novel adaptive neural network constrained control for a multi-area interconnected power system with hybrid energy storage. *IEEE Transactions on Industrial Electronics*, 65(8):6625–6634, 2017.

[10] Hanlei Wang. Adaptive control of robot manipulators with uncertain kinematics and dynamics. *IEEE Transactions on Automatic Control*, 62(2):948–954, 2016.

[11] Wang Leifeng, Li Ye, Liao Yulei, Pan Kaiwen, and Zhang Weixin. Adaptive heading control of unmanned wave glider with heading information fusion. *Control Engineering Practice*, 85:216–224, 2019.

[12] Jovan D Boskovic and Raman K Mehra. Intelligent adaptive control of a tailless advanced fighter aircraft under wing damage. *Journal of Guidance, Control, and Dynamics*, 23(5):876–884, 2000.

[13] Jin Young Choi, Dongkyoung Chwa, and Min-Soo Kim. Adaptive control for feedback-linearized missiles with uncertainties. *IEEE Transactions on Aerospace and Electronic Systems*, 36(2):467–481, 2000.

[14] Jean-Jacques E Slotine and Weiping Li. On the adaptive control of robot manipulators. *The international journal of robotics research*, 6(3):49–59, 1987.

[15] Jean-Jacques E Slotine and Weiping Li. Composite adaptive control of robot manipulators. *Automatica*, 25(4):509–519, 1989.

[16] Jean-Jacques E Slotine, Weiping Li, et al. *Applied nonlinear control*. Prentice hall Englewood Cliffs, NJ, 1991.

[17] Manuel A Duarte and Kumpati S Narendra. Combined direct and indirect approach to adaptive control. *IEEE Transactions on Automatic Control*, 34(10):1071–1075, 1989.

[18] Manuel A Duarte and Kumpati S Narendra. A new approach to model reference adaptive control. *International Journal of Adaptive Control and Signal Processing*, 3(1):53–73, 1989.

[19] Kumpati S Narendra and Manuel A Duarte. Application of robust adaptive control using combined direct and indirect methods. *International Journal of Adaptive Control and Signal Processing*, 3(2):131–142, 1989.

[20] Eugene Lavretsky. Combined/composite model reference adaptive control. *IEEE Transactions on Automatic Control*, 54(11):2692–2697, 2009.

[21] M Kemal Ciliz. Combined direct and indirect adaptive control for a class of nonlinear systems. *IET Control Theory & Applications*, 3(1):151–159, 2009.

[22] Parag M Patre, William MacKunis, Marcus Johnson, and Warren E Dixon. Composite adaptive control for euler–lagrange systems with additive disturbances. *Automatica*, 46(1):140–147, 2010.

[23] MK Ciliz. Adaptive backstepping control using combined direct and indirect adaptation. *Circuits, Systems & Signal Processing*, 26(6):911–939, 2007.

[24] Parag M Patre, Shubhendu Bhasin, Zachary D Wilcox, and Warren E Dixon. Composite adaptation for neural network-based controllers. *IEEE Transactions on Automatic Control*, 55(4):944–950, 2010.

[25] Yongping Pan, Yiqi Liu, and Haoyong Yu. Online data-driven composite adaptive backstepping control with exact differentiators. *International Journal of Adaptive Control and Signal Processing*, 30(5):779–789, 2016.

[26] Yongping Pan and Haoyong Yu. Composite learning from adaptive dynamic surface control. *IEEE Transactions on Automatic Control*, 61(9):2603–2609, 2015.

[27] Byoung-Ju Jeon, Hyo-Sang Shin, and Antonios Tsourdos. Composite adaptive backstepping control considering computational complexity and relaxation of persistent excitation. In *21st IFAC World Congress*. IEEE, 2020.

[28] Byoung-Ju Jeon, Hyo-Sang Shin, and Antonios Tsourdos. Composite adaptive control with new information matrix for parameter convergence without persistent excitation. *Automatica, Submitted*, 2020.

[29] Gang Tao. *Adaptive control design and analysis*, volume 37. John Wiley & Sons, 2003.

[30] Petar V Kokotovic. The joy of feedback: nonlinear and adaptive. *IEEE Control Systems Magazine*, 12(3):7–17, 1992.

Chapter 8

General Discussion : Comparative Study on Incremental and Composite Adaptive Backstepping Control

In Chapter 8, a comparative study between the incremental backstepping control (IBKS) in Chapter 2-4 and the new composite adaptive backstepping control (new C-ABKS) in Chapter 7 is performed through numerical simulations under various defects. Note that simulations are conducted with short period mode dynamics and 6-degree of freedom (6-DoF) dynamics of aircraft, respectively. In Section 8.1, two algorithms are compared under the short period mode dynamics where the analysis on IBKS in Chapter 2-4 holds. In Section 8.2, the dynamics is extended to the 6-DoF aircraft dynamics in order to check whether the characteristics observed in Section 8.1 are maintained under this extension.

8.1 Comparative Study on IBKS and new C-ABKS under Short Period Mode Dynamics

8.1.1 Simulation Setup

8.1.1.1 Aircraft Short Period Mode Dynamics

Short period mode dynamics (8.1) which has significant importance on flight control system design [1] is considered for this comparative study. Z_α^* is assumed to be known since it can be obtained with relatively high accuracy in general. The model parameters for the inner-loop dynamics, M_α^* and M_q^*, are set to be uncertain.

$$\dot{\boldsymbol{x}} = \boldsymbol{f}(\boldsymbol{x}) + \boldsymbol{g}(\boldsymbol{x})\boldsymbol{u} + \boldsymbol{\Delta}(\boldsymbol{x})$$

where

$$\begin{aligned}
&\boldsymbol{x} = [x_1, x_2]^T = [\alpha, q]^T \\
&\boldsymbol{x}_1' = [x_1]\,,\ \boldsymbol{x}_2' = [x_1, x_2]^T \\
&\boldsymbol{f}(\boldsymbol{x}) = \left[f_1(\boldsymbol{x}_1'), f_2(\boldsymbol{x}_2')\right]^T = [Z_\alpha^*\alpha, 0]^T \\
&\boldsymbol{g}(\boldsymbol{x}) = \mathrm{diag}\left\{\left[g_1(\boldsymbol{x}_1'), g_2(\boldsymbol{x}_2')\right]\right\} = \mathrm{diag}\left\{[1, M_\delta^*]\right\} \\
&\boldsymbol{u} = [u_1, u_2]^T = [q, \delta]^T \\
&\boldsymbol{\Delta}(\boldsymbol{x}) = \left[0, \Delta_2(\boldsymbol{x}_2')\right]^T
\end{aligned} \tag{8.1}$$

$\Delta_2(\boldsymbol{x}_2')$ in (8.1) is defined as (8.2).

$$\begin{aligned}
&\Delta_2(\boldsymbol{x}_2') = \boldsymbol{\theta}_2^T \boldsymbol{\phi}_2'(\boldsymbol{x}_2') \\
&\boldsymbol{\theta}_2 = \left[M_\alpha^*, M_q^*\right]^T \qquad \boldsymbol{\phi}_2'(\boldsymbol{x}_2') = [\alpha, q]^T
\end{aligned} \tag{8.2}$$

8.1.1.2 Flight Controllers with IBKS and new C-ABKS

In Section 8.1.1.2, flight control algorithms for the comparative study, IBKS and new C-ABKS, are briefly addressed with classical backstepping control (BKS) as a reference. Note that both algorithms are utilized for inner-loop control, and the outer-loop controller is designed with classical BKS since accurate Z_α^* is assumed to be available.

Backstepping Controller A flight control law with the classical BKS is given as (8.3) for the dynamics in (8.1). Note that detailed derivation of (8.3) is suggested in Chapter 2.

$$\begin{aligned} q_c &= -C_1 z_1 - Z_\alpha^* \alpha + \dot{\alpha}_c \\ \delta &= \frac{1}{\hat{M}_\delta^*} \left(-C_2 z_2 - z_1 - \hat{M}_\alpha^* \alpha - \hat{M}_q^* q + \dot{q}_c \right) \end{aligned} \tag{8.3}$$

Incremental Backstepping Controller The IBKS is applied to design the inner-loop controller for the dynamics (8.1), resulting in (8.4). Note that detailed derivation of (8.4) can be found in Chapter 2, 3 and 4.

$$\begin{aligned} q_c &= -C_1 z_1 - Z_\alpha^* \alpha + \dot{\alpha}_c \\ \delta &= \delta_0 + \Delta\delta \\ &= \frac{1}{\hat{M}_\delta^*} \left(-C_2 z_2 - z_1 - \dot{q}_0 + \dot{q}_c \right) + \delta_0 \end{aligned} \tag{8.4}$$

New Composite Adaptive Backstepping Controller A flight control algorithm is designed by applying new C-ABKS detailed in Chapter 7 to (8.1).

$$\begin{aligned} q_c &= -C_1 z_1 - Z_\alpha^* \alpha + \dot{\alpha}_c \\ \delta &= \frac{1}{\hat{M}_\delta^*} \left(-C_2 z_2 - z_1 - \hat{\boldsymbol{\theta}}_2^T \boldsymbol{\phi}_2(\boldsymbol{x}_2') + \dot{q}_c \right) \end{aligned} \tag{8.5}$$

The estimate on the uncertain parameter vector $\hat{\boldsymbol{\theta}}_2$ in (8.1) is obtained from the logarithmic regression-based composite adaptation law with new information matrix in Chapter 7.

8.1.1.3 Simulation Case Definitions and Parameter Settings

Simulation case definitions and parameter settings for the comparative study with short period mode dynamics are addressed in Section 8.1.1.3. The aerodynamic model of F-16 in [2] at the altitude of 4000ft and the velocity of 846.27ft/s is utilized for the simulations. The initial conditions on the state variables are $\alpha_0 = -0.6384^\circ$ and $q_0 = 0^\circ$. The control command on α is $\alpha_c = 1.5^\circ$. The common design parameters from the backstepping control structure, C_1 and C_2, are set to be $C_1 = 6$ and $C_2 = 3$. A set of design parameters for the logarithmic regression-based composite

adaptation law with new information matrix, which provides the best parameter estimation performance, is selected from a number of simulations. The selected design parameters are $\mathbf{\Gamma}_2 = \text{diag}\,[1000,\ 1000]$, $\lambda_2 = 1$, $p_2 = 1.2$, $q_2 = 1.5$, $k_{21} = 0.10$, $k_{22} = 0.15$.

Model uncertainties and measurement delays are considered in this comparative study. First, simulations are performed under the model uncertainties on the system matrix and the control effectiveness matrix, respectively. Note that the model parameters in the system matrix are replaced with the additional measurements in IBKS and with their estimates in new C-ABKS, while the control effectiveness information is still required for both algorithms. For the case with the model uncertainty on the system matrix, $\Delta_{M_\alpha^*}$ and $\Delta_{M_q^*}$ are set to be 0.5. The results for the case with the model uncertainty on the control effectiveness matrix are obtained under $\Delta_{M_\delta^*} = -0.2$ and $\Delta_{M_\delta^*} = 0.5$, respectively.

Second, simulations are conducted under the measurement delays with or without the model uncertainty on the control effectiveness information. Note that delays on state derivative and control surface deflection angle measurement are mainly considered for IBKS, and simulations with new C-ABKS mainly deal with delay on control surface deflection angle measurement. This is because the above two measurements are additionally utilized for IBKS comparing to BKS for its reduced model dependency, and the delay is considered in new C-ABKS for fair comparison. The defined simulation cases are listed in Table 8.1.

Table 8.1: Simulation Cases under τ_δ, $\tau_{\dot{q}}$ and $\Delta_{M_\delta^*}$

Case	$\Delta_{M_\delta^*}$	τ_δ	$\tau_{\dot{q}}$
1	-0.2	$0.01s$	$0s$, $0.001s$, $0.01s$, $0.011s$, $0.02s$
2	0	$0.01s$	$0s$, $0.001s$, $0.01s$, $0.011s$, $0.02s$
3	0.5	$0.01s$	$0s$, $0.01s$, $0.02s$, $0.021s$, $0.03s$

8.1.2 Simulation Results

8.1.2.1 Model Uncertainty

Model Uncertainty on System Matrix The simulation results with the model uncertainties on the system matrix are given in Fig. 8.1. It is shown in Fig. 8.1

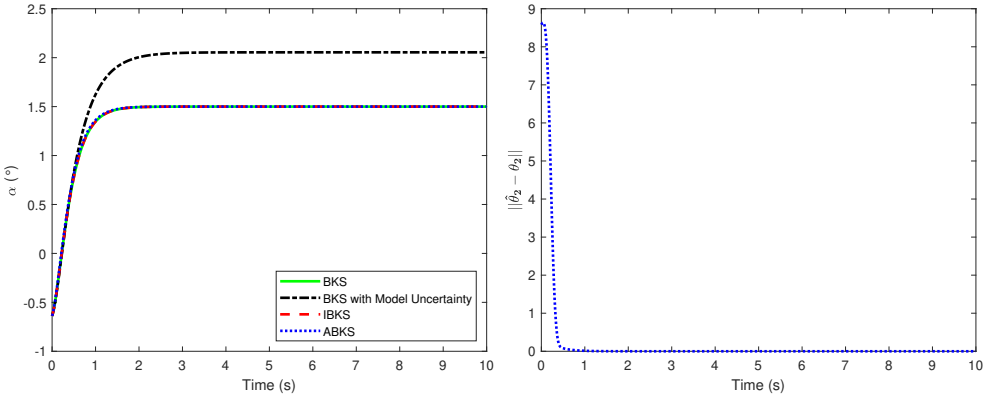

(a) Angle-of-Attack (b) Parameter Estimation Error with C-ABKS

Figure 8.1: System Response with $\Delta_{M_\alpha^*}$ and $\Delta_{M_q^*}$

that both IBKS and new C-ABKS have advantages from their reduced model dependency comparing to BKS as follows. BKS with the model uncertainties on M_α^* and M_q^* shows a steady-state error on α response. IBKS provides the same response with the nominal BKS. New C-ABKS takes some time for model parameter estimation, but this also shows the same performance with the nominal BKS after perfect adaptation.

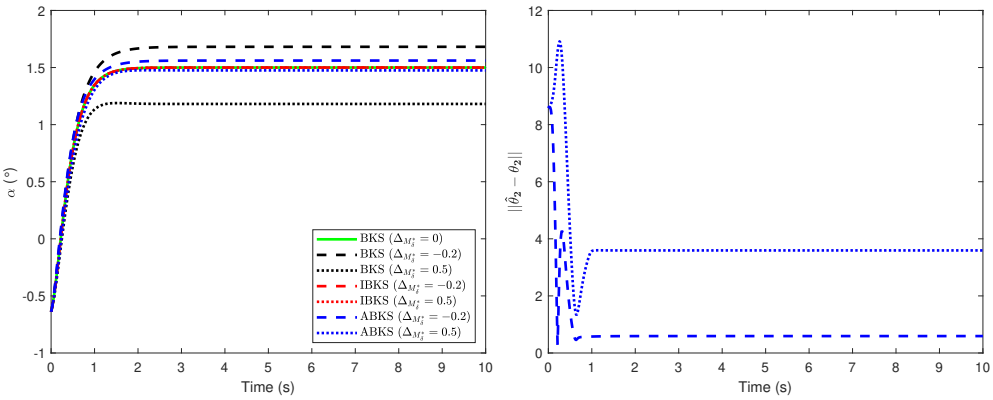

(a) Angle-of-Attack (b) Parameter Estimation Error with C-ABKS

Figure 8.2: System Response with $\Delta_{M_\delta^*}$

Model Uncertainty on Control Effectiveness Fig. 8.2 provides the simulation results with the uncertainty on the control effectiveness information. The closed-loop system with BKS shows large steady-state errors with the uncertainty in control effectiveness information. The IBKS shows the same response with the nominal BKS even with the uncertainty in control effectiveness information if the control input is calculated, transmitted, and reflected fast enough to the actual control surface. The

new C-ABKS with uncertainty in control effectiveness information shows parameter estimation errors, resulting in steady-state error in α response. This can be explained by (8.19) in Appendix A with $\tau_\delta = 0$; $\hat{\boldsymbol{\theta}}_2$ converges to $\boldsymbol{\theta}_2'$ which becomes different with $\boldsymbol{\theta}_2$ because of non-zero $\Delta_{M_\delta^*}$.

8.1.2.2 Delays on Additional Measurements and Model Uncertainty on Control Effectiveness

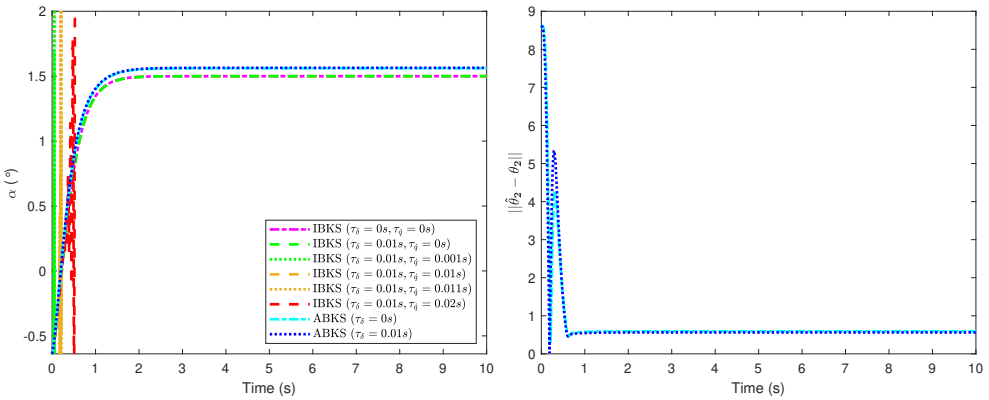

(a) Angle-of-Attack (b) Parameter Estimation Error with C-ABKS

Figure 8.3: System Response with τ_δ and $\tau_{\dot{q}}$ under $\Delta_{M_\delta^*} = -0.2$

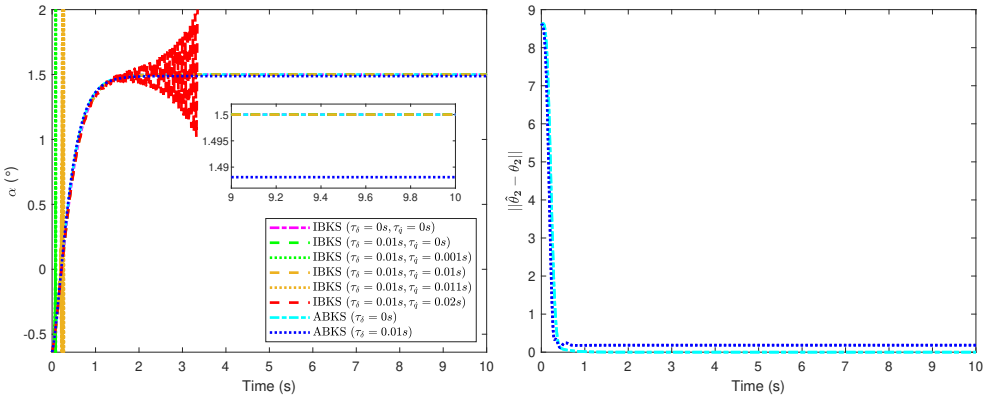

(a) Angle-of-Attack (b) Parameter Estimation Error with C-ABKS

Figure 8.4: System Response with τ_δ and $\tau_{\dot{q}}$ ($\Delta_{M_\delta^*} = 0$)

Fig. 8.4 shows the simulation results for case 2 with delays on the additional measurements and without model uncertainties. It is addressed in Fig. 8.4 that the closed-loop system with the IBKS is stable if there is no delay on the state derivative measurement or the non-zero delay on the state derivative measurement is

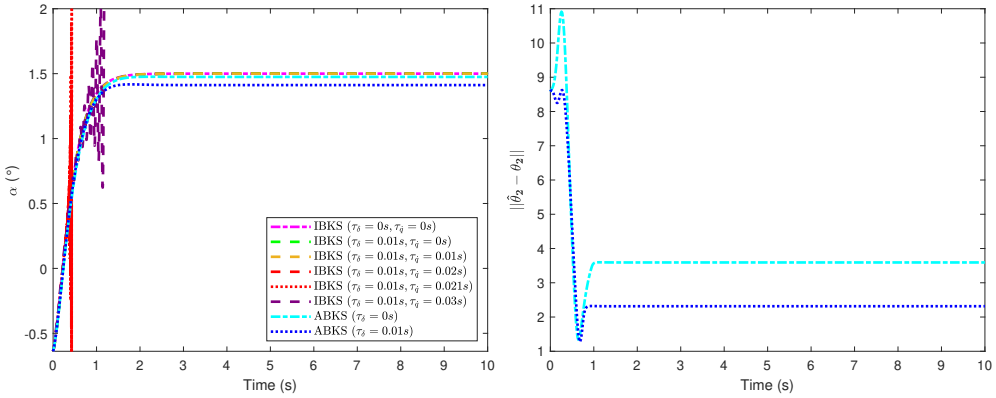

(a) Angle-of-Attack

(b) Parameter Estimation Error with C-ABKS

Figure 8.5: System Response with τ_δ and $\tau_{\dot{q}}$ under $\Delta_{M_\delta^*} = 0.5$

identical to the delay on the control surface deflection angle measurement. Even with very small deviation from this stability condition, the system with the IBKS becomes unstable as shown in Fig. 8.4. With the new C-ABKS, the closed-loop system shows stable response under delay on the additional measurement. However, as shown in Fig. 8.4, the delay induces parameter estimation error which results in tracking error.

The simulation results for the cases 1 and 3 considering both measurement delay and model uncertainty are provided in Fig. 8.3 and 8.5. Fig. 8.3 and 8.5 address that the stability condition for the IBKS about delays on the additional measurements is affected by the model uncertainty on control effectiveness information, resulting in different k_{max} for different model uncertainties. In this comparative study, $k_{max} = 1$ for $\Delta_{M_\delta^*} = -0.2$ and $\Delta_{M_\delta^*} = 0$, and $k_{max} = 2$ for $\Delta_{M_\delta^*} = 0.5$. It is also shown in Fig. 8.3 and 8.5 that the closed-loop system with the IBKS becomes unstable under the delays on the additional measurements which do not satisfy this stability condition with the model uncertainty by small difference. Fig. 8.3 and 8.5 indicate that the new C-ABKS under the delays on additional measurement and the model uncertainty on control effectiveness has parameter estimation errors which makes α response have a steady-state error.

Note that the detailed theoretical backgrounds for the above observations on the IBKS are provided in Chapter 4. The parameter estimation error of the new C-ABKS under delays on additional measurement can be explained with (8.19) in Appendix A which implies that non-zero τ_δ makes $\boldsymbol{\theta}_2'$ become different with $\boldsymbol{\theta}_2$ and the new C-ABKS drives $\hat{\boldsymbol{\theta}}_2$ to $\boldsymbol{\theta}_2'$.

8.2 Comparative Study on IBKS and new C-ABKS under 6-DoF Dynamics

8.2.1 Simulation Setup

8.2.1.1 Aircraft 6-DoF Dynamics

The 6-DoF dynamics with the model uncertainty $\boldsymbol{\Delta}_2$ is derived as (8.6) for comparative study in Section 8.2.

$$\frac{d}{dt}\begin{bmatrix} V \\ \alpha \\ \beta \end{bmatrix} = \boldsymbol{f}_1' + \boldsymbol{G}_1 \begin{bmatrix} T \\ q \\ r \end{bmatrix}$$

$$\frac{d}{dt}\begin{bmatrix} p \\ q \\ r \end{bmatrix} = \boldsymbol{f}_2' + \boldsymbol{G}_2 \begin{bmatrix} \delta_e \\ \delta_a \\ \delta r \end{bmatrix} + \boldsymbol{\Delta}_2$$

where

$$\boldsymbol{f}_1' = \boldsymbol{f}_1 + \boldsymbol{f}_g$$

$$\boldsymbol{f}_1 = \begin{bmatrix} \frac{1}{m}\left(X_T \cos\alpha\cos\beta + Y_T \sin\beta + Z_T \sin\alpha\cos\beta\right) \\ -p\cos\alpha\tan\beta + \frac{1}{mV\cos\beta}\left(Z_T\cos\alpha - X_T\sin\alpha\right) \\ p\sin\alpha + \frac{1}{mV}\left(-X_T\cos\alpha\sin\beta + Y_T\cos\beta - Z_T\sin\alpha\sin\beta\right) \end{bmatrix}$$

$$\boldsymbol{f}_g = \begin{bmatrix} g\left(-\sin\theta\cos\alpha\cos\beta + \cos\theta\sin\phi\sin\beta + \cos\theta\cos\phi\sin\alpha\cos\beta\right) \\ \frac{g}{V\cos\beta}\left(\cos\theta\cos\phi\cos\alpha + \sin\theta\sin\alpha\right) \\ \frac{g}{V}\left(\cos\theta\sin\phi\cos\beta + \sin\theta\cos\alpha\sin\beta - \cos\theta\cos\phi\cos\alpha\sin\beta\right) \end{bmatrix}$$

$$\boldsymbol{f}_2' = \begin{bmatrix} \left(c_2 p + c_1 r\right) q - c_4 b Y_T \frac{\bar{c}}{b} \\ c_5 pr + c_6\left(r^2 - p^2\right) + c_7 \bar{c} Z_T \left(x_{CG_R} - x_{CG}\right)\frac{\bar{c}}{b} \\ \left(c_8 p - c_2 r\right) q - c_9 b Y_T \frac{\bar{c}}{b} \end{bmatrix}$$

$$\boldsymbol{G}_1 = \begin{bmatrix} \frac{\cos\alpha\cos\beta}{m} & 0 & 0 \\ -\frac{\sin\alpha}{mV\cos\beta} & 1 & -\sin\alpha\tan\beta \\ -\frac{\cos\alpha\sin\beta}{mV} & 0 & -\cos\alpha \end{bmatrix} \quad \boldsymbol{G}_2 = \begin{bmatrix} 0 & c_3 L_{\delta_a} + c_4 N_{\delta_a} & c_3 L_{\delta_r} + c_4 N_{\delta_r} \\ c_7 M_{\delta_e} & 0 & 0 \\ 0 & c_4 L_{\delta_a} + c_9 N_{\delta_a} & c_4 L_{\delta_r} + c_9 N_{\delta_r} \end{bmatrix} \tag{8.6}$$

V, α and β represent velocity, angle-of-attack and sideslip angle. p,q, and r denote body angular rates and ϕ, θ, and ψ stand for Euler angles. T, δ_e, δ_a, and δr indicate thrust and elevator, aileron and rudder deflection angles, respectively. X_T, Y_T and Z_T are aerodynamic forces in body x, y, and z-axis which are assumed to be known [3] [4]. L_{δ_a}, L_{δ_r}, M_{δ_e}, N_{δ_a} and N_{δ_r} represent control effectiveness of the control surfaces to the aerodynamic moments. $c_{(.)}$ denote parameters related to moment of inertia as described in [5]. m is mass and g is the gravitational acceleration. x_{CG_R} is the x-coordinate of the reference center of gravity position and x_{CG} denotes the x-coordinate of the center of gravity position. $\bar{c}$ and b represent reference chord length and wing span, respectively.

$\mathbf{\Delta}_2$ in (8.6) is defined as (8.7).

$$\mathbf{\Delta}_2 = \begin{bmatrix} \boldsymbol{\theta}_p^T \boldsymbol{\phi'}_p & \boldsymbol{\theta}_q^T \boldsymbol{\phi'}_q & \boldsymbol{\theta}_r^T \boldsymbol{\phi'}_r \end{bmatrix}^T$$

where

$$\begin{aligned}
\boldsymbol{\theta}_p &= Sb \begin{bmatrix} \left(c_3 C_{l_0\beta} + c_4 C_{n_0\beta}\right) \\ \left(c_3 C_{l_{0\alpha\beta}} + c_4 C_{n_{0\alpha\beta}}\right) \\ \left(c_3 C_{l_{0\beta^2}} + c_4 C_{n_{0\beta^2}}\right) \\ \left(c_3 C_{l_{p0}} + c_4 C_{n_{p0}}\right) \\ \left(c_3 C_{l_{r0}} + c_4 C_{n_{r0}}\right) \end{bmatrix}^T \qquad \boldsymbol{\phi'}_p = \bar{q} \begin{bmatrix} \beta & \alpha\beta & \beta^2 & \frac{bp}{2V} & \frac{br}{2V} \end{bmatrix}^T \\
\boldsymbol{\theta}_q &= S\bar{c}c_7 \begin{bmatrix} C_{m_{0\,0}} \\ C_{m_{0\,\alpha}} \\ C_{m_{q\,0}} \\ C_{m_{q\,\alpha}} \end{bmatrix}^T \qquad \boldsymbol{\phi'}_q = \bar{q} \begin{bmatrix} 1 & \alpha & \frac{\bar{c}}{2V} q & \frac{\bar{c}}{2V} q\alpha \end{bmatrix}^T \\
\boldsymbol{\theta}_r &= Sb \begin{bmatrix} \left(c_4 C_{l_0\beta} + c_9 C_{n_0\beta}\right) \\ \left(c_4 C_{l_{0\alpha\beta}} + c_9 C_{n_{0\alpha\beta}}\right) \\ \left(c_4 C_{l_{0\beta^2}} + c_9 C_{n_{0\beta^2}}\right) \\ \left(c_4 C_{l_{p0}} + c_9 C_{n_{p0}}\right) \\ \left(c_4 C_{l_{r0}} + c_9 C_{n_{r0}}\right) \end{bmatrix}^T \qquad \boldsymbol{\phi'}_r = \bar{q} \begin{bmatrix} \beta & \alpha\beta & \beta^2 & \frac{bp}{2V} & \frac{br}{2V} \end{bmatrix}^T
\end{aligned} \tag{8.7}$$

S denotes wing area and $\bar{q}$ indicates dynamic pressure. $C_{(-)}$ are parameters to model

the aerodynamic coefficients in (8.23). The detailed derivations of (8.6) and (8.7) are provided in Appendix B.

The kinematics equation of the altitude h is given as (8.8).

$$\frac{d}{dt}h = V\left(\sin\theta\cos\beta\cos\alpha - \sin\phi\cos\theta\sin\beta + \cos\phi\cos\theta\cos\beta\sin\alpha\right) \tag{8.8}$$

The kinematics in (8.8) can be rewritten with small angle approximation on α as (8.9).

$$\begin{aligned} &\frac{d}{dt}h = f_h + g_h\alpha \\ &\text{where} \\ &f_h = V\left(\sin\theta\cos\beta\cos\alpha - \sin\phi\cos\theta\sin\beta\right) \\ &g_h = V\left(\cos\phi\cos\theta\cos\beta\right) \end{aligned} \tag{8.9}$$

8.2.1.2 Flight Controllers with IBKS and new C-ABKS

The flight control algorithms are designed in Section 8.2.1.2 for the comparative study with 6-DoF dynamics. The overall structure of the flight control algorithms is provided in Fig. 8.6.

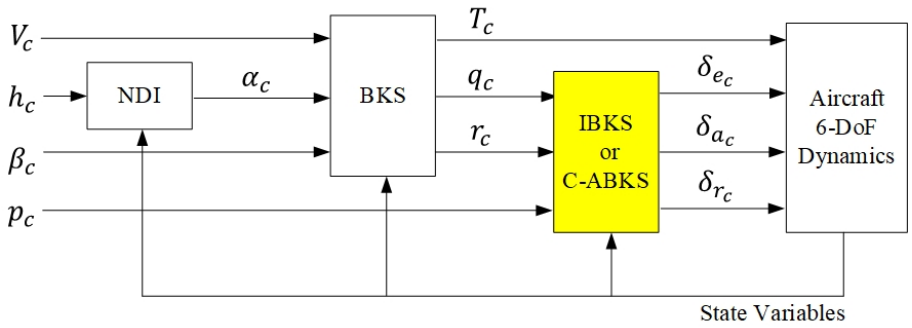

Figure 8.6: Block Diagram of Control System

The angle-of-attack command α_c to track h_c is generated as (8.10) with nonlinear dynamic inversion (NDI).

$$\alpha_c = \frac{1}{g_h}\left(-f_h - k_{hp}\left(h - h_c\right) - k_{hi}\int_0^t \left(h - h_c\right)d\tau\right) \tag{8.10}$$

where k_{hp} and k_{hi} are constant design parameters. Note that the altitude tracking error, $(h - h_c)$, follows the desired error dynamics in (8.11) when h_c is constant.

$$\frac{d}{dt}(h - h_c) = -k_{hp}(h - h_c) - k_{hi}\int_0^t (h - h_c)\, d\tau \tag{8.11}$$

The commands on thrust, pitch rate and yaw rates, T_c, q_c and r_c, are calculated as (8.12) from classical BKS to track V_c, α_c and β_c.

$$\begin{bmatrix} T_c \\ q_c \\ r_c \end{bmatrix} = \boldsymbol{G}_1^{-1} \left(-\mathbf{C}_1 \boldsymbol{z}_1 - \boldsymbol{f}_1' + \begin{bmatrix} \dot{V}_c \\ \dot{\alpha}_c \\ \dot{\beta}_c \end{bmatrix} \right) \tag{8.12}$$

IBKS and new C-ABKS are applied respectively for the design of the fin deflection angle commands, δ_{ec}, δ_{ac} and δ_{rc}, to track the body angular rate commands, p_c, q_c and r_c. The fin deflection angle commands in (8.13) are derived by utilizing the design procedures of IBKS in Chapter 2-4.

$$\begin{bmatrix} \delta_{ec} \\ \delta_{ac} \\ \delta_{rc} \end{bmatrix} = \boldsymbol{G}_2^{-1} \left(-\mathbf{C}_2 \boldsymbol{z}_2 - \boldsymbol{z}_1 - \begin{bmatrix} p_0 \\ q_0 \\ r_0 \end{bmatrix} + \begin{bmatrix} \dot{p}_c \\ \dot{q}_c \\ \dot{r}_c \end{bmatrix} \right) + \begin{bmatrix} \delta_{e0} \\ \delta_{a0} \\ \delta_{r0} \end{bmatrix} \tag{8.13}$$

The new C-ABKS in Chapter 7 is applied to obtain the fin deflection angle commands of (8.14).

$$\begin{bmatrix} \delta_{ec} \\ \delta_{ac} \\ \delta_{rc} \end{bmatrix} = \boldsymbol{G}_2^{-1} \left(-\mathbf{C}_2 \boldsymbol{z}_2 - \boldsymbol{z}_1 - \boldsymbol{f}_2' + \begin{bmatrix} \dot{p}_c \\ \dot{q}_c \\ \dot{r}_c \end{bmatrix} - \begin{bmatrix} \hat{\boldsymbol{\theta}}_p^T \boldsymbol{\phi}'_p \\ \hat{\boldsymbol{\theta}}_q^T \boldsymbol{\phi}'_q \\ \hat{\boldsymbol{\theta}}_r^T \boldsymbol{\phi}'_r \end{bmatrix} \right) \tag{8.14}$$

The estimates on the uncertain parameter vectors in (8.6), $\hat{\boldsymbol{\theta}}_p^T$, $\hat{\boldsymbol{\theta}}_q^T$ and $\hat{\boldsymbol{\theta}}_r^T$, utilized in (8.14) are obtained with the logarithmic regression-based composite adaptation law with the new information matrix proposed in Chapter 7.

8.2.1.3 Simulation Case Definitions and Parameter Settings

The parameter settings and simulation case definitions for the comparative study with 6-DoF dynamics are provided in Section 8.2.1.3. Note that the aerodynamic model of F-16 in [2] is utilized for the simulations. The initial conditions of the state variables are $[h\ V\ \alpha\ \beta\ p\ q\ r]_0^T = \left[4000\text{ft}\ 846.27\text{ft}/s\ -0.6384^\circ\ 0^\circ\ 0^\circ/s\ 0^\circ/s\ 0^\circ/s\right]^T$. The initial values of the Euler angles are set to be $[\phi\ \theta\ \psi]_0^T = [0^\circ\ -0.6384^\circ\ 0^\circ]^T$. The control commands are defined as $h_c = 4000\text{ft}$, $V_c = 855\text{ft}/s$, $\beta_c = 1^\circ$ and $p_c = 0^\circ/s$ for altitude hold, velocity increase, sideslip angle change and roll rate stabilization. The design parameters of the altitude controller are selected as $k_{hp} = 3$ and $k_{hi} = 1$. The common design parameters for the backstepping control structure are defined as $\mathbf{C}_1 = \text{diag}[20, 20, 20]$ and $\mathbf{C}_2 = \text{diag}[10, 10, 10]$. The design parameters for the logarithmic regression-based composite adaptation law with new information matrix are selected to show the best parameter estimation performance from a number of simulations. The parameter set for the new C-ABKS are $\mathbf{\Gamma}_p = \mathbf{\Gamma}_r = \text{diag}[0.1, 0.1, 0.1, 0.1, 0.1]$, $\mathbf{\Gamma}_q = \text{diag}[0.001, 0.001, 0.001, 0.001, 0.001]$, $\lambda_p = \lambda_q = \lambda_r = 1$, $p_p = p_q = p_r = 1.2$, $q_p = q_q = q_r = 1.5$, $k_1 = 0.1$, $k_2 = 0.15$, $k_3 = 0.2$, $k_4 = 0.25$, $k_5 = 0.3$.

The simulations with 6-DoF dynamics are performed to investigate whether the closed-loop characteristics observed from the comparative study with short period mode dynamics are retained under the extension to the 6-DoF dynamics. In the similar manner with the short period mode dynamics, the effects of model uncertainties and measurement delays on the closed-loop system are systematically examined with the 6-DoF dynamics. First, simulations are conducted with the model uncertainties on control effectiveness which is still required for both algorithms despite their reduced model dependency. The model uncertainties on control effectiveness information are set to be $\Delta_{(\star)} = -0.2$ and $\Delta_{(\star)} = 0.5$ for all $(\star) = L_{\delta_a},\ L_{\delta_r},\ M_{\delta_e},\ N_{\delta_a},\ N_{\delta_r}$. Second, simulations are performed under the measurement delays with or without model uncertainties on control effectiveness matrix. Due to the same reason explained in Section 8.1, delays on state derivative and control surface deflection angle measurements are mainly considered for IBKS, and simulations with new C-ABKS mainly deal with delays on control surface deflection angle measurements. Simulation cases are defined with model uncertainties and measurement delays as Table. 8.2. Note that $(\star) = L_{\delta_a},\ L_{\delta_r},\ M_{\delta_e},\ N_{\delta_a},\ N_{\delta_r}$, $(\cdot) = \delta_e,\ \delta_a,\ \delta_r$ and $(*) = \dot{p},\ \dot{q},\ \dot{r}$.

Table 8.2: Simulation Cases under $\tau_{(\cdot)}$, $\tau_{(*)}$ and $\Delta_{(\star)}$

Case	$\Delta_{(\star)}$	$\tau_{(\cdot)}$	$\tau_{(*)}$
a	-0.2	$0.01s$	$0s$, $0.001s$, $0.01s$, $0.011s$, $0.02s$
b	0	$0.01s$	$0s$, $0.001s$, $0.01s$, $0.011s$, $0.02s$
c	0.5	$0.01s$	$0s$, $0.01s$, $0.02s$, $0.021s$, $0.03s$

8.2.2 Simulation Results

8.2.2.1 Model Uncertainty on Control Effectiveness

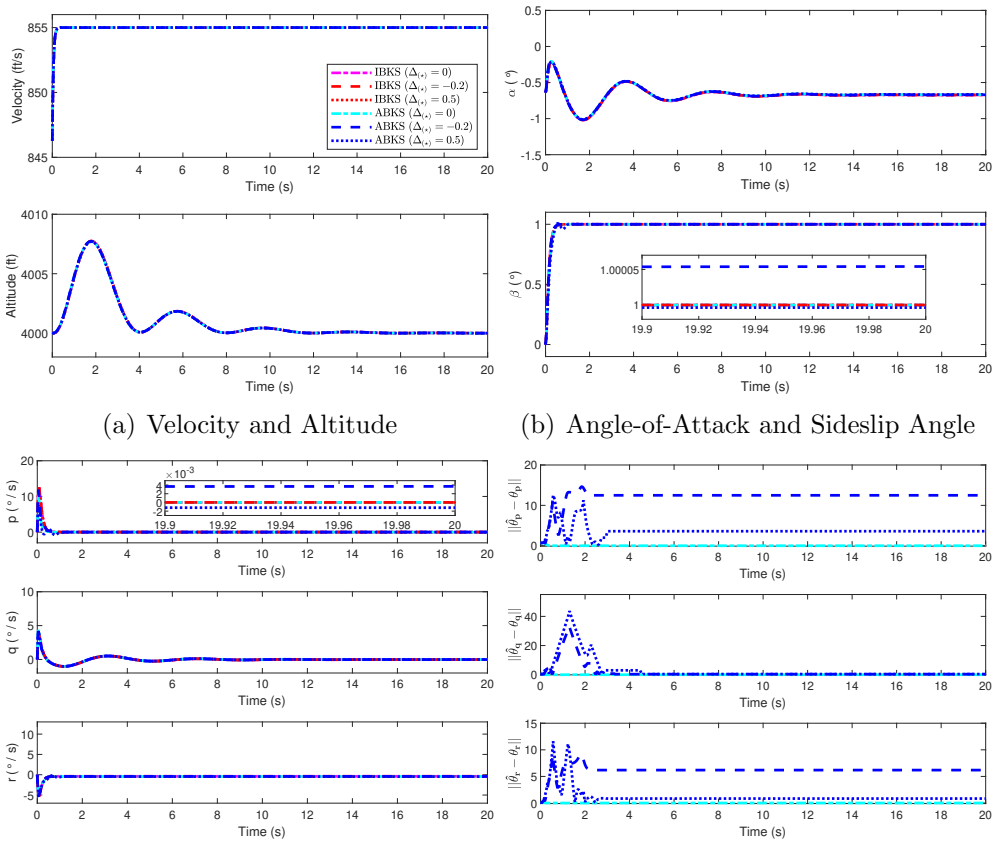

(a) Velocity and Altitude

(b) Angle-of-Attack and Sideslip Angle

(c) Body Angular Rates

(d) Parameter Estimation Error with C-ABKS

Figure 8.7: System Response with $\Delta_{(\star)}$

The 6-DoF simulation results with the IBKS and the new C-ABKS under model uncertainties on control effectiveness information are addressed in Fig. 8.7. It is observed in Fig. 8.7 that the closed-loop system with IBKS shows the same response regardless of the uncertainties on the control effectiveness if the control input

commands are generated, transmitted and reflected to the actual control surface actuators fast enough. The closed-loop system with the new C-ABKS is shown to be stable in Fig. 8.7. Note that the closed-loop system with the new C-ABKS appears to be stable for $-0.4 \leq \Delta_{(\star)} \leq 1.5$ from a number of simulations with different $\Delta_{(\star)}$ conducted to identify the effects of $\Delta_{(\star)}$ on the system. However, the system with the new C-ABKS have parameter estimation errors as addressed in Fig. 8.7(d) when the uncertainties on control effectiveness exist, which results in the steady-state errors on state outputs as shown in Fig. 8.7(b) and 8.7(c). Those observations on the closed-loop systems with the IBKS and the new C-ABKS coincide with the characteristics identified from the analysis and comparative studies with the short period mode dynamics.

8.2.2.2 Delays on Additional Measurements and Model Uncertainty on Control Effectiveness

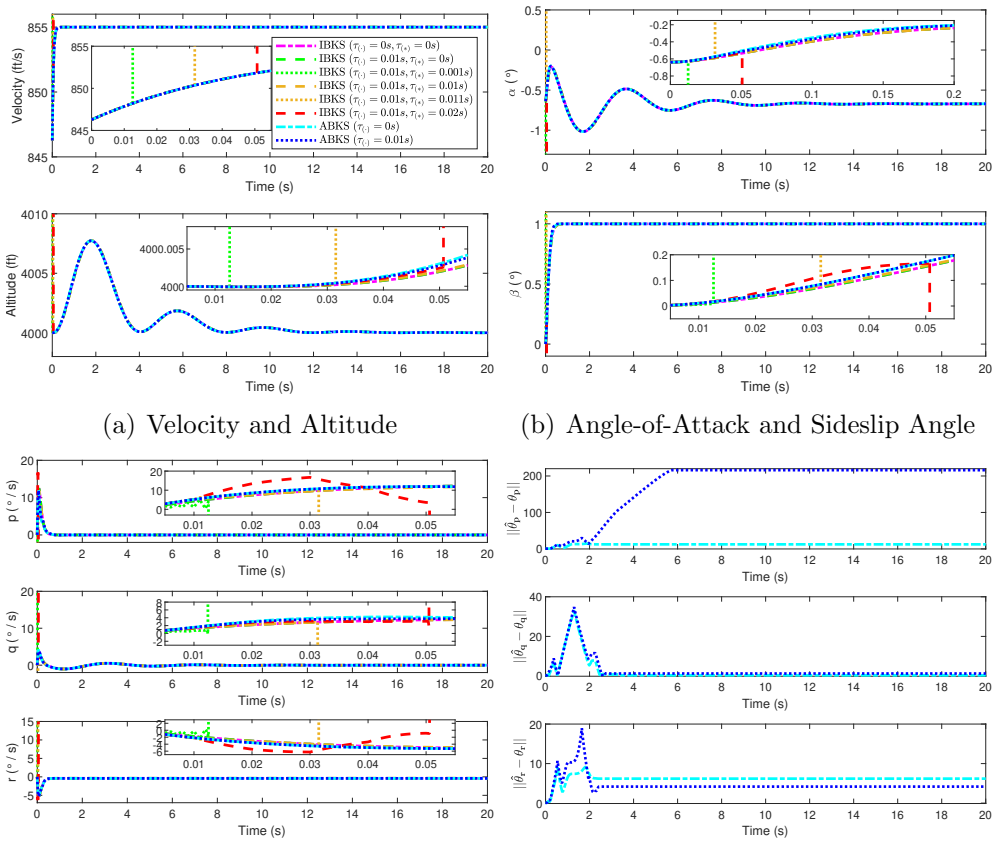

(a) Velocity and Altitude

(b) Angle-of-Attack and Sideslip Angle

(c) Body Angular Rates

(d) Parameter Estimation Error with C-ABKS

Figure 8.8: System Response with $\tau_{(\cdot)}$ and $\tau_{(*)}$ under $\Delta_{(\star)} = -0.2$

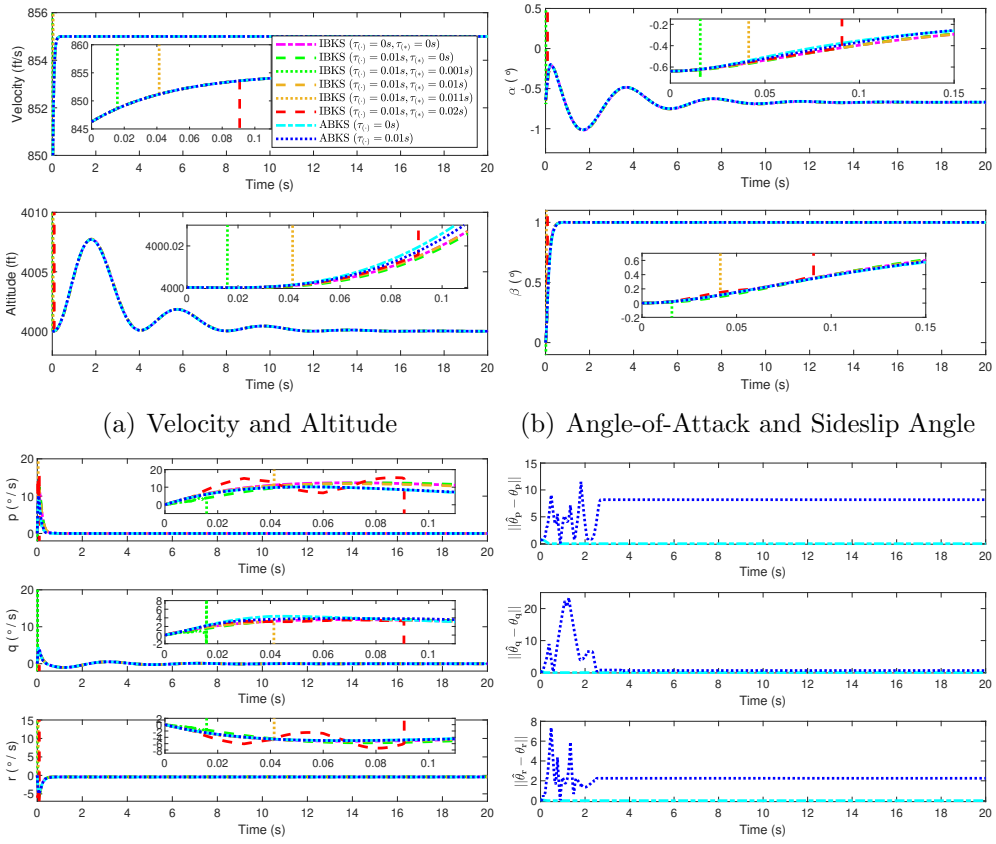

(a) Velocity and Altitude

(b) Angle-of-Attack and Sideslip Angle

(c) Body Angular Rates

(d) Parameter Estimation Error with C-ABKS

Figure 8.9: System Response with $\tau_{(\cdot)}$ and $\tau_{(*)}$ under $\Delta_{(\star)} = 0$

Fig. 8.9 addresses the simulation results for case b with delays on additional measurements and without model uncertainties. The closed-loop system with the IBKS is shown to be stable in Fig. 8.9 when the delays on state derivative measurements do not exist or the delays on state derivative measurements and control surface deflection angle measurements are the same. The closed-loop system with IBKS becomes unstable even with small deviations from this stability condition on measurement delays. The closed-loop system with the new C-ABKS is observed to be stable in Fig. 8.9. Note that the closed-loop system with the new C-ABKS appears to be stable for $\tau_{(\cdot)} \leq 0.06s$ from a number of simulations with different $\tau_{(\cdot)}$ conducted to identify the effects of $\tau_{(\cdot)}$ on the system. However, parameter estimation errors of the system with the new C-ABKS are induced by the measurement delays as shown in Fig. 8.9(d), which results in the the steady-state errors on state outputs as shown in Fig. 8.9(b) and 8.9(c). Note that properties of the IBKS and the new C-ABKS with delays under the 6-DoF dynamics are the same with the results under the short period mode dynamics.

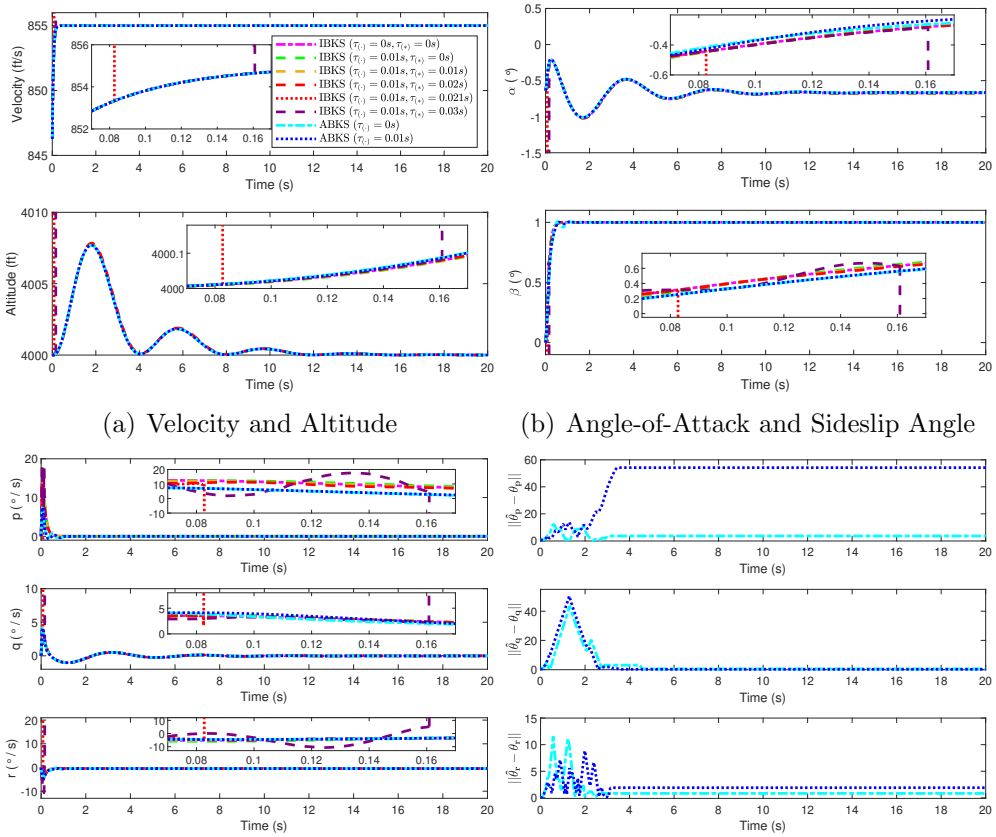

(a) Velocity and Altitude

(b) Angle-of-Attack and Sideslip Angle

(c) Body Angular Rates

(d) Parameter Estimation Error with C-ABKS

Figure 8.10: System Response with $\tau_{(\cdot)}$ and $\tau_{(*)}$ under $\Delta_{(\star)} = 0.5$

The simulation results for case a and c considering both measurement delays and model uncertainties are provided in Fig. 8.8 and 8.10. It is shown that the stability condition for the closed-loop system with the IBKS about delays on the additional measurements is affected by the model uncertainties on control effectiveness information; $k_{max} = 1$ for $\Delta_{(\star)} = -0.2$ while $k_{max} = 2$ for $\Delta_{(\star)} = 0.5$. It is also observed that the closed-loop system with the IBKS becomes unstable when this stability condition is not satisfied even with a small difference. The closed-loop system with the new C-ABKS is stable under delays on the additional measurements and the model uncertainties on control effectiveness information. However, the parameter estimation errors induced by these defects result in the steady-state errors of the state variables. These results address that the properties of the IBKS and the new C-ABKS under measurement delays and model uncertainties identified with the short period mode dynamics are maintained with the extension to the 6-DoF dynamics.

8.3 Conclusion

Numerical simulations are conducted for comparative studies between the IBKS and the new C-ABKS with the model uncertainties and delays on the additional measurements. Note that the short period mode and the 6-DoF dynamics are considered in the numerical simulations. The summary of the comparative studies is provided in Table 8.3.

Table 8.3: Summary of Comparative Study

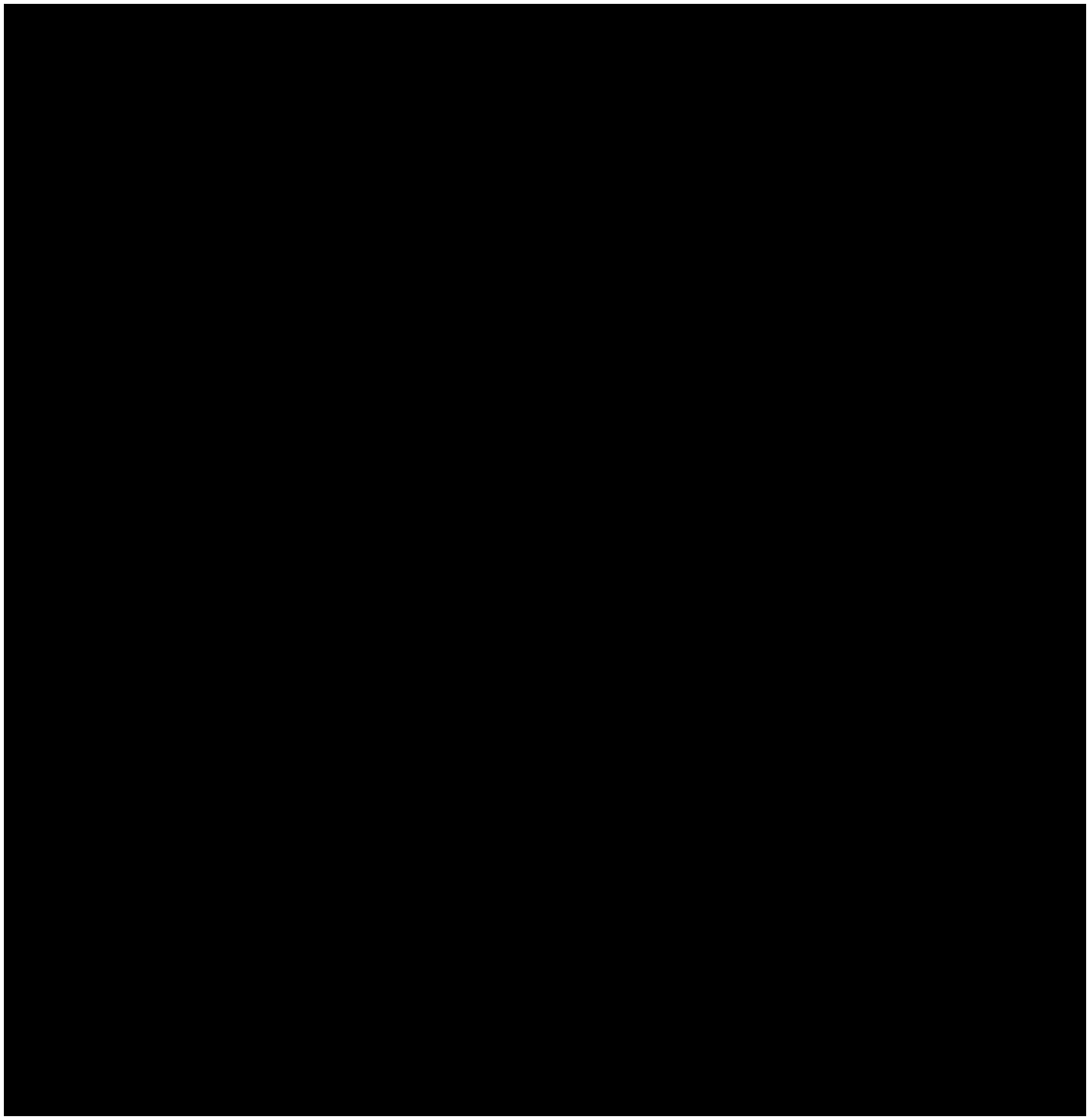

Appendix

A Estimation Error of C-ABKS with Model Uncertainty and Measurement Delay

The estimation error from the model uncertainty on control effectiveness information and the delay on the additional measurement is investigated in Appendix A for the comparative study. $\boldsymbol{r}_{2b}$ can be written from (7.17) in Chapter 7 with (8.1) as (8.15).

$$\boldsymbol{r}_{2b} = \boldsymbol{\Omega}_{2Hb}\boldsymbol{\theta}_2 = \boldsymbol{O}_{2b}\begin{bmatrix} \frac{1}{k_{21}}\left(x_{2b} - x_{2F_{21}b}\right) - M_\delta^*\delta_{F_{21}b} \\ \frac{1}{k_{22}}\left(x_{2b} - x_{2F_{22}b}\right) - M_\delta^*\delta_{F_{22}b} \end{bmatrix} \tag{8.15}$$

where $(\cdot)_b$ denotes $(\cdot)$ at $t = t_b$. If there exist $\Delta_{M_\delta^*}$ and τ_δ, $\boldsymbol{r}'_{2b}$ is obtained as follows.

$$\boldsymbol{r}'_{2b} = \boldsymbol{\Omega}'_{2Hb}\boldsymbol{\theta}'_2 = \boldsymbol{O}'_{2b}\begin{bmatrix} \frac{1}{k_{21}}\left(x'_{2b} - x'_{2F_{21}b}\right) - \hat{M}_\delta^*\delta'_{F_{21}b}(t-\tau_\delta) \\ \frac{1}{k_{22}}\left(x'_{2b} - x'_{2F_{22}b}\right) - \hat{M}_\delta^*\delta'_{F_{22}b}(t-\tau_\delta) \end{bmatrix} \tag{8.16}$$

where $(\cdot)'$ represents $(\cdot)$ under $\Delta_{M_\delta^*}$ and τ_δ. (8.16) can be rewritten as (8.17) with $d'_{F_{2_j b}} \triangleq \delta'_{F_{2_j b}}(t-\tau_\delta) - \delta'_{F_{2_j b}}$.

$$\boldsymbol{\Omega}'_{2Hb}\boldsymbol{\theta}'_2 = \boldsymbol{O}'_{2b}\begin{bmatrix} \left\{\frac{1}{k_{21}}\left(x'_{2b} - x'_{2F_{21}b}\right) - M_\delta^*\delta'_{F_{21}b}\right\} \\ \quad -M_\delta^*\Delta_{M_\delta^*}\delta'_{F_{21}b} - M_\delta^*\left(1+\Delta_{M_\delta^*}\right)d'_{F_{21}b} \\ \left\{\frac{1}{k_{22}}\left(x'_{2b} - x'_{2F_{22}b}\right) - M_\delta^*\delta'_{F_{22}b}\right\} \\ \quad -M_\delta^*\Delta_{M_\delta^*}\delta'_{F_{22}b} - M_\delta^*\left(1+\Delta_{M_\delta^*}\right)d'_{F_{22}b} \end{bmatrix} \tag{8.17}$$

(8.18) is derived from (8.1) with filtered dynamics (7.14) in Chapter 7.

$$\frac{1}{k_{2j}}\left(x'_{2b} - x'_{2F_{21}b}\right) = \theta_{21}x'_{1F_{2_j b}} + \theta_{22}x'_{2F_{2_j b}} + M_\delta^*\delta'_{F_{2_j b}} \tag{8.18}$$

Thus, $\boldsymbol{\Omega}'_{2Hb}\boldsymbol{\theta}'_2$ is rewritten by applying (8.18) to (8.17).

$$\boldsymbol{\Omega}'_{2Hb}\boldsymbol{\theta}'_2 = \boldsymbol{\Omega}'_{2Hb}\boldsymbol{\theta}_2 - M_\delta^*\boldsymbol{O}'_{2b}\left\{\Delta_{M_\delta^*}\begin{bmatrix}\delta'_{F_{21}b}\\ \delta'_{F_{22}b}\end{bmatrix} - \begin{bmatrix}d'_{F_{21}b}\\ d'_{F_{22}b}\end{bmatrix} - \Delta_{M_\delta^*}\begin{bmatrix}d'_{F_{21}b}\\ d'_{F_{22}b}\end{bmatrix}\right\} \tag{8.19}$$

It is shown in (8.19) that $\boldsymbol{\theta}_2'$ is different from $\boldsymbol{\theta}_2$ when $\Delta_{M_\delta^*}$ or τ_δ exist. Since the composite adaptation law makes $\boldsymbol{\Omega}_{2Hb}'\hat{\boldsymbol{\theta}}_2$ converge to $\boldsymbol{\Omega}_{2Hb}'\boldsymbol{\theta}_2'$, the parameter estimates have steady-state errors if $\Delta_{M_\delta^*}$ or τ_δ exist.

B Derivation of Equations for 6-DoF Dynamics with Uncertainties

The 6-DoF aircraft dynamics [5] is provided as (8.20).

$$\frac{d}{dt}\begin{bmatrix} V \\ \alpha \\ \beta \end{bmatrix} = \boldsymbol{f}_1 + \boldsymbol{f}_g + \boldsymbol{G}_1 \begin{bmatrix} T \\ q \\ r \end{bmatrix}$$

$$\frac{d}{dt}\begin{bmatrix} p \\ q \\ r \end{bmatrix} = \boldsymbol{f}_2 + \boldsymbol{G}_2 \begin{bmatrix} \delta_e \\ \delta_a \\ \delta r \end{bmatrix}$$

where

$$\boldsymbol{f}_1 = \begin{bmatrix} \frac{1}{m}\left(X_T \cos\alpha\cos\beta + Y_T \sin\beta + Z_T \sin\alpha\cos\beta\right) \\ -p\cos\alpha\tan\beta + \frac{1}{mV\cos\beta}\left(Z_T\cos\alpha - X_T\sin\alpha\right) \\ p\sin\alpha + \frac{1}{mV}\left(-X_T\cos\alpha\sin\beta + Y_T\cos\beta - Z_T\sin\alpha\sin\beta\right) \end{bmatrix}$$

$$\boldsymbol{f}_g = \begin{bmatrix} g\left(-\sin\theta\cos\alpha\cos\beta + \cos\theta\sin\phi\sin\beta + \cos\theta\cos\phi\sin\alpha\cos\beta\right) \\ \frac{g}{V\cos\beta}\left(\cos\theta\cos\phi\cos\alpha + \sin\theta\sin\alpha\right) \\ \frac{g}{V}\left(\cos\theta\sin\phi\cos\beta + \sin\theta\cos\alpha\sin\beta - \cos\theta\cos\phi\cos\alpha\sin\beta\right) \end{bmatrix}$$

$$\boldsymbol{f}_2 = \begin{bmatrix} \left(c_2 p + c_1 r\right) q + c_3 L_T + c_4 N_T \\ c_5 pr + c_6\left(r^2 - p^2\right) + c_7 M_T \\ \left(c_8 p - c_2 r\right) q + c_4 L_T + c_9 N_T \end{bmatrix}$$

$$\boldsymbol{G}_1 = \begin{bmatrix} \frac{\cos\alpha\cos\beta}{m} & 0 & 0 \\ -\frac{\sin\alpha}{mV\cos\beta} & 1 & -\sin\alpha\tan\beta \\ -\frac{\cos\alpha\sin\beta}{mV} & 0 & -\cos\alpha \end{bmatrix} \quad \boldsymbol{G}_2 = \begin{bmatrix} 0 & c_3 L_{\delta_a} + c_4 N_{\delta_a} & c_3 L_{\delta_r} + c_4 N_{\delta_r} \\ c_7 M_{\delta_e} & 0 & 0 \\ 0 & c_4 L_{\delta_a} + c_9 N_{\delta_a} & c_4 L_{\delta_r} + c_9 N_{\delta_r} \end{bmatrix} \tag{8.20}$$

L_T, M_T and N_T are aerodynamic moments in roll, pitch and yaw axis. Note that the definitions of the other parameters are provided in Section 8.2.1.1.

The equations for the aerodynamic forces and moments and the control effectiveness in (8.20) are listed in (8.21) and (8.22), respectively.

$$
\begin{aligned}
X_T &= \bar{q}S\left[C_{x_0}(\alpha) + C_{x_q}(\alpha)\frac{\bar{c}}{2V}q\right] \\
Y_T &= \bar{q}S\left[C_{y_0}(\beta) + C_{y_p}(\alpha)\frac{b}{2V}p + C_{y_r}(\alpha)\frac{b}{2V}r\right] \\
Z_T &= \bar{q}S\left[C_{z_0}(\alpha,\beta) + C_{z_q}(\alpha)\frac{\bar{c}}{2V}q\right] \\
L_T &= \bar{q}Sb\left[C_{l_0}(\alpha,\beta) + C_{l_p}(\alpha)\frac{b}{2V}p + C_{l_r}(\alpha)\frac{b}{2V}r\right] \\
M_T &= \bar{q}S\bar{c}\left[C_{m_0}(\alpha) + C_{m_q}(\alpha)\frac{\bar{c}}{2V}q + \left(C_{z_0}(\alpha,\beta) + C_{z_q}(\alpha)\frac{\bar{c}}{2V}q\right)\left(x_{CG_R} - x_{CG}\right)\frac{\bar{c}}{b}\right] \\
N_T &= \bar{q}Sb\left[C_{n_0}(\alpha,\beta) + C_{n_p}(\alpha)\frac{b}{2V}p + C_{n_r}(\alpha)\frac{b}{2V}r\right. \\
&\qquad \left. - \left(C_{y_0}(\beta) + C_{y_p}(\alpha)\frac{b}{2V}p + C_{y_r}(\alpha)\frac{b}{2V}r\right)\frac{\bar{c}}{b}\right]
\end{aligned}
\tag{8.21}
$$

$$
\begin{aligned}
L_{\delta_a} &= \bar{q}SbC_{l_{\delta_a}}(\alpha,\beta) \\
L_{\delta_r} &= \bar{q}SbC_{l_{\delta_r}}(\alpha,\beta) \\
M_{\delta_e} &= \bar{q}S\bar{c}C_{m_{\delta_e}}(\alpha,\delta_e) \\
N_{\delta_a} &= \bar{q}SbC_{n_{\delta_a}}(\alpha,\beta) \\
N_{\delta_r} &= \bar{q}SbC_{n_{\delta_r}}(\alpha,\beta)
\end{aligned}
\tag{8.22}
$$

where $C_{(\cdot)}$ is non-dimensional aerodynamic coefficient of $(\cdot)$.

The aerodynamic coefficients related to aerodynamic forces are assumed to be accurate which is reasonable as discussed in [3] and [4]. The uncertain aerodynamic coefficients for aerodynamic moments are modeled as (8.23) by simplifying the models in [2].

$$\begin{aligned}
C_{l_0}(\alpha,\beta) &= C_{l_{0\beta}}\beta + C_{l_{0\alpha\beta}}\alpha\beta + C_{l_{0\beta^2}}\beta^2 \\
C_{l_p}(-) &= C_{l_{p0}} \\
C_{l_r}(-) &= C_{l_{r0}} \\
C_{m_0}(\alpha) &= C_{m_{00}} + C_{m_{0\alpha}}\alpha \\
C_{m_q}(\alpha) &= C_{m_{q0}} + C_{m_{q\alpha}}\alpha \\
C_{n_0}(\alpha,\beta) &= C_{n_{0\beta}}\beta + C_{n_{0\alpha\beta}}\alpha\beta + C_{n_{0\beta^2}}\beta^2 \\
C_{n_p}(-) &= C_{n_{p0}} \\
C_{n_r}(-) &= C_{n_{r0}}
\end{aligned} \tag{8.23}$$

By substituting (8.21) and (8.23) into (8.20), the dynamic equation in (8.6) with (8.7) is derived.

References

[1] Donald McLean. *Automatic flight control systems*. Prentice Hall, New York, 1990.

[2] Eugene A Morelli. Global nonlinear parametric modelling with application to f-16 aerodynamics. In *Proceedings of the 1998 American Control Conference. ACC (IEEE Cat. No. 98CH36207)*, volume 2, pages 997–1001. IEEE, 1998.

[3] Pieter van Gils, Erik-Jan Van Kampen, Coen C de Visser, and Q Ping Chu. Adaptive incremental backstepping flight control for a high-performance aircraft with uncertainties. In *AIAA Guidance, Navigation, and Control Conference*, 2016.

[4] Paul Acquatella, E van Kampen, Qi Ping Chu, et al. Incremental backstepping for robust nonlinear flight control. *Proceedings of the EuroGNC*, 2013, 2013.

[5] Brian L Stevens and Frank L Lewis. *Aircraft Control And Simulation*. John Willey& Sons Inc., New York, 1992.

Chapter 9

Conclusions and Future Works

9.1 Conclusions

This thesis successfully innovates knowledge on nonlinear flight control algorithms with reduced model dependency, responding research gaps for their practical applications. Note that this thesis considers IBKS and C-ABKS which are obtained by applying the incremental and adaptive control schemes to BKS for reduced model dependency. The leading principle for each IBKS and C-ABKS to make the algorithm less dependent on model information can be summarized as follows. IBKS additionally utilizes state derivative and control surface deflection angle measurements to replace required model information except control effectiveness for its implementation. C-ABKS estimates uncertain model parameters online via adaptation law and utilizes these estimates in control input command calculation. The details on the contributions of the research with each algorithm are suggested as follows.

Extensive and systematic theoretical analyses under various defects are conducted to provide critical understandings on IBKS. As a starting point, closed-loop analyses under the model uncertainties are conducted with IBKS and BKS for theoretical interpretations on reduced model dependency in IBKS. A piecewise analysis method is utilized to obtain transfer functions with two algorithms under the model uncertainties. The characteristics of each algorithm are investigated by comparing them with the nominal results or with each other. As expected, stability and performance of the closed-loop system with IBKS are not affected by the model uncertainties, while they significantly influence the closed-loop characteristics with BKS. One interesting observation is that the uncertainty on the control effectiveness information, which

is still required to implement IBKS, does not have any impact on the closed-loop system with IBKS if the control input is calculated, transmitted and reflected fast enough to the actual control surface.

The discussions on the analysis with IBKS are broadened considering defects on the additional measurements along with the model uncertainties. First, the closed-loop characteristics with IBKS is analyzed under the biases on the additional measurements and the model uncertainties. A similar piecewise approach with the model uncertainty-only case is applied to acquire a transfer function under the measurement biases and the model uncertainties for theoretical analysis. The measurement biases result in a steady state error while not affecting the closed-loop system stability with IBKS. Unlike the analysis results only with the model uncertainties, the uncertainty in control effectiveness information has an impact on the steady-state error of the closed-loop system. Second, the closed-loop system with IBKS under the delays on the additional measurements and the model uncertainties is examined with the analysis framework proposed in this thesis. The transfer function of the closed-loop system with the measurement delays and the model uncertainties is derived under the piecewise approach as in the previous discussions. Since the measurement delays result in a highly nonlinear characteristic equation with exponential terms, the absolute stability is difficult to be examined in an analytical way. To this end, new numerical framework with optimization concept is proposed to systematically and efficiently test the closed-loop system stability under measurement delays. The key finding is that the delays on the additional measurements should satisfy a specific relationship for the closed-loop stability with IBKS. Besides, it is identified that this stability condition is affected by the uncertainty on control effectiveness information.

A new C-ABKS is designed to guarantee parameter convergence without PE and enhance the adaptation speed without excessive increase of the adaptation gain. There exist two main novel ideas for the design of the new C-ABKS to achieve this aim; a new modulation based approach for the information matrix design and a new logarithmic regression-based approach for the composite adaption law design. First, a new paradigm of the information matrix design is proposed by developing a modulation-based approach to accomplish parameter convergence under FE. A new information matrix is designed by utilizing linear independency between filtered regressor vectors from the multiple filters with different modulation effects. The filtered regressor vectors are modified to be orthogonal to each other while retaining their magnitudes before modifications, and the information matrix is con-

structed with these modified filtered regressor vectors. Second, a new logarithmic regression-based composite adaptive control is proposed to enhance the adaptation speed without excessive increase of the adapation gain. Since the linear regression term in previous studies is simply proportional to the estimation error, the adaptation speed of the linear regression term decreases fast at the later stage when the estimation error is small. The parameter convergence speed can be enhanced by slowing down the adaptation speed degeneration at the later stage; concave and monotonically increasing characteristics of the logarithmic function is utilized for the regression term in this research.

The key properties of the new logarithmic regression-based composite adaptive control with the new information matrix are investigated as follows. The closed-loop system with this new C-ABKS is shown to be asymptotically stable under FE by applying Lyapunov theory. The properties especially from the new information matrix constructed with modulation-based approach are addressed as follows. The new information matrix is proven to be positive definite for all the time from the beginning under FE, while the accumulation-based approach in previous studies requires uncertain amount of time to populate the information matrix to be full rank. Comparing to the accumulation-based approach, the new modulation-based approach provides advantages in adaptation speed and system robustness since the information matrix is designed to have all eigenvalues with moderate level of magnitudes. The properties originated from the logarithmic regression-based approach are given as follows. The logarithmic regression term is proven to be always larger than the linear regression term within the system boundary if its design parameters satisfy the suggested condition. In order to make the linear regression-based approach to become always faster than the logarithmic regression-based approach when its design parameters accomplish this condition, the adaptation gain of the linear regression term should be increased and this can result in reduced robustness.

The extensive theoretical findings on IBKS and C-ABKS are obtained and verified throughout the thesis. Note that a comparative study between IBKS and new C-ABKS is additionally performed via numerical simulations to address their differences especially under various defect circumstances.

9.2 Future Works

Researches presented in this thesis can be extended in several ways as follows.

Critical insights on the system characteristics with IBKS under the model uncertainties and the measurement delays are obtained from the analysis based on the short period mode dynamics due to its importance in flight control and simplicity in theoretical analysis. Further studies to examine and validate the properties of IBKS identified in this thesis with 6 degree-of-freedom dynamics would be beneficial.

From the closed-loop analysis with IBKS under model uncertainties and measurement delays, important stability condition is provided in terms of the relationship between delays on the state derivative and control surface deflection angle measurements. As can be seen in the numerical simulations, this condition is too strict, which could be disadvantageous for its practical applications. Hence, compensation algorithm against the delays on the additional measurements and the model uncertainties would be an interesting topic for the system with IBKS.

Most of the adaptive control algorithms are designed under the assumption of linearly structured uncertainty with constant unknown parameters satisfying the matching condition. The extension of the proposed C-ABKS algorithm to the problems with time-varying unknown parameters, unstructured uncertainty or unmatched uncertainty would be a challenging and interesting research topic.

Complete Bibliography

[1] Petar V Kokotovic. The joy of feedback: nonlinear and adaptive. *IEEE Control Systems Magazine*, 12(3):7–17, 1992.

[2] Taeyoung Lee and Youdan Kim. Nonlinear adaptive flight control using backstepping and neural networks controller. *Journal of Guidance, Control, and Dynamics*, 24(4):675–682, 2001.

[3] Jay Farrell, Manu Sharma, and Marios Polycarpou. Backstepping-based flight control with adaptive function approximation. *Journal of Guidance, Control, and Dynamics*, 28(6):1089–1102, 2005.

[4] Hann-Shing Ju and Ching-Chih Tsai. Longitudinal axis flight control law design by adaptive backstepping. *IEEE Transactions on Aerospace and Electronic Systems*, 43(1):311–329, 2007.

[5] Liang Sun and Wei Huo. 6-dof integrated adaptive backstepping control for spacecraft proximity operations. *IEEE Transactions on Aerospace and Electronic Systems*, 51(3):2433–2443, 2015.

[6] LR García Carrillo, Alejandro Dzul, and Rogelio Lozano. Hovering quad-rotor control: A comparison of nonlinear controllers using visual feedback. *IEEE Transactions on Aerospace and Electronic Systems*, 48(4):3159–3170, 2012.

[7] Xu Huang and Ye Yan. Saturated backstepping control of underactuated spacecraft hovering for formation flights. *IEEE Transactions on Aerospace and Electronic Systems*, 53(4):1988–2000, 2017.

[8] Lars Sonneveldt, QP Chu, and JA Mulder. Nonlinear flight control design using constrained adaptive backstepping. *Journal of Guidance, Control, and Dynamics*, 30(2):322–336, 2007.

[9] Baohua Lian and Hyochoong Bang. Momentum transfer-based attitude control of spacecraft with backstepping. *IEEE transactions on aerospace and electronic systems*, 42(2):453–463, 2006.

[10] Yoonsoo Kim and Byoung Soo Kim. Pitch autopilot design for agile missiles with uncertain aerodynamic coefficients. *IEEE Transactions on Aerospace and Electronic Systems*, 49(2):907–914, 2013.

[11] Jawhar Ghommam and Maarouf Saad. Autonomous landing of a quadrotor on a moving platform. *IEEE Transactions on Aerospace and Electronic Systems*, 53(3):1504–1519, 2017.

[12] Stephen H Lane and Robert F Stengel. Flight control design using non-linear inverse dynamics. *Automatica*, 24(4):471–483, 1988.

[13] Yunjun Xu. Multi-timescale nonlinear robust control for a miniature helicopter. *IEEE Transactions on Aerospace and Electronic systems*, 46(2):656–671, 2010.

[14] Romulus Lungu, Mihai Lungu, and Lucian Teodor Grigorie. Automatic control of aircraft in longitudinal plane during landing. *IEEE Transactions on Aerospace and Electronic Systems*, 49(2):1338–1350, 2013.

[15] Yuankai Li, Zhongliang Jing, and Guangjun Liu. Maneuver-aided active satellite tracking using six-dof optimal dynamic inversion control. *IEEE Transactions on Aerospace and Electronic Systems*, 50(1):704–719, 2014.

[16] Chang-Hun Lee, Byung-Eul Jun, and Jin-Ik Lee. Connections between linear and nonlinear missile autopilots via three-loop topology. *Journal of Guidance, Control, and Dynamics*, pages 1426–1432, 2016.

[17] Pieter van Gils, Erik-Jan Van Kampen, Coen C de Visser, and Q Ping Chu. Adaptive incremental backstepping flight control for a high-performance aircraft with uncertainties. In *AIAA Guidance, Navigation, and Control Conference*, 2016.

[18] Abdelouahed Ait Haddou Ali, Q Ping Chu, Erik-Jan Van Kampen, and Coen C de Visser. Exploring adaptive incremental backstepping using immersion and invariance for an f-16 aircraft. In *AIAA Guidance, Navigation, and Control Conference*, 2014.

[19] Paul Acquatella, E van Kampen, and Qi Ping Chu. Incremental backstepping for robust nonlinear flight control. In *Proceedings of the EuroGNC 2013, 2nd CEAS Specialist Conference on Guidance, Navigation and Control*, pages 1444–1463, 2013.

[20] Guillermo P Falconí, Valentin A Marvakov, and Florian Holzapfel. Fault tolerant control for a hexarotor system using incremental backstepping. In *2016 IEEE Conference on Control Applications (CCA)*, pages 237–242. IEEE, 2016.

[21] Jean-Jacques E Slotine and Weiping Li. On the adaptive control of robot manipulators. *The international journal of robotics research*, 6(3):49–59, 1987.

[22] Jean-Jacques E Slotine and Weiping Li. Composite adaptive control of robot manipulators. *Automatica*, 25(4):509–519, 1989.

[23] Hanlei Wang. Adaptive control of robot manipulators with uncertain kinematics and dynamics. *IEEE Transactions on Automatic Control*, 62(2):948–954, 2016.

[24] Nazli E Kahveci and Petros A Ioannou. Adaptive steering control for uncertain ship dynamics and stability analysis. *Automatica*, 49(3):685–697, 2013.

[25] J Van Amerongen. Model reference adaptive control applied to steering of ships. In *Methods and applications in adaptive control*, pages 199–208. Springer, 1980.

[26] HJ Tol, CC De Visser, LG Sun, E van Kampen, and QP Chu. Multivariate spline-based adaptive control of high-performance aircraft with aerodynamic uncertainties. *Journal of Guidance, Control, and Dynamics*, 39(4):781–800, 2016.

[27] Ye Zhou, Erik-Jan van Kampen, and QiPing Chu. Nonlinear adaptive flight control using incremental approximate dynamic programming and output feedback. *Journal of Guidance, Control, and Dynamics*, 40(2):493–496, 2016.

[28] Nhan Nguyen, Kalmanje Krishnakumar, John Kaneshige, and Pascal Nespeca. Flight dynamics and hybrid adaptive control of damaged aircraft. *Journal of guidance, control, and dynamics*, 31(3):751–764, 2008.

[29] DE Seborg, Thomas F Edgar, and SL Shah. Adaptive control strategies for process control: a survey. *AIChE Journal*, 32(6):881–913, 1986.

[30] A Galip Ulsoy and Yoram Koren. Applications of adaptive control to machine tool process control. *IEEE Control Systems Magazine*, 9(4):33–37, 1989.

[31] Chengshuai Wu, Jian Chen, Chenfeng Xu, and Zhiyang Liu. Real-time adaptive control of a fuel cell/battery hybrid power system with guaranteed stability. *IEEE Transactions on Control Systems Technology*, 25(4):1394–1405, 2016.

[32] Dezhi Xu, Jianxing Liu, Xing-Gang Yan, and Wenxu Yan. A novel adaptive neural network constrained control for a multi-area interconnected power system with hybrid energy storage. *IEEE Transactions on Industrial Electronics*, 65(8):6625–6634, 2017.

[33] Manuel A Duarte and Kumpati S Narendra. Combined direct and indirect approach to adaptive control. *IEEE Transactions on Automatic Control*, 34(10):1071–1075, 1989.

[34] Manuel A Duarte and Kumpati S Narendra. A new approach to model reference adaptive control. *International Journal of Adaptive Control and Signal Processing*, 3(1):53–73, 1989.

[35] Kumpati S Narendra and Manuel A Duarte. Application of robust adaptive control using combined direct and indirect methods. *International Journal of Adaptive Control and Signal Processing*, 3(2):131–142, 1989.

[36] Eugene Lavretsky. Combined/composite model reference adaptive control. *IEEE Transactions on Automatic Control*, 54(11):2692–2697, 2009.

[37] Parag M Patre, William MacKunis, Marcus Johnson, and Warren E Dixon. Composite adaptive control for euler–lagrange systems with additive disturbances. *Automatica*, 46(1):140–147, 2010.

[38] MK Ciliz. Adaptive backstepping control using combined direct and indirect adaptation. *Circuits, Systems & Signal Processing*, 26(6):911–939, 2007.

[39] Parag M Patre, Shubhendu Bhasin, Zachary D Wilcox, and Warren E Dixon. Composite adaptation for neural network-based controllers. *IEEE Transactions on Automatic Control*, 55(4):944–950, 2010.

[40] Yongping Pan, Yiqi Liu, and Haoyong Yu. Online data-driven composite adaptive backstepping control with exact differentiators. *International Journal of Adaptive Control and Signal Processing*, 30(5):779–789, 2016.

[41] Yongping Pan and Haoyong Yu. Composite learning from adaptive dynamic surface control. *IEEE Transactions on Automatic Control*, 61(9):2603–2609, 2015.

[42] Girish Chowdhary, Tansel Yucelen, Maximillian Mühlegg, and Eric N Johnson. Concurrent learning adaptive control of linear systems with exponentially convergent bounds. *International Journal of Adaptive Control and Signal Processing*, 27(4):280–301, 2013.

[43] Girish Chowdhary, Maximilian Mühlegg, and Eric Johnson. Exponential parameter and tracking error convergence guarantees for adaptive controllers without persistency of excitation. *International Journal of Control*, 87(8):1583–1603, 2014.

[44] Namhoon Cho, Hyo-Sang Shin, Youdan Kim, and Antonios Tsourdos. Composite model reference adaptive control with parameter convergence under finite excitation. *IEEE Transactions on Automatic Control*, 63(3):811–818, 2017.

[45] Hassan K Khalil. *Nonlinear systems*. Upper Saddle River, 1996.

[46] Jean-Jacques E Slotine, Weiping Li, et al. *Applied nonlinear control*. Prentice hall Englewood Cliffs, NJ, 1991.

[47] I. Kanellakopoulos M. Krstic and P. Kokotovic. *Nonlinear and Adaptive Control*. John Wiley and Sons, Inc., New York, 1995.

[48] B. Kim et al. *Flight Dynamics and Control*. Kyung Moon Sa, 2004.

[49] Farid Golnaraghi and Benjamin C Kuo. *Automatic Control Systems*. John Wiley and Sons Ltd, 2009.

[50] Donald McLean. *Automatic flight control systems*. Prentice Hall, New York, 1990.

[51] Gang Tao. *Adaptive control design and analysis*, volume 37. John Wiley & Sons, 2003.

[52] S Sieberling, QP Chu, and JA Mulder. Robust flight control using incremental nonlinear dynamic inversion and angular acceleration prediction. *Journal of guidance, control, and dynamics*, 33(6):1732–1742, 2010.

[53] Paul Acquatella, Wouter Falkena, Erik-Jan van Kampen, and Q Ping Chu. Robust nonlinear spacecraft attitude control using incremental nonlinear dynamic inversion. In *AIAA Guidance, Navigation, and Control Conference*, 2012.

[54] P Simplício, MD Pavel, E Van Kampen, and QP Chu. An acceleration measurements-based approach for helicopter nonlinear flight control using incremental nonlinear dynamic inversion. *Control Engineering Practice*, 21(8):1065–1077, 2013.

[55] Ewoud JJ Smeur, Qiping Chu, and Guido CHE de Croon. Adaptive incremental nonlinear dynamic inversion for attitude control of micro air vehicles. *Journal of Guidance, Control, and Dynamics*, 38(12):450–461, 2015.

[56] Xuerui Wang, Erik-Jan Van Kampen, Qiping Chu, and Peng Lu. Stability analysis for incremental nonlinear dynamic inversion control. *Journal of Guidance, Control, and Dynamics*, 42(5):1116–1129, 2019.

[57] Byoung-Ju Jeon, Min-Guk Seo, Hyo-Sang Shin, and Antonios Tsourdos. Understandings of the incremental backstepping control through theoretical analysis under the model uncertainties. In *2018 IEEE Conference on Control Technology and Applications (CCTA)*, pages 318–323. IEEE, 2018.

[58] B. Jeon, M. Seo, H. Shin, and A. Tsourdos. Understandings of classical and incremental backstepping controllers with model uncertainties. *IEEE Transactions on Aerospace and Electronic Systems*, 56(4):2628–2641, 2020.

[59] Byoung-Ju Jeon, Min-Guk Seo, Hyo-Sang Shin, and Antonios Tsourdos. Closed-loop analysis with incremental backstepping controller considering measurement bias. *IFAC-PapersOnLine*, 52(12):405–410, 2019.

[60] Fabian Grondman, Gertjan Looye, Richard O Kuchar, Q Ping Chu, and Erik-Jan Van Kampen. Design and flight testing of incremental nonlinear dynamic inversion-based control laws for a passenger aircraft. In *2018 AIAA Guidance, Navigation, and Control Conference*, page 0385, 2018.

[61] RD Driver, DW Sasser, and ML Slater. The equation x'(t)= ax (t)+ bx (t- τ) with "small" delay. *The American Mathematical Monthly*, 80(9):990–995, 1973.

[62] Steve Guillouzic, Ivan L'Heureux, and André Longtin. Small delay approximation of stochastic delay differential equations. *Physical Review E*, 59(4):3970, 1999.

[63] A Bahill. A simple adaptive smith-predictor for controlling time-delay systems: A tutorial. *IEEE Control systems magazine*, 3(2):16–22, 1983.

[64] Tamas Insperger. On the approximation of delayed systems by taylor series expansion. *Journal of Computational and Nonlinear Dynamics*, 10(2):024503, 2015.

[65] Nejat Olgac and Rifat Sipahi. An exact method for the stability analysis of time-delayed linear time-invariant (lti) systems. *IEEE Transactions on Automatic Control*, 47(5):793–797, 2002.

[66] ZV Rekasius. A stability test for systems with delays. In *Joint Automatic Control Conference*, number 17, page 39, 1980.

[67] Maxime Doublet, Cédric Join, and Frederic Hamelin. Stability analysis for unknown delayed systems controlled by model-free control. In *2017 21st International Conference on System Theory, Control and Computing (ICSTCC)*, pages 441–446. IEEE, 2017.

[68] Anup Parikh, Rushikesh Kamalapurkar, and Warren E Dixon. Integral concurrent learning: Adaptive control with parameter convergence using finite excitation. *International Journal of Adaptive Control and Signal Processing*, 2018.

[69] G Leitmann. Guaranteed asymptotic stability for some linear systems with bounded uncertainties. *Journal of Dynamic Systems, Measurement, and Control*, 101(3):212–216, 1979.

[70] Byoung-Ju Jeon, Hyo-Sang Shin, and Antonios Tsourdos. Composite adaptive backstepping control considering computational complexity and relaxation of persistent excitation. In *21st IFAC World Congress*. IEEE, 2020.

[71] Hae-In Lee, Hyo-Sang Shin, and Antonios Tsourdos. Concurrent learning adaptive control with directional forgetting. *IEEE Transactions on Automatic Control*, 64(12):5164–5170, 2019.

[72] Zachary T Dydek, Anuradha M Annaswamy, Jean-Jacques E Slotine, and Eugene Lavretsky. Composite adaptive posicast control for a class of lti plants with known delay. *Automatica*, 49(6):1914–1924, 2013.

[73] Yongping Pan and Haoyong Yu. Composite learning robot control with guaranteed parameter convergence. *Automatica*, 89:398–406, 2018.

[74] M Kemal Ciliz. Combined direct and indirect adaptive control for a class of nonlinear systems. *IET Control Theory & Applications*, 3(1):151–159, 2009.

[75] Byoung-Ju Jeon, Hyo-Sang Shin, and Antonios Tsourdos. Composite adaptive control with new information matrix for parameter convergence without persistent excitation. *Automatica, Submitted*, 2020.

[76] Wang Leifeng, Li Ye, Liao Yulei, Pan Kaiwen, and Zhang Weixin. Adaptive heading control of unmanned wave glider with heading information fusion. *Control Engineering Practice*, 85:216–224, 2019.

[77] Jovan D Boskovic and Raman K Mehra. Intelligent adaptive control of a tailless advanced fighter aircraft under wing damage. *Journal of Guidance, Control, and Dynamics*, 23(5):876–884, 2000.

[78] Jin Young Choi, Dongkyoung Chwa, and Min-Soo Kim. Adaptive control for feedback-linearized missiles with uncertainties. *IEEE Transactions on Aerospace and Electronic Systems*, 36(2):467–481, 2000.

[79] Dmitry I Ignatyev, Hyo-Sang Shin, and Antonios Tsourdos. Two-layer adaptive augmentation for incremental backstepping flight control of transport aircraft in uncertain conditions. *Aerospace Science and Technology*, page 106051, 2020.

[80] Lijia Cao, Xiaofeng Li, Yu Hu, Mingtao Liu, and Jiefu Li. Discrete-time incremental backstepping controller for unmanned aircrafts subject to actuator constraints. *Aerospace Science and Technology*, 96:105530, 2020.

[81] Yang Zhang, Sheng-hai Wang, Bin Chang, and Wen-hai Wu. Adaptive constrained backstepping controller with prescribed performance methodology for carrier-based uav. *Aerospace Science and Technology*, 92:55–65, 2019.

[82] Mihai Lungu. Auto-landing of uavs with variable centre of mass using the backstepping and dynamic inversion control. *Aerospace Science and Technology*, page 105912, 2020.

[83] Mihai Lungu. Backstepping and dynamic inversion combined controller for auto-landing of fixed wing uavs. *Aerospace Science and Technology*, 96:105526, 2020.

[84] Jan Roskam. *Airplane flight dynamics and automatic flight controls*. DARcorporation, 1998.

[85] Petros A Ioannou and Petar V Kokotovic. Instability analysis and improvement of robustness of adaptive control. *Automatica*, 20(5):583–594, 1984.

[86] Kumpatis Narendra and Anuradham Annaswamy. A new adaptive law for robust adaptation without persistent excitation. *IEEE Transactions on Automatic control*, 32(2):134–145, 1987.

[87] Tansel Yucelen and Wassim M Haddad. Low-frequency learning and fast adaptation in model reference adaptive control. *IEEE Transactions on Automatic Control*, 58(4):1080–1085, 2012.

[88] Chengyu Cao and Naira Hovakimyan. Design and analysis of a novel L_1 adaptive control architecture with guaranteed transient performance. *IEEE Transactions on Automatic Control*, 53(2):586–591, 2008.

[89] Tansel Yucelen and Anthony J Calise. Derivative-free model reference adaptive control. *Journal of Guidance, Control, and Dynamics*, 34(4):933–950, 2011.

[90] Eugene A Morelli. Global nonlinear parametric modelling with application to f-16 aerodynamics. In *Proceedings of the 1998 American Control Conference. ACC (IEEE Cat. No. 98CH36207)*, volume 2, pages 997–1001. IEEE, 1998.

[91] Brian L Stevens and Frank L Lewis. *Aircraft Control And Simulation*. John Willey& Sons Inc., New York, 1992.